The Biogeographic Origins of Iron Age Iapygians and Working-Class Romans from Southern Italy

Assessing Migration and Demographic Change in pre-Roman and Roman Period Southern Italy Using Whole-Mitochondrial DNA and Stable Isotope Analysis

By: Matthew Emery, B.A., M.A.

A Thesis Submitted to the School of Graduate Studies in the Partial Fulfillment of the Requirements for the Degree Doctor of Philosophy

DOCTOR OF PHILOSOPHY (2017) **McMaster University**

(Anthropology) Hamilton, Ontario

TITLE: Assessing Migration and Demographic Change in pre-Roman and Roman Period Southern Italy Using Whole-Mitochondrial DNA and Stable Isotope Analysis

AUTHOR: Matthew Emery, Hons. B.A. (Western University), M.A. (McMaster University)

SUPERVISORS: Dr. Tracy Prowse and Dr. Hendrik Poinar

NUMBER OF PAGES: XV, 176

Lay Abstract

With biochemical information obtained from teeth, this study examines the population structure and geographic origins in two archaeological communities located in southern Italy. Analysis of classical remains has traditionally been the subject of historical and archaeological inquiry. However, new applications evaluate these population changes with integrated stable isotope and ancient DNA techniques. Overall, the biochemical results suggest that the pre-Roman communities harbor deep maternal ancestry originating from eastern Europe and the eastern Mediterannean. These results, when compared to the genetic diversity of Roman and broader Mediterranean populations, indicate that the Romans share closer genetic similarity with ancient Stone and Bronze Age communites from Europe and the eastern Mediterranean, than with the pre-Roman community studied here. Furthermore, tooth chemistry results indicate a predominantly local population buried in the Roman period cemetery.

Abstract

Assessing population diversity in southern Italy has traditionally relied on archaeological and historic evidence. Although informative, these lines of evidence do not establish specific instances of within lifetime mobility, nor track population diversity over time. In order to investigate the population structure of ancient South Italy I sequenced the mitochondrial DNA (mtDNA) from 15 Iron Age (7^{th} – 4^{th} c. BCE) and 30 Roman period (1^{st} – 4^{th} c. BCE) individuals buried at Iron Age Botromagno and Roman period Vagnari, in southern Italy, and analyzed $\delta^{18}O$ and $^{87}Sr/^{86}Sr$ values from a subset of the Vagnari skeletal assemblage.

Phylogenetic analysis of 15 Iron Age mtDNAs together with 231 mtDNAs spanning European prehistory suggest that southern Italian *Iapygians* share close genetic affinities to Neolithic populations from eastern Europe and the Near East. Population pairwise analysis of Iron Age, Roman, and mtDNA datasets spanning the pan-Mediterranean region (n=357), indicate that Roman maternal genetic diversity is more similar to Neolithic and Bronze Age populations from central Europe and the eastern Mediterranean, respectively, than to Iron Age Italians. Genetic distance between population age categories imply moderate mtDNA turnover and constant population size during the Roman conquest of South Italy in the 3^{rd} century BCE.

In order to determine the local versus non-local demographic at Vagnari, I measured the $^{87}Sr/^{86}Sr$ and $^{18}O/^{16}O$ of composition of 43 molars, and the $^{87}Sr/^{86}Sr$ composition of an additional 13 molars, and constructed a preliminary $^{87}Sr/^{86}Sr$ variation map of the Italian peninsula using disparate $^{87}Sr/^{86}Sr$ datasets. The relationship between $^{87}Sr/^{86}Sr$ and previously published $\delta^{18}O$ data suggest a relatively low proportion of migrants lived at Vagnari (7%).

This research is the first to generate whole-mitochondrial DNA sequences from Iron Age and Roman period *necropoleis*, and demonstrates the ability to gain valuable information from the integration of aDNA, stable isotope, archaeological and historic evidence.

Acknowledgements

I am deeply indebted to the councel and supervision provided by my PhD committee members, Drs. Tracy Prowse, Hendrik Poinar, and Henry Schwarcz. Their wealth of knowledge and unwavering guidance over the years was crucial in seeding my academic development. Their unconditional support for my tenuous adventures, both in the field and within the university, allowed me to attain goals and objectives far outside the parameters of my own self-directed pursuits. Words cannot capture the respect and gratitude I feel towards these exceptional scholars, colleagues, and friends.

I would also like to thank my colleagues and friends (dare I say family members) at McMaster's Ancient DNA Centre and Department of Anthropology: Dr. Robert Stark, Dr. Stephanie Marciniak, Dr. Ana Duggan, Katherine Eaton, Emil Karpinski, Tyler Murchie, Jonathan Hughes, Jessica Hider, Mel Kuch, and Debi Poinar. I am truly fortunate to have met such a wonderfully talented group of like-minded individuals. Over the years at the centre I have been able to forge some exceptional relationships. Having no previous ancient DNA experience, their guidance helped expedite my skill-set and thus facilitated my own independent wet- and dry-laboratory research, which ultimately led to the successful completion of this dissertation. I am especially thankful to Dr. Stephanie Marciniak, Jennifer Klunk, Katherine Eaton, and Emil Karpinski, for their patience during my wet laboratory training, the outcome of which led to the successful results present in this body of work. I would, without question, fared poorly without their all-around dedicated support. Their passion for the field of ancient DNA is truly inspiring, and continues to motivate me on a daily basis. I would also like to thank the previous and current teachers, mentors, and scholars who impacted my early educational development, and laid the foundation for my long journey through graduate school: Drs. Alan Dickin, Christine White, Lisa Hodgetts, Holly Martelle, Peter Timmins, Eldon Molto, Andrew Walsh, Ian Colquhoun, Tina Moffat, Aubrey Cannon, Glen Caldwell, Cam Tsujita, and Steve Hicock, and to those that escape me at the moment - place your name here.

I would like to extend a very special thanks to Dr. Ana Duggan (our aDNA postdoc *extraordinaire*), whose careful guidance, knowledge, and quick problem solving skills were indispensable throughout the latter years of my PhD. The quality of the aDNA work herein is a direct reflection of her specific attention to detail, and is a testament of her ability to observe patience (especially in times of computer troubles), and teach complicated computational tasks quickly and with ease.

I would like to extend the deepest gratitude to my parents, Denise and Rosaire Emery, and younger brother, Christopher. Words cannot express my deep thanks for your unconditional support. You have been fans of my idealism since day one, and never once discouraged me from pursuing a career in the archaeo- and palaeosciences. You encouraged imagination over status quo and, now, with a few decades under my belt, I see no better philosophy by which to live.

I thank my best friends for life: Dr. Colin Labadie, Clayton DaSilva, Dr. Robert Stark, Tyler Murchie, and Ben Eldon, with whom our shared experiences, will certainly go down in the annals of life. And last but not least, to my dog, Maicoh, whose forever presence provided me the daily structure I so desperately needed to finish this damned document.

This dissertation is dedicated to the migrant families from East and North Africa, Syria, Palestine, and Iraq, who in search for better opportunities put their lives at risk for a chance at peace in a foreign land

Table of Contents

List of Figures

Chapter 2.0

Chapter 3.0

Chapter 4.0

List of Tables

Chapter 2.0

Chapter 3.0

Chapter 4.0

List of Abbreviations

aDNA	Ancient DNA
BCE	Before Common Era
BP	Before Present
bp	Base Pair
BWA	Burrows-Wheeler Aligner
C	Carbon
Ca	Calcium
$CaCl_2$	Calcium Chloride
CO_3	Carbonate
CE	Common Era
CF-IRMS	Continuous Flow Isotope Ratio Mass Spectrometer
CI	Crystallinity Index
DDT	Dithiothreitol
DNA	Deoxyribonucleic Acid
EDTA	Ethylenediaminetetraacetic Acid
FLD	Fragment Length Distribution
GIS	Geographic Information System
GNIP	Global Network of Isotopes in Precipitation
GuHCl	Guanadinium Hydrochloride
H	Hydrogen
HCl	Hydrochloric Acid
HPD	Highest Posterior Density
HVR	Hypervariable Region
IDW	Inverse Distance Weighting
ka	Thousand Years Ago
LGM	Last Glacial Maximum
MDS	Multi-Dimensional Scaling
M/m	Permanent Molar/Deciduous Molar
mL	Milliliter
MCC	Maximum Clade Credibility
mtDNA	Mitochondrial DNA
MQ	Map Quality
N	Nitrogen
NaClO	Sodium Hypochlorite
NGS	Next Generation Sequencing
nM	Nanomolar
NRY	Non-Recombining Region of the Y-Chromosome
O	Oxygen
OH	Hydroxide
Pb	Lead
pH	Potential of Hydrogen
PO	Phosphate
PTB	N-Phenacylthiazolium
PVP	Polyvinylpyrrolidone

qPCR	Quantitative Polymerase Chain Reaction
rCRS	Revised Cambridge Reference Sequence
rpm	Rounds Per Minute
S	Sulphur
SNP	Single Nucleotide Polymorphism
Sr	Strontium
TIMS	Thermal Ionization Mass Spectrometer
TLE	Trophic Level Effect
Tris-HCl	Tris Hydrochloride
µL	Microliter
µM	Micromolar
UV	Ultraviolet
VPDB	Vienna Pee Dee Belemnite
VSMOW	Vienna Standard Mean Ocean Water

Declaration of Authorship

I, Matthew EMERY, declare that this thesis titled "Assessing Migration and Demographic Change in pre-Roman and Roman Period Southern Italy Using Whole-Mitochondrial DNA and Stable Isotope Analysis" and the work presented in it are my own. I confirm that:

This dissertation is composed of three chapters that have been submitted for peer review to the *European Journal of Human Genetics*, *American Journal of Physical Anthropology*, and the *Journal of Archaeological Science*. As first author for all three papers I was the primary researcher involved in sample aquisition and prepration, laboratory experimentation, the processing of teeth samples, and was the primary contributor towards the analysis, interpretation, and manuscript writing. All coauthors listed in the Chapters 2, 3, and 4 contributed to editing each manuscript. Drs. Tracy Prowse, Hendrik Poinar, Henry Schwarcz, and Ana Duggan contributed to research question design and results interpretation; Spencer Elford and Robert Stark contributed to the GIS methodology included in both Chapters 3 and 4. Tyler Murchie contributed to figure design using Adobe Illustrator for Chapters 2, 3, and 4; Jennifer Klunk, Emil Karpinski, Katherine Eaton, and Jessica Hider aided in laboratory experimentation and question design and ancient DNA procedures outlined in Chapters 3 and 4.

Chapter 1.0

1.1 Introduction

The central theme of this dissertation is the process of human migration. The goal of this research is to situate this process at a local scale in classical period southern Italy using bone chemistry and ancient DNA (aDNA), and to consider the broader scale of human movement in the ancient Mediterranean region. Human migration in pre-Roman and Roman Italy has traditionally been studied through the archaeological and historic records (Benelli, 2001). These sources of information are highly informative, providing important lines of evidence about patterns in socio-economic trade (Fletcher, 2007; Garnsey and Saller, 2014), material production (Biers, 1992; Curti et al., 1996), food procurement and distribution (Bernard, 2016), military conquest (Dyson, 1985; Elton, 1996; Breeze, 2011), settlement construction (Cary, 1981; Burgers, 2004; Campagna, 2011), human kinship patterns (Gejvall and Henschen, 1968; Hassall, 1999), and migration and identity throughout classical antiquity (Fulford, 2010; Cool, 2010; De Ligt, 2012; Haeussler, 2013; De Ligt and Tacoma, 2016; Erdkamp, 2016). Historic and archaeological data shape our interpretations of past human behaviour at the local and broader social scales. However, these lines of information do not provide a complete picture of human migration, mobility, and the deep ancestry we carry within our genome at the individual level. In addition, historical documents are often biased representations of life in ancient Greece and Rome, because they were written by, and for, a select segment of ancient society. This narrow focus leads to the underrepresentation other members of society, such as children, women, and the rural inhabitants of Rome's hinterland (Foubert, 2016). In this respect, this research is the first to investigate origins and maternal ancestry of both rural Iron Age and Roman individuals outside of the confines of the city of Rome.

What follows is a comprehensive analysis of the origins and ancestral affiliations of Iron Age and rural Roman inhabitants located at the southern Italian archaeological sites of Botromagno (and the associated cemeteries of Padre Eterno and Parco San Stefano) (8^{th} – 4^{th} c. BCE) and Vagnari (1^{st} – 4^{th} c. CE). To date, no aDNA studies of Iron Age and Roman period Italians exist, leaving a major gap between what we know about the population history of pre-Roman and Roman Europe and modern European genetic diversity. The results contained herein add further stable isotope information to the growing body of bioarchaeological literature concerning migration in Roman Italy (Prowse et al., 2007, 2010; Killgrove, 2010; Killgrove and Montgomery, 2016; Prowse, 2016; Stark, 2016), but from the hinterland of Roman Italy, whose populations are not well represented in the current literature.

1.2 Research Questions and Objectives

This thesis addresses a number of interrelated research questions explored through aDNA and stable isotope analysis. A number of unanswered questions remain concerning the demographic makeup of Iron Age and Roman period communities in South Italy: How biologically diverse was southern Italy during the Roman period? Did Roman expansion, subjugation, and settlement of Roman colonies alter South Italy's pre-Roman demographic landscape? How genetically distant were Iron Age Italians and Romans from one another, and to other Mediterranean-bound populations? Can we identify deeper biological signatures embedded in the genetic structure of Iron Age and Roman period human remains? Are the burials with multiple individuals maternally related? These questions will be addressed through the analysis of aDNA from the Iron Age and Roman samples used in this study.

Further, were the inhabitants buried at Vagnari local or non-local to the region? If non-

local to Vagnari, where did the occupants likely originate? These questions will be addressed through the integrated analysis of oxygen and strontium isotopes. Finally, this thesis will address the question of integrating aDNA and stable isotope evidence and, specifically, what we can learn through the integration of these biochemical methodologies. Many of these social and biological questions concerning rural pre-Roman and Roman individuals have not been addressed in Roman bioarchaeological research. As such, the biochemical results provided in this dissertation directly link to ongoing debates concerning the origins and ancestry of pre-Roman communities, such as the Iron Age *Iapygians* of Apulia, and those of rural Imperial Roman workers at Vagnari.

1.3 Theoretical Orientation

The themes and results contained in this dissertation are interconnected through the expansive historical perspective of the *longue durée*, a theoretical idea first articulated by Fernand Braudel in his dissertation entitled: *La Méditerranée et le Monde Méditerranée à l'epoche de Philippe II* (Braudel, 1949) and subsequently elaborated in his treatise: *Histoire et Science Sociales: La Longue Durée* (Braudel, 1958). Archaeologists interested in long-term social and ecological changes adopted the French *Annales School* of historical thought about the structuring of temporal trends in the archaeological record (Braudel, 1958). A number of studies documenting long-term social changes exist, and Braudel's ideas have been adopted by archaeologists (Ames, 1991; Harding, 2005; Ben-Shlomo et al., 2009; Rosen and Rivera-Collazo, 2012; Batiuk, 2013), historians (Armitage, 2012; Guldi and Armitage, 2014), economists (Colombo et al., 2006), conservation ecologists (Redman and Kinzig, 2003), and archaeogeneticists (McEvoy et al., 2004; Soares et al., 2010). The success of this approach is owed to the inherent temporal depth required to obtain meaningful information about how social

variables change over time. The concept of the *longue durée* is a useful way to address changes in the archaeological record precisely because of the difficulties in recovering enough evidence to draw accurate conclusions over shorter time scales. The *longue durée* is also particularly useful in cases where diachronic analyses of related, or closely associated cemetery populations are found. Since Iron Age Botromagno and Roman Vagnari represent two populations that inhabited the same region in southern Italy at different times in its history, the genetic analysis of both skeletal assemblages, paired with Roman isotope data offer an exceptional case by which to explore population change over a period of occupation spanning a millennia, within the temporal lens of the *longue durée* in South Italy and the Mediterranean region.

1.4 Historical Background and Archaeological Context

1.4.1 A Sea of Traders: Iron Age Southern Italy from the 8th - 6th century BCE

The result of overcrowding, famine, and political destabilization in mainland Greece led to the dispersal and settlement of Greek inhabitants in Italy, Asia Minor (present day Turkey), and the Black Sea region (Dunbabin, 1979; Cornell, 1995). By 750 BCE many of these dispossessed Greeks landed on the Tyrrhenian coast, near the Bay of Naples, and established the first mainland settlements at Cumae and Pithekoussai, on the island of Ischia, to trade with the Etruscans situated further North (Reich, 1979; Smith, 1999). Two decades later the Greeks founded the oldest known sites on the island of Sicily, Naxos and Syracuse (Dunbabin, 1979; Finley, 1979), leading them into direct contact with the Italy's indigenous Iron Age communities. Historic evidence indicates that the Greeks contacted, quarreled, and traded with these Italic tribes, which included the Samnites, the Bruttians and Lucanians of southwestern Calabria and Potenza, and the Daunians, Peucetians, and Messapians, collectively known as *Iapygians*, of

Apulia (Guido, 1973; Graeme, 1995; La Torre, 2011). The *Iapygian* communities constructed settlements along the coast and mountainous interior, areas that were easily defensible positions. For *Iapygians* residing across the plains adjacent to the southern Apennines, scattered groups composed of small dwellings and tomb sites were interlinked with fortified defensive positions, which was a common tactic among Iron Age communities at this time (Fletcher, 2007). Many of the grave goods recovered from *Iapygian* tombs support the inference of cultural interaction and trade with the Greeks. Ceramic analysis of Corinthian pottery determined much of what is known about these cultural interactions, though debate continues as to whether these items were imported from mainland Greece or manufactured locally (Fletcher, 2007; Handberg and Jacobsen, 2011).

Archaeological evidence for the spread of Greek settlements by the Archaic Period (620 – 480 BCE) is strong, based on the discovery of permanent settlements built along the southeast coast, at Lakroi and Taras (Tarantum, or modern day Taranto), Metapontion (present day Metaponto) on the Ionian coast, and in the distribution of East Greek, Corinthian, and Spartan manufactured Laconian ceramics found throughout much of the southern peninsula (Dunbabin, 1979; Curti et al., 1996). Between 675 and 600 BCE, the archaeological data support a Corinthian dominated South, with Corinthian-style ceramics reaching as far northwest as the Greek settlement of Cumae.

The origins of ceramic imports to South Italy shifted by the last quarter of the 7th century BCE (625 BCE), suggesting changing trade relationships between local Italian groups and different Greek communities. For example, Corinthian style pottery represents over 83% of the ceramic materials recovered in southern Italy, whereas East Greek artifacts only accounted for 9.3% of these finds (Fletcher 2007). The archaeological evidence suggests that during this period

mainland Greek city-states were vying for economic and cultural dominance over their Italian colonies and the local inhabitants.

Recent reports by classical archaeologists and historians have focused on the cultural impact the Italic tribes had on Greek life (Colivicchi, 2011; Malfitana, 2011; Petersen, 2011). Despite the importance of Greek imports by artifact frequency, Handberg and Jacobsen (2011) note several occurrences during the 8th to mid-7th centuries BCE of a slow assimilation of Greek traditions at native Italian settlements. For example, at the 8th century indigenous settlement of Incoronata, Corinthian pottery occurred only in small numbers. By comparison, local matt-painted vessels represent the vast majority of finds at Incoronata (Colivicchi, 2011). The same pattern was discovered at Metaponto. Mixed Graeco-*Iapygian* ceramic assemblages at this site suggest that Metaponto may have been an indigenous settlement prior to the arrival of the Greeks. However, mixed ceramic traditions also suggest that local communities profoundly impacted Greek manufacturing traditions, and viewed locally procured materials as exotic items fit for both utilitarian and economic use (Dietler, 2007). Although marginal, the settlement on the slopes below Botromagno was also involved in trade with Ionian Greek colonies. This is indicated by Ionian style ceramic cups found in association with burials at Parco San Stefano (Small 1992). A detailed review of the archaeological and historical evidence for occupation at Parco San Stefano and Botromagno is found in Chapter 2, Supplementary 2A.

1.4.2 Southern Italy During the Late Iron Age: 6th - 3rd century BCE

The reduction in Corinthian middle- to late-geometric pottery during the early 6th century BCE coincided with an increase in East Greek material in southern Italian sites (Burgers, 2004). Yet, there are several difficulties in defining 'East Greek' artifacts since overlapping patterns in

style and decoration are also observed over the greater Aegean region, spanning East Greece and the western Anatolian Greek colonies at Samos, Chios, and Miletus, and in Lydia (present day central Turkey), at Sardis (Fletcher, 2007).

The archaeological evidence is clear that by the first quarter of the 6th century BCE, eastern Greek colonies, or at least their imported materials, were thriving. Interestingly, the distribution of these imports precisely mirrored trade-networks established two centuries earlier by the Levantines (under late Assyrian rule). Drastic changes in Levantine pottery types after the fall of Sidon (and the destruction of the Levantine Assyrian Empire by the Babylonians and Medes) showed East Greek influence (Hodos, 2009). This evidence supports the notion that East Greek hegemony extended the entirety of the Mediterranean. It similarly points to centuries of contact between East Greek and mainland Levantine communities from the eastern Mediterranean. This is shown by the reestablishment of 200-year old Laventine trade routes to South Italy by the East Greeks, and the expansive distribution of East Greek pottery to all of the southern Italian colonies until their decline after 550 BCE (Fletcher, 2007).

The 5th century BCE was a period of conflict in the eastern Mediterranean, both domestic and foreign, with wars fought between allied Greece and Persia (Greco-Persian Wars), and internally between the two dominant city-states, Athens and Sparta (Peloponnesian Wars) (Samuel, 1988; Morel, 2007; Lomas, 2016). After the Macedonian conquest and subsequent defeat of the Persian Empire (approximately 330 BCE) and the death of Alexander the Great (323 BCE), a renewed imperial stance for the Greeks in the greater Mediterranean region resumed (Samuel, 1988). Hellenism remained the dominant cultural tradition in the eastern Mediterranean until Roman legions invaded North Africa and the Levant during the latter half of the 1st century BCE (Revell, 2009).

In Italy, trade between the Etruscans and the Greek colonies on the southern Italian coast brought Etruria and the rest of southern Italy in closer contact with the greater Hellenic world (c. 507 – 323 BCE). Similarities in architectural and sculptural display show this influence was dominated by artistic and cultural centers in the regions of Apulia and eastern Lucania (Fischer-Hansen, 1993). These forms of artistic assimilation are evident in 5th century BCE Etruscan sculpture, and iconographic art in the form of plant, scroll ornamentation, and Apulian tomb reliefs that also show close ties to Etruscan motifs right up until the end of the 3rd century BCE (Fischer-Hansen, 1993). These artistic links meant that itinerant artisans of foreign origin, or at the very least foreign in their training, were adopted to incorporate stylistic elements in tomb architecture, paintings, and reliefs in the greater Apulian region.

Towards the end of the Iron Age, the region around Gravina in Puglia is characterized by a number of large, fortified Iron Age settlements on hilltops, like Botromagno, San Felice, and Monte Irsi, with smaller communities concentrated around these larger centers. Dramatic changes in the geopolitical landscape throughout the late 4th and early 3rd centuries BCE in South Italy were the result of several clashes between the expanding Roman Republic and Samnium (Salmon, 1955). After the eventual defeat of the Samnites (during the Second Samnite War, 328 BCE) at the end of the late 4th century BCE, Italic Apulians, Lucanians, and Bruttians sent envoys to Rome with the hope that these relations would end Samnite expansionism (Di Lieto, 2011). Despite this plea to the Roman Republic, it was clear that after the fall of Tarantum (272 BCE), conflict with the Romans over the control of *Magna Graecia* (the general name given to the Greek colonies in the South by the Romans) was imminent (Jeskins, 1998). The subsequent pact agreements (*foedera*) between Rome and the Greek *poleis* (few native Italian communities were involved) gave formal autonomy to the colonies, albeit at the clemency of Roman military

garrisons stationed throughout *Magna Graecia* (Gwynn, 2012). In exchange for the protection of lands and economic dealings, these local governments formed small aristocracies entrusted to the Roman senate (La Torre, 2011b). The consequence of Roman subjugation had more profound implications for the Lucanians and *Iapygian* populations, indicated by the gradual abandonment of their settlements by the early 3rd century BCE. This apparent decline was signified by the retraction of settlements across Italy, and was also noted to have taken place at Botromagno. This period coincides with the defeat of the *Iapygian* tribes by Rome and the reported enslavement of the population at Botromagno (Small, 2002). Alternatively, it is possible that the rise of Latin colonies, such as Paestum and Venusia, attracted many of these inhabitants to relocate closer to economically prosperous cities (Pedley, 1990; La Torre, 2011b).

1.4.3 Rise of the Roman Republic

Rome was a kingdom before it became a republic, established when, as legend has it, Romulus defeated Remus and became the founding monarch of the city in 753 BCE (Dudley, 1970; Christ, 1984; Cornell, 1995). Though only a small 16 km territory at its inception, Rome quickly grew as one of the most important ports on the Tyrrhenian coast, accessible by the River Tiber (Rostovtzeff, 1971; Crawford, 2001). In 509 BCE the Romans deposed the last reigning monarch, King Tarquin the Proud, and established a republic (Gwynn, 2012).

Rome's policy regarding migration was unique for its time. The Romans welcomed foreign migrants into their territorial confines and extended full citizenship (and the privileges that went with it) to those residing within its boundaries (Rostovtzeff, 1971). After the fall of the King Tarquin the Proud the Roman army protracted its garrisons by spanning their defensive efforts across a greater expanse of territory (Cornell, 1995). These army units were diffuse, so

much so that the tribal affiliates of greater Latium mounted an attack against the Romans at the Battle of Regillus, with the hope of ending further Roman expansion (499 BCE) (Cornell, 1995). The Romans narrowly escaped defeat. In turn, Rome immediately seized all Latin territory and established permanent settlements comprised of sections of their own population (Haywood, 2008).

In 340 BCE Latium and other non-Latin tribal affiliates rebelled against the Roman colonies (Salmon, 1955; La Torre, 2011b). While some Latin cities were incorporated into the Roman state, others remained autonomous but lost territory and were forced to provide military support to Rome during periods of war (Attema and van Leusen, 2004; La Torre, 2011b). Non-Latin tribes involved in the rebellion relinquished their territory to Rome in exchange for partial citizenship, which meant total allegiance to the military (by providing troops), taxation, but without the right to vote (Hopkins, 1980). *Silvium* (likely Botromagno) was sacked in 306 BCE, and according to the Greek historian Diodorus, the conquered population was removed and enslaved (Small, 2002).

Like the Greek and native Italian relationships of the 8th and 7th centuries, Graeco-Roman relations were often mutual in nature. Roman scholars and artisans readily adopted Greek architecture, art, literature, and philosophy into their cultural *annales* (Paoli, 1973; Biers, 1992). However, relations between *Magna Graecia* and Rome were unstable. Marcus Porcius Cato the Elder, being extremely familiar with Greek culture saw the Greeks as inferior and toxic to Roman culture (Rawson, 2001). Several conflicts arose amidst a series of complicated alliances between the Greek colonies, and with the defeat of Tarantum in particular, that eventually led to the Pyrrhic Wars (c. 280-275 BCE) (Winks and Mattern-Parkes, 2004).

1.4.4 Rome's Quarrel with Carthage

Originating from the city of Tyre (present-day Lebanon), the trade-faring Phoenicians founded ancient Carthage around 800 BCE (Negbi, 1992; Cornell, 1995). Their relocation to the north coast of modern Tunisia, at Tunis, was strategic in situating their efforts to dominate the western Mediterranean, and suited their maritime traditions of sea trading (Cary, 1981; Hodos, 2006). From this region the Carthaginians built an empire that extended from North Africa to Sardinia, Sicily, and Spain (Mattingly and Hitchner, 1995; Campagna, 2011). The political structure of Carthage was different than Rome, and its policies were dictated by an oligarchy of rich families instead of an elected senate. Carthage's army was comprised of 200 quinquiremes (military vessels armed with a bronze encased ram at the bow), with each quinquireme manned by 300 rowers and 120 on-deck soldiers for amphibious land-based assaults. The advanced Carthaginian military meant that Carthage had dominion over the western Mediterranean during the years leading up to war with Rome. These clashes culminated in the first (264 – 241 BCE) of three Punic Wars between Rome and Carthage, a period when Rome was nothing more than a regional power.

During the Pyrrhic War, Rome signed a treaty with Carthage allowing cooperative military action against Pyrrhus' army (Karlsson, 1993). However, after his defeat Rome's expansion into southern Italy and eventually to Sicily and Sardinia led to preliminary skirmishes during the opening months of the first Punic War (Van Dommelen, 1998). Despite being a conflict of attrition, the Romans made significant engineering advancements that helped them secure victory in conflict. Carthage, outpaced in manufacturing and naval power, signaled for peace after a naval defeat off the coast of Sicily in 241 BCE (Christ, 1984).

The loss of Sardinia and Sicily to Rome after the first Punic War forged further

Carthaginian expansion into Spain as an economic source to pay tribute and reparations for its hostilities (La Torre 2011). A preemptive attack on a Roman allied city in Spain by Hannibal in 219 BCE initiated the second Punic War (c. 218 – 201 BCE) (Haywood, 2008). The triumphant march of Hannibal's army across the Alps and subsequent victory at Cannae (216 BCE) inspired political change among the southern Italian communities, with most of the Roman allied South, both Greek and Italic, turning against the Republic (Lomas, 1993, 2000). Historical evidence suggests that this alliance was predominantly economic in nature, due to the financial surplus withheld from the lower classes by pro-Roman aristocracies (La Torre, 2011b).

Rome's vantage increased from a diplomatic stance to one of military and strategic dominance in South Italy. These political reformulations were based on two implemented actions. First, communities that betrayed Rome during the second Punic War had their lands confiscated, and the second was the granting of financial aristocratic freedoms to the communities who remained loyal to the republic (Rostovtzeff, 1971). Rome significantly increased its colonization efforts in the southern Italian territories, founding the settlements of *Croton* and *Sipontum* (Colivicchi, 2011). The remaining southern Italian communities were either captured or abandoned depending on whether or not they remained faithful to Rome.

More confrontations between the native Italians and Rome arose again during the Social Wars (91 – 88 BCE) (Bradley, 2000; Morley, 2001). By the end of these wars however, the Italic communities strained from the unrelenting economic pressure of the nascent empire, eventually capitulated (Wilson, 1966). Rome extended full citizenship to all Italic individuals, beginning a social reform that turned colonies into municipalities (*municipia*). In the foreground of victory over Carthage during the third Punic War (149 – 146 BC), and the subsequent establishment of North Africa as a Roman province, Rome's future imperial fate was founded (Dyson, 1985;

Winks and Mattern-Parkes, 2004). Most historians suggest that the Roman Empire was born when Julius Caesar was appointed with full authoritarian reign in 44 BCE (Dudley, 1970). However, other scholars maintain the birth of the empire following the Battle of Actium (31 BCE), when Octavian (who succeeded Julius Caesar) engaged and won a naval battle against an alliance formed between Mark Antony and Cleopatra (the last Pharaoh of Ptolemaïc Egypt) (Salmon, 1968; Morley, 2001). Another common agreement among historians is that despite these events the Roman Empire began with the highest of leadership titles, Augustus, granted to Octavian by the Roman senate in 27 BCE (North, 1991).

1.4.5 Roman Imperial Expansion and Decline

In order to maintain control over its territories, Rome relied heavily on a well-trained army. The Roman army was responsible for internal security and defense along its broad frontiers (Dyson, 1985). It also served an important socioeconomic role in the social mobility of its recruits and officers, a political tool to Romanize conquered populations, and as a financial catalyst in the areas where Roman legions were stationed (Wells, 1984). In order to carry on this military tradition, Augustus (Octavian) initiated further expansionist measures to acquire more territory (North, 1981; Breeze, 2011). The Roman Empire experienced little conflict during the 1st century CE, a period of *pax Romana* (Roman peace) for its citizens, although civil war erupted in 69 CE with rebellious uprisings in Celtic Gaul. Apart from this prolonged period of 'peace', the frontier regions continued to expand. Under the Roman emperor Claudius (41 – 54 CE), provinces were established in the east at *Judea* and Thrace, *Britannia* in the West, and in the North African territory of *Mauritania* (Whittaker, 1994). Indeed, a series of victorious campaigns supplemented Rome with the entire North African coastline, reaching as far west as

Tingis and *Volubilis*, beyond the Atlas Mountain range (Dudley, 1970).

Rome's expanding economy demanded a consistent work force to produce raw materials for building and agricultural production for food. Rural southern Italy provided the agrarian landscape and quarries for prolonged economic materials production. Notably, a number of rural villages (*vici*) were involved in producing food and materials for local Roman aristocrats. Archaeological evidence for the rural population at Vagnari suggests that its community was involved in agricultural and industrial production, likely comprised of low status workers, slaves and freedmen (Small and Small, 2007). Further information concerning Roman Vagnari is found in Chapters 3 and 4 (Supplementary 4A).

The Roman Empire reached its greatest extent in size during Trajan's reign (91 – 117 CE) (Williams, 1997). Internally, the Roman Imperial *pax Romana* remained consistent throughout the Nerva-Antonine dynasties (96 – 192 CE), a period of seven successive emperors that would define the 'golden age' of Roman Imperial ruling (i.e., Nerva, Trajan, Hadrian, Antonius Pius, Marcus Aurelius, Lucius Veras, and Commodus) (Breeze, 2011). However, signs of decline were already beginning to show by the mid-2nd century CE. Disease, demographic change, internal rebellions, and increased conflict along the frontier regions strained Rome's capacity to recover (Galinsky, 1992). As a result, more non-Roman citizens were inducted into the military, composed of conscripted individuals who had been former enemies of the Empire. This introduced a degree of rivalry between armies stationed in different provinces (Bradford, 1971). Furthermore, the expansive Roman border required a permanent military presence far too large to be maintained by non-Roman soldiers (Gibbon, 1869).

The middle of the 3rd century CE proved especially dangerous in the northern frontiers as the Teutonic peoples, the Goths, initiated a mass-scale migration from Scandinavia towards the

warmer seas of the South (Hedeager, 2000; Sampson, 2008). Military confrontations between the Romans and Goths extended the entirety of the northern European frontier, and were further exacerbated by battles as far South as the Danube (Hedeager, 1992). By 251 CE, the Romans retreated from *Dacia* (parts of modern Romania) leaving the Goths to control a greater portion of the Balkans. A year after the fall of Dacia the Goths raided posts surrounding the Black Sea, seizing Asia Minor, and in 263 CE sacked Athens, Sparta, and Corinth (Bradford, 1971). In addition to conflict in the East, the western half of the empire was thrown into political turmoil when in 285 CE Britania's Roman naval commander Carausius independently affirmed himself as Emperor (Sampson, 2008). In light of Carausius' decision, the Roman Emperor Diocletian partitioned the Roman state into eastern and western sections. This culminated in the establishment of the new Roman capital, Constantinople (modern-day Istanbul), founded by the Emperor Constantine in 330 CE (Parker, 1935). It was not until 476 CE that the last of the Roman Emperors, Romulus Augustulus, was met with defeat by a barbarian king, and the Emperor in Constantinople was informed of the collapse of the West (Sampson, 2008).

The historical review outlined above serves as a backdrop to the stable isotope, mtDNA results, and interpretations provided by the papers that follow below. It also establishes the historical and archaeological context from which to draw long-term inferences over the *long-durée*. A detailed narrative integrating the interpretations from all three papers is contained in Chapter 5.

1.6 Sandwich Thesis Structure

The structure of this dissertation follows the criteria outlined for the PhD 'sandwich thesis', and contains all relevant bioarchaeological, stable isotope, and aDNA data included in

Chapters 2, 3, and 4. Specific information about the archaeological sites is contained in greater detail in Chapters 2, 3, and 4. Stable isotope and aDNA methodological background, procedures, results, and interpretations are found in both the methods sections of the papers, and in supplementary information contained at the end of each chapter. Temporal chronology for the samples is set to BP (Before Present) in Chapter 2 and 5, and BCE (Before Common Era) for Chapters 3 and 4.

The first paper, entitled: *Italian Iron Age (Iapygian) Mitochondrial Genomes Suggest Close Genetic Affinities to Neolithic and Bronze Age Populations From the East*, investigates the ancestral origins of the Iron Age *Iapygians* from Botromagno through the comparative analysis of 15 Iron Age mtDNA sequences with 231 complete mitochondrial genomes obtained from publically available databases.

The second paper, entitled: *Mapping the Origins of Imperial Roman Workers (1st – 4th century CE) at Vagnari, Southern Italy, using $^{87}Sr/^{86}Sr$ and $\delta^{18}O$ Variability (American Journal of Physical Anthropology)*, presents newly analyzed strontium data (n=56) and previously published oxygen (n=43) isotope results obtained from a subset of the Vagnari skeletal assemblage. It also provides the first preliminary strontium isotope variation map (complete with >199 strontium isotope data points) of the Italian peninsula, an important tool from which to provenance the strontium isotope values obtained from archaeological specimens.

The third paper, titled: *Ancient Roman Mitochondrial Genomes and Isotopes Reveal Genetic Relationships and Geographic Origins at the Local and pan-Mediterranean Scales*, explores population continuity in South Italy. It compares the genetic affinities of the Vagnari Romans (n=30) with other ancient communities from the Mediterranean, European, North African, and western Asian regions (n=357), and the local social and demographic relationships

through an integrated genetic and isotopic approach. In addition, the paper explores the possibility of identifying kin-based relationships in the Vagnari cemetery through haplogroup mapping across associated burial assemblages.

Chapter 5 expands the narrative by integrating the results of Chapters 2, 3, and 4 into the *longue durée*, and details future directions for isotope and ancient DNA analysis of Iron Age and Roman period skeletal assemblages.

Chapter 2.0

Italian Iron Age (*Iapygian*) Mitochondrial Genomes Suggest Close Genetic Affinities to Neolithic and Bronze Age Populations From the East

*****Matthew V. Emery[1,2], Ana T. Duggan[1,2], Tyler J. Murchie[1,2], Jennifer Klunk[1,4], Katherine Eaton[1,2], Emil Karpinski[1,4], Tracy L. Prowse[2], and *Hendrik N. Poinar[1,2,3,4,5]

[1] McMaster Ancient DNA Centre, McMaster University, Hamilton, Ontario, Canada.
[2] Department of Anthropology, McMaster University, Hamilton, Ontario, Canada
[3]Institute of Infectious Disease Research, McMaster University, Hamilton, Ontario, Canada
[4]Department of Biology, McMaster University, Hamilton, Ontario, Canada
[5]Department of Biochemistry and Biomedical Sciences, Hamilton, Ontario, Canada

Short Title: Iron Age Mitochondrial Diversity in Southern Italy

Corresponding Authors:

*****Matthew Emery
McMaster Ancient DNA Centre, McMaster University
1280 Main Street West, Hamilton, Ontario
L8S 4L8
Phone: 905-515-1842
Email: emerymv@mcmaster.ca

*Hendrik Poinar
McMaster Ancient DNA Centre, McMaster University
1280 Main Street West, Hamilton, Ontario
L8S 4L8
Phone: 905-525-9140 x26331
Email: poinarh@mcmaster.ca

Keywords: ancient DNA; mitochondrial DNA; Iron Age; Southern Italy; *Iapygians*

2.1 Abstract

The 19th century German historian Theodor Mommsen hypothesized that the Iron Age tribes of southern Italy's Salentine coast, the *Iapygians*, were the oldest group of migrants to the region. Little information on southern Italy's Iron Age populations exists, and what we do know about the *Iapygians* derives from disparate archaeological reports. We present the whole-mitochondrial genomes of 15 *Iapygians* buried at the Iron Age settlement of Botromagno (~2.4 ka), located immediately West of the modern town of Gravina (Puglia, Italy). In addition, we compare southern Italian Iron Age haplogroup composition to 231 previously published complete ancient mtDNA genomes spanning the Upper Paleolithic (~45 ka) through the Iron Age (~2.2 ka).

Population pairwise Φ_{ST} values, and maximum clade credibility (MCC) tree reconstruction composed of 246 whole-mitochondrial genomes suggest that South Italy's Iron Age inhabitants share a close genetic relationship with Near East, eastern European Neolithic, Bronze and Iron Age populations. However, our analyses also point to the possibility that *Iapygian* mtDNA variation represents pre-Neolithic gene flow from the western Mediterranean, eastern Europe, and the Caucasus.

2.2 Introduction

Modern European mitochondrial DNA (mtDNA) diversity was shaped by a number of major demographic transitions following the initial colonization of Eurasia during the Upper Paleolithic (~55 ka) (Soares et al., 2010). These changes were driven by large-scale climatic fluctuations at the end of the Pleistocene, with the advance of continent-wide ice sheets during the Last Glacial Maximum (LGM) 22 to 19 ka, and the Younger Dryas cold snap (~11.5 ka) (Posth et al., 2016). MtDNA data obtained from ancient Europeans spanning these time periods suggest that human populations retracted to warmer climate refugia across Eurasia, concentrated in the Franco-Cantabrian region of Iberia, Italy, the Balkans, eastern Europe, and the Near East. These refuge populations then re-expanded into parts of northern Europe after the Late Glacial period (~14 ka) (Pereira et al., 2005; Pala et al., 2012; De Fanti et al., 2015). Subsequent contribution to the European mtDNA gene pool was influenced by waves of Neolithic farmers originating from the Levant and Anatolia (~12 ka), and during the late Neolithic/early Bronze Age from the eastern European plains (~5 ka) (Lazaridis et al., 2014; Haak et al., 2015; Omrak et al., 2016). However, speculation concerning the origins of Italic Iron Age tribes have been the focus of archaeological and historic inquiry, which questioned whether the ancestors of southern Italy's Iron Age inhabitants were present prior to the Neolithic, or represent post-Neolithic genetic influx into the region from western and/or eastern Europe (Peruzzi 2016).

Here, we provide complete mtDNA genomes as evidence for the ancestral origins of 15 Iron Age individuals from the hilltop site of Botromagno, South Italy (Fig. 1). We use published comparative ancient mtDNA genomes (n=231) from Europe to identify the ancestors of the Iron Age *Iapygians*, an Italic tribe that witnessed intensive Greek colonization of their homeland before Roman colonial expansion into South Italy around 2.2 ka (Small, 2002).

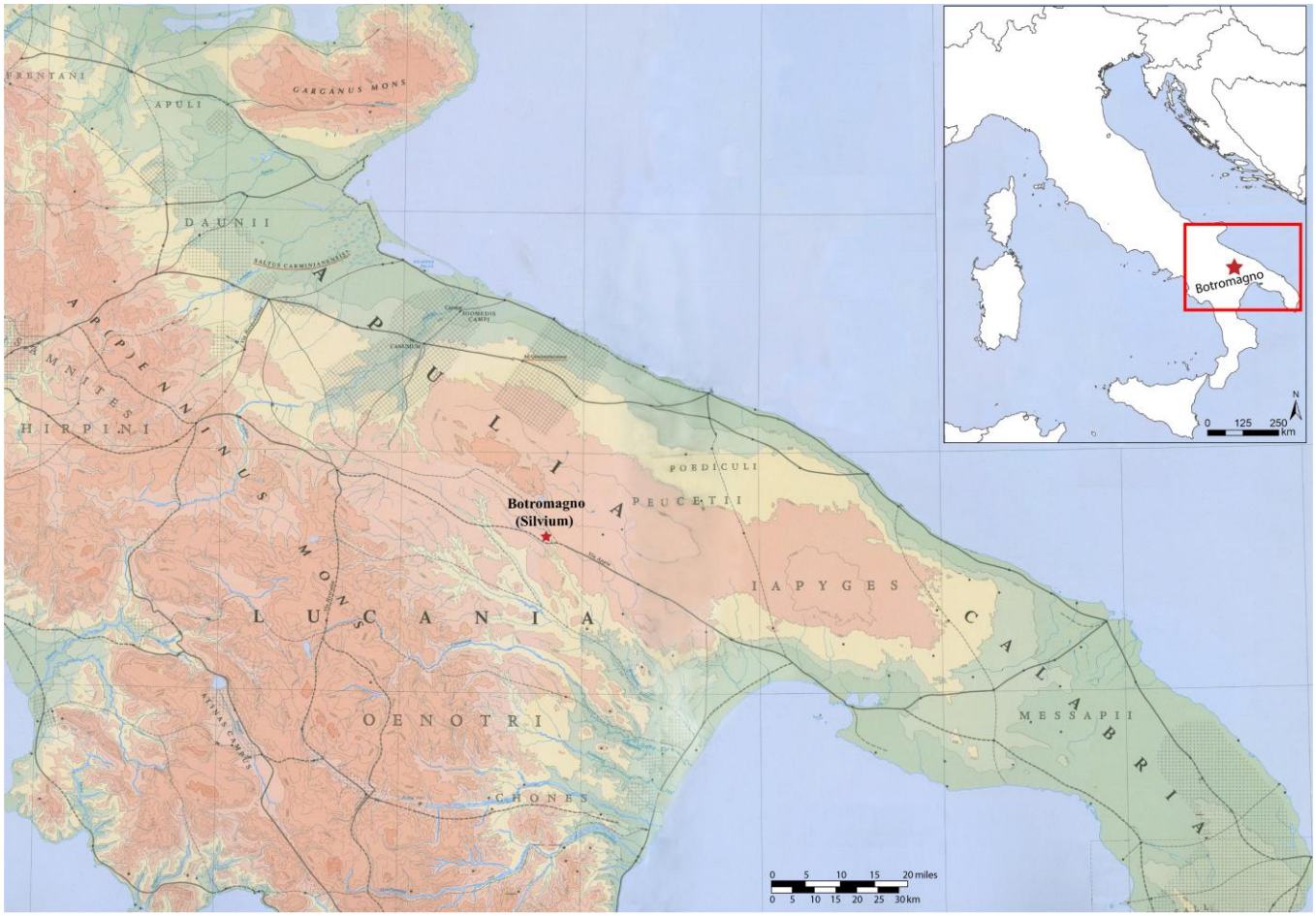

Figure 1: Map showing the location of Iron Age Botromagno, southern Italy.

2.3 Archaeogenetic Context

Genome-wide SNP data indicate that modern Europeans, in varying proportions, derive their ancestry from three basal populations: northern Paleolithic Eurasians, western European hunter-gatherers, and early Near Eastern Neolithic farmers (Lazaridis et al., 2014). In addition, ancient mtDNA evidence suggests that substantial population restructuring occurred at the Mesolithic-Neolithic transition, as suggested by the decrease in mtDNA haplogroups U2, U3, U5, and U8, and an increase in mtDNA haplogroups carried by early Neolithic farmers from the East (i.e., H, HV, J, K, I, V, X, W, and N) (Bramanti et al., 2009; Brandt et al., 2015). However,

ancient mtDNA diversity of Bronze Age and Iron Age populations, and their relatedness across space and time are only now being explored. Recent whole-genome data obtained from Mycenaean and Minoan skeletons from Greece and Anatolia revealed cross-Aegean and Neolithic Anatolian genetic relationships (Lazaridis et al., 2017). We hypothesize that Bronze Age Greeks and Iron Age Italians potentially share similar ancestral origins, based on the geographic and contemporaneous nature of the samples. Further, historic and archaeological sources suggest that the Iron Age *Iapygian* communities of southern Italy originate from an unknown pre-Iron Age population from Illyria, situated in the present-day Balkan region (Peruzzi 2016).

2.4 Materials and Methods

Teeth samples (n=38) were prepared in clean facilities dedicated to the extraction, amplification, and enrichment of ancient remains at the McMaster Ancient DNA Centre. In addition, we collected 231 ancient mtDNA genomes from GenBank for population pairwise (Φ_{ST}) analysis, Bayesian inference and maximum clade credibility (MCC) mtDNA tree reconstruction. All laboratory experimentation, read processing and analysis, and comparative sample database details are contained in Supplement 1.

2.5 Results and Discussion

We called consensus sequences and calculated contamination estimates for 38 samples, but selected samples with <90% coverage breadth across the mitochondrial genome, resulting in the retention of 15 out of the 38 original samples (Supplement Table S1 and S2). Fifteen mitochondrial genomes were sequenced to a depth of coverage ranging between 5x and 754x

(mean = 152.1x). Southern Italian Iron Age mtDNA variation was assessed with Haplogrep2 using Phylotree Build 17 (van Oven, 2015; Weissensteiner et al., 2016). The composition of the Iron Age population can be broadly summarized as containing haplogroups U (40%), H (40%), V (10%), and J (10%) (Supplement Tables S1 and S2).

Population pairwise Φ_{ST} suggest low population differentiation across geographic and temporal categories (Supplementary Tables S3-S4). Low genetic differentiation (i.e, Φ_{ST} <0.05; Hartl and Clark, 1997) was found between the Iron Age southern Italians and ancient samples from the Czech Republic (0.05), Germany (0.02), Russia (0.01), Spain (0.04), and Armenia (0.01), and temporally with European Neolithic (0.01), Bronze Age Aegean (0.03) and Armenian Iron Age populations (0.006), obtained from the geographic regions outlined in Fig. 2a (Fig. 2b; Supplementary Tables S3-S5). To better examine the relationships between post-Neolithic age categories, we removed the pre-LGM and Holocene (Fig. 2c), and pre-LGM and Mesolithic (Fig. 2d) age cohorts from MDS Figure 2d. MDS genetic distance indicates that the Iron Age Italians share similar mtDNA haplogroup compositions with Iron Age Armenians (i.e., Iron Age 2), Neolithic, and Bronze Age samples obtained from Anatolia and the Aegean (Fig. 2d). A 3-dimensional scaling model of the mtDNA data by country and age is provided in Supplement 1 (Fig. S4a/b).

MCC tree reconstruction shows that the Iron Age southern Italians harbour haplogroups with post-LGM coalescence dates (Fig. 3). These mtDNA sublineages likely arose in Ice Age eastern Europe (U2e3, U4a1, U4b1a1a1, U5a1, and J2b1c), the Near East and western Asia (H2 and H6a1a), and western Europe (U5b2c, H1, and H5'36), suggesting that subsequent post Late Glacial migrations out of these regions partially shaped the mtDNA gene pool in southern Italy (Pereira et al., 2005; Roostalu et al., 2007; Malyarchuk et al., 2010; Pala et al., 2012; Jones et al.,

2015). However, haplogroup U5b2c (and U5b3) possibly represents maternal continuity in Italy since the Late Glacial period, although it is currently unknown whether U5b2c originated in Iberia or Italy, since U5b2c was also detected in hunter-gatherer remains from Mesolithic Spain (Pala et al., 2009; Sánchez-Quinto et al., 2012). Further analysis of a larger South Italian Iron Age data set is required to determine whether Iron Age Italians have mtDNA signatures suggesting *in situ* genetic continuity since pre-Neolithic times.

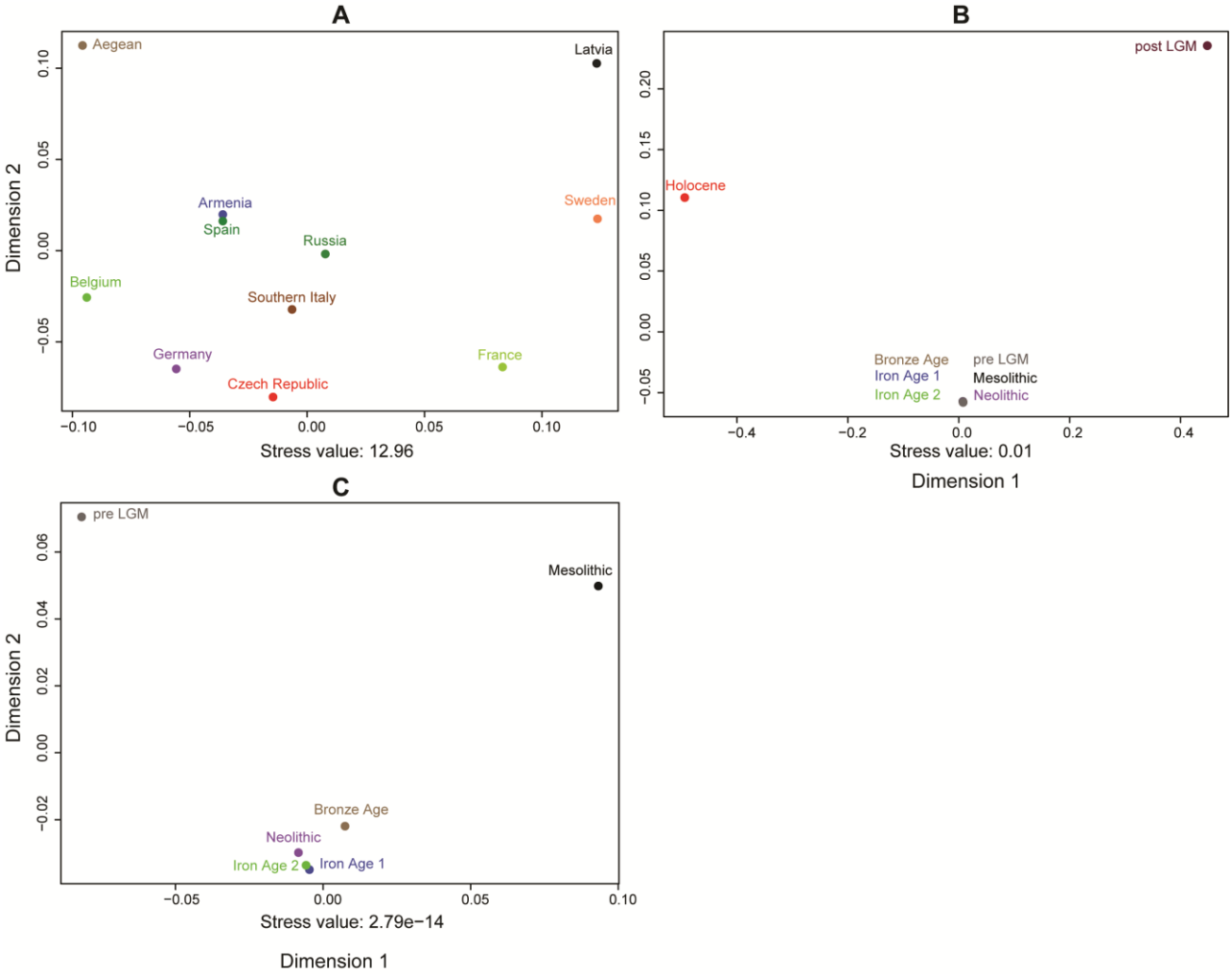

Figure 2a/b/c: Multi-dimensional Scaling plot composed of 224 mitochondrial genomes. Iron Age southern Italians are labeled as 'Southern Italy' in Fig. 2a for country/geographic region. For Fig. 2b/c, the Iron Age sample is labeled as 'Iron Age 1' by time period. Population and temporal categories with <5 representative samples were omitted from analysis. Scaling is

proportional to population pairwise Φ_{ST} distance by country and chronological age pairwise Φ_{ST} values <0.05 (low genetic differentiation), which are indicated in red in Supplementary Tables S3 and S4. a) MDS of mtDNAs by country/geographic region (n=11); b) MDS of mtDNAs by age categories spanning the Upper Paleolithic through the Iron Age (n=8) c) MDS of mtDNA age categories with 'post-LGM' and 'Holocene' chronological age categories removed.

Taken together, population pairwise Φ_{ST}, and the distribution of mtDNA haplotypes in relation to the comparative mtDNA data set show that the Iron Age southern Italians likely descended from early to late Neolithic farmers from Anatolia and possibly as far East as the Caucasus, and from migrants arriving from eastern Europe around the late Neolithic/early Bronze Age. These findings support previous hypotheses that the ancestors of the *Iapygians* may have originated in the eastern Balkan region, or derive shared ancestry with a common source population from eastern Europe. Alternatively, southern Italian Iron Age mtDNA variation might also reflect LGM gene flow between southwestern European, Mediterranean, and Carpathian basin refugia, which was suggested for haplogroup subclusters of U5 and J (Malyarchuk et al., 2010; Pala et al., 2012). Future mtDNA (and nuclear DNA) analysis comprised of a larger Iron Age data set from southern Italy is necessary to answer Theodor Mommsen's initial hypothesis that the *Iapygians* were the oldest immigrants to the southern Italian region.

Our investigation provides the first mtDNA evidence for the maternal ancestral affiliations of a subset of the *Iapygian* individuals recovered from southern Italy, and suggests a closer genetic link to European Neolithic and Iron Age Armenians, than to Bronze Age Aegeans. Future comparative ancient DNA data using whole-genome SNP, mtDNA, and NRY-chromosome analysis of pre-Roman populations will provide complementary evidence for the ancestral roots of understudied Iron Age individuals from Italy.

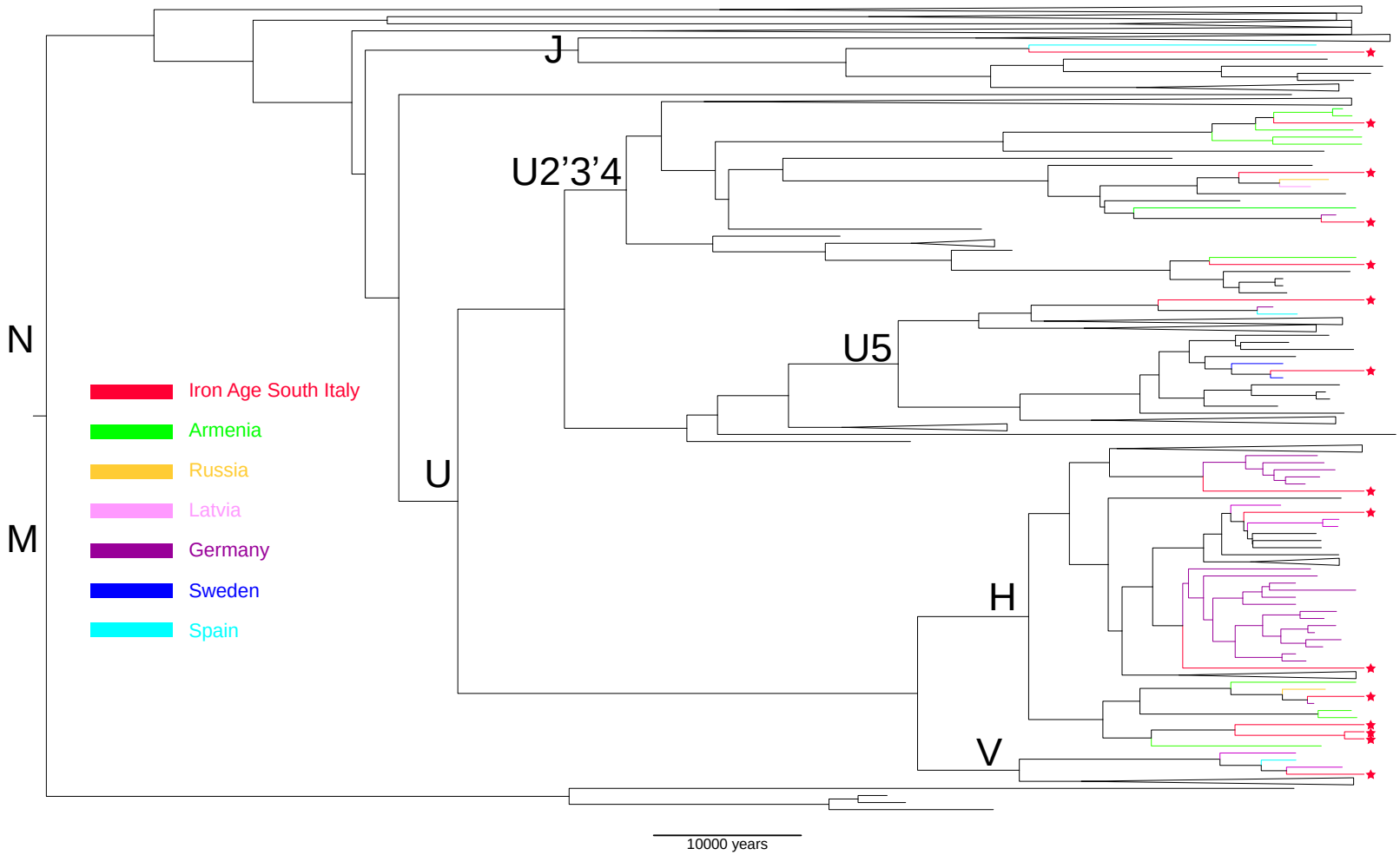
N
M
J
U2’3’4
U5
U
H
V
Iron Age South Italy
Armenia
Russia
Latvia
Germany
Sweden
Spain
10000 years

Figure 3: Maximum clade credibility tree reconstruction of 238 ancient mtDNA sequences. Red stars denote Iron Age samples from Botromagno. Subclades without Iron Age Italian representation were collapsed for clarification. Iron Age samples share subclades with mtDNA lineages found in Neolithic Near Eastern and eastern European assemblages.

Acknowledgements

Excavations at the Vagnari necropolis were granted by the Ministero per i Beni e le Attività Culturali to Tracy Prowse and Maureen Carroll, through the British School at Rome, with the help of Stefania Peterlini. Franco Taccogna (Gravina) provided critical technical support at the site. The Vagnari excavation team is grateful to a number of organisations and individuals for their support of the project, and in particular the landowner of Vagnari, Dott. Mario De Gemmis Pellicciari; the British School at Rome; the Soprintendenza per i Beni Archeologici della Puglia, especially Dott. Luigi LaRocca, Dttsa. Francesca Radina and Dottsa. Maria Rosaria Depalo from the Centro Operativo per l'Archeologia in Bari; and the Centro Operativo Fondazione Ettore Pomarici Santomasi, Gravina. We also thank and acknowledge the fieldwork conducted by students and volunteers from the Canada, the United Kingdom, and the United States.We thank members of the McMaster Ancient DNA Centre, Debi Poinar, Melanie Kuch, and Jessica Hider for their constructive feedback regarding this manuscript. We also thank colleagues who contributed mitochondrial consensus sequences upon request.

2A: Supplementary Information 1

Southern Italian Iron Age *Iapygian* Mitochondrial Genomes Suggest Close Genetic Affinities to Neolithic and Bronze Age Populations From the East

*****Matthew V. Emery, Ana T. Duggan, Tyler J. Murchie, Jennifer Klunk, Katherine Eaton, Emil Karpinski, Tracy L. Prowse, and *Hendrik N. Poinar

2.6.1 The Iron Age Settlement at Botromagno

The earliest archaeological evidence for human occupation at Botromagno dates to the Middle Neolithic (Small, 1992). A number of ceramic artifacts were recovered from this early encampment site, discovered North of the Iron Age settlement at Botromagno. These items included painted and impressed wares typical of the Neolithic archaeological traditions of South Italy. The lack of archaeological evidence at the end of the Neolithic suggests that the small settlement was eventually abandoned, and remained uninhabited until ~3950 ka, until the reoccupation of the site at the beginning of the Early Iron Age (Small, 1992).

The Iron Age site at Botromagno was established around 2950 ka, and was one among a number of Iron Age settlements constructed in South Italy at this time. A number of similar settlements were built within 22 km of Botromagno substantiated by excavations at Monte Irsi, Matera, and Altamura. Settlement construction at Botromagno, a *Peucetian* (an *Iapygian* sub-tribe) community, was composed of small, densely concentrated hollowed-in huts. The walls were likely constructed out of wattle (i.e., weaving thin branches into a woven lattice), and fortified using clay or mud (daub), and the floors underlain by stone rubble and gravel, and then overlaid with clay. Recovered pots and ceramic fragments were impressed and designed with simple geometric patterns. These geometric decorative motifs evolved into more elaborate forms through contact with Greek artisans who migrated and established permanent colonies along the Ionian coastline by ~2750 ka (Fletcher, 2007). Despite the evidence for sedentary occupation at

Botromagno, no burials dating to these earlier phases of occupation were recovered (Peruzzi, 2016).

Substantial cultural transitions developed by 2650 ka. These developments included the construction of small cemeteries within the limits of the village. Burials took the form of stone cut tombs and simple pit grave, a trend that remained unchanged throughout the greater Apulia region until 2350 ka, when increasingly elaborate chamber tombs were constructed (Small, 1992). Archaeological site reports described the construction of stone cut sarcophagi as a reflection of burial practices borrowed from the Ionian Greeks, since Ionian style 'cups' were also found interred with the deceased (Small, 1992). These burial patterns are consistent with the interpretation that Italic tribes, such as the Illyria-speaking *Peucetians*, shared economic and trade links with the Greek settlements along the coast. *Iapgygian* interest in assimilating Greek ceramic style and motif into their artistic repertoire was ubiquitous, however, Iron Age ceramic production continued to diversify on a distinct trajectory (Handberg and Jacobsen, 2011). Native ceramic production manifested in a traditional bichrome style, painted black and red against a pale background. The similarity in ceramic production, styles, and motifs, with other archaeological traditions of the Bradano basin suggest that Botromagno was socially and economically linked with Iron Age settlements to the West and East. These socio-political and economic links also extended into military connections, which culminated in a joint military campaign against the Greek Tarentines of Taras by 2450 ka (Dunbabin, 1979).

A second material transition occurred ~2450 ka, evidenced by an increase in Greek imports and the adoption of the potter's wheel. Between 2450 ka and 2350 ka, native production of hand-made geometric design decreased and was replaced by 'mixed styles' that assimilated Italic ceramic decoration with Greek impressions (i.e., simple bands and vegetable motifs).

Botromagno also transformed architecturally, and several terra cotta statues of Greek origin, including a water-spout in the form of lion's head, were recovered from the site (Small, 1992). Relations between the Italic tribes and the Greek colony at Taras were however often tumultuous. Historic evidence suggests that the Tarentines secured a defeat over the *Peucetians*, were slowed by the Messapians, but the Messapians were eventually defeated by the Tarentines shortly thereafter (La Torre, 2011). Botromagno experienced a period of decline around 2400 ka, a trend that lasted no more than two generations. One archaeological report draws comparison with Taras' war against the Iron Age village of Cavallino, where its military loss led to the enslavement of the population (Small, 1992). It is likely that the community at Botromagno suffered the same fate. Evidence for population decline at Botromagno was, however, short lived. Greek imports again increased, together with Italiote red-figure vases found in association with burials by 2350 ka (Guido, 1973).

The late Iron Age corresponds to an increase in settlement density across the plateau of the hill, indicating a period of prosperity at Botromagno. Although a number of structures and buildings were destroyed around 2150 ka, the foundations and wall footings remained relatively intact. Burial custom remained consistent with Apulian Iron Age traditions, with the dead inhumed in a flexed position, but found in association with an increasing number of lavish gravegoods and interred in elaborate *semicamera* tombs (Small, 1992). Another notable architectural achievement was the immense stonewall constructed around the settlement sometime around 2300 ka. Excavations indicate that the wall formed the entire perimeter of the site, for a total length of 3.75 km (Small, 1992). The amount of labour required to complete the fortification was likely immense, since the appropriation of stone material demanded a total of 37,500 blocks to complete the defensive barrier (Small, 1992). Walls of similar construction

were built around Iron Age communities throughout Apulia and Lucania at this time, suggesting a coordinated effort by the native Italic communities to thwart military conflict with the Greeks, Romans, and other Iron Age tribes situated to the North, such as the Samnites (La Torre, 2011). According to the historian Diodorus, a Roman consular army captured Botromagno (identified as Roman *Silvium*), which remained under Roman Republican control from 2250 ka onward (Small, 2002).

2.6.2 The Iron Age Skeletal Collection

Joan Du Plat Taylor and colleagues conducted archaeological excavations at Botromagno beginning in 1967 (Brooks et al., 1968; Ward-Perkins et al., 1969; Taylor et al., 1976). A total of 53 burials were excavated between 1967 and 1971 from three separate cemeteries located from within, and on the periphery of the hillside at Botromagno. These burials are attributed to successive chronological periods over the history of the settlement itself. Twenty-seven burials were dated between the 7th and 6th centuries BCE, 7 burials were from the 5th century BCE, and another 9 from the 4th century BCE. Chronology for the cemeteries was established through ceramic seriation. The remains were shipped from the Archaeological Superintendency in Gravina in Puglia to Dr. Tracy Prowse at McMaster University for stable isotope and aDNA analysis. The skeletal assemblage arrived in a highly fragmented and comingled condition prior to sampling. Further osteobiographical, isotopic, and palaeopathological analysis of the Botromagno skeletal assemblage is ongoing.

2.6.3 Sample Chronology

We retained the original ages and/or temporal chronologies of published ancient mtDNA sequences used for comparison in this study (Table S5). Since the geological epochs, such as the Pleistocene and Holocene, and archaeological and material cultural distinctions (i.e., Paleolithic, Mesolithic, Neolithic, Bronze and Iron Age) overlap with subsequent developments and material transitions, especially within the Holocene (~11,000 ka), we maintain that 'Holocene' denotes samples whose ages range between 10,652 and 8054 BP. This time range is approximately equivalent with Western Europe's Mesolithic period.

2.6.4 Laboratory Methodology and Experiments

2.6.5 Sub-sampling and Decontamination

All aDNA laboratory work was conducted in dedicated clean rooms at the McMaster Ancient DNA Centre. All laboratory bench space and tools were cleaned using a 6% solution of sodium hypochlorite (NaClO), and washed with UV-irradiated ultrapure water, including sampling implements (diamond cutting wheel, Dremel collar, and pulverizing tube mortar), and was repeated for every new sample. One root from each molar was cut using a diamond cutting wheel and the resulting material pulverized and transferred into 2 ml MAXYMum Recovery PCR Tubes (Axygen), then stored at -20°C for demineralization and digestion.

2.6.6 Demineralization and Enzymatic Digestion

Samples were demineralized in 500 µL of 0.5 M EDTA solution (pH 8.0) and shaken at 1,000 rpm in a Thermomixer at room temperature (22°C) for 24 hours. The supernatant was collected and dispensed into 1.7 ml Axygen MAXYMum Recovery PCR Tubes.

Demineralization was followed by enzymatic digestion in a 500 uL buffer comprised of 5 mM calcium chloride ($CaCl_2$), 20 mM Tris-HCl (pH 8.0), 2.5 mM N-phenacylthiazolium bromide (PTB), 50 mM dithiothreitol (DTT), 0.5% sarcosyl, 1% polyvinylpyrrolidone (PVP) and 20 mg/mL Proteinase K in nuclease free ultrapure H_2O for 24 hours, and shaken in a Thermomixer set to 25°C. 500 uL of digestion supernatant was collected and dispensed into tubes containing 500 µL of demineralization supernatant. This process was repeated for a second round for a total of 2 mL of supernatant for each sample.

2.6.7 DNA Extraction

DNA extractions were carried out according to established protocol (together with extract blanks using ultrapure H_2O at a sample:blank ratio of 7:1) to increase the concentration of ultra-short (~40 bp) DNA fragments (Dabney et al., 2013). Two mL of supernatant was added to a binding buffer containing 5 M guanidine hydrochloride (GuHCl), 40% isopropanol, Tween-20, 90 mM sodium acetate (pH 5.2), then added to High Pure Viral Nucleic Acid Large Volume Kit. Buffer solution was spun through the columns for 4 minutes at 1,500x *g*, rotated 90°, then spun again for 2 minutes at 1,500x *g*. The columns were removed from their internal reservoirs and placed in 1.5 mL MAXYMum recovery tubes, and washed with 750 µL Qiagen PE Buffer (centrifuged for 1 minute at 3,300x *g*), then dry spun for 1 minute at 16,100x *g*. Elution of DNA molecules was achieved by adding 25 µL of buffer EB to the silica-based membrane, and centrifuged at maximum speed for (16,100x *g*) for 30 seconds. This process was repeated a second time to increase the final extraction volume to 50 µL and the DNA extracts stored at -20°C for double-stranded library preparation.

2.6.8 Library Preparation and Post-Library Indexing

Library preparation for Illumina NGS platforms followed established protocol (Meyer and Kircher, 2010; Kircher et al., 2012). Extracts, negative controls, including two library blanks (UV-irradiated ultrapure H_2O) were converted to Illumina double-stranded libraries. Extracts were blunt-end repaired and purified. 20 µL were purified over Qiagen MinElute columns at a 5:1 ratio of Buffer PB to template according to manufacturer protocol. Adapter ligation master mix was comprised of T4 DNA Ligase Buffer, PEG-4000, Adapter mix (10 µM), and T4 DNA Ligase, ultrapure H_2O and sample extracts were incubated for 16 hours at 15°C, then purified again over Qiagen MinElute columns. Adapter Fill-in reactions were incubated for 30 minutes at 37°C followed by a final heat denaturation at 80°C for 20 minutes, and eluted in 40 µL buffer EB over Qiagen MinElute columns.

Samples were indexed using unique P5 and P7 primer combinations together with purified library template (Kircher et al., 2012). Post-library indexing used 18.8 µL of library with KAPA SYBR® FAST qPCR Master Mix (2X) in a reaction volume of 40 µL, an indexing primer concentration of 150 nM, and ultrapure H_2O. Libraries were indexed under the following PCR cycling conditions: denaturation at 95°C for 5 minutes, followed by 11 cycles of 95°C for 30 seconds, 60°C 45 seconds, and a final extension of 60°C for 3 minutes. Indexed libraries were stored at -20°C for mtDNA enrichment.

2.6.9 Mitochondrial DNA Enrichment

Targeted capture by in-solution enrichment was carried out in accordance with the manufacturer's protocol (MYcroarray, Ann Arbor, MI), with small modifications to hybridization temperature (55°C), time (24 hours), and bait concentration (50 ng), to enhance

target complexity for all baited reactions. Indexed libraries, including extraction and library blanks were enriched using mitochondrial RNAs synthesized from the *H. sapiens* Representative Global Diversity Panel (197 mtDNA sequences) (MYTObaits, MYcroarray, Ann Arbor, MI). Enrichment hybridization/capture and library master mixes were composed of (MYbaits manual v.3.02): (hybridization mix) 20X SSPE (Hyb #1), 0.5 M EDTA (Hyb #2), 50X Denhardt's solution (Hyb #3), 10% SDS, mitochondrial RNA baits (50 ng per rxn), and 20 U/µL RNase block SUPERase-IN (total hyb/cap master mix 14.5 µL); (library mastermix) human Cot1 DNA (Block #1), salmon sperm DNA (Block #2), and Illumina Bloligos (Block #3). 2.53 µL was added to high-profile strips containing indexed library template (5 µL) and ultrapure H_2O (5.75 µL). Hybridization/capture master mix was dispensed into a second set of high-profile PCR strips. PCR strips containing the library master mix were placed in a Thermocycler and heated to 95°C for 5 minutes, then reduced and held at 55°C. While heated, 12.75 µL of hybridization/capture mix was added to the library mastermix and left to hybridize for 24 hours. 960µl of streptavidin magnetic beads were dispensed into six 1.7 mL MAXYMum recovery PCR tubes and washed three times with 480µL of binding buffer before being re-suspended in 1.2mL of binding buffer. Baits were captured using 200µL of the bead suspension for 45 minutes at room temperature with rotation. Streptavidin magnetic beads were washed in 0.2X Wash Buffer 2 solution prepared in mix of 0.1% SDS, Hyb #4, and ultrapure H_2O. Enriched libraries were re-amplified using 18.8 µL of template in a 40 µL reaction according to the following scheme: KAPA SYBR ® FAST qPCR Master Mix (2X), primer combination IS5_long_amp.P5 (5'-AATGATACGGCGACCACCGA- 3') and IS6_ long_amp.P7 (5'-CAAGCAGAAGACGGCATACGA-3') at a concentration of 150 nM, and ultrapure H_2O, under the amplification conditions: 95°C for 5 minutes, 96°C for 30 seconds, 60°C for 45 seconds, and

a final 60°C for 3 minutes for 12 cycles. Post-amplification reactions were purified over MinElute columns and eluted with 10.75 µL of buffer EB for a second round of enrichment.

Enriched libraries were diluted to 1:1,000 and quantified against the 425–525 bp PhiX Control (Illumina) standard, and diluted in decreasing concentrations from 100 pM to 0.0625 pM. Quantification of enriched libraries used the primer combination IS5_long_amp.P5 and IS6_ long_amp.P7 (see above for primer sequences and concentrations) under the amplification conditions used for enriched library re-amplification. The qPCR conditions were the following: 150 nM of each primer, 1X KAPA SYBR ® FAST qPCR Master Mix (2X), 1:1,000 library dilutions, PhiX serial dilutions (4 µL) alongside two ultrapure H_2O blanks. Amplification proceeded following the re-amplifications conditions listed above. Enriched libraries were pooled in equimolar concentrations and size selected for DNA fragments ranging 150 bp and 600 bp in length using a gel cut. Gel plugs were purified using the QIAquick Gel Extraction Kit (Qiagen), according to the manufacturer's standard operating procedures for sequencing.

2.7.1 Sequencing

Enriched libraries were sequenced on an Illumina HiSeq 1500 platform at the Farncombe Family Digestive Health Research Institute (McMaster University, Hamilton ON, Canada) using 2 x 90 bp read chemistry.

2.7.1 Read Processing and Osteobiographical Analysis

2.7.2 Mitochondrial Genome Construction and Assembly

Raw reads were demultiplexed using bcl2fastq (ver. 2.17.1.14) then trimmed and merged with leeHom using ancient DNA parameters (--ancientdna) (Renaud et al., 2014). Trimmed and

merged reads were mapped to the human mitochondrial reference genome (revised Cambridge Reference Sequence, rCRS, NC_012920) using a modified version of BWA (https://github.com/mpieva/network-aware-bwa) (Li and Durbin, 2009), with the maximum edit distance set to 0.01(-n0.01), gap opening of (-o 2), seeding disabled (-1 16500). Mapped reads were filtered to merged or unmerged but properly paired (https://github.com/grenaud/libbam), and duplicates removed (https://github.com/udo-stenzel/biohazard. We restricted collapsed mtDNA reads to a minimum length of 35 bp and minimum map quality of 30. Consensus sequences and contamination rates were generated using Schmutzi using the Eurasian contamination database (Renaud et al., 2015). We called mitochondrial consensus sequences with Schmutzi (with quality filtering set to Q5) and haplogroups using HaploGrep2 employing PhyloTree Build 17 (Table S1) (van Oven, 2015; Weissensteiner et al., 2016). A total of 246 whole-mtDNA sequences (n = 231 from GenBank) were aligned using MUSCLE and the resulting alignment edited and pruned (polyC stretches removed between np 303 – 318 and 16,165 – 16,179) in Geneious for subsequent phylogenetic analysis (Kearse et al., 2012; Edgar et al., 2017) (Table S1-S5).

2.7.3 Ancient DNA Authentication

Ancient and degraded DNA molecules are typically shorter in length and exhibit a higher degree of DNA damage resulting from hydrolytic deamination, which can be quantified to support the authenticity of older samples. Negative controls (ultrapure H_2O blanks) were prepared in parallel during extraction and library preparation in order to monitor potential cross-contamination between samples, and contamination from the surrounding environment. Both extraction and library blanks show a low degree of reads mapping to the human mitochondrial

reference genome, indicating minimal exogenous contamination during sample processing. In addition, we performed *in silico* analysis to determine the authenticity of the filtered mtDNA reads obtained for the Iron Age individuals. We generated fragment length distribution (FLD) and terminal deamination (i.e., C→T and G→A transitions) plots for filtered mtDNA reads figures using mapDamage 2.0 (Table S2) (Jónsson et al., 2013). All Iron Age samples exhibit short FLD and misincorporation patterns expected of highly degraded or ancient molecules (Table S2). Contamination rates estimated by Schmutzi range between 1% and 17% (mean= 3.6%), suggesting low human contamination from the burial, storage, and laboratory environments (Renaud et al., 2015) (Table S1).

2.7.4 Age and Sex Estimation of the Botromagno Skeletal Sample

Age-at-death and sex was estimated using standard osteological methods (Buikstra and Ubelaker, 1994). Subadult and juvenile age was determined using long bone length, epiphyseal fusion of the long bones, and tooth development and eruption. Adult age was assessed using morphological changes to the auricular surface of the ilium and pubic symphysis, along with cranial suture closure. Sex was estimated using morphological features of the cranium and pelvis (Table S1).

2.7.5 Arlequin Analysis and Multi-Dimensional Scaling

Population pairwise Φ_{ST} values were generated with Arlequin ver. 3.5.2.2 using the Tamura-Nei substitution model, estimated by jmodeltest 2.1.10 (AIC corrected) (Table S5) (Excoffier et al., 1992; Darriba et al., 2012). Multi-dimensional scaling plots were composed using a customized script in R with the following CRAN-based packages: *plot3Drg, vegan,*

MASS. Countries or time periods represented with <5 mitochondrial sequences were omitted from MDS analysis in order to reduce scaling stress (from 246 to 224 mitochondrial genomes) (i.e., removing the countries of Ukraine, Italy and Sardinia, Romania, Luxembourg, Hungary, and China, and the Chalcolithic, Classical, Late Glacial, and Medieval temporal periods). We included n=11 countries (or geographic regions) represented by >5 mtDNAs (i.e., Aegean, Armenia, Belgium, Czech Republic, France, Germany, Latvia, Russia, South Italy, Spain, and Sweden), and by time period (n=8; Bronze Age, Holocene, Italian Iron Age1, Armenian Iron Age2, Mesolithic, Neolithic, post-LGM, and pre-LGM). Text files containing Φ_{ST} values were imported into R as matrices, and the stress values for in-text Figures 3a/b/c were calculated using the isoMDS function in *MASS* (Tables S3-S4).

2.7.6 BEAST Analysis

Samples without dates were omitted from Bayesian inference, which reduced sample size from 246 to 238. We reconstructed the coalescence dates for haplogroups comprising 238 mitochondrial sequences in BEAST ver. 1.8.4. Tip dates were obtained by averaging published calibrated ^{14}C ranges and previously published calibrated ^{14}C dates (Table S5). We currently have no ^{14}C dates for the Botromagno assemblage. Instead, we assigned an average date for the remains based on site occupation (i.e., $7^{th} – 4^{th}$ century BCE) in years before present (BP), or 2450 BP, to standardize the tip dates in BEAST. Calibrated ranges for samples referenced against BCE (Before Common Era) were adjusted by +1950 to BP for tip date molecular clock calibration. We used the substitution model Tamura-Nei 93 G+I estimated by jmodeltest 2.1.10 (AIC corrected; Darriba et al., 2012), and an uncorrelated relaxed lognormal clock model with the substitution rate set to 1.655×10^{-8} ($1\sigma = 1.479\times10^{-9}$) (Soares et al., 2009). Trees were

annotated using TreeAnnotator and visualized using FigTree ver. 1.4.3.

Figure S1a/b: 3D multi-dimensional scaling model showing scaling distance by a) country/region (stress value = 7.47) and b) time (stress value = 0.006). Country and age categories with < 5 mtDNA sequences were removed from MDS analysis.

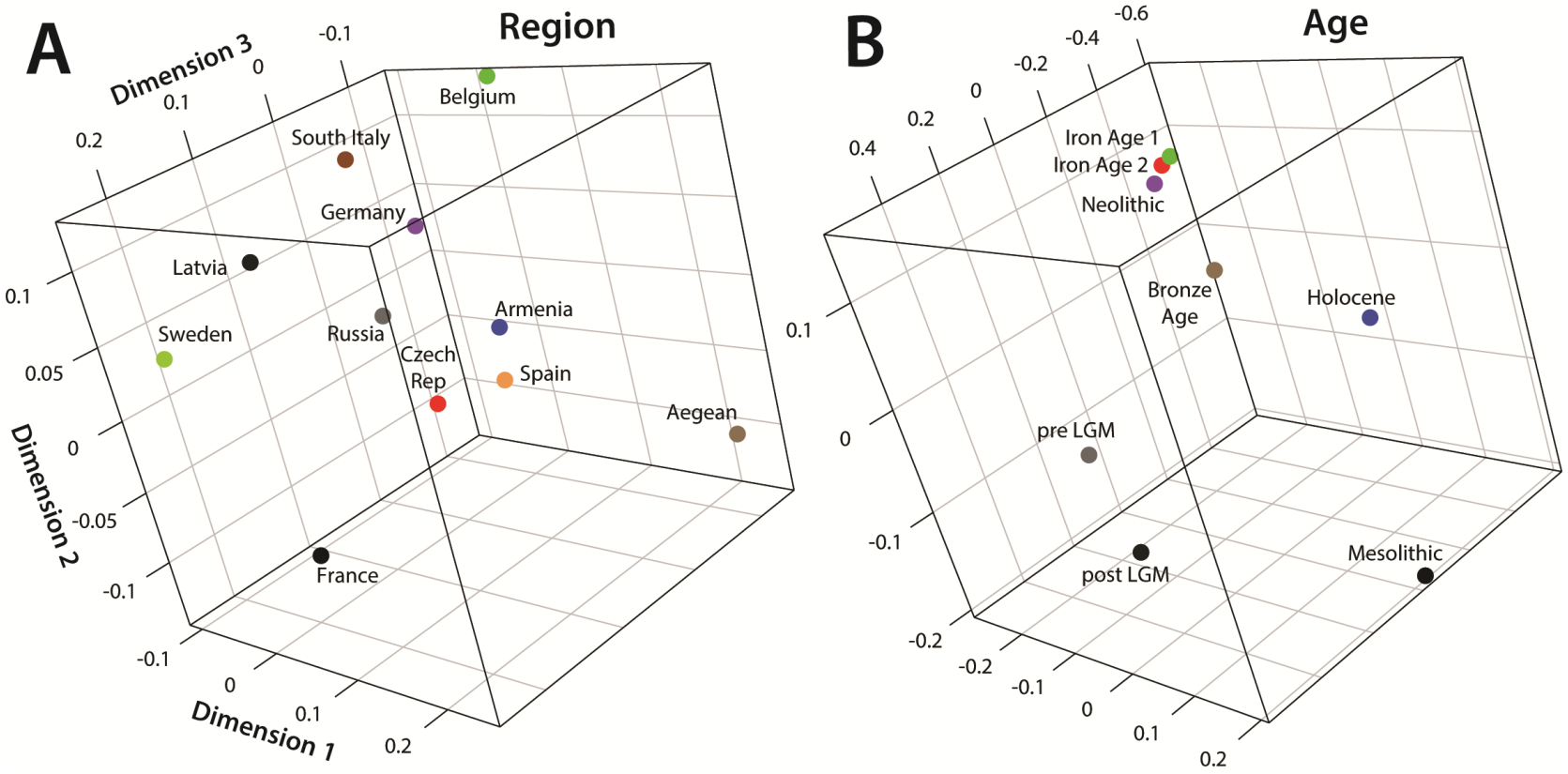

Table S1: Iron Age sample identification, mtDNA read data, and contamination estimates.

Library ID	Italian ID	Material Sampled	Age (Years)	Sex	Total Trimmed and Merged Reads	# of unique reads ≥ 35 bp MQ 30	Depth of Coverage (rCRS)	Haplogroup	Missing Data (# bp)	Schmutzi Contamination Estimate (%)
LIAV4	Tomba 11	Tooth Root	38.2 ± 70.9	F	1934979	75963	316x	U4b1a1a1	1	2
LIAV7	Scavi Latanzi F1, 5	Tooth Root	30.7 ± 8.1	F	2722239	170584	753.7x	V18	0	1
LIAV8	No Label Box#6	Tooth Root	Adult	Male?	27928515	95664	467.1x	H1	1	2
LIAV11	Tomba 18 Cranio	Tooth Root	n/a	n/a	108009	8566	41.8x	H6a1a	7	3
LIAV12	Site DB, Room 12	Tooth Root	n/a	n/a	2335939	25921	110.6x	J2b1a2	2	2
LIAV20	Settore III, T.2, h8, Dep 2 of 2	Tooth Root	n/a	n/a	1611460	4072	16.1x	U5b2c	87	2
LIAV29	GDA 68 R1 F1 L5	Tooth Root	14-15	U	4059624	6939	27.2x	H5'36	15	1
LIAV31	Area NB, Grave #3	Tooth Root	Adult	U	3775919	13508	66.4x	U5a1	2	11
LIAV32	G67/III p.1 c.1 layer 3 S7, Mandible 2	Tooth Root	n/a	n/a	1903030	7015	32.2x	H	10	2
LIAV33	G67/I P15 S19, cranium #1	Tooth Root	n/a	n/a	1714141	1251	5.6x	H	1385	4
LIAV37	F5 20108 Layer 1047, Skull	Tooth Root	Adult	M	4659123	27350	111x	U3b1b	0	1
LIAV38	G67/I 13 E2 S4 subadult Tomb 4	Tooth Root	Sub-adult	U	6560700	41907	221.4x	U4a1	2	2
LIAV40	G67 III, p1 c1, Tomba 7, loose molars	Tooth Root	n/a	n/a	3223409	8034	37.1x	H	7	3
LIAV43	Site DB, Room 12, Layer 1	Tooth Root	n/a	n/a	2134450	11630	62.2x	U2e3	4	2
LIAV45	G67/III no. p1 EI O of 3, Tomb 7	Tooth Root	n/a	n/a	3081617	2590	13.5x	H2	278	17
LIAV1Bl	n/a	n/a	n/a	n/a	41208	24	n/a	n/a	n/a	n/a
LIAV16Bl	n/a	n/a	n/a	n/a	6548	154	n/a	n/a	n/a	n/a
LIAV23Bl	n/a	n/a	n/a	n/a	978	25	n/a	n/a	n/a	n/a
LIAV27Bl	n/a	n/a	n/a	n/a	5447	30	n/a	n/a	n/a	n/a
LIAV34Bl	n/a	n/a	n/a	n/a	1708	7	n/a	n/a	n/a	n/a
LIAV41Bl	n/a	n/a	n/a	n/a	1250	11	n/a	n/a	n/a	n/a
Library Bl 1	n/a	n/a	n/a	n/a	16	2	n/a	n/a	n/a	n/a
Library Bl 2	n/a	n/a	n/a	n/a	786	0	n/a	n/a	n/a	n/a

Table S2: Misincorporation and Fragment Length Distribution (FLD) data for unique reads ≥35bp(MQ30)(Jónsson et al., 2013).

Sample ID	3' Deamination (%)	5' Deamination (%)	Avg. Insert Size (bp)
LIAV4	31	32	64.3
LIAV7	32	33	69.5
LIAV8	35	35	71.9
LIAV11	34	32	78
LIAV12	33	33	64.7
LIAV20	37	43	54
LIAV29	31	30	57
LIAV31	30	30	70.8
LIAV32	28	31	67.8
LIAV33	23	26	68.4
LIAV37	29	31	62.6
LIAV38	29	31	79.2
LIAV40	29	29	69.1
LIAV43	27	28	78.6
LIAV45	20	26	76.8

Table S3: Population pairwise Φ_{ST} results for mtDNA sequences categorized by geographic region.

Geographic Region	Aegean	Armenia	Belgium	CzechRep	France	Germany	Latvia	Russia	South Italy	Spain	Sweden
Aegean	0										
Armenia	0.09696	0									
Belgium	0.19391	0.05191	0								
Czech Rep.	0.20157	0.01739	0.10882	0							
France	0.27318	0.11886	0.18091	0.11591	0						
Germany	0.18931	0.01674	0.11408	0.06862	0.13299	0					
Latvia	0.22708	0.16812	0.24955	0.23048	0.16571	0.22704	0				
Russia	0.12233	0.0044	0.04962	0.00188	0.0905	0.01824	0.12601	0			
South Italy	0.17147	0.01787	0.08886	0.05399	0.13653	0.02242	0.16032	0.01136	0		
Spain	0.03373	-0.00156	0.06916	0.02104	0.08599	0.03726	0.19769	0.00781	0.04162	0	
Sweden	0.27718	0.1468	0.19581	0.20077	0.1155	0.19664	0.11286	0.09667	0.15117	0.14891	0

Table S4: Population pairwise Φ_{ST} results for mtDNA sequences categorized by temporal age.

Temporal Age	Bronze Age	Holocene	Iron Age1	Iron Age2	Mesolithic	Neolithic	Post-LGM	Pre-LGM
Bronze Age	0							
Holocene	0.23921	0						
Iron Age1	0.03621	0.26037	0					
Iron Age2	0.02081	0.28107	0.00626	0				
Mesolithic	0.06456	0.18757	0.09521	0.10582	0			
Neolithic	0.02308	0.20744	0.01715	0.00825	0.09365	0		
Post-LGM	0.16097	0.52178	0.22091	0.21962	0.23986	0.19034	0	
Pre-LGM	0.07785	0.38268	0.10597	0.09213	0.12459	0.0767	0.30128	0

***Φ_{ST} values in red indicate low genetic differentiation between categories (i.e, <0.05) (Hartl and Clark, 1997).**

Table S5: Published mtDNA Sequences Used for Multi-Dimensional Scaling and BEAST Analysis (n=231).

Library ID	Location	Time Period	Date (cal BP)/Ranges cal. BCE	Haplo-group	Publication
Kostenki14	Russia	preLGM	37985	U2	(Krause et al., 2010)
GoyetQ116-1	Belgium	preLGM	34795	M	(Posth et al., 2016)
GoyetQ376-3	Belgium	preLGM	33540	M	(Posth et al., 2016)
Cioclovina1	Romania	preLGM	33212	U	(Posth et al., 2016)
Paglicci133	Italy	preLGM	33000	U8c	(Posth et al., 2016)
DolniVestonice13	Czech Republic	preLGM	31155	U8	(Fu et al., 2013)
DolniVestonice14	Czech Republic	preLGM	31155	U5	(Fu et al., 2013)
DolniVestonice15	Czech Republic	preLGM	31155	U5	(Fu et al., 2013)
DolniVestonice16	Czech Republic	preLGM	29977	U5	(Posth et al., 2016)
DolniVestonice43	Czech Republic	preLGM	29977	U5	(Posth et al., 2016)
Paglicci108	Italy	preLGM	28396	U2'3'4'7'8'9	(Posth et al., 2016)
GoyetQ53-1	Belgium	preLGM	27975	U2	(Posth et al., 2016)
LaRochette	France	preLGM	27592	M	(Posth et al., 2016)
GoyetQ55-2	Belgium	preLGM	27520	U2	(Posth et al., 2016)
GoyetQ376-19	Belgium	preLGM	27515	U2	(Posth et al., 2016)
Goyet2878-21	Belgium	preLGM	26662	U5	(Posth et al., 2016)
GoyetQ56-16	Belgium	preLGM	26320	U2	(Posth et al., 2016)
Paglicci71	Italy	postLGM	18585	U5b2b	(Posth et al., 2016)
HohleFels79	Germany	postLGM	15909	U8a	(Posth et al., 2016)
HohleFels10	Germany	postLGM	15470	U8a	(Posth et al., 2016)
HohleFels49	Germany	postLGM	15470	U8a	(Posth et al., 2016)
Rigney1	France	postLGM	15465	U2'3'4'7'8'9	(Posth et al., 2016)
GoyetQ-2	Belgium	postLGM	15005	U8a	(Posth et al., 2016)
Brillenhohle	Germany	postLGM	14780	U8a	(Posth et al., 2016)
Burkhardtshohle	Germany	postLGM	14615	U8a	(Posth et al., 2016)
Oberkassel1998	Germany	Late Glacial	14020	U5b1	(Fu et al., 2013)
Iboussieres39	France	postLGM/LateGlacial	11820	U5b2b	(Posth et al., 2016)
Iboussieres25-1	France	postLGM/LateGlacial	11820	U5b2b	(Posth et al., 2016)
Iboussieres31-2	France	postLGM/LateGlacial	11820	U5b1	(Posth et al., 2016)
Rochedane	France	postLGM/LateGlacial	12960	U5b2b	(Posth et al., 2016)
BLA20	Germany	Holocene	10652	U5a2c3	(Bollongino et al., 2013)
Ranchot88	France	Holocene	10084	U5b1	(Posth et al., 2016)
LesCloseaux3	France	Holocene	9905	U5a2	(Posth et al., 2016)
MareuilLesMea.	France	Holocene	9290	U5a2	(Posth et al., 2016)

Falkenstein	Germany	Holocene	9201	U5b2a	(Posth et al., 2016)
Felsdach	Germany	Holocene	8680	U5a2c	(Posth et al., 2016)
HohlensteinStadel	Germany	Holocene	8628	U5b2c1	(Posth et al., 2016)
Ofnet	Germany	Holocene	8292	U5b1d1	(Posth et al., 2016)
CuiryLesChaudardes1	France	Holocene	8205	U5b1b	(Posth et al., 2016)
Bockstein	Germany	Holocene	8173	U5b1d1	(Posth et al., 2016)
BerryAuBac1	France	Holocene	7244	U5b1a	(Posth et al., 2016)
Loschbour	Luxembourg	Holocene	8054	U5b1a	(Fu et al., 2013)
Motala1	Sweden	Neolithic	7953	U5a1	(Lazaridis et al., 2014)
Motala12	Sweden	Neolithic	7953	U2e1	(Lazaridis et al., 2014)
Motala2	Sweden	Neolithic	7953	U2e1	(Lazaridis et al., 2014)
Motala3	Sweden	Neolithic	7953	U5a1	(Lazaridis et al., 2014)
Motala4	Sweden	Neolithic	7953	U5a2d	(Lazaridis et al., 2014)
Motala6	Sweden	Neolithic/Holocene	7953	U5a2d	(Lazaridis et al., 2014)
Motala9	Sweden	Neolithic/Holocene	7953	U5a2	(Lazaridis et al., 2014)
arm1	Armenia	Early Bronze Age	4942	K3	(Margaryan et al., 2017)
arm10	Armenia	Classical	2580	H13a1a2	(Margaryan et al., 2017)
arm11	Armenia	Late Bronze Age	3200	U3b	(Margaryan et al., 2017)
arm12	Armenia	Medieval	1179	J1d6	(Margaryan et al., 2017)
arm13	Armenia	Early Iron Age	3000	U2e2a1	(Margaryan et al., 2017)
arm14	Artsakh	Medieval	300	U1a1a	(Margaryan et al., 2017)
arm15	Armenia	Late Bronze Age	3314	H15a1a1	(Margaryan et al., 2017)
arm16	Armenia	Late Bronze Age	3314	K1a12a	(Margaryan et al., 2017)
arm18	Armenia	Late Bronze Age	3314	H15a1a1	(Margaryan et al., 2017)
arm19	Armenia	Late Bronze Age	3314	K1a1b1e	(Margaryan et al., 2017)
arm2	Armenia	Early Bronze Age	4942	R1a1	(Margaryan et al., 2017)
arm20	Armenia	Late Bronze Age	3314	H8a1	(Margaryan et al., 2017)
arm21	Armenia	Early Iron Age	3161	HV12b1	(Margaryan et al., 2017)
arm22	Armenia	Early Iron Age	3161	H2a	(Margaryan et al., 2017)
arm23	Armenia	Late Bronze Age	3400	R1a1a	(Margaryan et al., 2017)
arm24	Armenia	Early Iron Age	3161	U5a1b	(Margaryan et al., 2017)
arm26	Armenia	Early Iron Age	3161	J1d1b1	(Margaryan et al., 2017)
arm27	Armenia	Early Iron Age	3161	HV	(Margaryan et al., 2017)
arm28	Armenia	Late Bronze Age	3300	K1a4c1	(Margaryan et al., 2017)
arm29	Armenia	Late Bronze Age	3300	R1b1	(Margaryan et al., 2017)
arm3	Armenia	Early Bronze Age	4942	K3	(Margaryan et al., 2017)
arm30	Armenia	Late Bronze Age	3400	U8b1a2b	(Margaryan et al., 2017)
arm31	Armenia	Late Bronze Age	3300	T1a9	(Margaryan et al., 2017)
arm32	Armenia	Late Bronze Age	3300	HV1a2	(Margaryan et al., 2017)
arm33	Armenia	Late Bronze Age	3300	W3b	(Margaryan et al., 2017)

arm34	Armenia	Late Bronze Age	3264	U3b	(Margaryan et al., 2017)
arm35	Armenia	Middle Bronze Age	3900	U3b	(Margaryan et al., 2017)
arm36	Armenia	Late Bronze Age	3400	U2e1e	(Margaryan et al., 2017)
arm37	Armenia	Early Iron Age	3000	H	(Margaryan et al., 2017)
arm39	Armenia	Neolithic	7811	I1	(Margaryan et al., 2017)
arm4	Armenia	Classical	2000	J1d1b1	(Margaryan et al., 2017)
arm40	Armenia	Early Bronze Age	5353	H14b2	(Margaryan et al., 2017)
arm42	Armenia	Early Bronze Age	5353	T1	(Margaryan et al., 2017)
arm43	Armenia	Middle Bronze Age	3700	U4a	(Margaryan et al., 2017)
arm44	Armenia	Late Iron Age	2609	U3b3	(Margaryan et al., 2017)
arm45	Armenia	Middle Bronze Age	3700	T	(Margaryan et al., 2017)
arm46	Armenia	Middle Bronze Age	3700	HV1a1	(Margaryan et al., 2017)
arm48	Armenia	Late Iron Age	2609	I4	(Margaryan et al., 2017)
arm49	Armenia	Late Iron Age	2609	I4	(Margaryan et al., 2017)
arm5	Armenia	Early Bronze Age	4942	J1b1b1	(Margaryan et al., 2017)
arm51	Armenia	Late Iron Age	2609	U3b3	(Margaryan et al., 2017)
arm52	Artsakh	Chalcolithic	6411	U8b1a1	(Margaryan et al., 2017)
arm7	Armenia	Neolithic	7811	H2+152	(Margaryan et al., 2017)
arm9	Armenia	Neolithic	7811	H15a1	(Margaryan et al., 2017)
rise396	Armenia	Early Iron Age	3007	H6b	(Margaryan et al., 2017)
rise397	Armenia	Early Iron Age	2909	T1a2	(Margaryan et al., 2017)
rise407	Armenia	Early Iron Age	2935	H8a1	(Margaryan et al., 2017)
rise408	Armenia	Early Iron Age	3049	I5c	(Margaryan et al., 2017)
rise412	Armenia	Early Iron Age	3016	U4c1	(Margaryan et al., 2017)
rise413	Armenia	Middle Bronze Age	3766	T2c1f	(Margaryan et al., 2017)
rise423	Armenia	Late Bronze Age	3249	T2a3	(Margaryan et al., 2017)
HAL16	Germany	Unetice_EBA	2022-1937 calBCE	V	(Haak et al., 2015)
HAL25	Germany	LBK_EN	5206-5052 calBCE	K1a	(Haak et al., 2015)
ESP5	Germany	Corded_Ware_LN	2800-2050 BCE	U5a2d	(Haak et al., 2015)
ESP22	Germany	Corded_Ware_LN	2454-2291 calBCE	X2b4	(Haak et al., 2015)
HAL5	Germany	LBK_EN	5206-5004 calBCE	T2c1d'e'f	(Haak et al., 2015)
ALB2	Germany	Alberstedt_LN	2494-2344 calBCE	H3b	(Haak et al., 2015)
HAL36C	Germany	Halberstadt_LBA	1113-1021 calBCE	H23	(Haak et al., 2015; (Brotherton et al., 2013)
QUEXII6	Germany	Bell_Beaker_LN	2340-2190 calBCE	H13a1a2	(Haak et al., 2015)
ALB3	Germany	Alberstedt_LN	2459-2345 calBCE	HV6'17	(Haak et al., 2015)
ESP26	Germany	Corded_Ware_LN	2454-2291 calBCE	T2a1b1	(Haak et al., 2015)
ESP2	Germany	Unetice_EBA_relative_of_I0117	2131-1979 calBCE	I3a	(Haak et al., 2015)
ESP11	Germany	Corded_Ware_LN	2473-2348 calBCE	U4b1a1a1	(Haak et al., 2015)
ROT3	Germany	Bell_Beaker_LN	2500-2050 BCE	K1a2c	(Haak et al., 2015)
HAL15	Germany	LBK_EN	5030-4948 calBCE	N1a1a1a	(Haak et al., 2015)

				3	
HAL4	Germany	LBK_EN	5032-4946 calBCE	N1a1a1a	(Haak et al., 2015)
ROT4	Germany	Bell_Beaker_LN	2414-2333 calBCE	H3	(Haak et al., 2015)
ESP16	Germany	Corded_Ware_LN	2566-2477 calBCE	W6a	(Haak et al., 2015)
QUEXII4	Germany	Bell_Beaker_LN	2290-2130 calBCE	J1c5	(Haak et al., 2015)
ROT6	Germany	Bell_Beaker_LN	2497-2436 calBCE	H5a3	(Haak et al., 2015; Brotherton et al., 2013)
ESP3	Germany	Unetice_EBA	1931-1780 calBCE	U5a1	(Haak et al., 2015)
ESP29	Germany	Unetice_EBA	2199-2064 calBCE	I3a	(Haak et al., 2015)
ESP4	Germany	Unetice_EBA	2118-1961 calBCE	W3a1	(Haak et al., 2015)
QUEVIII6	Germany	Unetice_EBA	2012-1919 calBCE	U5b2a1	(Haak et al., 2015)
HAL13	Germany	Rössen_EN	5500-4775 BCE	V1a	(Haak et al., 2015)
BAL16a	Hungary	Lengyel_Neolithic	4900-4500 BCE	N1a1a1	(Haak et al., 2015)
BZH12	Germany	BenzigerodeHeimburg_LN	2204-2136 calBCE	U5a1a2a	(Haak et al., 2015)
BAM25a	Hungary	Starcevo_EN	5710-5530 calBCE	N1a1a1	(Haak et al., 2015)
OSH7	Germany	Rössen_EN	4582-4407 calBCE	H5b	(Haak et al., 2015; Brotherton et al., 2013)
OAW1	Germany	Gatersleben_EN	4475-3950 BCE	HV6'17	Haak et al., 2015
OSH1	Germany	Rössen_EN	4625-4250 BCE	H16a'c'd	(Haak et al., 2015; Brotherton et al., 2013)
SZEH4b	Hungary	LBKT_EN	5210-4940 calBCE	N1a1a1a3	(Haak et al., 2015)
OSH9	Germany	Rössen_EN	4625-4250 BCE	U5b1b	(Haak et al., 2015)
UzOO74	Russia	Karelia_HG	5500-5000 BCE	C1g	(Haak et al., 2015)
UWS4	Germany	LBK_EN	5209-5070 calBCE	J1c17	(Haak et al., 2015)
BZH4	Germany	BenzigerodeHeimburg_LN	2283-2146 calBCE	H1e	(Haak et al., 2015; Brotherton et al., 2013)
BZH6	Germany	BenzigerodeHeimburg_LN	2286-2153 calBCE	H1/H1b'ad	(Haak et al., 2015; Brotherton et al., 2013)
HAL14	Germany	LBK_EN	5206-5052 calBCE	T2b(8)	(Haak et al., 2015)
HAL34	Germany	LBK_EN	5207-5067 calBCE	N1a1a1	(Haak et al., 2015)
HQU5	Germany	Baalberge_MN	3631-3561 calBCE	T2c1d1	(Haak et al., 2015)
Troc7	Spain	Spain_EN	5177-5068 calBCE	V	(Haak et al., 2015)
Troc4	Spain	Spain_EN_relative_of_I0410	5303-5204 calBCE	K1a2a	(Haak et al., 2015)
Mina18a	Spain	Spain_MN	3900-3600 BCE	pre-U5b1i	(Haak et al., 2015)
Mina2	Spain	Spain_MN	3900-3600 BCE	J2a1a1	(Haak et al., 2015)
Troc3	Spain	Spain_EN	5178-5066 calBCE	pre-T2c1d2	(Haak et al., 2015)
Mina6b	Spain	Spain_MN	3900-3600 BCE	K1b1a1	(Haak et al., 2015)
Troc5	Spain	Spain_EN	5310-5206 calBCE	N1a1a1	(Haak et al., 2015)
Mina3	Spain	Spain_MN	3900-3600 BCE	K1a1b1	(Haak et al., 2015)
Troc1	Spain	Spain_EN	5311-5218 calBCE	J1c3	(Haak et al., 2015)
DEB36	Germany	LBK_EN	5500-4775 BCE	U5a1a'g	(Haak et al., 2015)
QLB18A	Germany	Baalberge_MN	3640-3510 calBCE	T2e1	(Haak et al., 2015)

KAR22A	Germany	Karsdorf_LN	2564-2475 cal BCE	T1a1	(Haak et al., 2015)
QLB15D	Germany	Baalberge_MN	3645-3537 calBCE	HV6'17	(Haak et al., 2015)
QLB6B	Germany	Baalberge_MN	3950-3400 BCE	U5b2a2	(Haak et al., 2015)
BENZ18/BENZ15?	Germany	Bernburg_MN	3101-2919 calBCE	W1c'i	(Haak et al., 2015)
SALZ7A	Germany	Salzmünde_MN	3400-3025 BCE	H5	(Haak et al., 2015)
SALZ3B	Germany	Salzmünde_MN	3400-3025 BCE	U3a1	(Haak et al., 2015)
BENZ14	Germany	Bernburg_MN	3104-2919 cal BCE	U5a2b4	(Haak et al., 2015)
QLB2A	Germany	Baalberge_MN	3950-3400 BCE	U8a1	(Haak et al., 2015)
SALZ88A	Germany	Salzmünde_MN	3237-3171 calBCE	J1c	(Haak et al., 2015)
HAL2	Germany	LBK_EN	5066-4979 calBCE	N1a1a1a2	(Haak et al., 2015)
ESP24	Germany	Esperstedt_MN	3360-3086 calBCE	T2b	(Haak et al., 2015)
SALZ21B	Germany	Schöningen_MN	4100-3950 BCE	H1e	(Haak et al., 2015; Brotherton et al., 2013)
SALZ18A	Germany	Schöningen_MN	4172-4089 calBCE	H10e'f'g	(Haak et al., 2015; Brotherton et al., 2013)
QLB28b	Germany	Bell_Beaker_LN	2296-2206 calBCE	H1	(Haak et al., 2015; Brotherton et al., 2013)
EUL41a	Germany	Unetice_EBA	2115-1996 calBCE	H4a1a1	(Haak et al., 2015; Brotherton 2013)
QLB26a	Germany	Bell_Beaker_LN	2360-2190 calBCE	H1	(Haak et al., 2015; Brotherton et al., 2013)
SALZ57A	Germany	Salzmünde_MN	3334-3262 calBCE	H3	(Haak et al., 2015; Brotherton et al., 2013)
HAL24	Germany	LBK_EN	5034-4942 calBCE	pre-X2d1	(Haak et al., 2015)
EUL57b	Germany	Unetice_EBA	2131-1982 calBCE	H3	(Haak et al., 2015; Brotherton et al., 2013)
KAR16A	Germany	LBK_EN	5500-4775 BCE	H46b	(Haak et al., 2015; Brotherton et al., 2013)
KAR11B	Germany	LBK_EN	5500-4775 BCE	H	(Haak et al., 2015; Brotherton et al., 2013)
HQU3	Germany	Baalberge MN	3630-3581 calBCE	K1e	(Haak et al., 2015)
SALZ77A	Germany	Salzmünde_MN	3400-3025 BCE	H3	(Haak et al., 2015; Brotherton et al., 2013)
HAL37	Germany	LBK_EN	5298-5247 calBCE	W1c'i	(Haak et al., 2015)
ESP30	Germany	Baalberge_MN	3887-3797 calBCE	H1e1a	(Haak et al., 2015; Brotherton et al., 2013)
HQU4	Germany	Baalberge_MN	3950-3400 BCE	H7d	(Haak et al., 2015; Brotherton et al., 2013)
LBK1992	Germany	LBK_EN	5500-4800 BCE	T2b	(Haak et al., 2015)
LBK2172	Germany	LBK_EN	5500-4800 BCE	H40	(Haak et al., 2015)
LBK2155	Germany	LBK_EN	5500-4800 BCE	T2b	(Haak et al., 2015)
LBK1979	Germany	LBK_EN	5500-4800 BCE	H	(Haak et al., 2015)
LBK1254	Germany	LBK_EN	5500-4800 BCE	HV6'17	(Haak et al., 2015)
LBK1581	Germany	LBK_EN	5500-4800 BCE	T2b	(Haak et al., 2015)
LBK1976	Germany	LBK_EN	5500-4800 BCE	T2e	(Haak et al., 2015)
LBK1988	Germany	LBK_EN	5500-4800 BCE	W1c'i	(Haak et al., 2015)
LBK1577	Germany	LBK_EN	5500-4800 BCE	T2e	(Haak et al., 2015)
SVP3	Russia	Yamnaya	2910-2875 calBCE	U4a1	(Haak et al., 2015)

SVP10	Russia	Yamnaya	3500-2700 BCE	H13a1a1	(Haak et al., 2015)
SVP44	Russia	Samara_HG	5650-5555 calBCE	U5a1d	(Haak et al., 2015)
SVP57	Russia	Yamnaya	3500-2700 BCE	W3a1a	(Haak et al., 2015)
SVP5	Russia	Yamnaya	3090-2910 calBCE	W6c	(Haak et al., 2015)
SVP2	Russia	Yamnaya	3500-2700 BCE	K1b2a	(Haak et al., 2015)
SVP38	Russia	Yamnaya	3339-2917 calBCE	T2c1a2	(Haak et al., 2015)
SVP50	Russia	Yamnaya	3021-2635 calBCE	U5a1a1	(Haak et al., 2015)
SVP52	Russia	Yamnaya	3305-2925 calBCE	U5a1a1	(Haak et al., 2015)
SVP58	Russia	Yamnaya	3335-2881 calBCE	H6a1b	(Haak et al., 2015)
SVP54	Russia	Yamnaya	3010-2622 calBCE	H2b	(Haak et al., 2015)
BLA7	Germany	Neolithic	3666	H5	(Bollongino et al., 2013)
BLA10	Germany	Neolithic	3418	H1c3	(Bollongino et al., 2013)
BLA11	Germany	Neolithic	-	U5b2b	(Bollongino et al., 2013)
BLA13	Germany	Neolithic	3513	H5	(Bollongino et al., 2013)
Theo5	Greece/Anatolia	Mesolithic	7605-7529	K1c	(Hofmanova et al., 2016)
Theo1	Greece/Anatolia	Mesolithic	7288-6771	K1c	(Hofmanova et al., 2016)
Rev5	Greece/Anatolia	Neolithic	6438-6264	X2b	(Hofmanova et al., 2016)
Bar31	Greece/Anatolia	Neolithic	6419-6238	X2m	(Hofmanova et al., 2016)
Bar8	Greece/Anatolia	Neolithic	6212-6030	K1a2	(Hofmanova et al., 2016)
Pal7	Greece/Anatolia	Neolithic	4452-4350	J1c1	(Hofmanova et al., 2016)
Klei10	Greece/Anatolia	Neolithic	4230-3995	K1a2	(Hofmanova et al., 2016)
StPet12	Ukraine	Neolithic	4519-4343	U5b2	(Jones et al., 2017)
StPet2	Ukraine	Mesolithic	9193-8641	U4a1d	(Jones et al., 2017)
ZVEJ28	Latvia	Neolithic	3089-2676	U5a1	(Jones et al., 2017)
ZVEJ31	Latvia	Neolithic	4229-3800	U4	(Jones et al., 2017)
ZVEJ26	Latvia	Neolithic	4251-3976	U4a1	(Jones et al., 2017)
ZVEJ27	Latvia	Neolithic	5302-4852	U5a2d	(Jones et al., 2017)
ZVEJ25	Latvia	Neolithic	5841-5636	U2e1	(Jones et al., 2017)
ZVEJ32	Latvia	Neolithic	6467-6249	U5a1c	(Jones et al., 2017)
LaBrana1	Spain	Mesolithic	6980 +/-50	U5b2c1	(Sanchez-Quinto et al., 2012)
CroMagnon	France	Medieval	690 +/- 39	T2b1	(Fu et al., 2013)
BS11	China	Neolithic	7368 +/- 34	B4c1a	(Fu et al., 2013)
ESP15	Germany	Neolithic	3904 +/- 47	H6a1a	(Brotherton et al., 2013)
ROT2	Germany	Neolithic?	n/a	H5a3	(Brotherton et al., 2013)
OSH2	Germany	Neolithic?	n/a	H89	(Brotherton et al., 2013)
HAL11	Germany	Neolithic?	n/a	H	(Brotherton et al., 2013)
DEB9	Germany	Neolithic?	n/a	H88	(Brotherton et al., 2013)
HAL32	Germany	Neolithic?	n/a	H26	(Brotherton et al., 2013)
KAR6a	Germany	Neolithic?	n/a	H1	(Haak et al., 2015; Brotherton et al., 2013)

Mina4	Germany	Neolithic	3900-3600 BCE	H1	(Haak et al., 2015)
Sardinia	Sardinia	Neolithic	3398 +/-26	H1aw1	(Brotherton et al., 2013)
OSH3	Germany	Neolithic	n/a	H1	(Brotherton et al., 2013)
DEB21	Germany	Neolithic	6151 +/-27	H1j	(Brotherton et al., 2013)
HAL39	Germany	Neolithic	6145+/-30	H1e	(Brotherton et al., 2013)
ALB1	Germany	Neolithic	3858 +/-57	H3b	(Brotherton et al., 2013)

2.8 References

Bollongino R, Nehlich O, Richards MP, Orschiedt J, Thomas MG, Sell C, Fajkošová Z, Powell A, Burger J. 2013. 2000 years of parallel societies in stone age central Europe. Science 342:479

Bramanti B, Thomas MG, Haak W, Unterlaender M, Jores P, Tambets K, Antanaitis-Jacobs I, Haidle MN, Jankauskas R, Kind C-J, Lueth F, Terberger T, Hiller J, Matsumura S, Forster P, Burger J. 2009. Genetic discontinuity between local hunter-gatherers and central Europe's first farmers. Science 326:137–140.

Brandt G, Szécsényi-Nagy A, Roth C, Alt KW, Haak W. 2015. Human paleogenetics of Europe - the known knowns and the known unknowns. J Hum Evol 79:73–92.

Brooks R, Small A, Ward-Perkins J. 1966. Trial excavations on the site of Botromagno, Gravina di Puglia, 1966. Pap Br Sch Rome1 34:131–150.

Brotherton P, Haak W, Templeton J, Brandt G, Soubrier J, Jane Adler C, Richards SM, Sarkissian C Der, Ganslmeier R, Friederich S, Dresely V, van Oven M, Kenyon R, Van der Hoek MB, Korlach J, Luong K, Ho SYW, Quintana-Murci L, Behar DM, Meller H, Alt KW, Cooper A, Adhikarla S, Ganesh Prasad AK, Pitchappan R, Varatharajan Santhakumari A, Balanovska E, Balanovsky O, Bertranpetit J, Comas D, Martínez-Cruz B, Melé M, Clarke AC, Matisoo-Smith EA, Dulik MC, Gaieski JB, Owings AC, Schurr TG, Vilar MG, Hobbs A, Soodyall H, Javed A, Parida L, Platt DE, Royyuru AK, Jin L, Li S, Kaplan ME, Merchant NC, John Mitchell R, Renfrew C, Lacerda DR, Santos FR, Soria Hernanz DF, Spencer Wells R, Swamikrishnan P, Tyler-Smith C, Paulo Vieira P, Ziegle JS. 2013. Neolithic mitochondrial haplogroup H genomes and the genetic origins of Europeans. Nat Commun [Internet] 4:1764. Available from: http://dx.doi.org/10.1038/ncomms2656

Buikstra J, Ubelaker D. 1994. Standards for Data Collection from Human Skeletal Remains. Arkansas Archeological Survey, Fayetteville.

Dabney J, Knapp M, Glocke I, Gansauge M-T, Weihmann A, Nickel B, Valdiosera C, García N, Pääbo S, Arsuaga J-L, Meyer M. 2013. Complete mitochondrial genome sequence of a middle Pleistocene cave bear reconstructed from ultrashort DNA fragments. Proc Natl Acad Sci 110:15758–63.

Darriba D, Taboada GL, Doallo R, Posada D. 2012. jModelTest 2: more models, new heuristics and parallel computing. Nat Methods 9:772–772.

Dunbabin TJ. 1979. The Western Greeks: The History of Sicily and South Italy From the Foundation of the Greek Colonies to 480 BC. Chicago: ARES Publisher Inc.

Edgar RC, Drive RM, Valley M. 2017. MUSCLE : multiple sequence alignment with high accuracy and high throughput. Nucleic Acids Res 32:1792–1797.

Excoffier L, Smouse PE, Quattro JM. 1992. Analysis of molecular variance inferred from metric distances among DNA haplotypes: Application to human mitochondrial DNA restriction data. Genetics 131:479–491.

De Fanti S, Barbieri C, Sarno S, Sevini F, Vianello D, Tamm E, Metspalu E, Van Oven M, Hübner A, Sazzini M, Franceschi C, Pettener D, Luiselli D. 2015. Fine dissection of human mitochondrial DNA haplogroup HV lineages reveals paleolithic signatures from European Glacial refugia. PLoS One 10:1–19.

Fletcher RN. 2007. Patterns of Imports in Iron Age Italy. Oxford: Archeopress.

Guido M. 1973. Southern Italy: An Archaeological Guide: The Main Prehistoric, Greek, and Roman Sites. New Jersey: Noyes Press.

Haak W, Lazaridis I, Patterson N, Rohland N, Mallick S, Llamas B, Brandt G, Nordenfelt S, Harney E, Stewardson K, Fu Q, Mittnik A, Bánffy E, Economou C, Francken M, Friederich S, Pena RG, Hallgren F, Khartanovich V, Khokhlov A, Kunst M, Kuznetsov P, Meller H, Mochalov O, Moiseyev V, Nicklisch N, Pichler SL, Risch R, Rojo Guerra M a., Roth C, Szécsényi-Nagy A, Wahl J, Meyer M, Krause J, Brown D, Anthony D, Cooper A, Alt KW, Reich D. 2015. Massive migration from the steppe was a source for Indo-European languages in Europe. Nature 522:207–211.

Handberg S, Jacobsen JK. 2011. Greek or Indigenous? From Potsherd to Identity in Early Colonial Encounters. In: Gleba M, Horsnaes HW, editors. Communicating Identity in Italic Iron Age Communities. Oxford: Oxford Books:177–197.

Hartl D, Clark A. 1997. Principles of Population Genetics. 3rd Editio. Sunderland, Massachusetts: Sinauer Associates.

Hofmanova Z, Kreutzer S, Hallenthal G, Sell C, Diekmann Y. 2016. Early farmers from across Europe directly descended from Neolithic Aegeans. Proc Natl Acad Sci 113:6886–6891.

Jones ER, Gonzalez-Fortes G, Connell S, Siska V, Eriksson A, Martiniano R, McLaughlin RL, Gallego Llorente M, Cassidy LM, Gamba C, Meshveliani T, Bar-Yosef O, Müller W, Belfer-Cohen A, Matskevich Z, Jakeli N, Higham TFG, Currat M, Lordkipanidze D, Hofreiter M, Manica A, Pinhasi R, Bradley DG. 2015. Upper Palaeolithic genomes reveal deep roots of modern Eurasians. Nat Commun 6: 8912.

Jones ER, Zarina G, Moiseyev V, Manica A, Pinhasi R, Bradley DG, Lightfoot E, Nigst PR. 2017. The Neolithic transition in the Baltic was not driven by admixture with early European farmers. Curr Biol 27:576–582.

Jónsson H, Ginolhac A, Schubert M, Johnson PLF, Orlando L. 2013. MapDamage2.0: Fast approximate Bayesian estimates of ancient DNA damage parameters. Bioinformatics 29:1682–1684.

Kearse M, Moir R, Wilson A, Stones-Havas S, Cheung M, Sturrock S, Buxton S, Cooper A, Markowitz S, Duran C, Thierer T, Ashton B, Meintjes P, Drummond A. 2012. Geneious Basic: An integrated and extendable desktop software platform for the organization and analysis of sequence data. Bioinformatics 28:1647–1649.

Kircher M, Sawyer S, Meyer M. 2012. Double indexing overcomes inaccuracies in multiplex sequencing on the Illumina platform. Nucleic Acids Res 40:1–8.

Krause J, Briggs AW, Kircher M, Maricic T, Zwyns N, Derevianko A, Pääbo S. 2010. A Complete mtDNA Genome of an Early Modern Human from Kostenki, Russia. Curr Biol 20:231–236.

Lazaridis I, Mittnik A, Patterson N, Mallick S, Rohland N, Pfrengle S. 2017. Genetic origins of the Minoans and Mycenaeans. Nature 548:214–218.

Lazaridis I, Patterson N, Mittnik A, Renaud G, Mallick S, Kirsanow K, Sudmant PH, Schraiber JG, Castellano S, Lipson M, Berger B, Economou C, Bollongino R, Fu Q, Bos KI, Nordenfelt S, Li H, de Filippo C, Prüfer K, Sawyer S, Posth C, Haak W, Hallgren F, Fornander E, Rohland N, Delsate D, Francken M, Guinet J-M, Wahl J, Ayodo G, Babiker H a., Bailliet G, Balanovska E, Balanovsky O, Barrantes R, Bedoya G, Ben-Ami H, Bene J, Berrada F, Bravi CM, Brisighelli F, Busby GBJ, Cali F, Churnosov M, Cole DEC, Corach D, Damba L, van Driem G, Dryomov S, Dugoujon J-M, Fedorova S a., Gallego Romero I, Gubina M, Hammer M, Henn BM, Hervig T, Hodoglugil U, Jha AR, Karachanak-Yankova S, Khusainova R, Khusnutdinova E, Kittles R, Kivisild T, Klitz W, Kučinskas V, Kushniarevich A, Laredj L, Litvinov S, Loukidis T, Mahley RW, Melegh B, Metspalu E, Molina J, Mountain J, Näkkäläjärvi K, Nesheva D, Nyambo T, Osipova L, Parik J, Platonov F, Posukh O, Romano V, Rothhammer F, Rudan I, Ruizbakiev R, Sahakyan H, Sajantila A, Salas A, Starikovskaya EB, Tarekegn A, Toncheva D, Turdikulova S, Uktveryte I, Utevska O, Vasquez R, Villena M, Voevoda M, Winkler CA, et al. 2014. Ancient human genomes suggest three ancestral populations for present-day Europeans. Nature 513:409–13.

Li H, Durbin R. 2009. Fast and accurate short read alignment with Burrows-Wheeler transform. Bioinformatics 25:1754-1760.

Malyarchuk B, Derenko M, Grzybowski T, Perkova M, Rogalla U, Vanecek T, Tsybovsky I. 2010. The peopling of Europe from the mitochondrial haplogroup U5 perspective. PLoS One 5:16–20.

Margaryan A, Derenko M, Hovhannisyan H, Malyarchuk B, Heller R, Khachatryan Z, Avetisyan P, Badalyan R, Bobokhyan A, Melikyan V, Sargsyan G, Piliposyan A, Simonyan H, Mkrtchyan R, Denisova G, Yepiskoposyan L, Willerslev E, Allentoft ME. 2017. Eight millennia of matrilineal genetic continuity in the South Caucasus. Curr Biol 27:2023–2028.

Meyer M, Kircher M. 2010. Illumina sequencing library preparation for highly multiplexed target capture and sequencing. Cold Spring Harb Protoc 5:10.1101/pdb.prot5448.

Omrak A, Günther T, Valdiosera C, Svensson EM, Malmström H, Kiesewetter H, Aylward W, Storå J, Jakobsson M, Götherström A. 2016. Genomic evidence establishes Anatolia as the source of the European Neolithic gene pool. Curr Biol 26:270–275.

van Oven M. 2015. PhyloTree Build 17: Growing the human mitochondrial DNA tree. Forensic Sci Int Genet Suppl Ser 5:392–394.

Pala M, Achilli A, Olivieri A, Kashani BH, Perego UA, Sanna D, Metspalu E, Tambets K, Tamm E, Accetturo M, Carossa V, Lancioni H, Panara F, Zimmermann B, Huber G, Al-Zahery N, Brisighelli F, Woodward SR, Francalacci P, Parson W, Salas A, Behar DM, Villems R, Semino O, Bandelt HJ, Torroni A. 2009. Mitochondrial haplogroup U5b3: a distant echo of the epipaleolithic in Italy and the legacy of the early Sardinians. Am J Hum Genet 84:814–821.

Pala M, Olivieri A, Achilli A, Accetturo M, Metspalu E, Reidla M, Tamm E, Karmin M, Reisberg T, Kashani BH, Perego UA, Carossa V, Gandini F, Pereira JB, Soares P, Angerhofer N, Rychkov S, Al-Zahery N, Carelli V, Sanati MH, Houshmand M, Hatina J, MacAulay V, Pereira L, Woodward SR, Davies W, Gamble C, Baird D, Semino O, Villems R, Torroni A, Richards MB. 2012. Mitochondrial DNA signals of late glacial recolonization of europe from near eastern refugia. Am J Hum Genet 90:915–924.

Pereira L, Richards M, Goios A, Alonso A, Albarrán C, Garcia O, Behar DM, Gölge M, Hatina J, Al-Gazali L, Bradley DG, Macaulay V, Amorim A. 2005. High-resolution mtDNA evidence for the late-glacial resettlement of Europe from an Iberian refugium. Genome Res 15:19–24.

Peruzzi B. 2016. Populating Peucetia: Central Apulian Grave Good Assemblages From the Classical Period (late 6th-3rd centuries B.C.). Unpublished PhD Dissertation, University of Cincinnat, Arts and Sciences: Classics.

Posth C, Renaud G, Mittnik A, Drucker DG, Rougier H, Cupillard C, Valentin F, Thevenet C, Furtwängler A, Wißing C, Francken M, Malina M, Bolus M, Lari M, Gigli E, Capecchi G, Crevecoeur I, Beauval C, Flas D, Germonpré M, Van Der Plicht J, Cottiaux R, Gély B, Ronchitelli A, Wehrberger K, Grigorescu D, Svoboda J, Semal P, Caramelli D, Bocherens H, Harvati K, Conard NJ, Haak W, Powell A, Krause J. 2016. Pleistocene mitochondrial genomes suggest a single major dispersal of non-africans and a late glacial population turnover in Europe. Curr Biol 26:827–833.

Renaud G, Slon V, Duggan AT, Kelso J. 2015. Schmutzi: estimation of contamination and endogenous mitochondrial consensus calling for ancient DNA. Genome Biol 16:1–18.

Renaud G, Stenzel U, Kelso J. 2014. LeeHom: Adaptor trimming and merging for Illumina sequencing reads. Nucleic Acids Res 42:e141.

Roostalu U, Kutuev I, Loogväli EL, Metspalu E, Tambets K, Reidla M, Khusnutdinova EK, Usanga E, Kivisild T, Villems R. 2007. Origin and expansion of haplogroup H, the dominant human mitochondrial DNA lineage in west Eurasia: The Near Eastern and Caucasian perspective. Mol Biol Evol 24:436–448.

Sánchez-Quinto F, Schroeder H, Ramirez O, Ávila-Arcos MC, Pybus M, Olalde I, Velazquez AM V, Marcos MEP, Encinas JMV, Bertranpetit J, Orlando L, Gilbert MTP, Lalueza-Fox C. 2012. Genomic affinities of two 7,000-year-old Iberian hunter-gatherers. Curr Biol 22:1494–1499.

Small A. 1992. Botromagno: An Introduction. In: Small A, editor. Gravina: An Iron Age and Republican Settlement in Apulia. Volume 1: London: British School at Rome:3–15.

Small A. 2002. Apulia before and after the Roman conquest: Recent evidence from Botromagno. J Rom Archaeol 15:375–379.

Soares P, Achilli A, Semino O, Davies W, Macaulay V, Bandelt HJ, Torroni A, Richards MB. 2010. The archaeogenetics of Europe. Curr Biol 20:174–183.

Soares P, Ermini L, Thomson N, Mormina M, Rito T, Röhl A, Salas A, Oppenheimer S, Macaulay V, Richards MB. 2009. Correcting for purifying selection: an improved human mitochondrial molecular clock. Am J Hum Genet 84:740–759.

Taylor J, Dorrell P, Small A. 1976. Gravina-Di-Puglia III Houses and a Cemetery of the Iron Age and Classical Period. Pap Br Sch Rome1 44:48–132.

La Torre GF. 2011. Reflections on the Lucanians and Bruttians in Calabria Between Hannibal and the Principate: Coloniae, Foederatae, Municipia. In: Colivicchi F, editor. Local Cultures of South Italy and Sicily in the Late Republican Period: Between Hellenism and Rome. Journal of Roman Archaeology, Supplementary Series Number 83:139-159.

Ward-Perkins J, Cotton M, Vander Poel H, Macnamara E, Taylor J, Carter A. 1969. Excavations at Botromagno, Gravina di Puglia: Second Interim Report, 1967-68. Pap Br Sch Rome 37:100–157.

Weissensteiner H, Pacher D, Kloss-Brandstätter A, Forer L, Specht G, Bandelt H-J, Kronenberg F, Salas A, Schönherr S. 2016. HaploGrep 2: mitochondrial haplogroup classification in the era of high-throughput sequencing. Nucleic Acids Res 44:58-63.

Chapter 3.0

Mapping the Origins of Imperial Roman Workers (1st – 4th century CE) at Vagnari, Southern Italy, using $^{87}Sr/^{86}Sr$ and $\delta^{18}O$ Variability

Matthew V. Emery[1,2], Robert J. Stark[1], Tyler J. Murchie[1,2], Spencer Elford[3], Henry P. Schwarcz[3], Tracy L. Prowse[1]

[1]Department of Anthropology, McMaster University, Hamilton, Canada
[2]McMaster Ancient DNA Centre, McMaster University, Hamilton, Canada
[3]School of Geography and Earth Sciences, McMaster University, Hamilton, Canada

Short Title: *Geographic Origins of Roman Imperial Workers, Southern Italy*

Key Words: oxygen and strontium isotopes; migration and mobility; Roman Italy; ArcGIS analysis; strontium isotope variation

Corresponding Author:

Matthew V. Emery, PhD Candidate*
Department of Anthropology, McMaster University
1280 Main St. West, L8S 4L8
Hamilton, Ontario, Canada
Home Phone: 905-515-1842
Work Phone Number: 905-525-9140 x 24423
emerymv@mcmaster.ca

3.1 Abstract

We obtained the oxygen and strontium isotope composition of teeth from Roman period (1^{st} – 4^{th} century CE) inhabitants buried in the Vagnari cemetery (southern Italy), and present the first strontium isotope variation map of the Italian peninsula using previously published data sets and new strontium data. We test the hypothesis that the Vagnari population was predominantly composed of local individuals, instead of migrants originating from abroad.

We analyzed the oxygen ($^{18}O/^{16}O$) and strontium ($^{87}Sr/^{86}Sr$) isotope composition of 43 teeth. We also report the $^{87}Sr/^{86}Sr$ composition of an additional 13 molars, $^{87}Sr/^{86}Sr$ values from fauna (n=10), and soil (n=5) samples local to the area around Vagnari. The $^{87}Sr/^{86}Sr$ variation map of Italy uses $^{87}Sr/^{86}Sr$ values obtained from previously published data sources from across Italy (n=199).

Converted tooth carbonate ($\delta^{18}O_{DW}$) and $^{87}Sr/^{86}Sr$ data indicate that the majority of individuals buried at Vagnari were local to the region. ArcGIS bounded Inverse Distance Weighting (IDW) interpolation of the pan-Italian $^{87}Sr/^{86}Sr$ dataset approximates the expected $^{87}Sr/^{86}Sr$ range of Italy's geological substratum, producing the first strontium map of the Italian peninsula.

Results suggest that only 7% of individuals buried at Vagnari were born elsewhere and migrated to Vagnari, while the remaining individuals were either local to Vagnari (58%), or from the southern Italian peninsula (34%). Our results are consistent with the suggestion that Roman Imperial lower-class populations in southern Italy sustained their numbers through local reproduction measures, and not through large-scale immigration from outside the Italian peninsula.

3.2 Introduction

Roman period mobility is traditionally studied through archaeological and epigraphic evidence, as well as Graeco-Roman texts, census data, and funerary inscriptions (e.g., Attema and van Leusen, 2004; Bagnall and Frier, 1994; Benelli, 2001; Curti, Dench, and Patterson, 1996; DeLigt and Tacoma, 2016; Noy, 2000). Documentary sources and archaeological evidence are useful for understanding mobility at a population level. However, isotopic data can be uniquely effective in investigating mobility at the individual and local level (e.g., Leach, Eckardt, Chenery and Müldner, 2010; Knudson, Tung, Nystrom, Price, and Fullagar, 2005; Knudson, Pestle, Torres-Rouff, and Pimentel, 2012), and at larger geographic scales, provided that adequate regional isotope information exists. A number of isotope studies have documented mobility in Roman Britain (e.g., Chenery, 2008; Chenery, Pashley, Lamb, Sloane, and Evans, 2010; Chenery, Eckardt, and Müldner, 2011; Eckardt et al., 2009, 2010; Eckardt, Müldner, and Lewis, 2014; Evans, Stoodley, and Chenery, 2006; Leach, Lewis, Chenery, Müldner, and Eckardt, 2009; Montgomery, Evans, Chenery, Pashley, and Killgrove, 2010; Müldner, Chenery, and Eckardt, 2011; Shaw, Montgomery, Redfern, Gowland, and Evans, 2016), with additional Roman cases reported from Bavaria (Schweissing and Grupe, 2003) and Croatia (Lightfoot, Šlaus, and O'Connell, 2014). In contrast, there are relatively few stable isotope studies that investigate mobility in Roman Italy, and those that have done so focus on the center of the Roman Empire around the city of Rome (e.g., Casal Bertone and Castellaccio Europarco), or nearby on the Tyrrhenian coast (e.g., Velia and Isola Sacra) (Prowse et al., 2007; Killgrove 2010a, b, c; Killgrove and Montgomery, 2016; Stark, 2017). Most of these sites are located in areas of Roman Italy expected to experience high levels of mobility due to their nature as either a bustling metropolis or a major port city. What is still poorly understood is life outside the urban

centers of the Roman world, that is, life for the vast majority of people living and working in rural Roman Italy. This study uses strontium and oxygen isotope analysis to investigate the degree and pattern of mobility at the rural site of Vagnari in southern Italy (Fig. 1), and explores what these results can tell us about the population history of southern Italy after its subjugation by the expanding Roman Empire.

The Imperial Roman cemetery at Vagnari (1^{st} – 4^{th} century CE) provides a unique opportunity to explore mobility and geographic origins of a rural working class population. These results are interpreted within a broader historical and archaeological context of the region, and debates about the source of Roman Imperial workers and slaves in rural Italy (e.g., Brunt, 1971; Lo Cascio, 1999; Scheidel, 2001, 2007). Further, the increased use of strontium isotope analysis as a tool to investigate mobility in Roman Italy has prompted our analysis of strontium isotope variation across the peninsula itself, in order to accurately provenance the strontium signatures obtained from Italian archaeological remains. The development of a strontium isotope variation map for Italy will greatly improve the ability of bioarchaeologists to identify potential regional origins of their archaeological samples.

3.3 The Genesis and Development of Roman Imperial Estates in Southern Italy

Prior to the 4^{th} century BCE, Rome was a small Republic while the rest of Italy was occupied by local indigenous Iron Age communities, along with a number of Greek colonies established along the southern coast of Italy from the 8^{th} through 3^{rd} centuries BCE. The Roman Republic began campaigns to extend its territory throughout the Italian mainland starting in the 5^{th} century BCE, and by the 3^{rd} century BCE southern Italy experienced political and social upheaval associated with military attempts at Roman expansion (e.g., the Pyrrhic and Punic

wars). During the second Punic War (c. 218 – 201 BCE), Rome confiscated the lands of Italian communities that opposed them, while granting financial freedom to the communities who remained loyal to the Republic (Rostovtzeff, 1971). The remaining southern Italian communities were either captured or abandoned. More confrontations between the indigenous Italians and the Roman Republic arose again during the Social Wars (91 – 88 BCE) (Bradley, 2000; Morley, 2001). By the end of these wars the Italic communities eventually capitulated under strain from the unrelenting economic pressure of the nascent Roman Empire (Wilson, 1966).

Some researchers posit that some lower class Roman labourers and slaves were acquired through military conquest during the Roman Republican period (509 – 27 BCE) (e.g., Bradley, 1987; Yavetz, 1988). As the Empire expanded, the demand for servile labour increased, and scholars have debated whether the lower class and slave populations of Roman Italy were maintained through immigration/importation from the new Roman-controlled frontiers, or through intra-community reproduction (Bradley, 1987; Harris, 1999; Scheidel, 2001, 2004, 2007). Scheidel (1997) and Harris (1999) suggest that North Africa and the Near East were the main geographic regions of origin of foreign, non-Italian workers or slaves. It is unknown, however, what fraction of these individuals (and their families) was forced, or willing, to migrate to Italy to work for wealthy Roman patricians and managers of Imperial estates (Scheidel, 1999).

After the continued expansion of the Roman Republic throughout Italy in the 2nd century BCE, some of the local southern Italian indigenous populations were conscripted into working on rural villas and estates (Bradley, 1994; Rathbone, 1983). Vagnari was one such Imperial estate, located 14 km northeast of Gravina in Puglia (Fig. 1). The Roman phase of Vagnari is composed of a core central village (*vicus*) and a cemetery for its inhabitants, in use between the 1st and 4th centuries CE (Carroll, 2014; Carroll and Prowse, 2014; Small 2011). The first

excavations of the cemetery began in 2002 and over 140 burials have been excavated to-date. The *'alla cappuccina'* tombs commonly found in the cemetery are constructed out of large *tegulae* (roof tiles) arranged in a gabled pattern over the body, occasionally with *tegulae* placed under the body or interred without *tegulae* in a simple pit (Small and Small, 2005; Prowse, Barta, von Hunnius, and Small, 2010). Libation tombs are another prominent grave structure in the cemetery. These are tile burials connected to the surface through a vertical tube made of curved tiles for the purpose of making offerings to the dead (Prowse, 2016). Grave goods include plain-ware and painted pots, bent iron nails, lamps, glass vessels, bronze coins, bone pins, iron blades, and hobnails (Brent and Prowse, 2014; Prowse, Barta, von Hunnius, and Small, 2010). Some graves contained select jewelry items, such as bracelets, rings, and pendants, which were typically manufactured out of iron or bronze alloy (Brent and Prowse, 2014; Small and Small 2005). While imported items are present in some of the burials (e.g., African Red slip wares, Butrint pottery from Albania), there is no clear evidence for the presence of 'foreigners' based on atypical grave goods in the burials. Several inscribed tombstones of Imperial freedmen have been recovered from the surrounding countryside; however, no funerary inscriptions have been found at Vagnari (Prowse, 2016), so there is no biographical information about the people who were living and working on this site. Thus, the composition of this population as local tenants or imported workers (or slaves) remains unknown. A preliminary oxygen isotope and ancient DNA (aDNA) analysis of the Vagnari assemblage reported little isotopic and maternal genetic (mitochondrial DNA) variability. However, Prowse et al. (2010) identified two individuals from the Vagnari sample with mtDNA haplogroups characteristic of African (haplogroup L) and eastern Eurasian (haplogroup D) maternal descent, providing tantalizing evidence of foreign-born members of this population. The Vagnari sample represents one of the largest skeletal

collections from Roman southern Italy, and presents an opportunity to investigate the lives and mobility of rural residents in this relatively unexplored region of the Roman Empire.

Figure 1: Map of Italy showing the location of Vagnari, indicated by a star (Image – T. Murchie and M. Emery).

3.4 The Strontium and Oxygen Isotope Composition of Tooth Enamel

The oxygen ($^{18}O/^{16}O$) and strontium ($^{87}Sr/^{86}Sr$) isotope composition of teeth is correlated with the isotope composition of the food and water ingested at the time of tissue formation (Bentley, 2006; Bowen, 2010). The crowns of deciduous molars form *in utero* and therefore reflect the $^{18}O/^{16}O$ and $^{87}Sr/^{86}Sr$ dietary sources ingested by the mother at the time of formation, beginning approximately 14-20 weeks post-fertilization (Scheuer and Black, 2000). The crowns of the 1st permanent molars begin mineralization at birth and are complete between the ages of two to four years, while the 2nd molar crowns initiate development around three-and-a-half years of age, and are complete between the ages of six to eight years (White and Folkens, 2005). The 3rd molar crowns initiate and terminate mineralization between the ages of eight and 14 years (Scheuer and Black, 2000; White and Folkens, 2005). Since tooth development, mineralization, and eruption rates are well known, it is possible to obtain isotopic information from birth up to age ~18 years of age from teeth, thus providing information on whether an individual was local to the area during childhood.

The $^{87}Sr/^{86}Sr$ ratio is useful in migration studies because the $^{87}Sr/^{86}Sr$ of regional soils is incorporated into plant tissues and passed on unaltered by the metabolism of consumers throughout the food chain (Beard and Johnson, 2000; Flockheart, Kyeser, Chipley, Miller, and Norris, 2015). Strontium (^{87}Sr) is incorporated into bone and tooth bioapatite via ionic substitution for calcium (Ca), providing a way in which to identify where individuals were residing when those tissues were formed (Burton, Price, and Middleton, 1999; Burton, Price, Cahue, and Wright, 2003). Strontium isotope values obtained from archaeological human remains can, in turn, be compared to regional $^{87}Sr/^{86}Sr$ variation maps (provided they exist for the region in question), or to locally derived faunal $^{87}Sr/^{86}Sr$ values (i.e. bioavailable sources) as

a means to identify individuals who fall within or outside local $^{87}Sr/^{86}Sr$ ranges.

Alteration of mineral bioapatite is influenced by diagenetic factors from the surrounding burial environment (Kohn, Schoeninger, and Barker, 1999). However, it is generally accepted that tooth enamel is less susceptible to diagenetic modifications than bone bioapatite and tooth dentine due to their smaller crystalline structure and larger pore spaces (Hoppe, Koch, and Furutani, 2003; Lee-Thorp and Sponheimer, 2003). Overlapping $^{87}Sr/^{86}Sr$ values are problematic across geographic regions with a high degree of geological variation, making it difficult to provenance human strontium values with accuracy. The best solution to this problem is to integrate strontium isotope data with another provenance-based isotope, such as oxygen.

The oxygen isotope composition of human skeletal tissue reflects the $^{18}O/^{16}O$ composition of ingested water at the time of bone and tooth development, and is captured as either CO_3 or PO_4 in mineral hydroxyapatite, $Ca_{10}(PO_4)_6(OH)_2$. $^{18}O/^{16}O$ variation in meteoric precipitation (rainwater) is determined by thermal and geographic variables, such as distance from the coast, latitude, altitude, and evapotranspiration, as well as groundwater exchange with ^{18}O from geological sources, and $^{18}O/^{16}O$ mixing with river systems fed by high altitude precipitation (Gat, 2005; Lightfoot and O'Connell, 2016). Culturally mediated factors, like brewing and stewing have been shown to slightly alter the oxygen isotope values of water consumed with food by enriching ^{18}O (due to the preferential evaporation of ^{16}O during boiling) before entering the body (Brettell, Montgomery, and Evans, 2012). Breastfeeding also enriches ^{18}O in developing tissues, an enrichment that has been documented in the crowns of permanent 1^{st} molars, and requires adjustment by -0.7‰ to control for this trophic level effect (TLE) from nursing (Wright and Schwarcz, 1998; Britton, Fuller, Tütken, Mays, and Richards, 2015).

GNIP (Global Network for Isotopes in Precipitation) stations monitor global $^{18}O/^{16}O$

variability across the planet. These data provide a substantial database from which to build $^{18}O/^{16}O$ variation maps for particular geographic regions (GNIP, 2015). Oxygen ($^{18}O/^{16}O$) ratios are denoted as δ values in parts per mil (‰, or parts per thousand), and calculated using the following equation (VSMOW) (Hoefs, 2004):

$$\delta^{18}O = \left(\frac{R(sample) - R(standard)}{R(standard)}\right) \times 1000$$

where $R=^{18}O/^{16}O$ is the sample being examined, and standard refers to an international measurement standard (e.g., NBS-19).

Previous research showed that bone and tooth PO_4 is strongly correlated with $\delta^{18}O$ of precipitation, allowing for a direct comparison between drinking water ($\delta^{18}O_{DW}$) and isotopic analysis of skeletal PO_4 (Daux et al., 2008; Longinelli, 1984; Luz, Kolodny, and Horowitz, 1984). It is also possible to obtain this information from $\delta^{18}O$ analyses of the CO_3 component of bone and tooth mineral ($\delta^{18}O_C$) (Iacumin, Bocherens, Mariotti, and Longinelli, 1996). In this study we use the equation devised by Chenery, Pashley, Lamb, Sloane, and Evans (2012) for enamel carbonate to estimate the oxygen isotopic composition of ancient drinking water.

3.5 Materials and Methods

The Vagnari dental sample used in this study is comprised of 43 permanent M1s, four permanent M2s, three permanent M3s, four deciduous m1s, and one deciduous m2. We were not able to measure the $^{18}O/^{16}O$ composition of 13 teeth, restricting the bivariate (bagplot) analysis to 43 teeth, with each tooth representing one individual. Consequently, a large portion of the teeth with only $^{87}Sr/^{86}Sr$ values, including the $^{87}Sr/^{86}Sr$ Vagnari faunal and soil samples, were solely subject to univariate analysis. Three ungulate teeth were collected from the Vagnari assemblage, and five ungulate teeth, two snail shells, and five soil samples were collected from the nearby (10 km East of Vagnari) Iron Age sites at Botromagno and Parco San Stefano (7^{th} – 4^{th} centuries

BCE) as a means to determine the local (bioavailable) $^{87}Sr/^{86}Sr$ variation of the landscape.

3.5.1 Age and Sex Determination

Age and sex of the Vagnari sample was assessed using standard osteological methods outlined by Buikstra and Ubelaker (1994). Adult age was determined using the pubic symphysis, auricular surface of the innominate, and cranial suture closure. Adult sex was assessed using the morphology of the pelvis and cranium. Subadult and juvenile age was estimated based on tooth development and eruption, and epiphyseal fusion of the long bones. Sex was not estimated for subadults and juveniles.

3.5.2 $^{87}Sr/^{86}Sr$ Preparation and Analysis

Teeth were manually cleaned in distilled water, dried, drilled, and the resulting enamel powder dissolved in 1.3 ml of 4 M ultra-pure hydrochloric acid (HCl). Following dissolution the samples were centrifuged for 10 minutes and loaded into cation exchange columns (AG 50W-X12, 200-400 mesh cation exchange resin), the samples were eluted, and the resulting salts collected for analysis. Sr isotope fractionation was corrected to $^{86}Sr/^{88}Sr = 0.1194$. Strontium isotope of tooth enamel was measured using a dynamic multi-collection VG 354 thermal ionization mass spectrometer (TIMS) in the Radiogenic Isotope Laboratory of the School of Geography and Earth Sciences at McMaster University. Regular analysis of the NBS 987 standard gave an average $^{87}Sr/^{86}Sr$ value of 0.710246 with a population standard deviation of 0.000022 (1σ).

The methodology for oxygen isotope analysis is presented in Prowse (2016), where the data were originally published. All first molar $\delta^{18}O_C$ (carbonate) values were adjusted by -0.7‰

to control for the possible effects of weaning, which has been shown to enrich $\delta^{18}O$ values of pre-weaned teeth by approximately +0.7‰ (Wright and Schwarcz, 1998; Prowse, 2016).

3.5.3 $^{87}Sr/^{86}Sr$ Map Development

A number of $^{87}Sr/^{86}Sr$ variation maps have been produced for the purpose of provenancing $^{87}Sr/^{86}Sr$ values obtained from archaeological and forensic remains (e.g., Bataille and Bowen, 2012; Bataille, Laffoon, and Bowen, 2012; Brennan et al., 2014; Evans, Montgomery, Wildman, and Boulton, 2010; Hartman and Richards, 2014; Laffoon, Davies, Hoogland, and Hofman, 2012; Laffoon et al., 2017; Nafplioti, 2011; Voerkelius et al., 2010; Willmes et al., 2014), but there is currently no $^{87}Sr/^{86}Sr$ variation map for Italy. To remedy this lack of baseline information for the Italian peninsula, we constructed a $^{87}Sr/^{86}Sr$ variation map of Italy using archaeological human and faunal data, modern wine, beef, cheese, sediment, natural spring water, fossil, and tomato sauce, in addition to the faunal and soil $^{87}Sr/^{86}Sr$ results from this study (Supplement 1; Boari et al., 2008; Durante et al., 2015; Marchionni et al., 2013; Matano, Barbieri, Di Nocera, and Torre, 2005; Pellegrini et al., 2008; Petrini et al., 2015; Reinhardt, Cavazza, Patterson, and Blenkinsop, 2000; Rossmann et al., 2000; Rummel et al., 2012; Schülter, Steuber, and Parente, 2008; Trincherini, Baffi, Barbero, Pizzoglio, and Spalla, 2014; Vander Auwera and Andre, 1991; Voerkelius et al., 2010).

Biospheric $^{87}Sr/^{86}Sr$ is constrained by the $^{87}Sr/^{86}Sr$ composition of the underlying geological substrate, specifically the decay of $^{87}Rb \rightarrow ^{87}Sr$, and inversely reflects the amount of radiogenic ^{87}Rb (half-life = 48.8×10^9 years) in igneous, metamorphic, and siliciclastic rocks (Bataille and Bowen, 2012; Dickin, 2005). The non-radiogenic isotope ^{86}Sr fixes during initial mineral formation, and as a consequence, the $^{87}Sr/^{86}Sr$ ratio evolves according to its original $^{87}Sr/^{86}Sr$ and ^{87}Rb composition, and the decay of ^{87}Rb to ^{87}Sr (Bentley, 2006; Hodell, Quinn,

Brenner, and Kamenov, 2004). The $^{87}Sr/^{86}Sr$ composition of sedimentary carbonates evolves differently than siliciclastic sedimentary, metamorphic, or igneous rocks. Only trace amounts of Rb are contained in marine-derived carbonates, which reflect the $^{87}Sr/^{86}Sr$ of seawater at the time of their formation (Veizer, 1989). Prior research on the evolution of $^{87}Sr/^{86}Sr$ in carbonate rocks showed that the $^{87}Sr/^{86}Sr$ of seawater steadily increased from the late Cretaceous (~0.707) to the modern value of ~0.70924 (Veizer, 1989).

Since bioavailable and non-bioavailable (i.e., whole-rock, fossil, and spring water) sources of ^{87}Sr and ^{86}Sr are constrained by the evolution of the geological substrate from which they derive (Bowen, 2010), the strontium isotope ranges should approximate the predicted $^{87}Sr/^{86}Sr$ composition of the regional substratum (Supplement 1; Atlante Tematico d'Italia, 1989). We recognize the complex geological processes associated with modeling $^{87}Sr/^{86}Sr$ from non-bioavailable sources, and across large geographic regions (e.g., mixing, transportation, small datasets, contribution of atmospheric Sr, intra-whole rock $^{87}Sr/^{86}Sr$ variation) and present this as a preliminary strontium map, using a mixture of bioavailable and geological $^{87}Sr/^{86}Sr$ values, that contributes to a future, more finely resolved strontium variation map of Italy.

We collected the $^{87}Sr/^{86}Sr$ values from data sets spanning the Italian peninsula (n=199) and generated a strontium map based on those sample points. $^{87}Sr/^{86}Sr$ values for locations with more than one strontium isotope value were averaged and digitized into a cloud hosted GIS-system and attributed $^{87}Sr/^{86}Sr$ values were assigned to each individual polygon-point. The entire spatial dataset was then imported into ArcMap version 10.4 through one of two methods: i) the data were imported through ArcGIS and housed within a referenced feature dataset (UTM zone 33n), then saved as a "Shapefile" or Feature Class, or ii) the data were downloaded as a CSV file containing both longitude and latitude points then imported as a table into ArcMap as XY data.

The $^{87}Sr/^{86}Sr$ values were interpolated using the bounded Inverse Distance Weighting (IDW) function under geo-processing tools. The output was evaluated against the processing extent defined by ArcMap environments. IDW parameters were then adjusted to best fit the average $^{87}Sr/^{86}Sr$ values for each sample point.

3.6 Results

The corrected $\delta^{18}O_{DW}$ results for 43 molars used in this study range between -10.2‰ and -3.2‰ (mean = -7.1‰; 1σ = 1.2‰; 2σ = 2.5‰) suggesting differential access to water sources by the Vagnari occupants outside of the regional $\delta^{18}O$ range (-8‰ to -6‰) during childhood (Table 1) (Giustini et al., 2016; Prowse, 2016). The $^{87}Sr/^{86}Sr$ results for the 56 molars range between 0.70705 and 0.71064 (mean = 0.70862; 1σ = 0.00055; 2σ = 0.00111) (Table 1). Faunal and soil $^{87}Sr/^{86}Sr$ values fall within a small range, 0.70802 - 0.70901, for the site (mean= 0.70867; 1σ=0.00023; 2σ=0.00046) (Table 2). For individuals discernible by sex (Females n=16; Males n=20) a Mann-Whitney-Wilcoxon *t* test determined no significant differences between male and female $\delta^{18}O_{DW}$ (p = 0.8735) and $^{87}Sr/^{86}Sr$ (p = 0.8112) values, suggesting no significant differences in access to food and water between the sexes as children.

Table 1: Converted $\delta^{18}O_C$ (VPDB-VSMOW), $\delta^{18}O_{DW}$ and $^{87}Sr/^{86}Sr$ values for 43 individuals, and $^{87}Sr/^{86}Sr$ values for an additional 13 molars obtained from the Vagnari dental assemblage. Identified males and females (represented by the letter M and F, respectively), and unidentified sex (represented by the letter U), estimated using the methods outlined by Buikstra and Ubelaker (1994). Cappucina and libation burials are denoted as cap and lib, respectively, and disturbed as 'dist'.

Sample ID	Tooth Sampled	Burial Type	Age	Sex	$\delta^{18}O_C$ VPDB (‰)	$\delta^{18}O_C$ (VPDB) Adjusted - 0.7‰	$\delta^{18}O_C$ VSMOW (‰)	$\delta^{18}O_{DW}$ VSMOW (‰)	$^{87}Sr/^{86}Sr$
F35	M1	libation	adult	M	-4.6	-5.3	25.3	-8.2	0.70856
F39	molar crown	cap	3 yrs ± 12 mo.	U	-3.3	-4	26.7	-6.1	0.70865
F40	M1	cap	15-17 yrs	F	-3.8	-4.5	26.2	-6.9	0.7072

F42	M1	cap	28.7 yrs ± 6.5	M	-4.1	-4.8	25.9	-7.4	0.70857
F42A	M1	dist	adult	M	-4.4	-5.1	25.6	-7.9	0.70705
F49	M1	cap	8 yrs ± 2 yrs	U	-5.8	-6.5	24.1	-10.2	0.70812
F55	M1	cap	5-6 yrs	U	-3.8	-4.5	26.2	-6.9	0.70858
F59	M1	lib	5 yrs ± 6 mo.	U	-3.6	-4.3	26.3	-6.6	0.7072
F67	M1	cap	19-21 yrs	M	-4.6	-5.3	25.4	-8.1	0.70971
F92A	M1	cap	old adult	M	-3.5	-4.2	26.5	-6.4	0.70869
F92B	M3	cap	old adult	M	-3.9	-4.6	26.1	-7	0.70861
F93	M1	cap	adult	F	-4.2	-4.9	25.8	-7.5	0.70852
F95	M1	cap	young adult	F	-3.7	-4.4	26.3	-6.7	0.70863
F96A	M1	dist	adult	M	-4	-5	25.7	-7.6	0.70827
F117	M1	cap	20-25	F	-3.5	-4.2	26.5	-6.4	0.70882
F126	M1	cap	20-25 yrs	M	-3.3	-4	26.7	-6	0.70863
F127	M1	dist	15-20 yrs	F	-4.8	-5.5	25.2	-8.5	0.70862
F130	M1	dist	old adult	F	-1.5	-2.2	28.6	-3.1	0.70829
F131	M1	lib	35.2 ± 9.4	M	-2.1	-2.8	27.9	-4.1	0.70837
F132	M1	dist	15-16 yrs	F	-4.1	-4.8	25.9	-7.4	0.70899
F137A	M1	tile	21-24 yrs	M?	-3.7	-4.4	26.3	-6.7	0.70871
F200	M2	cap	old adult	M?	-4	-4.7	25.9	-7.3	0.70867
F204	M1	cap	39.4 ± 9.1	F	-3.9	-4.6	26.1	-7	0.70868
F205	M3	cap	young adult	F	-4.3	-5	25.7	-7	0.70863
F206	M1	cap	old adult	F	-3.9	-4.6	26.1	-7	0.70826
F207	M1	cap	young adult	M	-3.3	-4	26.7	-6.1	0.7085
F208	M1	cap	12-14.5 yrs	F?	-3.8	-4.5	26.2	-6.8	0.70779
F209	M1	lib	14-16 yrs	F	-3.7	-4.4	26.3	-6.7	0.70913
F210	M1	cap	9 yrs ± 24 mo	U	-4.9	-5.6	25.1	-8.7	0.70865
F211	M1	cap	young adult	F	-2.8	-3.5	27.2	-5.3	0.7088
F212	M1	cap	adult	U	-4.8	-5.5	25.2	-8.5	0.70861
F214	M1	cap	45-59 yrs	M	-4	-4.7	26	-7.1	0.70895
F215	M1	cap	38.2 ± 10.9	F	-3.8	-4.5	26.2	-6.9	0.70866
F216	M1	cap	35.2 ± 9.4	M	-3.6	-4.3	26.4	-6.5	0.70875
F220	M2	cap	40-44 yrs	M	-4.1	-4.8	25.8	-7.4	0.70877
F226	M1	cap	8.0 yrs	U	-5.2	-5.9	24.8	-9.2	0.7084
F231	M1	lib	adult	M	-3.3	-4	26.7	-6.1	0.70974
F234	M1	cap	35.2 ± 9.4	M	-4.9	-5.6	25.1	-8.6	0.70801
F235	M1	soil	50 yrs ± 12.6	M	-2.8	-3.5	27.2	-5.2	0.70916
F245	M1	cap	19-22 yrs	F	-4	-4.7	26	-7.2	0.70864
F249	M1	cap	adult	M?	-4.4	-5.1	25.5	-7.9	0.70857

F250	M1	cap	35-39 years	M	-4	-4.7	26	-7.1	0.70792
F252	M1	cap	17-22.5 yrs	F	-4.9	-5.6	25.1	-8.7	0.70868
F246	M1	cap	Adult	U	-	-	-	-	0.70865
F247	M1	cap	Old Adult	M	-	-	-	-	0.70863
F248	M1	cap	~20 years	M	-	-	-	-	0.70878
F280	M1	cap	Adult	F?	-	-	-	-	0.70912
F287	M2	cap	Old Adult	M	-	-	-	-	0.70917
F286A	M1	cap	16-18 years	U	-	-	-	-	0.7087
F286B	M1	cap	13-14 years	U	-	-	-	-	0.70894
F288	M1	cap	30-40 years	M	-	-	-	-	0.70856
F294	M2	cap	Old Adult	M	-	-	-	-	0.70878
F296	M1	cap	25-29	F	-	-	-	-	0.70868
F298	M1	cap	Adult	U	-	-	-	-	0.71064
F306	M1	cap	Adult	F	-	-	-	-	0.70889
F312	M1	cap/soil	Young Adult	M	-	-	-	-	0.70868

Table 2: The $^{87}Sr/^{86}Sr$ composition of faunal (n=10) and soil (n=5) samples collected from the cemeteries at Vagnari and Botromagno.

Sample ID	Material Sampled	$^{87}Sr/^{86}Sr$
FS186	Ungulate Tooth	0.70802
FS188	Ungulate Tooth	0.70874
FS195	Ungulate Tooth	0.70849
FSPSS	Ungulate Tooth	0.70851
FSG67	Ungulate Tooth	0.70865
FSG66	Ungulate Tooth	0.70855
FSP13	Ungulate Tooth	0.70866
FSS73	Ungulate Tooth	0.70877
SST15	Soil	0.70878
SSB70	Soil	0.70886
SST11	Soil	0.70881
SSG66	Soil	0.70872
SST1968	Soil	0.7087
FS189A	Snail Shell	0.70901
FS189B	Snail Shell	0.7089

Bivariate bagplot analysis of the $^{87}Sr/^{86}Sr$ and $\delta^{18}O_{DW}$ for 43 molars was conducted in R statistical programming using the package *aplpack* (Fig. 2). Three individuals (F67, F131, F231) were identified as outliers, while the remaining sample points fall within the fence of the bagplot for both $\delta^{18}O$ and $^{87}Sr/^{86}Sr$ datasets (Lightfoot and O'Connell, 2016). A univariate statistical comparison between the faunal and soil $^{87}Sr/^{86}Sr$ values and the $^{87}Sr/^{86}Sr$ obtained from human molars indicate that 7/56 (13%) of the $^{87}Sr/^{86}Sr$ values sampled fall outside the local $^{87}Sr/^{86}Sr$ for the site (Fig. 3; Table 2). These results are consistent with the original interpretation of solely the $\delta^{18}O$ data by Prowse (2016), in which it was determined that 9% of the sample was not local to Vagnari.

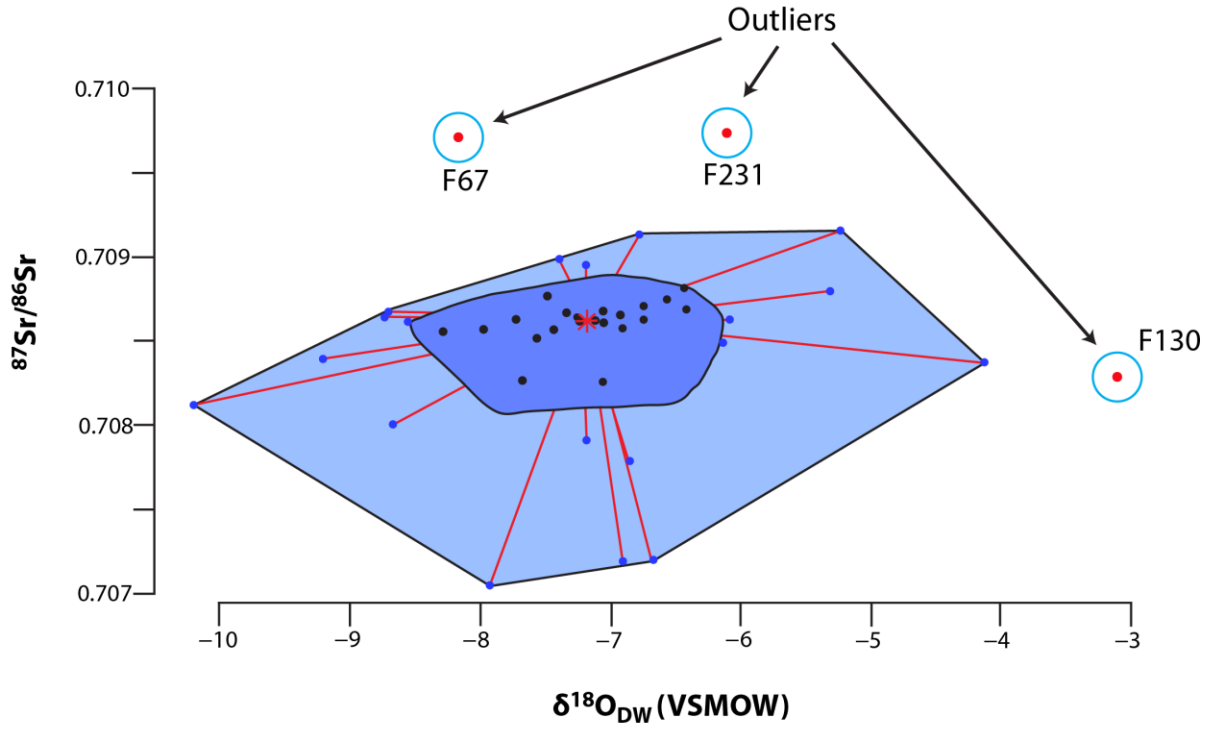

Figure 2: A bagplot (bivariate boxplot) diagram depicting the relationship between $\delta^{18}O$ and $^{87}Sr/^{86}Sr$. Statistical outliers are represented by red dots outside of the bag and circled in black. The bagplot (also known as a starburst plot) was generated using R's statistical package, *aplpack*.

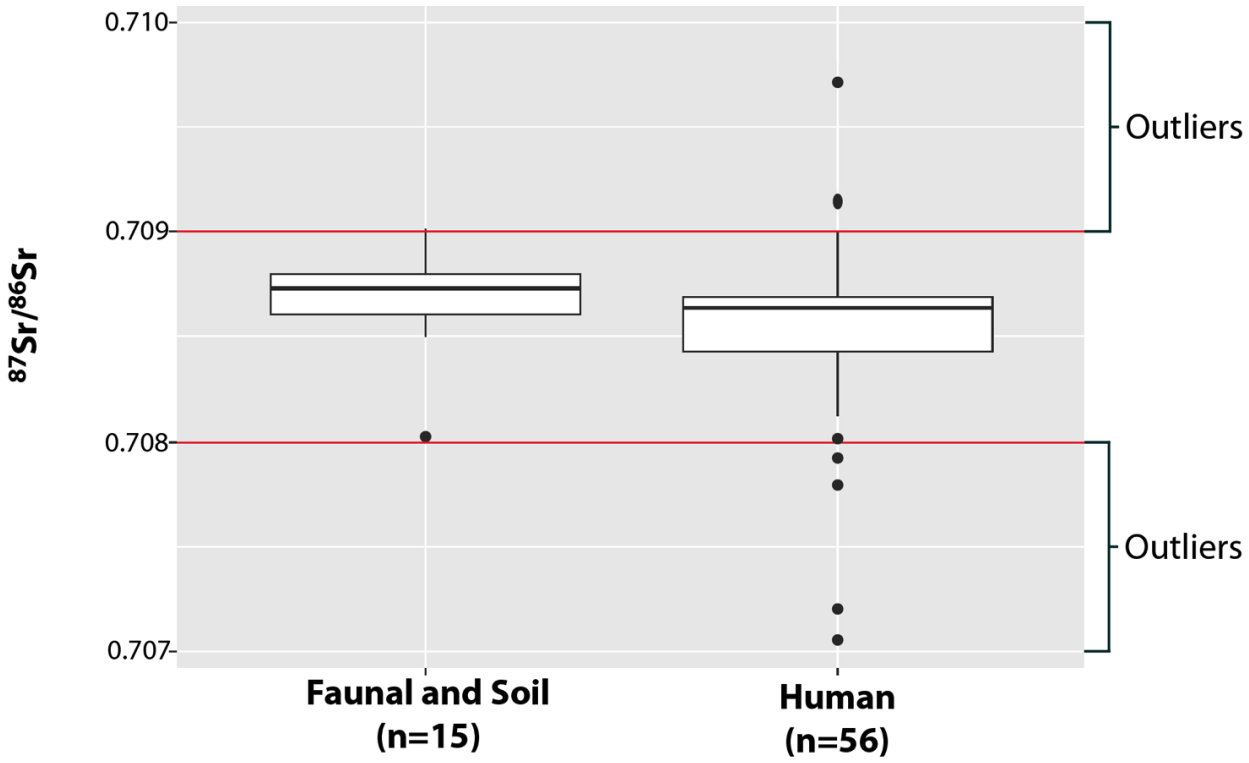

Figure 3: A Univariate (boxplot) comparison between the faunal, soil, and human tooth (molars) $^{87}Sr/^{86}Sr$ values. The red lines represent the $^{87}Sr/^{86}Sr$ baseline range (i.e. 0.708-0.709) for Vagnari. Individuals falling outside the red lines represent potential migrants at the site.

3.7 Discussion

3.7.1 Defining the $^{87}Sr/^{86}Sr$ and $^{18}O/^{16}O$ Variation of the Italian Peninsula

As expected, the $^{87}Sr/^{86}Sr$ range (~0.70370 - 0.77600) of the Italian peninsula reflects Italy's complex geological history (Fig. 4). The distribution of $^{87}Sr/^{86}Sr$ across the Italian landmass follows a North/South gradient, with higher $^{87}Sr/^{86}Sr$ values (i.e. > 0.710) concentrated in the Italian Alps. These high $^{87}Sr/^{86}Sr$ values are characteristic of the older granitic and metamorphic sequences that define the alpine late Mesozoic and Cenozoic-era orogeny (d'Italia, 1989). $^{87}Sr/^{86}Sr$ variation of central and southern Italy typically ranges less than 0.710,

constrained by carbonate CO_3 (including dolomites, $CaMg(CO_3)_2$), evaporite ($CaSO_4$), and young igneous (i.e. Rome, Naples, and eastern Sicily) geological substrate of the rest of the peninsula. This is especially apparent in southern Italy, where large limestone outcrops (deposited between the Jurassic and Miocene, 135 - 5.3 mya) and their associated weathered products (dating between the Pliocene and Quaternary, ~ 5.3 mya to 11.5 kya), cover the landscape (with the exception of western Calabria where older Paleozoic granites are predominant). Since marine-derived carbonates fix $^{87}Sr/^{86}Sr$ composition at their time of formation, and research has shown that the $^{87}Sr/^{86}Sr$ composition of seawater has steadily increased from ~0.707 during the late Cretaceous Period to the modern-day seawater value of 0.70924, the $^{87}Sr/^{86}Sr$ ranges defined by our bounded IDW algorithm fits within this expected range based on the collected sample points for the southern peninsula (i.e. 0.707 to 0.709; Fig. 4) (Veizer, 1989).

Longinelli and Selmo (2003) constructed the first $\delta^{18}O$ gradient map of the Italian peninsula, resulting in an approximate $\delta^{18}O$ range of precipitation between > -5‰ and <-9‰. However, a recent $\delta^{18}O$ variation map utilizing GNIP points (n=56) and an additional 210 points obtained from previously compiled $\delta^{18}O$ data increased the lower limit of the $\delta^{18}O$ range to < -12‰ (Fig. 5; Giustini et al., 2016). As expected, the $\delta^{18}O$ variation of Italy follows an East/West gradient with higher values measured along the Tyrrhenian coastline and the Salentine peninsula (> -6‰), and lower values measured further inland progressing towards the Apennines and North of the Alps (~ -7‰ and -12‰) (Longinelli and Selmo, 2003; Giustini et al., 2016).

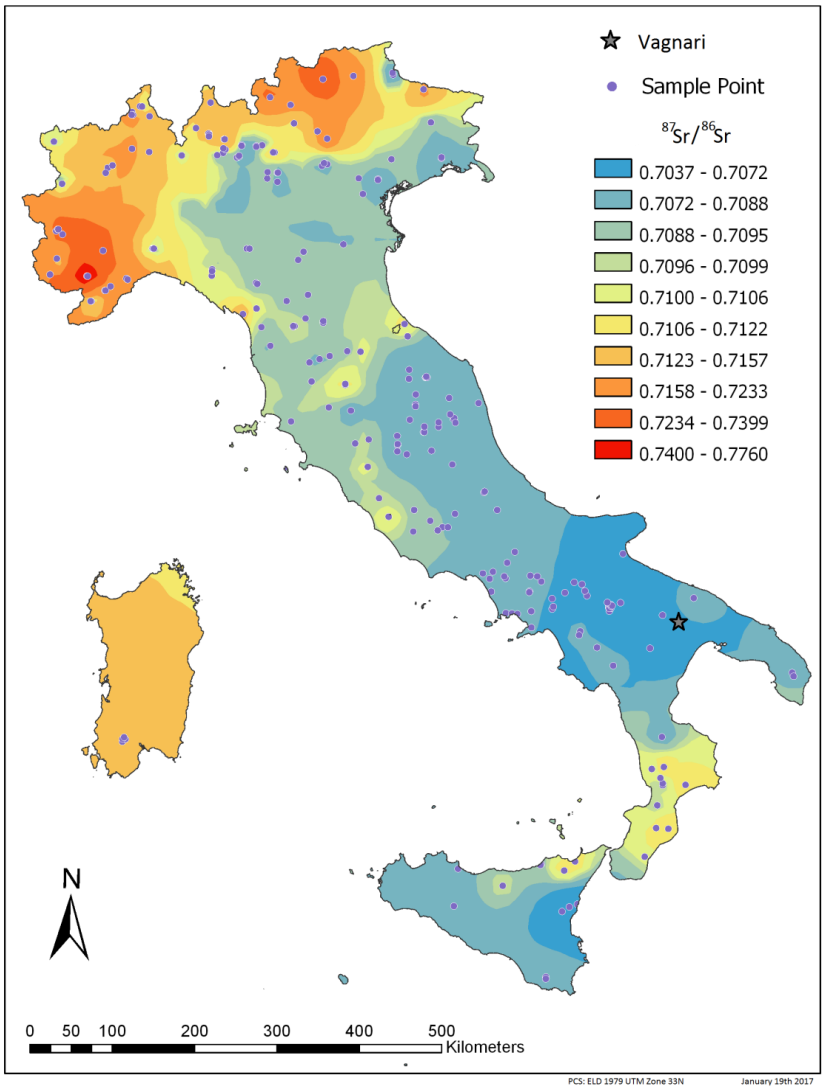

Figure 4: $^{87}Sr/^{86}Sr$ variation map of the Italy using disparate sources of $^{87}Sr/^{86}Sr$ sources and interpolated using a bounded Inverse Distance Weighting (IDW) algorithm (Supplementary Table S1) (Image – M. Emery and T. Murchie).

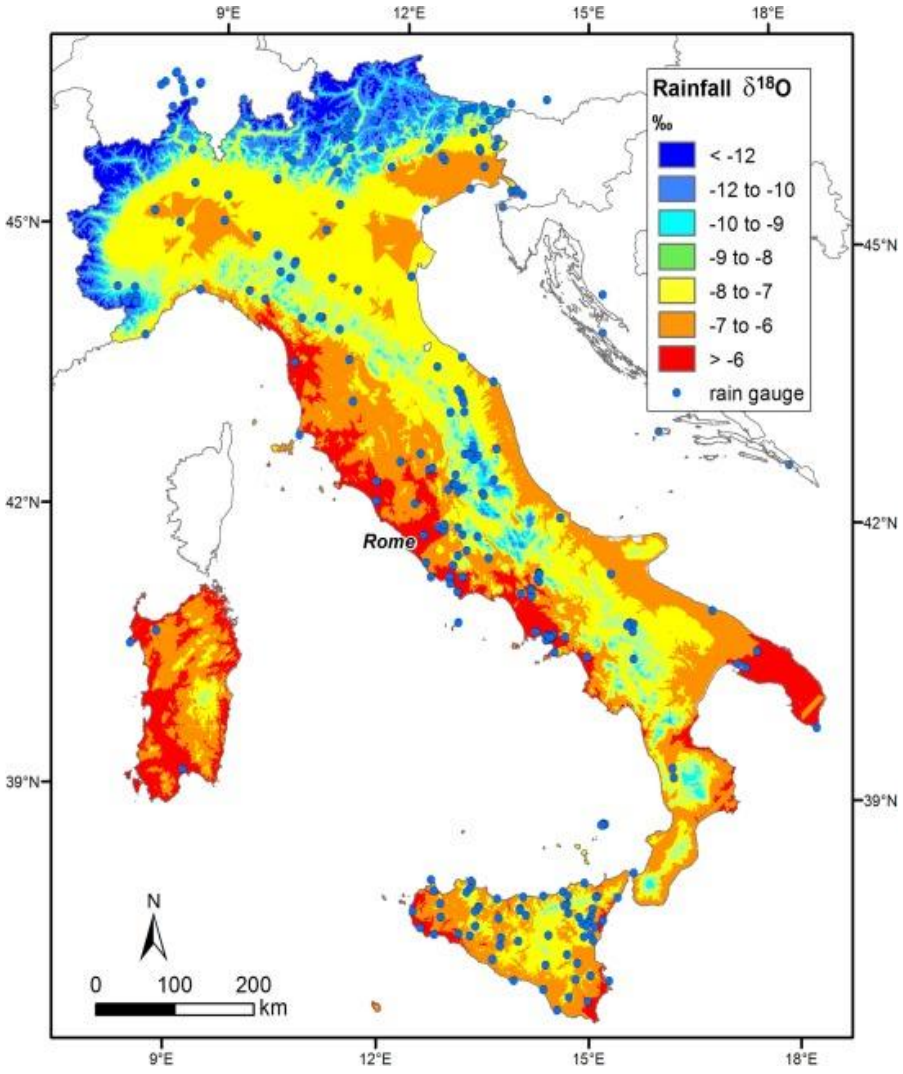

Figure 5: Map of spatial distribution of δ18O (‰) of precipitations in Italy (as published in Giustini et al., 2016).

3.7.2 The Regional Origins of the Vagnari Sample

The $^{87}Sr/^{86}Sr$ results for 56 molars suggest that a total of 49/56 individuals (88%; Fig. 3 and 13) originated from the region of Vagnari and/or the southern Italian peninsula. These results conform to the measured spatial $^{87}Sr/^{86}Sr$ variation for the southern Italian region, according to our $^{87}Sr/^{86}Sr$ variation map (Fig. 4; Table S1). However, restricting bagplot analysis to the 43 individuals with $^{87}Sr/^{86}Sr$ and $\delta^{18}O_{DW}$ values (Fig. 2), the number of potential locally born

individuals at Vagnari increases to (93%, 40/43 individuals) with respect to the measured intra-sample $^{87}Sr/^{86}Sr$ and $\delta^{18}O_{DW}$ variability. Interestingly two outliers (F67 and F231) identified in Figure 2 fall within the $^{87}Sr/^{86}Sr$ and $\delta^{18}O_{DW}$ variation of South Italy, despite falling outside the statistical range of within-sample $^{87}Sr/^{86}Sr$ and $\delta^{18}O_{DW}$ variation (Fig. 2 and Fig. 6), suggesting that although they were not local to Vagnari, they were likely local to the southern end of the peninsula. Instead, a different pair of young individuals, F49 and F226, are identified as non-local to the southern peninsula, based on their $\delta^{18}O_{DW}$ values (-10.2‰ and -9.2‰, respectively), which fall lower than the measured meteoric precipitation $\delta^{18}O_{DW}$ range (-8‰ to >-6‰) for Puglia and Basilicata (Fig. 5; Giustini, et al., 2016; Longinelli and Selmo, 2003). These two individuals, both with an estimated age-at-death of 8 years of age, likely originated from central Calabria (see Giustini et al., 2016), near the Apennine mountain range of central Italy, or northern Italy, geographic areas with associated $^{87}Sr/^{86}Sr$ ranges that span the $^{87}Sr/^{86}Sr$ values obtained for F49 (0.70812) and F226 (0.7084). The $\delta^{18}O_{DW}$ value for one individual, F130, was significantly higher than the rest of the sample, measured at -3.1‰, but with an associated $^{87}Sr/^{86}Sr$ value of 0.70829, a value characteristic of the limestones that compose the eastern Mediterranean basin rim (Roveri et al., 2014). F130 possibly originated from North Africa or southern Spain, areas where meteoric $\delta^{18}O_{DW}$ reach as high as -3‰. The remaining 40 individuals have $^{87}Sr/^{86}Sr$ and $\delta^{18}O_{DW}$ values that fall within the $^{87}Sr/^{86}Sr$ and $\delta^{18}O_{DW}$ range for southern Italy. Notably, 25 individuals (58%) have $^{87}Sr/^{86}Sr$ and $\delta^{18}O_{DW}$ values that place their geographic origins directly at Vagnari, suggesting that over half of the Vagnari sample spent their childhoods and, presumably, their entire adult lives on the Imperial estate (Fig. 6).

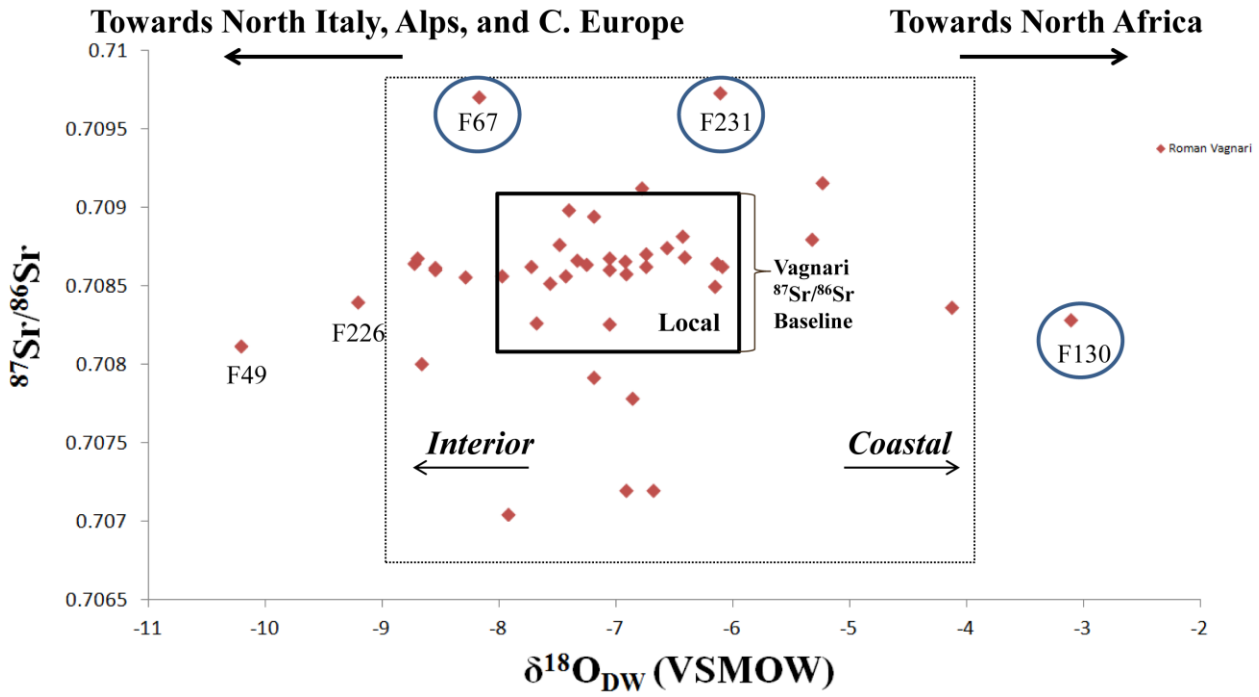

Figure 6: The $^{87}Sr/^{86}Sr$ and $\delta^{18}O_{DW}$ relationship for 43 individuals recovered from the Vagnari necropolis. Individuals circled in blue (F67, F231, and F130) were isolated as outliers in the bagplot (Fig. 2). Samples in the solid black line fall within the $^{87}Sr/^{86}Sr$ and $\delta^{18}O_{DW}$ range for Vagnari. Individuals outside the solid line but within the dashed black line likely originated from South Italy, as these samples fall within the broader $^{87}Sr/^{86}Sr$ and $\delta^{18}O_{DW}$ range of the southern peninsula. Again, three individuals (F49, F226, and F130) fall outside the southern Italian $^{87}Sr/^{86}Sr$ and $\delta^{18}O_{DW}$ range and likely represent migrants at buried at Vagnari.

The $^{87}Sr/^{86}Sr$ and $\delta^{18}O_{DW}$ evidence obtained from the Vagnari assemblage supports the hypothesis that this population was likely sustained through intra-community reproductive measures rather than by immigration from abroad, whether they were workers, freedmen, or slaves. Territorial acquisition during the Republic and Imperial periods provided new source of workers and slaves, including the sack of nearby *Silvium* (Botromagno) in 306 BCE by the Romans, during which ~5000 Samnites were captured and enslaved by the Romans (Diodorus, 20.80, translated by Geer, 1954; Small, 2002). However, it is likely that once territory was secured by Rome, subsequent maintenance of the working classes was achieved through children born to local parents (intra-community reproduction), and not through importation of new

workers/slaves. The integrated $^{87}Sr/^{86}Sr$ and $\delta^{18}O_{DW}$ results presented with our preliminary $^{87}Sr/^{86}Sr$ map of Italy suggest that the majority of the Vagnari occupants (58%) were local to the site, while an additional 34% likely originated from southern Italy, a trend that fits with these historic patterns, especially those proposed by Scheidel (1999, 2004, 2005, 2007). Only three individuals, all adult males, were identified as being non-local to southern Italy, with possible origins in northern Italy or further afield from Western Europe (n=2) and North Africa (n=1). These results are in line with historic evidence that suggests that Imperial Roman working classes employed at agricultural and industrial sites were primarily derived from areas close to rural settlements in Rome's hinterland (Bradley, 1987; Scheidel, 2007).

In contrast to rural settlements, integrated $^{87}Sr/^{86}Sr$ and $\delta^{18}O$ analysis of remains recovered from coastal communities such as Velia and *Portus Romae*, and of skeletal samples from larger city centers like Rome revealed that a larger proportion of these assemblages were composed of immigrants. For example, at the Roman necropoleis of Casal Bertone and Castellaccio Europarco Killgrove and Montgomery (2016) discovered 4 individuals whose $^{87}Sr/^{86}Sr$ and $\delta^{18}O$ values were different from the predicted $^{87}Sr/^{86}Sr$ and measured $\delta^{18}O$ variation of Rome's regional substratum and precipitation composition, respectively, and found that another 4 individuals were possibly non-local to Rome (out of a total of 55 individuals). Oxygen isotope analysis by Prowse et al. (2007) and more recently, an integrated $^{87}Sr/^{86}Sr$ and $\delta^{18}O$ by Stark (2016) of Roman period remains recovered from the cemetery of Isola Sacra showed that approximately one-third of the samples were non-local to the port-city, but migrated to *Portus Romae* as children. These studies shed light on the contrast that exists between necropoleis located in major and portside cities, versus those found further inland and further away from major portside commercial trade routes along the Tyrrhenian coast.

3.8 Conclusion

Our $^{87}Sr/^{86}Sr$ variation map provides preliminary data on the distribution of $^{87}Sr/^{86}Sr$ values across the Italian landscape, especially with respect to the known geological composition of the peninsula itself (Fig. 4; Supplement 1). More bioavailable strontium data are required to further refine the $^{87}Sr/^{86}Sr$ ranges, but we have nonetheless taken the first step in mapping the $^{87}Sr/^{86}Sr$ variation of Italy. In addition, improved spatial algorithms will lead to more accurate geo-provenancing of isotope values obtained from forensic and archaeological subjects (e.g. Emery, Prowse, Elford, Schwarcz, and Brickley, 2017; Laffoon et al., 2017).

The growth of the Roman Empire between the 1st and 4th centuries CE fostered new ties between the Mediterranean region, continental Europe, and parts of Asia, the Middle East, and Africa through conquest, colonization, and assimilation. Roman Italy's demographic landscape, especially its free versus slave classes, has long been the subject of intense debate (e.g., Beloch, 1886; Brunt, 1971; Harris, 1999; Lo Cascio, 1994; Scheidel, 1999, 2001, 2005, 2007). The Imperial working class population at Vagnari, whether enslaved or employed, was composed primarily of local inhabitants, corroborating historical evidence about subjugated populations after Roman expansion into southern Italy, a trend that is mirrored by the $^{87}Sr/^{86}Sr$ and $\delta^{18}O_{DW}$ values of the Vagnari occupants. The people at Vagnari living under Roman rule likely spent the majority of their lives from childhood onwards living, working, and eventually dying on the Vagnari estate. The results presented here provide new individual and local evidence to address questions surrounding the demographic composition of rural Roman Italy, its slave and free classes, by way of stable isotope analysis of ancient human remains. There is still a need for further isotopic inquiry into the demographic profiles of lesser-known rural Roman archaeological populations, in order to better understand how chemical analyses of the human

skeleton might complement the rich sources of textual, epigraphic, and archaeological information, among other data sets (e.g., censuses) available for study in quantifying Imperial Roman mobility and population diversity.

Acknowledgements

Excavations at the Vagnari necropolis were granted by the Ministero per i Beni e le Attività Culturali to Tracy Prowse and Maureen Carroll, through the British School at Rome, with the help of Stefania Peterlini. Franco Taccogna (Gravina) provided critical technical support at the site. The Vagnari excavation team is grateful to a number of organizations and individuals for their support of the project, and in particular the landowner of Vagnari, Dott. Mario De Gemmis Pellicciari; the British School at Rome; the Soprintendenza per i Beni Archeologici della Puglia, especially Dott. Luigi LaRocca, Dottsa. Francesca Radina and Dottsa. Maria Rosaria Depalo; the Centro Operativo and the Fondazione Ettore Pomarici Santomasi, Gravina. We also thank and acknowledge the fieldwork conducted by students and volunteers from Canada, the United Kingdom, and the United States. We would like to thank Professor Alan Dickin for running the strontium isotope analysis of the Vagnari tooth sample. We also thank members of McMaster's Ancient DNA Centre, Dr. Hendrik Poinar, Deb Poinar, Mel Kuch, Jessica Hider, Emil Karpinski, Dr. Ana Duggan, and Jennifer Klunk, as well as former members Jonathan Hughes and Dr. Stephanie Marciniak for their help troubleshooting figures and maps included in this paper.

Table S1: Italian baseline $^{87}Sr/^{86}Sr$ data used for map construction.

Region	$^{87}Sr/^{86}Sr$	Source Material	North	East	Published Source
Ivrea	0.7102	Dioritic rock	45°28'02.19"	7°52'48.21"	Vander Auwera and Andre (1991)
Ivrea	0.7109	Dioritic rock	45°28'02.19"	7°52'48.21"	Vander Auwera and Andre (1991)
Ivrea	0.71064	Dioritic rock	45°28'02.19"	7°52'48.21"	Vander Auwera and Andre (1991)
Ivrea	0.71028	Dioritic rock	45°28'02.19"	7°52'48.21"	Vander Auwera and Andre (1991)
Ivrea	0.70966	Dioritic rock	45°28'02.19"	7°52'48.21"	Vander Auwera and Andre (1991)
Ivrea	0.7101	Dioritic rock	45°28'02.19"	7°52'48.21"	Vander Auwera and Andre (1991)
Ivrea	0.71059	Dioritic rock	45°28'02.19"	7°52'48.21"	Vander Auwera and Andre (1991)
Ivrea	0.7102	Epidote	45°28'02.19"	7°52'48.21"	Vander Auwera and Andre (1991)
Ivrea	0.70876	Dolomitic marble	45°28'02.19"	7°52'48.21"	Vander Auwera and Andre (1991)
Ivrea	0.70876	Dolomitic marble	45°28'02.19"	7°52'48.21"	Vander Auwera and Andre (1991)
Ivrea	0.70971	Dolomitic marble	45°28'02.19"	7°52'48.21"	Vander Auwera and Andre (1991)
Ivrea	0.70953	Dolomitic marble	45°28'02.19"	7°52'48.21"	Vander Auwera and Andre (1991)
Ivrea	0.7088	Skarn Minerals early stages	45°28'02.19"	7°52'48.21"	Vander Auwera and Andre (1991)
Ivrea	0.70918	Skarn Minerals early stages	45°28'02.19"	7°52'48.21"	Vander Auwera and Andre (1991)
Ivrea	0.70915	Skarn Minerals early stages	45°28'02.19"	7°52'48.21"	Vander Auwera and Andre (1991)
Ivrea	0.7103	Skarn Minerals early stages	45°28'02.19"	7°52'48.21"	Vander Auwera and Andre (1991)
Ivrea	0.70988	Skarn Minerals early stages	45°28'02.19"	7°52'48.21"	Vander Auwera and Andre (1991)
Ivrea	0.7095	Skarn Minerals early stages	45°28'02.19"	7°52'48.21"	Vander Auwera and Andre (1991)
Ivrea	0.7104	Skarn Minerals early stages	45°28'02.19"	7°52'48.21"	Vander Auwera and Andre (1991)
Ivrea	0.71259	Skarn Minerals early stages	45°28'02.19"	7°52'48.21"	Vander Auwera and Andre (1991)
Ivrea	0.71028	Skarn minerals first hydroxylation	45°28'02.19"	7°52'48.21"	Vander Auwera and Andre (1991)
Ivrea	0.7103	Skarn minerals first hydroxylation	45°28'02.19"	7°52'48.21"	Vander Auwera and Andre (1991)
Ivrea	0.71092	Skarn minerals first hydroxylation	45°28'02.19"	7°52'48.21"	Vander Auwera and Andre (1991)
Ivrea	0.71303	Skarn minerals sulphidation stage	45°28'02.19"	7°52'48.21"	Vander Auwera and Andre (1991)
Ivrea	0.71373	Skarn minerals sulphidation stage	45°28'02.19"	7°52'48.21"	Vander Auwera and Andre (1991)
Grotta Polesini	0.708613	Cervus elaphus M2	41°57'40.37"	12°47'38.31	Pellegrini et al. 2008
Grotta Polesini	0.70873	Cervus elaphus M2	41°57'40.37"	12°47'38.31	Pellegrini et al. 2008
Grotta Polesini	0.708837	Cervus elaphus M2	41°57'40.37"	12°47'38.31	Pellegrini et al. 2008
Grotta Polesini	0.708756	Cervus elaphus M2	41°57'40.37"	12°47'38.31	Pellegrini et al. 2008
Grotta Polesini	0.708786	Cervus elaphus M2	41°57'40.37"	12°47'38.31	Pellegrini et al. 2008
Grotta Polesini	0.708788	Equs hydruntinus M or P	41°57'40.37"	12°47'38.31	Pellegrini et al. 2008
Grotta Polesini	0.708734	Equs hydruntinus M or P	41°57'40.37"	12°47'38.31	Pellegrini et al. 2008
Grotta Polesini	0.708686	Equs hydruntinus M or P	41°57'40.37"	12°47'38.31	Pellegrini et al. 2008
Grotta Polesini	0.708743	Equs hydruntinus M or P	41°57'40.37"	12°47'38.31	Pellegrini et al. 2008

Grotta Polesini	0.708753	Equs hydruntinus M or P	41°57'40.37"	12°47'38.31	Pellegrini et al. 2008
Grotta di Pozzo	0.70871	Cervus elaphus M2	42°00'18.10"	14°00'14.19"	Pellegrini et al. 2008
Grotta di Pozzo	0.708746	Cervus elaphus M2	42°00'18.10"	14°00'14.19"	Pellegrini et al. 2008
Grotta di Pozzo	0.708759	Cervus elaphus M2	42°00'18.10"	14°00'14.19"	Pellegrini et al. 2008
Grotta di Pozzo	0.708784	Cervus elaphus M2	42°00'18.10"	14°00'14.19"	Pellegrini et al. 2008
Grotta di Pozzo	0.708828	Cervus elaphus M2	42°00'18.10"	14°00'14.19"	Pellegrini et al. 2008
Grotta di Pozzo	0.70875	Equs hydruntinus M or P	42°00'18.10"	14°00'14.19"	Pellegrini et al. 2008
Grotta di Pozzo	0.708761	Equs hydruntinus M or P	42°00'18.10"	14°00'14.19"	Pellegrini et al. 2008
Grotta di Pozzo	0.708793	Equs hydruntinus M or P	42°00'18.10"	14°00'14.19"	Pellegrini et al. 2008
Grotta di Pozzo	0.708788	Equs hydruntinus M or P	42°00'18.10"	14°00'14.19"	Pellegrini et al. 2008
Grotta di Pozzo	0.70882	Equs hydruntinus M or P	42°00'18.10"	14°00'14.19"	Pellegrini et al. 2008
Grotta Settecannelle	0.708902	Cervus elaphus M2	42°40'02.92"	11°54'48.74"	Pellegrini et al. 2008
Grotta Settecannelle	0.708946	Cervus elaphus M2	42°40'02.92"	11°54'48.74"	Pellegrini et al. 2008
Grotta Settecannelle	0.708989	Cervus elaphus M2	42°40'02.92"	11°54'48.74"	Pellegrini et al. 2008
Grotta Settecannelle	0.708913	Cervus elaphus M2	42°40'02.92"	11°54'48.74"	Pellegrini et al. 2008
Grotta Settecannelle	0.709038	Cervus elaphus M2	42°40'02.92"	11°54'48.74"	Pellegrini et al. 2008
Vado all'Arancio	0.708845	Equs hydruntinus M or P	42°53'31.00"	10°57'50.10"	Pellegrini et al. 2008
Vado all'Arancio	0.708844	Equs hydruntinus M or P	42°53'31.00"	10°57'50.10"	Pellegrini et al. 2008
Vado all'Arancio	0.708896	Equs hydruntinus M or P	42°53'31.00"	10°57'50.10"	Pellegrini et al. 2008
Vado all'Arancio	0.708661	Equs hydruntinus M or P	42°53'31.00"	10°57'50.10"	Pellegrini et al. 2008
Vado all'Arancio	0.708735	Equs hydruntinus M or P	42°53'31.00"	10°57'50.10"	Pellegrini et al. 2008
Rionero in Vulture	0.707812	wine 2001	40°55'40"	15°40'31"	Marchionni et al. 2013
Rionero in Vulture	0.707896	wine 2003	40°55'40"	15°40'31"	Marchionni et al. 2013
Rionero in Vulture	0.707824	wine 2002	40°55'40"	15°40'31"	Marchionni et al. 2013
Rionero in Vulture	0.70788	wine 2004	40°55'40"	15°40'31"	Marchionni et al. 2013
Rionero in Vulture	0.707897	wine 2005	40°55'40"	15°40'31"	Marchionni et al. 2013
Venosa	0.708175	wine 2003	40°57'32"	15°48'00"	Marchionni et al. 2013
Venosa	0.708306	wine 2004	40°57'32"	15°48'00"	Marchionni et al. 2013
Venosa	0.707896	wine 2007	40°57'32"	15°48'00"	Marchionni et al. 2013
Rionero in Vulture	0.707589	wine 2005	40°55'32"	15°40'39	Marchionni et al. 2013
Rionero in Vulture	0.707479	wine 2008	40°55'32"	15°40'39	Marchionni et al. 2013
Barile	0.706793	wine 2005	40°56'47"	15°40'24"	Marchionni et al. 2013
Pian dell'Altare	0.707124	wine 2002	40°55'28"	15°42'09"	Marchionni et al. 2013
Rionero in Vulture	0.70785	wine 2002	40°55'32"	15°40'39	Marchionni et al. 2013
Cesinali	0.708439	wine 2004	40°53'58"	14°49'30"	Marchionni et al. 2013
Massa di Faicchio	0.708427	wine 2009	41°15'41"	14°30'45"	Marchionni et al. 2013
Santa Lucia	0.708277	Wine 2009	41°00'37"	14°49'13"	Marchionni et al. 2013
Napoli	0.708445	wine 2005	40°50'52"	14°09'35"	Marchionni et al. 2013
Napoli	0.708342	wine 2009	40°50'52"	14°09'35"	Marchionni et al. 2013
Paupisi	0.708432	wine 2006	41°11'43"	14°40'02"	Marchionni et al. 2013
Nola	0.708646	wine 2009	40°52'41"	14°30'33"	Marchionni et al. 2013

Guardia Sanframondi	0.708614	wine 2008	41°15'06"	14°34'32	Marchionni et al. 2013
Guardia Sanframondi	0.708442	wine 2008	41°15'06"	14°34'32	Marchionni et al. 2013
Atripalda	0.70822	wine 2004	40°55'23"	14°49'54"	Marchionni et al. 2013
Sant'Agata dei Goti	0.708219	wine 2004	41°05'12"	14°30'10"	Marchionni et al. 2013
San Terzano	0.708349	wine 2005	41°13'02"	13°54'49"	Marchionni et al. 2013
San Terzano	0.708351	wine 2004	41°13'02"	13°54'49"	Marchionni et al. 2013
Lettere	0.707723	wine 2002	40°42'17"	14°33'05"	Marchionni et al. 2013
Napoli	0.707991	wine 2009	40°50'52"	14°09'35"	Marchionni et al. 2013
Sant'Agata dei Goti	0.707958	wine 2009	41°05'12"	14°30'10"	Marchionni et al. 2013
Colle Faggiano	0.709046	wine 2005	41°52'48"	13°06'27"	Marchionni et al. 2013
Colle Faggiano	0.708978	wine 2009	41°52'48"	13°06'27"	Marchionni et al. 2013
Colle Faggiano	0.709025	wine 2010	41°52'48"	13°06'27"	Marchionni et al. 2013
Colle Cotoverio	0.709965	wine 2008	41°43'13"	13°06'11"	Marchionni et al. 2013
Colle Cotoverio	0.709989	wine 2009	41°43'13"	13°06'11"	Marchionni et al. 2013
Colle Cotoverio	0.71001	wine 2010	41°43'13"	13°06'11"	Marchionni et al. 2013
San Giovenale	0.709168	wine 2003	41°50'53"	13°02'24	Marchionni et al. 2013
San Giovenale	0.709177	wine 2005	41°50'53"	13°02'24	Marchionni et al. 2013
San Giovenale	0.709174	wine 2006	41°50'53"	13°02'24	Marchionni et al. 2013
Cerreto	0.710586	wine 2010	41°50'53"	13°02'24	Marchionni et al. 2013
Isola del Giglio	0.709371	wine 2008	42°22'31"	10°52'31	Marchionni et al. 2013
Isola del Giglio	0.710969	wine 2009	42°22'31"	10°52'31	Marchionni et al. 2013
isola del Giglio	0.711305	wine 2010	42°22'31"	10°52'31	Marchionni et al. 2013
Barberino Val D'Elsa	0.709	wine 2006	43°32'24"	11°09'54"	Marchionni et al. 2013
Figline Valdarno	0.710689	wine 2006	43°38'23"	11°25'19"	Marchionni et al. 2013
Figline Valdarno	0.709849	wine 2006	43°38'23"	11°25'19"	Marchionni et al. 2013
Vulture volcanic rocks	0.70695	rock	n/a	n/a	Marchionni et al. 2013
Neapolitan volcanic rocks	0.70746	rock	n/a	n/a	Marchionni et al. 2013
Roccamonfina volcanic rocks	0.7082	rock	n/a	n/a	Marchionni et al. 2013
Central Latium volcanic rocks	0.71038	rock	n/a	n/a	Marchionni et al. 2013
Southern Tuscany sedimentary rocks	0.71472	rock	n/a	n/a	Marchionni et al. 2013
Giglio Island granite	0.71755	rock	n/a	n/a	Marchionni et al. 2013
Aglianico del Vulture	0.70771	wine	n/a	n/a	Marchionni et al. 2013
Piedirosso	0.70789	wine	n/a	n/a	Marchionni et al. 2013
Aglianico Campano	0.7084	wine	n/a	n/a	Marchionni et al. 2013
Cesanese	0.70951	wine	n/a	n/a	Marchionni et al. 2013
Chianti Classico	0.70958	wine	n/a	n/a	Marchionni et al. 2013
Giglio Island	0.71055	wine	n/a	n/a	Marchionni et al. 2013
Emilia-Romagna (sub-alpine northern-central)	0.70817	tomato	n/a	n/a	Trincherini et al. 2014
Apulia and Campania (southern)	0.70793	tomato	n/a	n/a	Trincherini et al. 2014
Emilia-Romagna (sub-alpine northern-central)	0.70866	wine	n/a	n/a	Durante et al. 2015

Modena near the village of Sorbara	0.708762	wine	n/a	n/a	Durante et al. 2015
Modena near the village of Sorbara	0.708725	wine	n/a	n/a	Durante et al. 2015
Modena near the village of Sorbara	0.708668	wine	n/a	n/a	Durante et al. 2015
7 miles (11 km) west of the village Sorbara	0.708675	wine	n/a	n/a	Durante et al. 2015
7 miles (11 km) west of the village Sorbara	0.708702	wine	n/a	n/a	Durante et al. 2015
7 miles (11 km) west of the village Sorbara	0.708647	wine	n/a	n/a	Durante et al. 2015
7 miles (11 km) west of the village Sorbara	0.708677	wine	n/a	n/a	Durante et al. 2015
south of the town of Modena	0.709145	wine	n/a	n/a	Durante et al. 2015
south of the town of Modena	0.709017	wine	n/a	n/a	Durante et al. 2015
south of the town of Modena	0.70882	wine	n/a	n/a	Durante et al. 2015
Montalcino, 80 Km, south of Florence	0.709402	wine	n/a	n/a	Durante et al. 2015
Montalcino, 80 Km, south of Florence	0.709374	wine	n/a	n/a	Durante et al. 2015
Montalcino, 80 Km, south of Florence	0.709508	wine	n/a	n/a	Durante et al. 2015
Barolo (piedmont)	0.70907	wine	n/a	n/a	Durante et al. 2015
Barolo (piedmont)	0.709061	wine	n/a	n/a	Durante et al. 2015
Barolo (piedmont)	0.709096	wine	n/a	n/a	Durante et al. 2015
Lonigo (Veneto region N/E Italy)	0.70706	wine must	n/a	n/a	Petrini et al. 2015
S. Anna (Veneto region N/E Italy)	0.71049	wine must	n/a	n/a	Petrini et al. 2015
Peraro (Veneto region N/E Italy)	0.70947	wine must	n/a	n/a	Petrini et al. 2015
Broscagin (Veneto region N/E Italy)	0.70907	wine must	n/a	n/a	Petrini et al. 2015
Braga (Veneto region N/E Italy)	0.71066	wine must	n/a	n/a	Petrini et al. 2015
Pattarello (Veneto region N/E Italy)	0.71215	wine must	n/a	n/a	Petrini et al. 2015
Bottazzo (Veneto region N/E Italy)	0.70919	wine must	n/a	n/a	Petrini et al. 2015
Gaiarine (Veneto region N/E Italy)	0.70919	wine must	n/a	n/a	Petrini et al. 2015
Aleandri (Veneto region N/E Italy)	0.71022	wine must	n/a	n/a	Petrini et al. 2015
Nardin-Lison (Veneto region N/E Italy)	0.70977	wine must	n/a	n/a	Petrini et al. 2015
Lonigo (Veneto region N/E Italy)	0.70772	soil labile fraction	n/a	n/a	Petrini et al. 2015
S. Anna (Veneto region N/E Italy)	0.71097	soil labile fraction	n/a	n/a	Petrini et al. 2015
Peraro (Veneto region N/E Italy)	0.70899	soil labile fraction	n/a	n/a	Petrini et al. 2015
Broscagin (Veneto region N/E Italy)	0.7088	soil labile fraction	n/a	n/a	Petrini et al. 2015
Braga (Veneto region N/E Italy)	0.70986	soil labile fraction	n/a	n/a	Petrini et al. 2015
Pattarello (Veneto region N/E Italy)	0.71064	soil labile fraction	n/a	n/a	Petrini et al. 2015
Bottazzo (Veneto region N/E Italy)	0.70941	soil labile fraction	n/a	n/a	Petrini et al. 2015
Gaiarine (Veneto region N/E Italy)	0.70839	soil labile fraction	n/a	n/a	Petrini et al. 2015
Aleandri (Veneto region N/E Italy)	0.70956	soil labile fraction	n/a	n/a	Petrini et al. 2015

Nardin-Lison (Veneto region N/E Italy)	0.70955	soil labile fraction	n/a	n/a	Petrini et al. 2015
Trentino	0.708979	Butter	n/a	n/a	Rossmann et al. 2000
Modena	0.708818	Butter	n/a	n/a	Rossmann et al. 2000
Padua	0.708899	Butter	n/a	n/a	Rossmann et al. 2000
Sassari	0.712126	Butter	n/a	n/a	Rossmann et al. 2000
Sicily	0.708614	Beef	n/a	n/a	Rummel et al. 2012
Sicily	0.709185	Beef	n/a	n/a	Rummel et al. 2012
Sicily	0.710649	Beef	n/a	n/a	Rummel et al. 2012
Sicily	0.708891	Beef	n/a	n/a	Rummel et al. 2012
Sicily	0.709009	Beef	n/a	n/a	Rummel et al. 2012
Sicily	0.709555	Beef	n/a	n/a	Rummel et al. 2012
Sicily	0.709051	Beef	n/a	n/a	Rummel et al. 2012
Sicily	0.708621	Beef	n/a	n/a	Rummel et al. 2012
Sicily	0.709045	Beef	n/a	n/a	Rummel et al. 2012
Sicily	0.709079	Beef	n/a	n/a	Rummel et al. 2012
Sicily	0.707454	Beef	n/a	n/a	Rummel et al. 2012
Sicily	0.708457	Beef	n/a	n/a	Rummel et al. 2012
Sicily	0.708803	Beef	n/a	n/a	Rummel et al. 2012
Sicily	0.709258	Beef	n/a	n/a	Rummel et al. 2012
Sicily	0.709255	Beef	n/a	n/a	Rummel et al. 2012
Sicily	0.709172	Beef	n/a	n/a	Rummel et al. 2012
Sicily	0.709053	Beef	n/a	n/a	Rummel et al. 2012
Sicily	0.708586	Beef	n/a	n/a	Rummel et al. 2012
Sicily	0.708928	Beef	n/a	n/a	Rummel et al. 2012
Sicily	0.710869	Beef	n/a	n/a	Rummel et al. 2012
Tuscany	0.709073	Beef	n/a	n/a	Rummel et al. 2012
Tuscany	0.709138	Beef	n/a	n/a	Rummel et al. 2012
Tuscany	0.709302	Beef	n/a	n/a	Rummel et al. 2012
Tuscany	0.709307	Beef	n/a	n/a	Rummel et al. 2012
Tuscany	0.709027	Beef	n/a	n/a	Rummel et al. 2012
Tuscany	0.709175	Beef	n/a	n/a	Rummel et al. 2012
Tuscany	0.708818	Beef	n/a	n/a	Rummel et al. 2012
Tuscany	0.708767	Beef	n/a	n/a	Rummel et al. 2012
Tuscany	0.708841	Beef	n/a	n/a	Rummel et al. 2012
Tuscany	0.708789	Beef	n/a	n/a	Rummel et al. 2012
Tuscany	0.709346	Beef	n/a	n/a	Rummel et al. 2012
Tuscany	0.709504	Beef	n/a	n/a	Rummel et al. 2012
Tuscany	0.70916	Beef	n/a	n/a	Rummel et al. 2012
Tuscany	0.709057	Beef	n/a	n/a	Rummel et al. 2012
Tuscany	0.709449	Beef	n/a	n/a	Rummel et al. 2012

Tuscany	0.715717	Beef	n/a	n/a	Rummel et al. 2012
Tuscany	0.70932	Beef	n/a	n/a	Rummel et al. 2012
Tuscany	0.709377	Beef	n/a	n/a	Rummel et al. 2012
Tuscany	0.709229	Beef	n/a	n/a	Rummel et al. 2012
Tuscany	0.709526	Beef	n/a	n/a	Rummel et al. 2012
Trentino	0.708682	Beef	n/a	n/a	Rummel et al. 2012
Trentino	0.710073	Beef	n/a	n/a	Rummel et al. 2012
Trentino	0.708174	Beef	n/a	n/a	Rummel et al. 2012
Trentino	0.707703	Beef	n/a	n/a	Rummel et al. 2012
Trentino	0.708549	Beef	n/a	n/a	Rummel et al. 2012
Trentino	0.710417	Beef	n/a	n/a	Rummel et al. 2012
Trentino	0.7089	Beef	n/a	n/a	Rummel et al. 2012
Trentino	0.708539	Beef	n/a	n/a	Rummel et al. 2012
Trentino	0.708888	Beef	n/a	n/a	Rummel et al. 2012
Trentino	0.708188	Beef	n/a	n/a	Rummel et al. 2012
Trentino	0.708372	Beef	n/a	n/a	Rummel et al. 2012
Trentino	0.708506	Beef	n/a	n/a	Rummel et al. 2012
Trentino	0.708643	Beef	n/a	n/a	Rummel et al. 2012
Trentino	0.708543	Beef	n/a	n/a	Rummel et al. 2012
Trentino	0.709057	Beef	n/a	n/a	Rummel et al. 2012
Trentino	0.707749	Beef	n/a	n/a	Rummel et al. 2012
Trentino	0.708972	Beef	n/a	n/a	Rummel et al. 2012
Trentino	0.709418	Beef	n/a	n/a	Rummel et al. 2012
Trentino	0.708536	Beef	n/a	n/a	Rummel et al. 2012
Trentino	0.70761	Beef	n/a	n/a	Rummel et al. 2012
Trentino	0.708663	Beef	n/a	n/a	Rummel et al. 2012
Trentino	0.708956	Beef	n/a	n/a	Rummel et al. 2012
Trentino	0.706278	Beef	n/a	n/a	Rummel et al. 2012
Trentino	0.709166	Beef	n/a	n/a	Rummel et al. 2012
Trentino	0.7104	Beef	n/a	n/a	Rummel et al. 2012
Basilicata	0.707816	wine	n/a	n/a	Boari et al. 2008
Basilicata	0.708333	wine	n/a	n/a	Boari et al. 2008
Basilicata	0.708177	wine	n/a	n/a	Boari et al. 2008
Basilicata	0.707752	wine	n/a	n/a	Boari et al. 2008
Basilicata	0.707838	wine	n/a	n/a	Boari et al. 2008
Campania	0.708222	wine	n/a	n/a	Boari et al. 2008
Campania	0.707637	wine	n/a	n/a	Boari et al. 2008
Campania	0.707615	wine	n/a	n/a	Boari et al. 2008
Latium	0.709177	wine	n/a	n/a	Boari et al. 2008
Latium	0.709174	wine	n/a	n/a	Boari et al. 2008
Tuscany	0.708764	wine	n/a	n/a	Boari et al. 2008

Tuscany	0.708767	wine	n/a	n/a	Boari et al. 2008
Tuscany	0.708801	wine	n/a	n/a	Boari et al. 2008
Tuscany	0.708784	wine	n/a	n/a	Boari et al. 2008
Tuscany	0.709	wine	n/a	n/a	Boari et al. 2008
Tuscany	0.71069	wine	n/a	n/a	Boari et al. 2008
Tuscany	0.709845	wine	n/a	n/a	Boari et al. 2008
Cervaro River	0.70898	gypsum	n/a	n/a	Matano et al. 2005
Cervaro River	0.70898	gypsum	n/a	n/a	Matano et al. 2005
Cervaro River	0.70901	gypsum	n/a	n/a	Matano et al. 2005
Ferrara Mt.	0.7089	gypsum	n/a	n/a	Matano et al. 2005
Ferrara Mt.	0.70902	gypsum	n/a	n/a	Matano et al. 2005
Ferrara Mt.	0.709	gypsum	n/a	n/a	Matano et al. 2005
Pianerottolo	0.70895	gypsum	n/a	n/a	Matano et al. 2005
Scampitella	0.709	gypsum	n/a	n/a	Matano et al. 2005
Scampitella	0.709	gypsum	n/a	n/a	Matano et al. 2005
Scampitella	0.70901	gypsum	n/a	n/a	Matano et al. 2005
Scampitella	0.70897	gypsum	n/a	n/a	Matano et al. 2005
Scampitella	0.70893	gypsum	n/a	n/a	Matano et al. 2005
Scampitella	0.70899	gypsum	n/a	n/a	Matano et al. 2005
Scampitella	0.709	gypsum	n/a	n/a	Matano et al. 2005
Scampitella	0.709	gypsum	n/a	n/a	Matano et al. 2005
Scampitella	0.70897	gypsum	n/a	n/a	Matano et al. 2005
Scampitella	0.70902	gypsum	n/a	n/a	Matano et al. 2005
Difesa Grande	0.70904	gypsum	n/a	n/a	Matano et al. 2005
Difesa Grande	0.70899	gypsum	n/a	n/a	Matano et al. 2005
Difesa Grande	0.70895	gypsum	n/a	n/a	Matano et al. 2005
Monteleone	0.70853	gypsum	n/a	n/a	Matano et al. 2005
Monteleone	0.7085	gypsum	n/a	n/a	Matano et al. 2005
Monteleone	0.70858	gypsum	n/a	n/a	Matano et al. 2005
Monteleone	0.7085	gypsum	n/a	n/a	Matano et al. 2005
Monteleone	0.70855	gypsum	n/a	n/a	Matano et al. 2005
Monteleone	0.70848	gypsum	n/a	n/a	Matano et al. 2005
Monteleone	0.70851	gypsum	n/a	n/a	Matano et al. 2005
Monteleone	0.70848	gypsum	n/a	n/a	Matano et al. 2005
Monteleone	0.70851	gypsum	n/a	n/a	Matano et al. 2005
Monteleone	0.70853	gypsum	n/a	n/a	Matano et al. 2005
Oscata	0.70874	gypsum	n/a	n/a	Matano et al. 2005
Oscata	0.70876	gypsum	n/a	n/a	Matano et al. 2005
Oscata	0.70887	gypsum	n/a	n/a	Matano et al. 2005
Oscata	0.70878	gypsum	n/a	n/a	Matano et al. 2005
Oscata	0.70871	gypsum	n/a	n/a	Matano et al. 2005

Oscata	0.70881	gypsum	n/a	n/a	Matano et al. 2005
Oscata	0.70882	gypsum	n/a	n/a	Matano et al. 2005
Oscata	0.70877	gypsum	n/a	n/a	Matano et al. 2005
Gravina	0.70802	Ungulate Tooth	n/a	n/a	This study
Gravina	0.70874	Ungulate Tooth	n/a	n/a	This study
Gravina	0.70849	Ungulate Tooth	n/a	n/a	This study
Gravina	0.70901	Snail Shell	n/a	n/a	This study
Gravina	0.7089	Snail Shell	n/a	n/a	This study
Gravina	0.70851	Ungulate Tooth	n/a	n/a	This study
Gravina	0.70865	Ungulate Tooth	n/a	n/a	This study
Gravina	0.70855	Ungulate Tooth	n/a	n/a	This study
Gravina	0.70866	Ungulate Tooth	n/a	n/a	This study
Gravina	0.70877	Ungulate Tooth	n/a	n/a	This study
Gravina	0.70878	Soil	n/a	n/a	This study
Gravina	0.70886	Soil	n/a	n/a	This study
Gravina	0.70881	Soil	n/a	n/a	This study
Gravina	0.70872	Soil	n/a	n/a	This study
Gravina	0.7087	Soil	n/a	n/a	This study
Calabria	0.709033	Bulk Rock	n/a	n/a	Reinhardt et al. (2000)
Calabria	0.709033	Bulk Rock	n/a	n/a	Reinhardt et al. (2000)
Calabria	0.709044	Bulk Rock	n/a	n/a	Reinhardt et al. (2000)
Calabria	0.709068	Bulk Rock	n/a	n/a	Reinhardt et al. (2000)
Calabria	0.708996	Bulk Rock	n/a	n/a	Reinhardt et al. (2000)
Calabria	0.709053	Bulk Rock	n/a	n/a	Reinhardt et al. (2000)
Calabria	0.709043	Bulk Rock	n/a	n/a	Reinhardt et al. (2000)
Calabria	0.709057	Bulk Rock	n/a	n/a	Reinhardt et al. (2000)
Calabria	0.709063	Bulk Rock	n/a	n/a	Reinhardt et al. (2000)
Calabria	0.70906	Bulk Rock	n/a	n/a	Reinhardt et al. (2000)
Calabria	0.709055	Bulk Rock	n/a	n/a	Reinhardt et al. (2000)
Calabria	0.709071	Bulk Rock	n/a	n/a	Reinhardt et al. (2000)
Calabria	0.709072	Bulk Rock	n/a	n/a	Reinhardt et al. (2000)
Calabria	0.709056	Bulk Rock	n/a	n/a	Reinhardt et al. (2000)
Calabria	0.709061	Bulk Rock	n/a	n/a	Reinhardt et al. (2000)
Calabria	0.709045	Bulk Rock	n/a	n/a	Reinhardt et al. (2000)
Calabria	0.709048	Bulk Rock	n/a	n/a	Reinhardt et al. (2000)
Calabria	0.709046	Bulk Rock	n/a	n/a	Reinhardt et al. (2000)
Calabria	0.709046	Bulk Rock	n/a	n/a	Reinhardt et al. (2000)
Calabria	0.709045	Bulk Rock	n/a	n/a	Reinhardt et al. (2000)
Calabria	0.709047	Bulk Rock	n/a	n/a	Reinhardt et al. (2000)
Calabria	0.709053	Bulk Rock	n/a	n/a	Reinhardt et al. (2000)
Calabria	0.709035	Bulk Rock	n/a	n/a	Reinhardt et al. (2000)

Calabria	0.709064	Bulk Rock	n/a	n/a	Reinhardt et al. (2000)
Calabria	0.709057	Bulk Rock	n/a	n/a	Reinhardt et al. (2000)
Salentine Coast	0.707769	Bulk Rock	n/a	n/a	Schulter et al. (2008)
Salentine Coast	0.707761	Bulk Rock	n/a	n/a	Schulter et al. (2008)
Salentine Coast	0.707779	Bulk Rock	n/a	n/a	Schulter et al. (2008)
Salentine Coast	0.707767	Bulk Rock	n/a	n/a	Schulter et al. (2008)
Salentine Coast	0.707786	Bulk Rock	n/a	n/a	Schulter et al. (2008)
Salentine Coast	0.707419	Bulk Rock	n/a	n/a	Schulter et al. (2008)
Salentine Coast	0.707685	Bulk Rock	n/a	n/a	Schulter et al. (2008)
Salentine Coast	0.70758	Bulk Rock	n/a	n/a	Schulter et al. (2008)
Salentine Coast	0.707569	Bulk Rock	n/a	n/a	Schulter et al. (2008)
Salentine Coast	0.707574	Bulk Rock	n/a	n/a	Schulter et al. (2008)
Salentine Coast	0.707575	Bulk Rock	n/a	n/a	Schulter et al. (2008)
Salentine Coast	0.707633	Bulk Rock	n/a	n/a	Schulter et al. (2008)
Salentine Coast	0.707676	Bulk Rock	n/a	n/a	Schulter et al. (2008)
Salentine Coast	0.707591	Bulk Rock	n/a	n/a	Schulter et al. (2008)
Salentine Coast	0.707813	Bulk Rock	n/a	n/a	Schulter et al. (2008)
Salentine Coast	0.707828	Bulk Rock	n/a	n/a	Schulter et al. (2008)
Salentine Coast	0.707794	Bulk Rock	n/a	n/a	Schulter et al. (2008)
Salentine Coast	0.707933	Bulk Rock	n/a	n/a	Schulter et al. (2008)

3.9 References

Atlante Tematico d'Italia. 1989. Consiglio Nazionale delle Ricerche (Italy). Milano: Touring Club Italiano, 1989–1992.

Attema P, van Leusen A. 2004. The Early Roman Colonization of South Lazio: A Survey of Three Landscapes. In: Attema P, editor. Centralization, Early Urbanization, and Colonization in First Millenium BC Italy and Greece. Leuven: Peeters:157–195.

Bagnall R, Frier B. 1994. The Demography of Roman Egypt. Cambridge: Cambridge University Press.

Bataille CP, Bowen GJ. 2012. Mapping 87Sr/86Sr variations in bedrock and water for large scale provenance studies. Chem Geol 304–305:39–52.

Bataille CP, Laffoon J, Bowen GJ. 2012. Mapping multiple source effects on the strontium isotopic signatures of ecosystems from the circum-Caribbean region. Ecosphere 3:1–24

Beard BL, Johnson CM. 2000. Strontium isotopes composition of skeletal material can determine the birth place and geographic mobility of humans and animals. J Forensic Sci 45:1049–1061.

Beloch J. 1886. Die Bevölkerung der Griechisch-Römischer Welt. Leipzig: Verlag von Duncker & Humblot.

Benelli E. 2001. The Romanization of Italy Through the Epigraphic Record. In: Keays S, Terrenato N, editors. Italy and the West: Comparative Issues in Romanization. Oxford: Oxbow Books:7–17.

Bentley RA. 2006. Strontium isotopes from the earth to the archaeological skeleton: a review. J Archaeol Method Theory 13:135–187.

Boari E, Tommasini R, Mercurio M, Morra V, Mattei M, Mulinacci N, Conticelli S. 2008. 87Sr/86Sr of some central and southern Italian wines and its use as fingerprints for geographic origins. In: Proceedings of OIV 2008 - 31st World Congress of Vine and Wine.

Bowen GJ. 2010. Isoscapes: spatial pattern in isotopic biogeochemistry. Annu Rev Earth Planet Sci 38:161–187.

Bradley KR. 1987. On the Roman slave supply and slavebreeding. Slavery Abolit 8:42–64.

Bradley KR. 1994. Slavery and Society at Rome. Cambridge: Cambridge University Press.

Brennan SR, Fernandez DP, Mackey G, Cerling TE, Bataille CP, Bowen GJ, Wooller MJ. 2014. Strontium isotope variation and carbonate versus silicate weathering in rivers from across Alaska: implications for provenance studies. Chem Geol 389:167–181.

Brent L, Prowse T. 2014. Grave Goods, Burial Practices and Patterns of Distribution in the Vagnari Cemetery. In: Small A, editor. Beyond Vagnari: New Themes in the Study of Roman South Italy. Bari: Edipuglia:99–110.

Brettell R, Montgomery J, Evans J. 2012. Brewing and stewing: the effect of culturally mediated behaviour on the oxygen isotope composition of ingested fluids and the implications for human provenance studies. J Anal At Spectrom 27:778–758.

Britton K, Fuller BT, Tutken T, Mays S, Richards MP. Oxygen isotope analysis of human bone phosphate evidences weaning age in archaeological populations. Am J Phys Anthropol 157:226 –241.

Brunt PA. 1971. Italian Manpower 225 B.C.-A.D. 14. (1987) O (repr., editor.). Oxford: Oxford University Press.

Buikstra J, Ubelaker D. 1994. Standards for Data Collection from Human Skeletal Remains. Arkansas Archeological Survey, Fayetteville.

Burton JH, Price TD, Cahue L, Wright LE. 2003. The use of barium and strontium abundances

in human skeletal tissues to determine rheir geographic origins. Int J Osteoarchaeol 13:88–95.

Burton JH, Price TD, Middleton WD. 1999. Correlation of bone Ba/Ca and Sr/Ca due to biological purification of calcium. J Archaeol Sci 26:609–616.

Carroll M. 2014. New Work in the Vicus by the University of Sheffield. In: Small A, editor. Beyond Vagnari: New Themes in the Study of Roman South Italy. Bari: Edipuglia: 79–88.

Carroll M, Prowse TL. 2014. Exploring the Vicus and the Necropolis at the Roman Imperial Estate at Vagnari (commune di Gravina in Puglia, provincia di Bari, regione, Puglia). Papers of the British School at Rome 82:353–356.

Chenery CA, Pashley V, Lamb AL, Sloane HJ, Evans JA. 2012. The oxygen isotope relationship between the phosphate and structural carbonate fractions of human bioapatite. Rapid Commun Mass Spectrom 26:309–319.

Chenery C, Müldner G, Evans J, Eckardt H, Lewis M. 2010. Strontium and stable isotope evidence for diet and mobility in Roman Gloucester, UK. J Archaeol Sci 37:150–163.

Curti E, Dench E, Patterson J. 1996. The archaeology of central and southern Roman Italy: recent trends and approaches. J Rom Archaeol 86:170–189.

D'Italia AT. 1989. Consiglio nazionale delle ricerche (Italy). Milano: Touring Club Italiano, 1989-1992.

Daux V, Lécuyer C, Héran MA, Amiot R, Simon L, Fourel F, Martineau F, Lynnerup N, Reychler H, Escarguel G. 2008. Oxygen isotope fractionation between human phosphate and water revisited. J Hum Evol 55:1138–1147.

De Ligt L, Tacoma L. 2016. Approaching Migration in the Early Roman Empire. In: De Ligt L, Tacoma L, editors. Migration and Mobility in the Early Roman Empire. Leiden: Brill:1–22.

Dickin A. 2005. Radiogenic Isotope Geology, Second Edition. Cambridge: Cambridge University Press.

Durante C, Baschieri C, Bertacchini L, Bertelli D, Cocchi M, Marchetti A, Manzini D, Papotti G, Sighinolfi S. 2014. An analytical approach to Sr isotope ratio determination in Lambrusco wines for geographical traceability purposes. Food Chem 173:557–563.

Eckardt H, Chenery C, Booth P, Evans JA, Lamb A, Müldner G. 2009. Oxygen and strontium isotope evidence for mobility in Roman Winchester. J Archaeol Sci 36:2816–2825.

Eckardt H, Chenery C, Leach S, Lewis M, Muldner G, Nimmo E. 2010. A Long Way From

Home: Diaspora Communities in Roman Britain. In: Eckardt H, editor. Roman Diasporas: Archaeological Approaches to Mobility and Diversity in the Roman Empire. Portsmouth: Journal of Roman Archaeology Supplementary Series 78: 99–130.

Edmonson J. 2011. Slavery and the Roman Family. In: Bradley K, Cartledge P, editors. The The Cambridge World History of Slavery, 1: The Ancient Mediterranean World. Cambridge: Cambridge University Press:337–361.

Eckardt H, Müldner G, Lewis M. 2014. People on the move in Roman Britain. World Archaeol 46:534–550.

Emery MV, Prowse TL, Elford S, Schwarcz HP, Brickley M. 2017. Geographic origins of a War of 1812 skeletal sample integrating oxygen and strontium isotopes with GIS-based multi-criteria evaluation analysis. J Archaeol Sci Reports 14:323–331.

Evans J, Montgomery J, Wildman G, Boulton N. 2010. Spatial variation in biosphere 87Sr/86Sr in Britain. J Geol Soc London 167:1–4.

Evans J, Stoodley N, Chenery C. 2006. A strontium and oxygen isotope assessment of a possible fourth century immigrant population in a Hampshire cemetery, southern England. J Archaeol Sci 33:265–272.

Flockhart DTT, Kyser TK, Chipley D, Miller NG, Norris DR. 2015. Experimental evidence shows no fractionation of strontium isotopes (87Sr/86Sr) among soil, plants, and herbivores: implications for tracking wildlife and forensic science. Isotopes Environ Health Stud 51:372–381.

Gat J. 2005. Some Classical Concepts of Isotope Hydrology: "Rayleigh Fractionation, Meteoric Water Lines, the Dansgaard Effects (Altitude, Latitude, Distance From the Coast and Amount Effects) and the D-Excess Parameter. In: Aggarwal P, Gat J, Froehlich K, editors. Isotopes in the Water Cycle: Past, Present, and Future of a Developing Science. Dordrecht, The Netherlands: Spinger:127–139.

Geer RM, translator. 1954. Diodorus Siculus. Library of History, Volume X (Books 19.66–20) Loeb Classical Library. Cambridge, MA: Harvard University Press.

George M. 2013. Roman Slavery and Material Culture. Toronto: Toronto University Press.

Giustini F, Brilli M, Patera A. 2016. Mapping oxygen stable isotopes of precipitation in Italy. J Hydrol Reg Stud 8:162–181.

GNIP. 2015. Global Network of Isotopes in Precipitation (GNIP). http://www-naweb.iaea.org/napc/ih/IHS_resources_gnip.html.

Harris W. 1980. Towards a Study of the Roman Slave Trade. In: D'Arms JH, Kopff EC, editors.

The Seaborne Commerce of Ancient Rome: Studies in History and Archaeology. Memoirs of the American Academy in Rome 36:117–140.

Harris W. 1999. Demography, Geography, and the Sources of Roman Slaves. J Rom Stud 89:62–75.

Hartman G, Richards MP. 2014. Mapping and defining sources of variability in bioavailable strontium isotope ratios in the eastern Meditearranean. Geochim Cosmochim Acta 126: 250–264.

Hodell DA, Quinn RL, Brenner M, Kamenov G. 2004. Spatial variation of strontium isotopes (87Sr/86Sr) in the Maya region: A tool for tracking ancient human migration. J Archaeol Sci 31:585–601.

Hoefs J. 2004. Stable Isotope Geochemistry. Berlin-Heidelberg: Springer-Verlag.

Hoppe KA, Koch PL, Furutani TT. 2003. Assessing the preservation of biogenic strontium in fossil bones and tooth enamel. Int J Osteoarch 13: 20–28.

Iacumin P, Bocherens H, Mariotti A, Longinelli A. 1996. Oxygen isotope analyses of co-existing carbonate and phosphate in biogenic apatite: a way to monitor diagenetic alteration of bone phosphate? Earth Planet Sci Lett 142:1–6.

Killgrove K. 2010a. Migration and Mobility in Imperial Rome. Unpublished PhD Dissertation, University of North Carolina, Chapel Hill.

Killgrove K. 2010b. Identifying Immigrants to Imperial Rome Using Strontium Isotope Analysis. In: Eckardt H, editor. Roman Diasporas: Archaeological Approaches to Mobility and Diversity in the Roman Empire. Portsmouth: Journal of Roman Archaeology Supplementary Series 78:157–174.

Killgrove K. 2010c. Response to C. Bruun "Water, Oxygen Isotopes and Immigration to Ostia-Portus." J Rom Archaeol 23:133–136.

Killgrove K, Montgomery J. 2016. All roads lead to Rome: Exploring human migration to the eternal city through biochemistry of skeletons from two imperial-era cemeteries (1st-3rd c AD). PLoS One 11:1–30.

Knudson KJ, Tung T, Nystrom KN, Price TD, Fullagar PD. 2005. The origin of the Juch'uypampa cave mummies: strontium isotope analysis of archaeological remains from Bolivia. J Archeol Sci 32:903–913.

Knudson KJ, Pestle WJ, Torres-Rouff C, Pimental G. 2012. Assessing the life history of an Andean traveller through biogeochemistry: stable and radiogenic isotope analysis of archaeological human remains from northern Chile. Int J Osteoarchaeol 22: 435–451.

Kohn MJ, Schoeninger MJ, Barker WW. 1999. Altered states: effects of diagenesis on fossil

tooth chemistry. Geochim Cosmochim Act 63: 2737–2747.

Laffoon JE, Sonnemann TF, Shafie T, Hofman CL, Brandes U, Davies GR. 2017. Investigating human geographic origins using dual-isotope (87Sr/86Sr, δ18O) assignment approaches. PLoS One: DOI 10.1371/journal.pone.0172562.

Leach S, Lewis M, Chenery C, Muldner G, Eckardt H. 2009. Migration and diversity in Roman Britain: A multidisciplinary approach to the identification of immigrants in Roman York, England. Am J Phys Anthropol 140:546–561.

Lee-Thorp JA, Sponheimer M. 2003. Three case studies used to reasses the reliability of fossil bone and enamel isotope signals for paleodietary studies. J Anthropol Archaeol 22: 208–216.

Lightfoot E, O'Connell TC. 2016. On the use of biomineral oxygen isotope data to identify human migrants in the archaeological record: intra-sample variation, statistical methods and geographical considerations. PLoS One 11:e0153850.

Lightfoot E, Šlaus M, O'Connell TC. 2014. Water consumption in Iron Age, Roman, and Early Medieval Croatia. Am J Phys Anthropol 154:535–543.

Lo Cascio J. 1999. The Population of Roman Italy in Town and Country. In: Intlilff B, Sbonias K, editors. Reconstructing Past Population Trends in Mediterranean Europe (3000 BC– AD 1800) Oakville CT: Oxbow Books: 161–172.

Longinelli A. 1984. Oxygen isotopes in mammal bone phosphate: A new tool for paleohydrological and paleoclimatological research? Geochim Cosmochim Acta 48:385–390.

Longinelli A, Selmo E. 2003. Isotopic composition of precipitation in Italy: A first overall map. J Hydrol 270:75–88.

Luz B, Kolodny Y, Horowitz M. 1984. Fractionation of oxygen isotopes between mammalian bone-phosphate and environmental drinking water. Geochim Cosmochim Acta 48:1689–1693.

Madden J. 1996. Slavery in the Roman Empire: Numbers and Origins. Dublin, Ireland: University College.

Marchionni S, Braschi E, Tommasini S, Bollati A, Cifelli F, Mulinacci N, Mattei M, Conticelli S. 2013. High-precision 87Sr/86Sr analyses in wines and their use as a geological fingerprint for tracing geographic provenance. J Agric Food Chem 61:6822–6831.

Matano F, Barbieri M, Di Nocera S, Torre M. 2005. Stratigraphy and strontium geochemistry of

Messinian evaporite-bearing successions of the southern Apennines foredeep, Italy: Implications for the Mediterranean "salinity crisis" and regional palaeogeography. Palaeogeogr Palaeoclimatol Palaeoecol 217:87–114.

Montgomery J, Evans J, Chenery C, Pashley V, Killgrove K. 2010. Gleaming, White and Deadly: Using Lead to Track Human Exposure and Geographic Origins in the Roman Period in Britain. In: Eckardt H, editor. Roman Diasporas: Archaeological Approaches to Mobility and Diversity in the Roman Empire. Portsmouth: Journal of Roman Archaeology Supplementary Series 78:199–226.

Morley N. 2001. The transformation of Italy, 225-28 BC. J Roman Studies 91: 50–62.

Müldner G, Chenery C, Eckardt H. 2011. The "Headless Romans": Multi-isotope investigations of an unusual burial ground from Roman Britain. J Archaeol Sci 38:280–290.

Nafplioti A. 2011. Tracing population mobility in the Aegean using isotope geochemistry: A first map of local biologically available 87Sr/86Sr signatures. J Archaeol Sci 38:1560–1570.

Noy D. 2000. Foreigners of Rome: Citizens and Strangers. London UK: Gerald Duckworth & Co, Ltd.

Pellegrini M, Donahue R, Chenery C, Evans J, Lee-Thorp J, Montgomery J, Mussi M. 2008. Faunal migration in late-glacial central Italy: implications for human resource exploitation. Rapid Commun Mass Spectrom 22:1714–1726.

Petrini R, Sansone L, Slejko FF, Buccianti A, Marcuzzo P, Tomasi D. 2015. The 87Sr/86Sr strontium isotopic systematics applied to Glera vineyards: A tracer for the geographical origin of the Prosecco. Food Chem 170:138–144.

Prowse TL. 2016. Isotopes and Mobility in the Ancient Roman World. In: De Ligt L, Tacoma L, editors. Migration and Mobility in the Early Roman Empire. Leiden: Brill:205–233.

Prowse TL, Barta J, Hunnius T, Small A. 2010. Stable isotope and mtDNA evidence for geographic origins at the site of Vagnari, South Italy. In: Eckardt H, editor. Roman Diasporas: Archaeological Approaches to Mobility and Diversity in the Roman Empire. Portsmouth: Journal of Roman Archaeology Supplementary Series 78:175–198.

Prowse TL, Schwarcz HP, Garnsey P, Knyf M, Macchiarelli R, Bondioli L. 2007. Isotopic evidence for age-related immigration to imperial Rome. Am J Phys Anthropol 128:2–13.

Rathbone DW. 1983. The slave mode of production in Italy. J Roman Studies 73: 160–168.

Reinhardt EG, Cavazza W, Patterson RT, Blenkinsop J. 2000. Differential diagenesis of sedimentary components and the implication for strontium isotope analysis of carbonate rocks. Chem Geol 164:331–343.

Rossmann A, Haberhauer G, Hölzl S, Horn P, Pichlmayer F, Voerkelius S. 2000. The potential of multielement stable isotope analysis for regional origin assignment of butter. Eur Food Res Technol 211:32–40.

Rostovtzeff M. 1971. The Social and Economic History of the Roman Empire. Oxford: Oxford University Press.

Roveri M, Lugli S, Manzi V, Gennari R, Schreiber BC. 2014. High-resolution strontium isotope stratigraphy of the messinian deep mediterranean basins: Implications for marginal to central basins correlation. Mar Geol 349:113–125.

Rummel S, Dekant CH, Holzl S, Kelly SD, Baxter M, Marigheto N, Quetel CR, Larcher R, Nicolini G, Fr??schl H, Ueckermann H, Hoogewerff J. 2012. Sr isotope measurements in beef-analytical challenge and first results. Anal Bioanal Chem 402:2837–2848.

Scheidel W. 1997. Quantifying the Sources of Slaves in the Roman Empire. J Rom Archaeol 87:159–169.

Scheidel W. 1999. The Slave Population of Roman Italy: Speculations and Constraints. Topoi 9:129–144.

Scheidel W. 2001. Debating Roman Demography. Leiden: Brill.

Scheidel W. 2004. Human Mobility in Roman Italy I: The Free Population. J Rom Stud 94:1–26.

Scheidel W. 2005. Human Mobility in Roman Italy II: The Slave Population. J Rom Stud 95:64–79.

Scheidel W. 2007. The Roman Slave Supply. Princeton/Stanford Papers in Classics. In: Bradley P, Cartledge P, editors. The Cambridge World History of Slavery, 1: The Ancient Mediterranean World. Cambridge: Cambridge University Press:287–310.

Scheuer L, Black S. 2000. Developmental Juvenile Osteology. San Diego, California: Elsevier Academic Press.

Schlüter M, Steuber T, Parente M. 2008. Chronostratigraphy of Campanian-Maastrichtian platform carbonates and rudist associations of Salento (Apulia, Italy). Cretac Res 29:100–114.

Schweissing MM, Grupe G. 2003. Stable strontium isotopes in human teeth and bone: A key to migration events of the late Roman period in Bavaria. J Archaeol Sci 30:1373–1383.

Small A. 2002. Apulia before and after the Roman conquest: Recent evidence from Botromagno. J Rom Archaeol 15:375–379.

Small A, Small C. 2005. Defining an Imperial Estate: The Environs of Vagnari in South Italy: In: Attema P, Nijboer A, Zifferero A, editors. Communities and Settelements From the Neolithic to the early Medieval Period, Vol. II. Proceedings of the 6th Conference of Italian Archaeology, University of Groningen, April 15–17. Oxford: BAR: 894–902.

Small A. 2011. Vagnari. Il Villagio, L'artigianato, La proprieta imperiale. Bari: Edipuglia.

Stark R. 2016. Ancient Lives in Motion. Unpublished PhD Dissertation, McMaster University, Hamilton, Canada.

Trincherini PR, Baffi C, Barbero P, Pizzoglio E, Spalla S. 2014. Precise determination of strontium isotope ratios by TIMS to authenticate tomato geographical origin. Food Chem 145:349–355.

Vander-Auwera J, Andre L. 1991. Trace elements (REE) and isotopes (O, C, Sr) to characterize the metasomatic fluid sources: evidence from the skarn deposit (Fe, W, Cu) of Traversella (Ivrea, Italy). Contrib to Mineral Petrol 106:325–339.

Veizer J. 1989. Strontium isotopes in seawater through time strontium isotope systematics. Ann Rev Earth Planet Sci 17:14167.

Voerkelius S, Lorenz GD, Rummel S, Quétel CR, Heiss G, Baxter M, Brach-Papa C, Deters-Itzelsberger P, Hoelzl S, Hoogewerff J, Ponzevera E, Van Bocxstaele M, Ueckermann H. 2010. Strontium isotopic signatures of natural mineral waters, the reference to a simple geological map and its potential for authentication of food. Food Chem 118:933–940.

White T, Folkens P. 2005. The Human Bone Manual. Burlington, MA: Elsevier Academic Press.

Willmes M, McMorrow L, Kinsley L, Armstrong R, Aubert M, Eggins S, Falguères C, Maureille B, Moffat I, Grün R. 2014. The IRHUM (Isotopic Reconstruction of Human Migration) database - Bioavailable strontium isotope ratios for geochemical fingerprinting in France. Earth Syst Sci Data 6:117–122.

Wilson A. 1966. Emigration From Italy in Republican Rome. Manchester, UK: Manchester University Press.

Wright LE, Shchwacz HP. 1996. Infrared Isotopic Evidence for Diagenesis of Bone Apatite at Dos Pilas, Guatemala: Paleodietary Implications. J Archaeol Sci 23: 933–944.

Wright LE, Schwarcz HP. 1998. Stable carbon and oxygen isotopes in human tooth enamel: Identifying breastfeeding and weaning in prehistory. Am J Phys Anthropol 106:1–18.

Yavetz Z. 1988. Slaves and Slavery in Ancient Rome. London, UK: Transaction Publishers.

Chapter 4.0

Ancient Roman Mitochondrial Genomes and Isotopes Reveal Relationships and Geographic Origins at the Local and pan-Mediterranean Scales

*Matthew V. Emery[1,2], Ana T. Duggan[1,2], Tyler J. Murchie[1,2], Robert J. Stark[2], Jennifer Klunk[1,5], Jessica Hider[1,2], Katherine Eaton[1,2], Emil Karpinski[1,5], Henry P. Schwarcz[3], Hendrik N. Poinar[1,2,4,5,6] and Tracy L. Prowse[2]

[1]McMaster Ancient DNA Centre, McMaster University, Hamilton, Canada
[2]Department of Anthropology, McMaster University, Hamilton, Canada
[3]School of Geography and Earth Sciences, McMaster University, Hamilton, Canada
[4]Institute of Infectious Disease Research, McMaster University, Hamilton, Canada
[5]Department of Biology, McMaster University, Hamilton, Canada
[6]Department of Biochemistry and Biomedical Sciences, McMaster University, Hamilton, Canada

Short Title: The mtDNA Diversity of Roman Italian Workers

*Corresponding Author

Matthew Emery, PhD Candidate
McMaster Ancient DNA Centre, McMaster University
1280 Main Street West, Hamilton, Ontario
L8S 4L8
Phone: 905-515-1842
Email: emerymv@mcmaster.ca

Keywords: Roman Italy; ancient DNA; mtDNA diversity; isotope analysis; bioarchaeology; Iron Age; maternal ancestry

4.1 Abstract

Rome initiated several campaigns to expand, conquer, and enslave local Italic populations following the establishment of the republic in 504 BCE. However, the cultural and biological changes resulting from Roman subjugation across Italy remain a topic of intense historical debate. Although important, historic and archaeological lines of evidence fail to track the impact of forced enslavement and enculturation at individual and broader genetic scales and, more broadly, offer fewer clues regarding the potential affinities of Roman period Italians to European, Near Eastern, western Asian and North African populations at this time.

In this paper, we present the whole mitochondrial (mtDNA) genomes of 30 Roman period (1^{st} - 4^{th} centuries CE) individuals buried in the Vagnari *necropolis* in southern Italy. We integrate the mtDNA data with previously published bioarchaeological and isotope ($\delta^{18}O$ and $^{87}Sr/^{86}Sr$) data for the Vagnari assemblage, and compare Roman haplogroup composition to 15 mitochondrial genomes obtained from a pre-Roman Iron Age skeletal assemblage, located in close proximity to Vagnari. Additionally, we contrast our South Italian dataset to a further 357 complete mtDNA genomes from the pan-Mediterranean region, Europe, western Asia and North African regions.

Population pairwise Φ_{ST} values suggest that Roman Italians share closer genetic similarity to Neolithic and Bronze Age populations from Europe and the eastern Mediterranean than with Iron Age Italians, Armenians, and Roman period Egyptians. Vagnari individuals with $\delta^{18}O$, $^{87}Sr/^{86}Sr$, and mtDNA data suggest a predominantly local demographic was employed at the site. However, two individuals belong to eastern Eurasian haplogroup D4b1c, indicating that the maternal ancestors of these two individuals migrated to South Italy prior to the 1^{st} century CE. Additionally, we provide the first genetic evidence for possible maternal relatedness in a Roman period skeletal assemblage. Our research highlights the significance of integrating multiple lines of bioarchaeological data to inform interpretations about Roman colonial expansion and its impact on population structure.

4.2 Introduction

The application of ancient DNA (aDNA) and stable isotope analysis has greatly improved our understanding of population-wide demographic changes and disease in past populations (Skoglund et al., 2012; Wagner et al., 2014; Haak et al., 2015; Bos et al., 2016; Duggan et al., 2016; Schuenemann et al., 2017; Wong et al., 2017). A growing interest in the paleodemography of ancient Mediterranean populations has prompted the biomolecular analysis of skeletal assemblages from this historically complex region (Bouwman et al., 2008; Chilvers et al., 2008; Lacan et al., 2011; Olalde et al., 2015; Lazaridis et al., 2017). Despite increased interest and a growing number of publicly available aDNA datasets, investigations detailing the genetic makeup of southern Italian pre-Roman and Roman period populations are absent. Detailed genetic and isotopic analyses of classical Italian remains stand to elucidate important demographic questions inaccessible through artifactual, textual, and epigraphic evidence alone. Traditional approaches to studying the effects of Roman expansion and colonialism rely primarily on literary sources and archaeological evidence (Salmon, 1955; Whittaker, 1994; Attema and van Leusen, 2004; De-Ligt and Northwood, 2008; Stek and Pelgrom, 2014). The historical sources focused on their audience of literate, privileged, male, and dominant patriarchs of Rome while marginalizing other members of Roman society, such as women, children, and lower class individuals living in rural areas (Paoli, 1973; Bradley, 1994; Williams, 1997; Crawford, 2001). More recent investigations have concentrated on integrating several lines of ancient DNA (aDNA), historic, bioarchaeological, and isotopic data from a broad spectrum of Roman society to inform their interpretations about past mobility and the prevalence of disease (Prowse et al., 2010; Killgrove and Montgomery, 2016; Marciniak et al., 2016; Prowse, 2016). Although research has focused on how Roman subjugation of the indigenous Italic and Greek

colonial populations impacted the demographic composition of Roman Italy, little is known about the biological composition of populations in southern Italy as a result of these military and political conquests. This paper investigates how pre-Roman and Roman genetic diversity changed over time, and the genetic relationships Roman period South Italians had with contemporaneous populations across Europe, western Asia, the Near East, and North Africa, before and during the classical period.

Our research integrates previously analyzed $\delta^{18}O$ and $^{87}Sr/^{86}Sr$ isotope data (i.e., Emery et al., in review; Prowse 2016) and bioarchaeological data (n=43), which provides information on geographic origins on the sample from Roman Vagnari, with whole mitochondrial DNA (mtDNA) sequences obtained from Iron Age Botromagno (7^{th} – 4^{th} centuries BCE) (n=15) and Roman period Vagnari (1^{st} – 4^{th} centuries CE) (n=30). We compare southern Italian Iron Age and Roman mtDNA haplogroup compositions to ancient mtDNA sequences (n=357) spanning the Upper Paleolithic through the Roman periods and document a case of possible maternal relations in the Roman *necropolis*. We analyze the population history of pre-Roman and Roman period southern Italy within the context of social and political upheaval at the local and broader Mediterranean scales.

4.3 Iron Age Botromagno and Roman Period Vagnari

4.3.1Botromagno (7th – 4th century BCE)

Following the establishment of the Roman republic in 504 BCE, Rome conquered and expanded its territory into central and southern Italy. Roman armies conquered and acquired territories in central Italy starting in the 5^{th} century BCE, defeating the Samnites over the span of three major wars (343 – 290 BCE), and expanded to areas of southern Italy by the 3^{rd} century

BCE (Cornell, 1995). The Iron Age settlement at Botromagno is a hilltop settlement located West of the modern town of Gravina in Puglia (Fig. 1). The settlement was home to a prosperous *Peucetian* community (7^{th} – 4^{th} century BCE) at a time of intense Greek colonization

Figure 1: Map of Italy showing the location of Iron Age Botromagno and Roman Vagnari.

of South Italy (*Magna Graecia*) (Small, 1992). Historic records indicate that Botromagno (recognized as Roman *Silvium*) was secured by a Roman consular army in 306 BCE (Small, 2002). Southern Italy's Italic and Greek communities were subjected to repeated conflicts between Greece and Rome (Pyrrhic Wars) and Rome and Carthage (Punic Wars). These conflicts coincided with an apparent depopulation of the southern Italian Iron Age sites between the 4th and 3rd centuries BCE, and by the 2nd century BCE with the establishment of Roman colonies (*coloniae*).

Early archaeological excavations at Botromagno were conducted on behalf of the British School at Rome between 1965 and 1974 by Joan Taylor (Brooks et al., 1966; Ward-Perkins et al., 1969; Taylor et al., 1976; Small, 1992). Excavations uncovered a substantial number of groticella tombs, associated artifacts, and a modest settlement composed of small house-dwellings, courtyards, and two *necropoli* at the base of the hill, known locally as Padreterno and Parco San Stefano (Small, 1992). No public spaces or centralized governing quarters were identified, suggesting that the site was likely a dependent rural village (*vicus* or *pagus*) (Small, 2002). Burials were interred with grave goods characteristic of native Apulian pottery traditions with shifting burial customs ranging from Iron Age Italic to Hellenistic in nature. Evidence suggests that individuals were interred according to both local and Greek customs, with tomb structures during the 6th century BCE taking the form of pit extensions and sarcophagi. However, the flexed burial positions at Botromagno are consistent with Italic traditions of the Early to Middle southern Italian Iron Age, remaining unchanged until larger, increasingly elaborate *semicamara* tombs were constructed in the 4th century BCE (Small, 1992; Peruzzi, 2016).

4.3.2 Vagnari (1st - 4th century CE)

Vagnari is a 1st - 4th century CE Roman period site located 14 km northwest of Gravina in Puglia (Fig. 1). The cemetery is located adjacent to a small rural village (*vicus*) and early Roman villa (1st c. BCE - 1st c. CE) (San Felice), located on a hill to the South of the cemetery (Small et al., 2000). Excavations at the Roman *necropolis* began in 2002 when subsurface tombs were identified. Since then, over 130 burials have been recovered including a number of grave goods interred with the deceased. Five tomb 'types' were identified at Vagnari: *'alla cappuccina*', cremation, funnel burials for libation offerings, soil burials, and disturbed graves (Small and Small, 2007; Brent and Prowse, 2014). A select number of grave goods recovered to date include fragmentary and intact ceramic pots, oil lamps, coins, bronze vessels, hobnails, glass vessels, bracelets and necklaces, and various iron and bronze weapons, such as pruning hooks and spearheads (Brent and Prowse, 2014). Current evidence points to a community engaged in agricultural and industrial production likely driven by slaves, lower-class workers, and/or freedmen who lived onsite at the adjacent *vicus*.

Preliminary mtDNA data generated by Prowse et al., (2010) targeting the HVR-1 region of the mitochondrial genome, assessed the haplogroups of 10 Vagnari individuals, and identified haplogroups typical of Eurasian populations (haplogroups H, J, K, and T). Two individuals harboured haplogroups characteristic to Africa (L) and eastern Eurasia (D).

4.3.3 $\delta^{18}O$ and $^{87}Sr/^{86}Sr$ Analysis of the Vagnari Assemblage

The $\delta^{18}O$ an $^{87}Sr/^{86}Sr$ composition of bones and teeth directly reflect the water ($\delta^{18}O$) and foods ($^{87}Sr/^{86}Sr$) consumed during life (Schweissing and Grupe, 2003; Chenery et al., 2012). By integrating $\delta^{18}O$ and $^{87}Sr/^{86}Sr$ data that are known to vary geographically, it may be possible to

determine the geographic region of origin (or long-term residency before death) of human remains by matching tooth $\delta^{18}O$ and $^{87}Sr/^{86}Sr$ values with the local $\delta^{18}O$ (rainwater) and $^{87}Sr/^{86}Sr$ (geological substrate) baseline variation (Bentley, 2006; Bowen, 2010). As a result, isotopic analysis of archaeological remains has provided a substantial amount of information regarding migration and mobility in the past (Pellegrini et al., 2016; Barberena et al., 2017; Gregoricka and Sheridan, 2017; Marsteller et al., 2017; Perry et al., 2017; Peschel et al., 2017; Wilhelmson and Price, 2017). The $\delta^{18}O$ and $^{87}Sr/^{86}Sr$ values in teeth reflect the isotopic composition of food and water consumed during childhood.

It is necessary to obtain local baseline $\delta^{18}O$ and $^{87}Sr/^{86}Sr$ estimates of the study region to determine the geographic provenance of archaeological remains. $^{87}Sr/^{86}Sr$ values for the Italian peninsula generally increase from southern Italy to the Alps along a North-South axis (Emery et al., in review). Italian meteoric $\delta^{18}O$ variation generally follows an East-West gradient, with heavier $\delta^{18}O$ values (>-6‰) recorded along the Italy's coastlines, progressing to lighter values (<-9‰) towards the interior (Longinelli and Selmo, 2003; Giustini et al., 2016). Previous $\delta^{18}O$ analyses conducted on a subset of the Vagnari assemblage determined that the majority of the occupants buried in the *necropolis* were born at Vagnari (>90%), falling within the local $\delta^{18}O$ range (-10‰ to -6‰) of the southern Italian region (Prowse et al., 2010; Prowse, 2016). More recent $\delta^{18}O$ and $^{87}Sr/^{86}Sr$ analysis obtained from a larger portion of the Vagnari assemblage, together with new $^{87}Sr/^{86}Sr$ baseline information for the Italian peninsula, found that over half of the Vagnari occupants (58%) were local to the site, while a further 34% were identified as originating from southern Italy (Emery et al., in review). Approximately 7% of the individuals analyzed were likely born outside of South Italy, from either northern Italy or further afield from Europe and North Africa (Emery et al., in review). To further refine the possible geographic

origins of the Vagnari skeletal sample, mtDNA analysis provides another line of evidence for mobility by identifying potential genetic relationships that exist between the Romans themselves, as well as the possible genetic affinities between the ancient southern Italians (Iron Age and Roman individuals) and pre-Roman and Roman populations from Eurasia.

4.4 Materials and Methods

A total of 41 Vagnari teeth, each representing one individual, were selected for aDNA processing. In order to maximize interpretation and contextualize the mtDNA results, we included samples with complementary bioarchaeological, $\delta^{18}O$, and $^{87}Sr/^{86}Sr$ data. Previously published mtDNA data on 15 Iron Age samples from the site of Botromagno was included as provisional data (from Emery et al., in review). In addition, we obtained 357 whole-mtDNA sequences from GenBank and the ENA (European Nucleotide Archive) for comparative mtDNA analysis. Egyptian sequence data (Schuenemann et al., 2017) was downloaded from the ENA (ID ERP017224) and re-processed according to the parameters outlined in Supplement 1. Stable and radiogenic isotope laboratory methodology is provided in Supplement 1.

4.4.1 Age and Sex Estimation of the Vagnari Skeletal Sample

We estimated age-at-death and sex using standard osteological methods, outlined in Buikstra and Ubelaker (1994). The ages of subadult and juvenile skeletons were determined using long bone length, epiphyseal fusion of the long bones, and tooth development and eruption. The age of adult skeletons was assessed using morphological changes to the auricular surface of the ilium and pubic symphysis, along with cranial suture closure. Sex was determined using standard morphological features of the cranium and pelvis (see Table 1).

4.4.2 Demineralization, Enzymatic Digestion, and DNA Extraction

All aDNA laboratory work for the Roman samples was conducted in dedicated clean rooms at the McMaster Ancient DNA Centre. All laboratory bench space and tools were cleaned using a 6% solution of sodium hypochlorite (NaClO), and washed with UV-irradiated ultrapure water. Molar roots were cut using a diamond-cutting wheel and the resulting material pulverized and transferred into 2 ml MAXYMum Recovery PCR Tubes (Axygen). Teeth sub-samples were stored at -20°C for demineralization and digestion.

Samples were demineralized in 500 µL of 0.5 M EDTA solution (pH 8.0) and the supernatant collected and dispensed into 1.7 ml MAXYMum Recovery PCR Tubes. Enzymatic digestion was performed using 500 uL buffer comprised of 5 mM calcium chloride ($CaCl_2$), 20 mM Tris-HCl (pH 8.0), 2.5 mM N-phenacylthiazolium bromide (PTB), 50 mM dithiothreitol (DDT), 0.5% sarcosyl, 1% polyvinylpyrrolidone (PVP) and 20 mg/mL Proteinase K in nuclease free ultrapure H_2O. 500 uL of digestion supernatant was collected and dispensed into tubes containing 500 µL of demineralization supernatant. This process was repeated for a second round for a total of 2 mL of supernatant for each sample.

DNA extractions were carried out according to established protocol (Dabney et al., 2013). Two mL of supernatant was added to a binding buffer containing 5 M guanidine hydrochloride (GuHCl), 40% isopropanol, Tween-20, 90 mM sodium acetate (pH 5.2), then added to Roche biopurification columns. Silica membranes were washed with 750 µL PE Buffer (Qiagen), and then eluted with 25 µL of buffer EB. This process was repeated a second time for a final extraction volume to 50 µL. Final DNA extracts were stored at -20°C for double-stranded library preparation and indexing.

4.4.3 Double Stranded Library Preparation and Post-Library Indexing

Library preparation followed established protocol for Illumina sequencing (Meyer and Kircher, 2010; Kircher et al., 2012). All processed extracts and extraction blanks, in addition to two library blanks, were converted to double-stranded DNA libraries. DNA extracts were blunt-end repaired with a master mix comprised of NE Buffer 2, BSA, dNTPs, ATP, T4 polynucleotide kinase, T4 DNA polymerase, and ultrapure H_2O according to standardized concentrations, incubated at 25°C (15 minutes) and 12°C (15 minutes), then purified over Qiagen MinElute columns. 20 µL were purified over Qiagen MinElute columns at a 5:1 ratio of Buffer PB to template according to manufacturer protocol. Adapter ligation master mix was composed of T4 DNA Ligase Buffer, PEG-4000, Adapter mix (10 µM), and T4 DNA Ligase, ultrapure H_2O and sample extracts were incubated for 16 hours at 15°C, and purified over Qiagen MinElute columns. Adapter fill-in reactions were incubated for 30 minutes at 37°C followed by a final heat denaturation at 80°C for 20 minutes, and eluted in 40 µL buffer EB using Qiagen MinElute columns. Roman samples were indexed using unique P5 and P7 primer combinations together with purified library template according to the following scheme: 12.5 µL of library with KAPA SYBR® FAST qPCR Master Mix (2X), an indexing primer concentration of 750 nM, ultrapure H_2O (Kircher et al., 2012).

4.4.4 mtDNA Enrichment

The targeted capture of mtDNA molecules was carried out in accordance with the manufacturer's protocol (MYcroarray, Ann Arbor, MI), with minor alterations to time (24 hours), bait concentration (50 ng), and hybridization temperature (55°C). Indexed libraries, including both extraction and library blanks, were enriched using mitochondrial RNAs

synthesized from the *H. sapiens* Representative Global Diversity Panel (197 mtDNA sequences) (MYTObaits, MYcroarray, Ann Arbor, MI). Enrichment hybridization/capture and library master mixes were composed of (MYbaits manual v.3.02): 20X SSPE, 0.5 M EDTA, 50X Denhardt's solution, 10% SDS, mitochondrial RNA baits (50 ng per rxn), and 20 U/µL RNase block SUPERase-IN; human Cot1 DNA, salmon sperm DNA, and Illumina Bloligos. Enriched libraries were re-amplified using 18.8 µL of template in a 40 µL reaction for a second round of enrichment.

4.4.5 Sequencing

Enriched Roman libraries were pooled at equimolar concentrations then size selected for DNA fragments ranging from 150 bp to 500 bp in length using a gel cut. Gel plugs were purified using the QIAquick Gel Extraction Kit (Qiagen). Roman libraries were sequenced on an Illumina HiSeq 1500 platform at the Farncombe Family Digestive Health Research Institute (McMaster University, Hamilton ON, Canada) using 2 x 90 bp read chemistry.

4.4.6 Read Processing, mtDNA, and Osteobiographical Analysis

Details concerning read processing, mitochondrial genome assembly, aDNA authentication, and contamination estimates are contained in Supplement 1. We generated population pairwise Φ_{ST} values using Arlequin (v. 3.5.2.2) and conducted Bayesian Skygrid analysis with BEAST (v. 1.8.0). Further information concerning mtDNA analysis is also contained in Supplement 1.

4.5 Results

Eleven Roman samples were omitted from further analysis due to low mapping quality

and/or >10% missing data resulting in the retention of 30 out of 41 samples for population pairwise Φ_{ST} and Bayesian inference analysis. Of the thirty Roman mtDNA genomes that did meet our quality control criteria, the average mtDNA genome coverage was 176.0x (min 8.7x, max 586.1x) (Table 1; Table S1).

Table 1: Mitochondrial DNA Haplogroup, osteobiographic, $\delta^{18}O_{DW}$, $^{87}Sr/^{86}Sr$ results for the Vagnari skeletal assemblage.

Library ID	Feature No.	Age	Sex	Haplogroup	$\delta^{18}O_{DW}$ VSMOW (‰)	$^{87}Sr/^{86}Sr$
LRV 76	F34	Adult	M	D4b1c	-6.3	-
LRV 77	F37	45-49	F	D4b1c	-	-
LRV 92	F95	Adult	F	T2j1	-7.6	0.70827
LRV 93	F96a	Young Adult	M	X2e2a	-6.7	0.70863
LRV 95	F100	Adult	U	T2j1	-	-
LRV 97	F126	20-25	M	N1a1a1a	-6.0	0.70863
LRV 101	F132	Old Adult	F	H1t	-7.4	0.70899
LRV 102	F131	35.2 +/- 9.5	M	J1b1a1+146	-4.1	0.70837
LRV 103	F137A	20-25	M	H16d	-6.7	0.70871
LRV 104	F137B	Adult	U	J1b4	-	-
LRV 105	F67	19-21	M	K2a9	-8.1	0.70971
LRV 110	F206	Old Adult	F	N1b1a2	-7.0	0.70826
LRV 112	F211	Young Adult	F	H50	-5.3	0.70880
LRV 114	F214	Adult (45-49)	M	I5a2	-7.1	0.70895
LRV 118	F215	38.2 ± 10.9 yrs	F	HV	-6.9	0.70866
LRV 119	F216	35.2 ± 9.4 yrs	M	H5'36	-6.5	0.70875
LRV 122	F234	35.2 ± 9.4 yrs	M	K1a12a1a	-8.6	0.70801
LRV 128	F252	17-22.5 yrs	F	H	-8.7	0.70868
LRV 135	F287	Old Adult	M?	H47	-	0.70917
LRV 137	F283	Subadult	U	T2a1b1	-	-
LRV 138	F254	35-45	M	N1a1a1a	-	-
LRV 143	F246	Adult	U	H2	-	0.70865
LRV 146	F292	3 ± 1 year	U	H+73	-	-
LRV 148	F289	?	?	X2+225	-	-
LRV 149	F312	Young Adult	M	H5b	-	0.70868
LRV 151	F280	Adult	F?	T2+16189	-	0.70912
LRV 152	F306	Adult	F?	H5a3a	-	0.70889
LRV 153	F286A	Ind A 16-18 years	U	H2a1b	-	0.70870
LRV 154	F286B	Ind. B 13-14 years	U	T2g	-	0.70894
LRV 156	F247	Adult	M	H15a	-	-

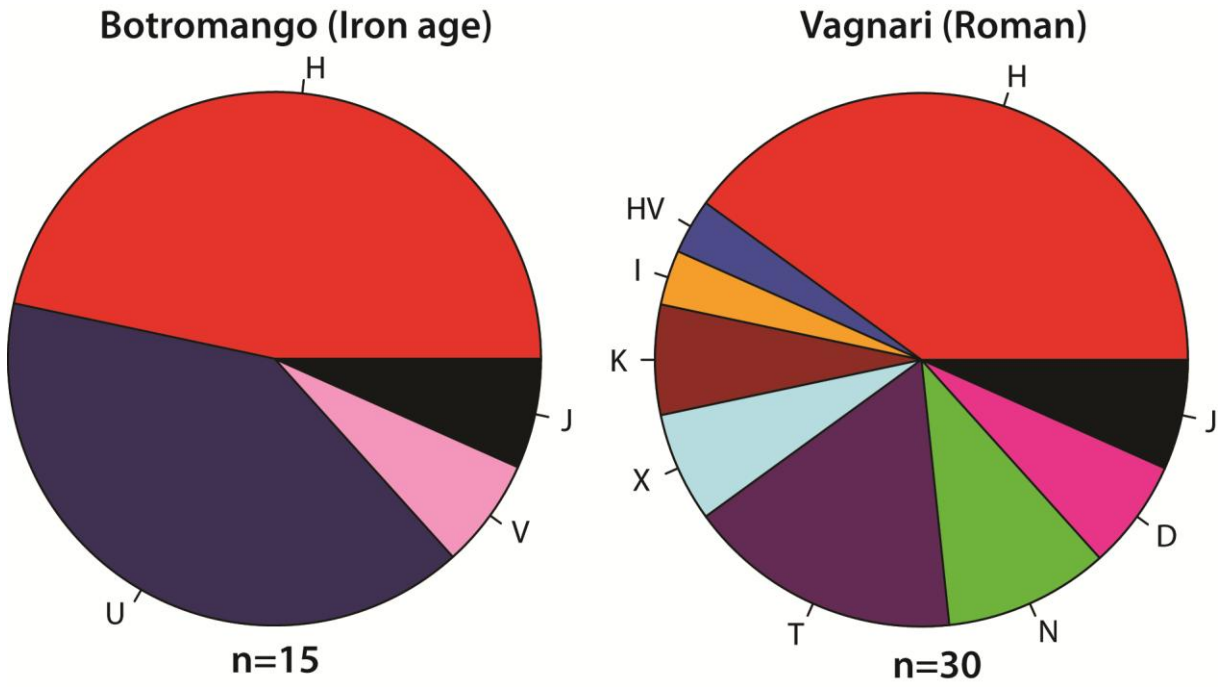

Figure 2: mtDNA haplogroup composition between Botromagno (7th – 4th century BCE; n=15) and Vagnari (1st – 4th century CE; n=30) skeletal assemblages.

Contamination estimates were low to moderate, ranging between 1% and 20% (mean = 3.3%), suggesting minimal human contamination from the burial and laboratory environments (Table S1). We identified the haplogroups consistent with Eurasian ancestry for all samples (Table 1; Fig. 2; Table S1).

Population pairwise Φ_{ST} across geographic categories indicate that the Roman period southern Italian population shares low genetic differentiation (Φ_{ST} = <0.05; Hartl and Clark, 1997) with ancient populations from Armenia (0.01), the Czech Republic (0.05), Egypt (0.02), Germany (0.005), Greece (0.008), and Spain (0.02), and through time with Bronze Age (0.01), Italian Iron Age (0.04), Armenian Iron Age (0.01), the Third Intermediary (0.02), Late (0.008),

Ptolemaic (0.02), and Roman (0.02) periods of Egypt, and Neolithic (0.02) populations, from the same geographic regions (Supplementary Tables S3-S4). Multi-dimensional scaling plots constructed from population pairwise Φ_{ST} values are shown in Figures 3a/b (Fig. S1a/b). Since effective population size is a direct function of genetic diversity and generation time, we employed Bayesian nonparametric demographic modeling in BEAST and generated Skygrid plots (Gill et al., 2013). Skygrid reconstruction using Iron Age and Roman mtDNA diversity data sets show comparable effective female population sizes between the Iron Age and Roman periods in southern Italy (Fig. 4; Supplement 1).

To determine potential maternal relations across the Vagnari cemetery, we superimposed Roman haplogroups (distinguished by colour) over their respective burials using a base map of the Vagnari cemetery (Fig. 5). We hypothesize that shared mtDNAs between burials in close proximity potentially represent maternally related individuals. We identified shared mtDNA haplogroups between burial features F95 and F100 (i.e., T2j1), F34 and F37 (i.e., D4b1c). In addition, the isotope data for F34 and F95 indicate that they were born at, or around, Vagnari. Interestingly, two double burials (F137A/B and F286A/B) contained non-maternally related individuals. We do not have isotope data for one of two individuals in each pair, so we cannot comment on their respective geographic origins. Two individuals recovered from burial feature F137A/B belong to mtDNA haplogroups H16d and J1b4, while another two individuals from F286A/B were identified as belonging to haplogroups H2a1b and T2g, respectively. Delta ^{18}O and $^{87}Sr/^{86}Sr$ from a larger representative Vagnari sample can be found in Prowse (2016) and Emery et al. (in review), and from individuals with both mtDNA, $\delta^{18}O$, and $^{87}Sr/^{86}Sr$ results presented in Table 1.

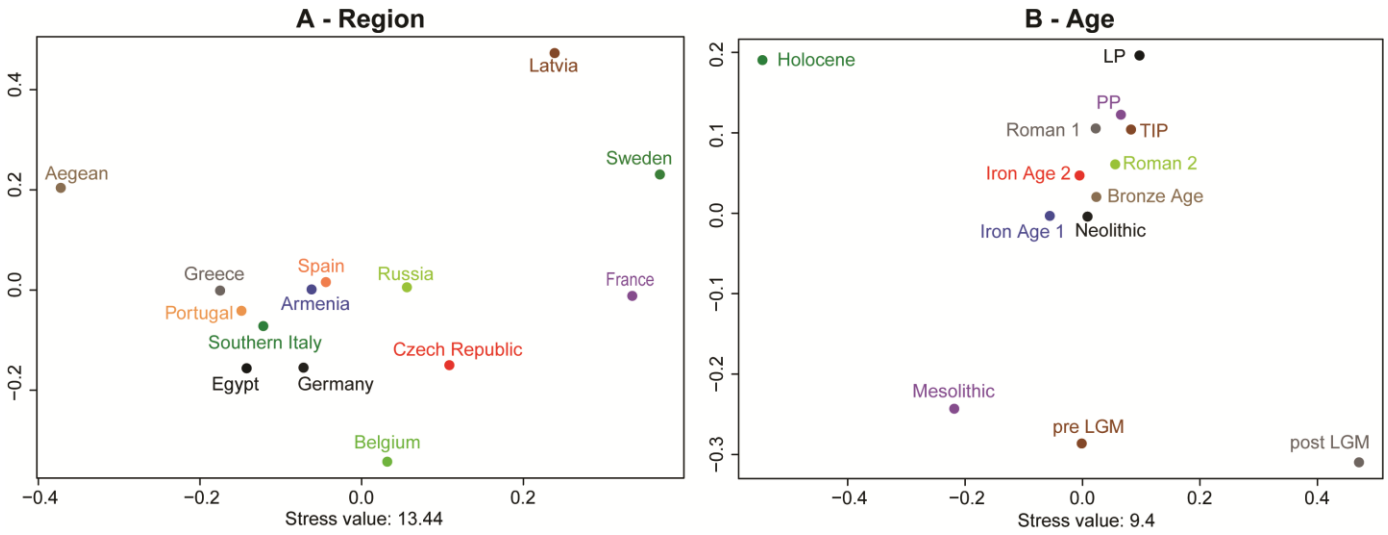

Figure 3a/b: Multi-dimensional scaling plots showing pairwise Φ_{ST} values by a) age and b) country. We removed age and geographic categories with <5 mtDNA sequence representation to reduce scaling stress, which decreased the sample size from 402 mtDNAs to n = 378 by age, and n= 382 by country. a) MDS plot of the mtDNA categorized by country of origin; b) MDS of mtDNA dataset by age spanning the Upper Paleolithic (pre-LGM) to the Roman period. IronAge 1 = Italian Iron Age samples; IronAge 2 = Armenian Iron Age samples; Roman 1 = Italian Roman samples; Roman 2 = Egyptian Roman samples; TIP = Third Intermediary Period (Egypt); LP = Late Period (Egypt); PP = Ptolemaic Period (Egypt).

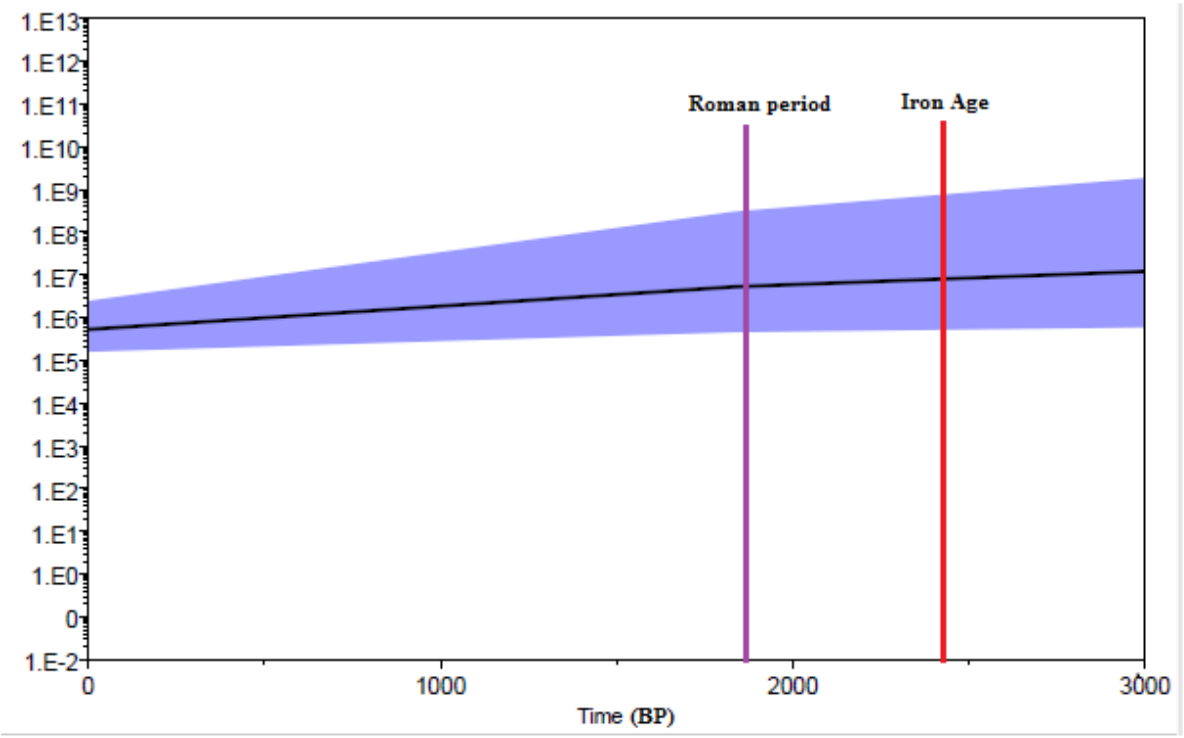

Figure 4: Bayesian Skygrid plot depicting continuous effective female population size over the average time interval between the Iron Age and Roman periods.

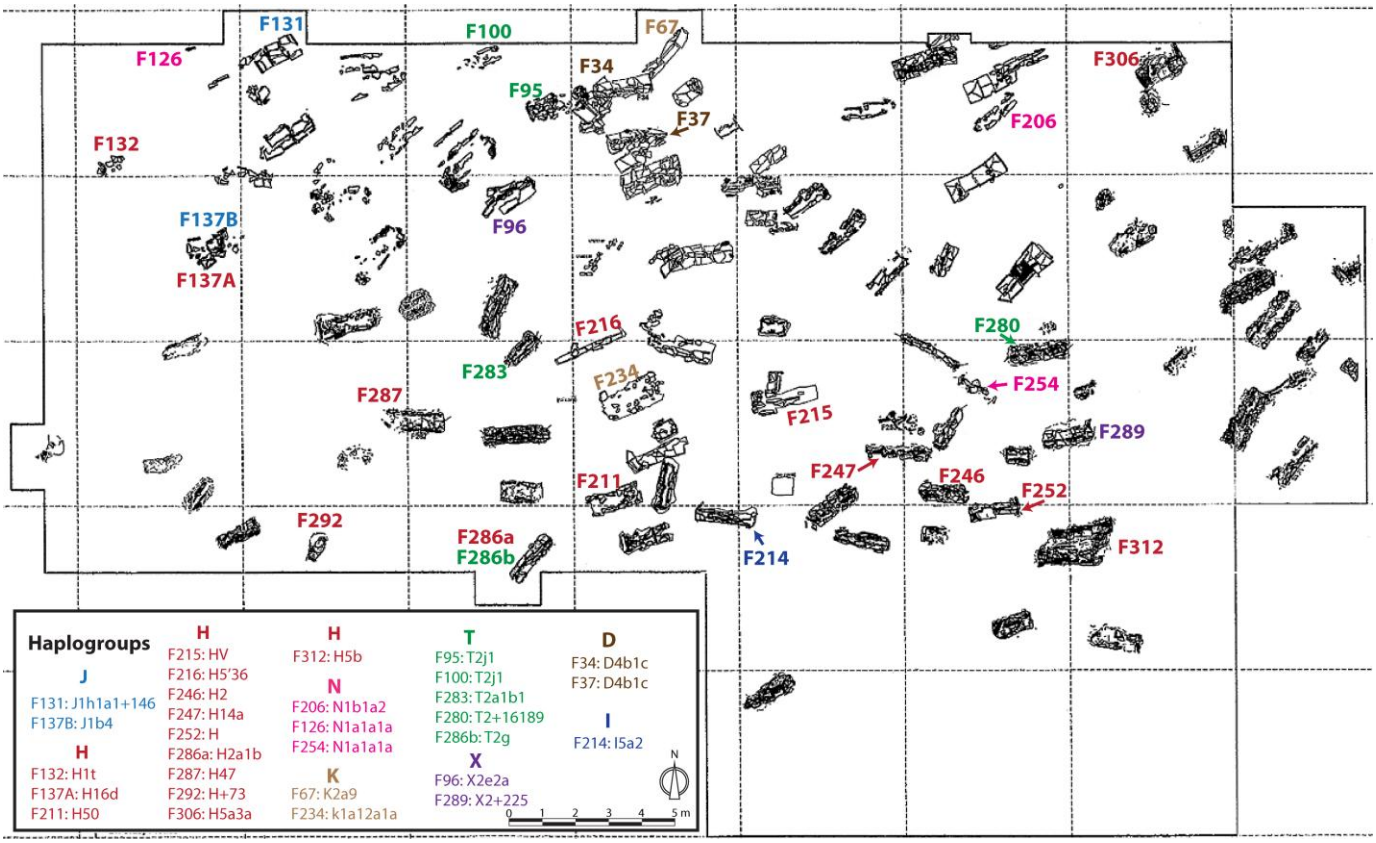

Figure 5: Map of the Vagnari cemetery with haplogroups superimposed (and colour coded) over associated grave structures.

4.6 Discussion

MtDNA data for 14 individuals are supported by $\delta^{18}O$ and $^{87}Sr/^{86}Sr$ values. One individual is represented by $\delta^{18}O$ and mtDNA data, while another 7 individuals by mtDNA and $^{87}Sr/^{86}Sr$ data. Eight individuals yielded mtDNA data, but are without $\delta^{18}O$ and $^{87}Sr/^{86}Sr$ representation. With the exception of F34 and F37, who both belong to haplogroup D4b1c (eastern Eurasian), the remaining 28 individuals have mtDNA haplogroups typically found among western Eurasian populations (Table 1) (Derenko et al., 2010; Brandt et al., 2015). HVR-1 analysis of 10 individuals by Prowse et al., (2010) showed that 8 individuals harboured western Eurasian haplogroups K, J, H, and T (F95), and that another two individuals belonged to

haplogroups L (F96a) and D (F37), two haplogroups associated with maternal origins from Africa and eastern Eurasia, respectively. Our results confirm that individual F37 has eastern Eurasian maternal ancestry. Further, our whole mitochondrial genome re-analysis of F37, F96a, and F95, revealed finer mtDNA resolution of subclusters D4b1c (F37) and T2j1 (F95), while F96a (formerly haplogroup L based on HVR-1 analysis) was reclassified as belonging to haplogroup X2e2a due to higher resolution across the whole mitochondrial genome (Table 1).

The $\delta^{18}O$ and $^{87}Sr/^{86}Sr$ values for these 14 individuals with combined isotopic and mtDNA data fall within the $\delta^{18}O$ (-8‰ to -6‰) and $^{87}Sr/^{86}Sr$ (~0.708) baseline variation for rainwater and known $^{87}Sr/^{86}Sr$ variation for the region (Emery et al. in review; Longinelli and Selmo, 2003; Giustini et al., 2016). Likewise, the $^{87}Sr/^{86}Sr$ values for 7 individuals (without associated $\delta^{18}O$ data) place their childhood origins at Vagnari. The $\delta^{18}O$ value for one individual (F34) without $^{87}Sr/^{86}Sr$ data also suggests an upbringing at the site. The discovery of haplogroup D (F37) by Prowse et al., (2010) indicates that migration between western and eastern Eurasia was likely common in classical antiquity. Additional reanalysis of the same individual, plus another (F34), confirm mtDNA influx from non-western Eurasian haplogroups at the cemetery. Although it is impossible to determine whether these individuals migrated to South Italy within their lifetime based on their mtDNA haplogroup alone, the tooth $\delta^{18}O$ value for F34 falls within the local $\delta^{18}O$ range for meteoric precipitation, placing their childhood upbringing within the greater Apulia region. Instead, it is likely that the ancestors of F34 and F37 originated from eastern Eurasia (possibly Asia proper) sometime prior to the 1st century CE. Whether this move was willingly initiated or forced remains unknown.

Population genomic studies using modern and ancient Italian samples revealed that Italy likely served as a refuge for human populations during the Last Glacial Maximum (LGM), and

as an area for introgression between Epipaleolithic (i.e., Mesolithic) populations and Neolithic migrants arriving from the eastern Mediterranean and Anatolia (Quintana-Murci et al., 2003; Capelli et al., 2007; Pala et al., 2009; Lacan et al., 2011; Di Gaetano et al., 2012; Boattini et al., 2013; Capocasa et al., 2014; Lazaridis et al., 2014; De Fanti et al., 2015a; Sarno et al., 2016). Population pairwise mtDNA distance across time period reflects the later part of this population history, with greater Φ_{ST} disparity between pre- and post-Neolithic samples (Fig. 3a/b). Although the scaling distance for mtDNAs by country show that South Italy shares closer mtDNAs with Portugal, Greece, Armenia, and Spain, Φ_{ST} values are skewed by disproportionate mtDNAs from different time periods (Fig. 3a). Instead, scaling distance by time period shows mtDNA structuring. Multi-dimensional scaling shown in Figure 3a support the hypothesis that post-LGM admixture in southern Italy was driven by early Neolithic migrants stemming from the Near East (possibly out of Anatolia following a Mediterranean route), indicated here by low differentiation Φ_{ST} values (and scaling distance) between Neolithic and post-Neolithic time periods (Chilvers et al., 2008; Skoglund et al., 2012; Brotherton et al., 2013; Haak et al., 2015; Omrak et al., 2016). Similar results were found between ancient Etruscan and modern Tuscan mtDNAs, which have argued for a deeper Near Eastern (possibly Anatolian) heritage, dating back to the Neolithic, although the origins of the Etruscans remains contentious (Ghirotto et al., 2013; Tassi et al., 2013; Gomez-Carballa et al., 2015). Roman Italian mtDNA population pairwise distance suggests greater genetic affinities with Neolithic and Bronze Age populations from central and southern Europe, than to either Iron Age Italian or Armenian age categories, and samples spanning the Third Intermediary through the Roman periods of Egypt (Fig. 3b). Interestingly, the higher Φ_{ST} disparity between Iron Age and Roman period southern Italians than with Bronze Age Aegeans, Greeks, and Neolithic samples from across Europe possibly indicates moderate

mtDNA influx following the subjugation of Italic tribes and installation of Roman colonies (*coloniae*) after the 3rd century BCE (Cornell, 1995; Small, 2002; La Torre, 2011) (Fig. 3b).

Archaeological and historic data point to a period of depopulation of southern Italy's Iron Age communities between the 4th and 3rd centuries BCE, a population retraction linked to prolonged conflict and warfare (i.e, the Pyrrhic and Punic Wars) (Small, 1992; Peruzzi, 2016). In order to test this assumption we employed Bayesian Skygrid analysis to obtain information about the effective female population size between the Iron Age and Roman periods. We hypothesize that Iron Age and Roman populations represent continuous occupation of the Puglia region over a 650-year period, so we used the 15 Iron Age and 30 Roman mtDNA sequences for demographic modelling in BEAST. Coalescent Skygrid results suggest that, despite this documented period of conflict, the effective female population size was comparable between the Iron Age and the Roman period, potentially pointing to a continuous effective female population size between these two time periods (Fig. 4). However, considerably more mtDNA representation for the interim period (3rd - 2nd centuries BCE) between the Iron Age and Roman period is required to fully assess whether prolonged warfare and enslavement contributed to population decline during the period immediately after Roman conquest (i.e., 3rd century BCE) of South Italy.

4.6.1 Identifying Maternal Kinship in the Vagnari Cemetery

Roman mtDNA distribution across the Vagnari necropolis indicates that at least some of the burial assemblages were constructed along kin-based lines (Fig. 5). Noted above, burials F34 (adult male) and F37 (45 – 49 yr old female) share the same mtDNA haplogroup (D4b1c), grave orientation (N-E), and are located in close proximity to one another (<2 meters). It is possible

that these two burials share the same maternal ancestor. These burials are also in close proximity to 5 adult (F36, F41, F67, F68, and F95) and two juvenile burials (F44 and F43), a pattern that indicates the possibility of family-linked burials plots within the cemetery. Two adult burials, F95 (male) and F100 (unknown sex) share haplogroup T2j1. These burial features are also located in close proximity (<2 meters) to one another, and share the same grave orientation (N-E). F95 and F100 are found in close association with F34 and F37 (D4b1c), and possibly represent another pair of maternally related individuals. Further genetic analysis of skeletons from the surrounding burial environment is required to substantiate other kin-based relationships in the North end of the *necropolis*.

Burial feature F137A/B (H16d/J1b4) is comprised of one male (A 20-25 yr) and another adult of unidentified sex (B). The $\delta^{18}O$ (-6.7‰) and $^{87}Sr/^{86}Sr$ (0.70871) tooth values for F137A suggest that he grew up in close proximity to, if not directly at Vagnari (Emery et al. in review; Giustini et al., 2016; Prowse, 2016). Although not maternally related, these two individuals may have shared paternal ancestry, were involved in a conjugal relationship, or were entirely unrelated but maintained non-kinship based relations during life. Double burial F286A/B contains two young adult (A=16-18 yr; B=13-14 yr) individuals of unknown sex, with mtDNA haplogroups (H2a1b/T2g) that indicate no maternal affiliation. The $^{87}Sr/^{86}Sr$ composition of their teeth (A=0.70870; B=0.70894) indicates that they were likely born at Vagnari (Emery et al. in review). Apart from the possibility of a paternal relationship, it is not clear why these two individuals were buried together.

4.7 Conclusion

Our investigation has provided insight into the population dynamics of a Roman period

population at both the local and regional scales. The mtDNA haplogroup composition of the Vagnari occupants is typical of western Eurasian populations, with the exception of two individuals belonging to haplogroup D4b1c, which is commonly found in eastern Eurasian populations, although the $\delta^{18}O$ for one individual places their origins directly at the site. In addition, the $\delta^{18}O$ and $^{87}Sr/^{86}Sr$ results suggest that the individuals analyzed here grew up at or in close proximity to Vagnari.

Comparative mtDNA analysis of geographically and temporally disparate data demonstrate that Roman period southern Italians had genetic affinities with Neolithic, Bronze, and Iron Age samples from Europe, the Near East, and western Asia. Population pair-wise Φ_{ST} analysis of Iron Age and Roman mtDNAs suggests that Roman conquest and eventual occupation of South Italy likely altered the genetic landscape of the region thereafter. However, our demographic modeling results indicate that population size of South Italy remained relatively stable despite centuries of warfare, Roman enslavement, and colony building, by the turn of the millennium. Possible maternal relationships were identified within the cemetery itself. Two pairs of individuals buried in the North end of the cemetery share the same haplogroup and burial characteristics, while a further two double burials contain non-maternally related individuals. The former suggests a possible shared maternal ancestor while the latter points to a yet unidentified familial/null relationship pattern in the cemetery. Future aDNA research of the Vagnari skeletal assemblage, paired with the growing number of publicly accessible aDNA datasets, will lead to a better understanding of the complex population dynamics at the local southern Italian, and broader Mediterranean scales.

Acknowledgements

Archaeological excavations at Vagnari were permitted by the Ministero per i Beni e le Attività Culturali through the British School at Rome to Tracy Prowse and Maureen Carroll, with the aid of Franco Taccogna and Stefania Peterlini. The Vagnari excavation team is thankful to the landowner of Vagnari, Dott. Mario De Gemmis Pellicciari; the Soprintendenza per i Beni Archeologici della Puglia, especially Dott. Luigi LaRocca, Dttsa. Francesca Radina and Dottsa Maria Rosaria DePalo, the British School at Rome, and the Centro Operativo and Fondazione Ettore Pomarici Santomasi, Gravina in Puglia. We are also grateful and acknowledge the fieldwork conducted by students and volunteers from Canada, the United Kingdom, and the United States. Additionally, we would like to thank Professor Alan Dickin for running the strontium isotope analysis of the Vagnari tooth samples. We also thank members of the McMaster Ancient DNA Centre, Debi Poinar and Melanie Kuch, as well as former members Jonathan Hughes and Dr. Stephanie Marciniak for their help with troubleshooting figures and maps included in this paper. We also thank the many colleagues who contributed mitochondrial consensus sequences upon request.

4A: Supplemental Information 1

Ancient Roman Mitochondrial and Isotopic Evidence Reveal Relationships at the Local and pan-Mediterranean Scales

*Matthew V. Emery, Ana T. Duggan, Tyler J. Murchie, Robert J. Stark, Jennifer Klunk, Jessica Hider, Katherine Eaton, Emil Karpinski, Henry P. Schwarcz, Hendrik N. Poinar and *Tracy L. Prowse

4.8 $^{18}O/^{16}O$ and $^{87}Sr/^{86}Sr$ Methodology

Oxygen isotope analysis was undertaken at the Hatch Stable Isotope Laboratory located at the University of Ottawa. Isotope measurements were performed on a Thermo Finnigan Delta XP and a Gas Bench II IRMS. Analytical precision (2σ) was measured to +/- 0.1‰. Oxygen values were converted from VPDB to VSMOW using the equation: $\delta\,^{18}O_{VSMOW} = 1.0309\ \delta\,^{18}O_{VPDB} + 30.92$, then to drinking water ($\delta^{18}O_{DW}$ VSMOW) using the equation devised by Chenery et al., (2012): $\delta^{18}O_{DW} = 1.590 \times \delta^{18}O_C - 48.6$ (‰ VSMOW). All first molars $\delta^{18}O_C$ values were adjusted by -0.7‰ to control for the possible effects of weaning which has been show to enrich $\delta^{18}O$ values of pre-weaned teeth by approximately +0.7‰ (Wright and Schwarcz, 1998).

Teeth selected for strontium isotope analysis were washed in distilled water, dried, drilled. The resulting enamel powder dissolved in 1.3 ml of ca. 4 M ultra-pure hydrochloric acid (HCl). The solution was centrifuged for 10 minutes, loaded into cation exchange columns (AG 50W-X12, 200-400 mesh cation exchange resin), eluted, and the resulting salts collected for thermal ionization mass spectrometry (TIMS). Within run isotope fractionation was corrected to $^{86}Sr/^{88}Sr = 0.1194$, using a dynamic multi-collection VG 354 thermal ionization mass spectrometer in the Radiogenic Isotope Laboratory of the School of Geography and Earth Sciences at McMaster University. Analysis of the NBS 987 standard resulted in an average $^{87}Sr/^{86}Sr$ value of 0.710246 with a population standard deviation of 0.000022 (1σ).

4.9 Read Processing, Age, and Sex Determination

4.9.1 MtDNA Construction and Assembly

Sequenced reads were demultiplexed using bcl2fastq (ver. 2.17.1.14). Adapter sequences were trimmed and paired-end reads merged with leeHom using ancient DNA parameters (--ancientdna) (Renaud et al., 2014). Trimmed and merged reads were mapped to the human mitochondrial reference genome (revised Cambridge Reference Sequence, rCRS, NC_012920) with a modified version of BWA (https://github.com/mpieva/network-aware-bwa), with seeding disabled (-1 16500), gap opening (-o 2), and a maximum edit distance set to 0.01 (-n0.01) (Li and Durbin, 2009). We filtered mapped mtDNA reads to merged or unmerged but paired (https://github.com/grenaud/libbam), removed duplicated reads (https://github.com/udo-stenzel/biohazard), then restricted collapsed mtDNA reads to a minimum length of 35 bp and minimum map quality of 30. Mitochondrial consensus sequences and contamination rates were generated using Schmutzi (Q5), and haplogroups called using HaploGrep2 and PhyloTree Build 17 (Table S1) (Renaud et al., 2015; van Oven, 2015; Weissensteiner et al., 2016). A total of 402 mtDNA sequences were aligned with MUSCLE, and the resulting alignment edited and pruned (polyC stretches removed between np 303 – 317 and 16,165 – 180) in Geneious for analysis (Kearse et al., 2012; Edgar et al., 2017).

4.9.2 Ancient DNA Authentication

Negative controls (ultrapure H_2O blanks) were prepared in tandem during DNA extraction and library preparation. Extraction and library blank reads show a low degree of reads mapping to the rCRS, indicating minimal exogenous contamination during laboratory experimentation (Table S1). We performed *in silico* analysis to determine the authenticity of the

filtered mtDNA reads. Fragment length distributions (FLDs) and terminal deamination plots (i.e., C→T and G→A transitions) were generated for mtDNA reads using mapDamage 2.0 (Table S2) (Jónsson et al., 2013). All Roman samples exhibit short FLD and misincorporation patterns expected of highly degraded or ancient molecules (Supplementary Table S2).

4.9.3 Arlequin Analysis and Multi-Dimensional Scaling

Population pairwise Φ_{ST} values were calculated using Arlequin ver. 3.5.2.2 using the Tamura-Nei substitution model, estimated by jmodeltest 2.1.10 (AIC corrected) (Excoffier et al., 1992; Darriba et al., 2012). Multi-dimensional scaling plots were generated using a customized script in R using the packages *plot3Drg, vegan,* and *MASS*. We omitted temporal and country categories represented with <5 mitochondrial sequences to reduce scaling stress from the total mtDNA alignment (n=402) to n=382 for time period and n=378 for country. Population pairwise Φ_{ST} values were imported into R as matrices, and the resulting stress values calculated using the isoMDS function in *MASS* (Tables S3-S4).

4.9.4 Bayesian Skygrid Analysis Using BEAST

We conducted Bayesian Skygrid analysis using 45 Iron Age and Roman samples to assess the impact of Roman occupation on effective female population size. Unfortunately, we have no ^{14}C dates for the Iron Age or Roman skeletons. However, we assigned an average date to the Iron Age (500 BCE) and Roman (150 CE) assemblage based on the length of site occupation, and adjusted by +1950 to BP for tip date molecular clock calibration (i.e, Iron Age = 2450 BP; Roman = 1800 BP). We used the substitution model Tamura-Nei accounting for a gamma distribution and invariant sites as estimated by jmodeltest 2.1.10 (AIC corrected; Darriba et al.,

2012), and a strict clock model with the substitution rate set to 1.655×10^{-8} ($1\sigma = 1.479\times10^{-9}$) (Soares et al., 2010).

Table S1: Roman sample identification, mtDNA read data, and contamination estimates.

Library ID	Sample ID	Tissue Type	Trimmed and Merged Reads	# of unique reads (min35MQ3) mapped to rCRS	Depth of Coverage	Haplogroup	N of Missing Data (bp)	Schmutzi Contamination Estimate (%)
LRV 76	F34	Tooth Root	587325	39024	156.4x	D4b1c	1	1
LRV 77	F37	Tooth Root	4793091	58152	227.6x	D4b1c (formerly Hap D)	0	1
LRV 92	F96A	Tooth Root	2286160	4789	18x	T2j1	597	2
LRV 93	F95	Tooth Root	5269122	146157	529x	X2e2a (formerly Hap L)	0	3
LRV 95	F100	Tooth Root	3517733	37602	128x	T2j1	18	3
LRV 97	F126	Tooth Root	9664148	109112	390x	N1a1a1a	1	1
LRV 101	F132	Tooth Root	1645531	8514	23.8x	H1t	75	1
LRV 102	F131	Tooth Root	2077002	15377	50.3x	J1b1a1+146	6	2
LRV 103	F137A	Tooth Root	4711324	80445	326.2x	H16d	2	1
LRV 104	F137B	Tooth Root	1557585	63612	210.2x	J1b4	1	2
LRV 105	F67	Tooth Root	3727026	38032	129x	K2a9	14	2
LRV 110	F206	Tooth Root	2621886	9206	30.9x	N1b1a2	181	3
LRV 112	F211	Tooth Root	8347171	78903	275.6x	H50	1	1
LRV 114	F214	Tooth Root	6969494	140585	553.2x	I5a2	0	17
LRV 118	F215	Tooth Root	6212454	147492	586.1x	HV	0	1
LRV 119	F216	Tooth Root	2950345	31103	123.7x	H5'36	5	20
LRV 122	F234	Tooth Root	1355434	47387	173.1x	K1a12a1a	6	1
LRV 128	F252	Tooth Root	599651	2226	9.6x	H	1152	3

Library ID	Sample ID	Tissue Type	Trimmed and Merged Reads	# of unique reads (min35MQ3) mapped to rCRS	Depth of Coverage	Haplogroup	N of Missing Data (bp)	Schmutzi Contamination Estimate (%)
LRV 135	F287	Tooth Root	528783	9491	36x	H47	218	2
LRV 137	F283	Tooth Root	6612872	97632	503.1x	T2a1b1	0	2
LRV 138	F254	Tooth Root	1160794	2909	9.7x	N1a1a1a	1511	1
LRV 143	F246	Tooth Root	2145190	2310	8.7x	H2	1264	8
LRV 146	F292	Tooth Root	1166288	5492	28.1x	H+73	25	2
LRV 148	F289	Tooth Root	1551658	49495	187.1x	X2+225	2	4
LRV 149	F312	Tooth Root	2806178	65374	232.1x	H5b	0	1
LRV 151	F280	Tooth Root	3190094	2926	12.5x	T2+16189	291	6
LRV 152	F306	Tooth Root	7042850	47772	174.2x	H5a3a	1	1
LRV 153	F286A	Tooth Root	2993264	7714	24.1x	H2a1b	127	5
LRV 154	F286B	Tooth Root	2195085	12783	39.6x	T2g	21	2
LRV 156	F247	Tooth Root	723999	27187	89.1x	H15a	78	1
LRV 84 Bl	Extraction Blank	Extraction Blank	303	14	Extraction Blank	Extraction Blank	Extraction Blank	Extraction Blank
LRV 115 Bl	Extraction Blank	Extraction Blank	799	85	Extraction Blank	Extraction Blank	Extraction Blank	Extraction Blank
LRV 139 Bl	Extraction Blank	Extraction Blank	695	58	Extraction Blank	Extraction Blank	Extraction Blank	Extraction Blank
LRV 155 Bl	Extraction Blank	Extraction Blank	239	5	Extraction Blank	Extraction Blank	Extraction Blank	Extraction Blank
Lib Bl 1	Library Blank	Library Blank	207	2	Library Blank	Library Blank	Library Blank	Library Blank
Lib Bl 2	Library Blank	Library Blank	249	0	Library Blank	Library Blank	Library Blank	Library Blank
Lib Bl 3	Library Blank	Library Blank	657	39	Library Blank	Library Blank	Library Blank	Library Blank

Table S2: mtDNA read deamination and average insert length (bp).

Sample ID	3' Deamination (%)	5' Deamination (%)	Avg. Insert Length (bp)
LRV 76	26	24	66.3
LRV 77	32	31	64.8
LRV 92	32	29	64
LRV 93	27	27	59.9
LRV 95	32	30	56.6
LRV 97	32	32	59
LRV 101	33	36	46.3
LRV 102	34	32	54.1
LRV 103	31	31	67.1
LRV 104	35	34	54.7
LRV 105	34	34	56.1
LRV 110	32	31	55.5
LRV 112	33	32	57.5
LRV 114	26	25	65.1
LRV 118	33	33	65.6
LRV 119	30	29	65.7
LRV 122	30	30	60.4
LRV 128	31	26	71.5
LRV 135	31	29	62.8
LRV 137	25	27	85.2
LRV 138	36	37	55.3
LRV 143	24	25	62.5
LRV 146	25	27	84.5
LRV 148	36	35	62.6
LRV 149	33	32	58.6
LRV 151	21	20	70.8
LRV 152	32	31	60.3
LRV 153	32	33	51.6
LRV 154	33	31	51.3
LRV 156	36	31	54.3

Table S3: Population pairwise Φ_{ST} results for mtDNA sequences categorized by temporal age.

	BronzeAge	Holocene	IronAge1	IronAge2	LP	Mesolithic	Neolithic	postLGM	preLGM	PP	Roman2	Roman1	TIP
BronzeAge	0												
Holocene	0.21639	0											
IronAge 1	0.02287	0.25867	0										
IronAge 2	0.00803	0.27945	0.00626	0									
***LP**	0.04506	0.49762	0.08093	0.05678	0								
Mesolithic	0.07359	0.18634	0.09522	0.10582	0.24872	0							
Neolithic	0.00511	0.20386	0.01735	0.00984	0.0612	0.08578	0						
postLGM	0.16784	0.51563	0.22045	0.2189	0.42592	0.24424	0.18603	0					
preLGM	0.07018	0.37782	0.10378	0.08993	0.30565	0.12383	0.07224	0.29923	0				
***PP**	0.02985	0.25813	0.06879	0.03027	-0.00722	0.13981	0.04186	0.20959	0.10182	0			
Roman 2	0.00406	0.26814	0.05064	0.01333	0.01727	0.1006	0.02711	0.19052	0.08913	-0.00164	0		
Roman 1	0.01999	0.28602	0.04065	0.01353	0.00819	0.15264	0.02038	0.23173	0.12297	0.02785	0.02126	0	
***TIP**	0.0303	0.25906	0.06835	0.02225	-0.00033	0.13402	0.04673	0.19798	0.09953	-0.00498	-0.00872	0.02125	0

***Abbreviated categories LP, PP, and TIP, stand for Late Period, Ptolemaic Period, and Third Intermediary Period, respectively. Φ_{ST} values in red indicate low genetic differentiation between relevant population age categories (i.e, <0.05) (Hartl and Clark, 1997).**

Table S4: Population pairwise Φ_{ST} results for mtDNA sequences categorized by geographic region.

	Aegean	Armenia	Belgium	CzechRep	Egypt	France	Germany	Greece	Latvia	Portugal	Russia	SouthItaly	Spain	Sweden
Aegean	0													
Armenia	0.09697	0												
Belgium	0.19392	0.05191	0											
Czech Rep	0.19596	0.01915	0.115	0										
Egypt	0.13341	0.02261	0.07958	0.04974	0									
France	0.27105	0.11833	0.17997	0.11711	0.1332	0								
Germany	0.188	0.01699	0.11443	0.06823	0.04054	0.13225	0							
Greece	0.11493	0.00722	0.11942	0.06006	0.0338	0.15969	0.02251	0						
Latvia	0.22708	0.16813	0.24956	0.2282	0.22037	0.16401	0.22643	0.22005	0					
Portugal	0.13377	0.00765	0.1293	0.08732	0.0338	0.11851	0.00002	-0.0056	0.24093	0				
Russia	0.12233	0.0044	0.04963	0.00128	0.02907	0.08923	0.01794	0.01452	0.12601	0.01817	0			
South Italy	0.14075	0.01037	0.08418	0.05319	0.02926	0.1422	0.0057	0.00825	0.20821	-0.00267	0.01869	0		
Spain	0.03271	-0.00171	0.06983	0.02274	0.02619	0.08561	0.03688	0.02284	0.19736	-0.0097	0.00728	0.0243	0	
Sweden	0.27719	0.1468	0.19581	0.20376	0.17789	0.11471	0.19646	0.19894	0.11287	0.20855	0.09668	0.17752	0.14952	0

Φ_{ST} values in red indicate low genetic differentiation between relevant population categories by country (i.e, <0.05) (Hartl and Clark, 1997).

Figure S1a/b: 3D Multi-dimensional scaling plots depicting genetic distance using population pairwise Φ_{ST} values by a) country (stress value = 8.01) and b) age (stress value = 5.42).

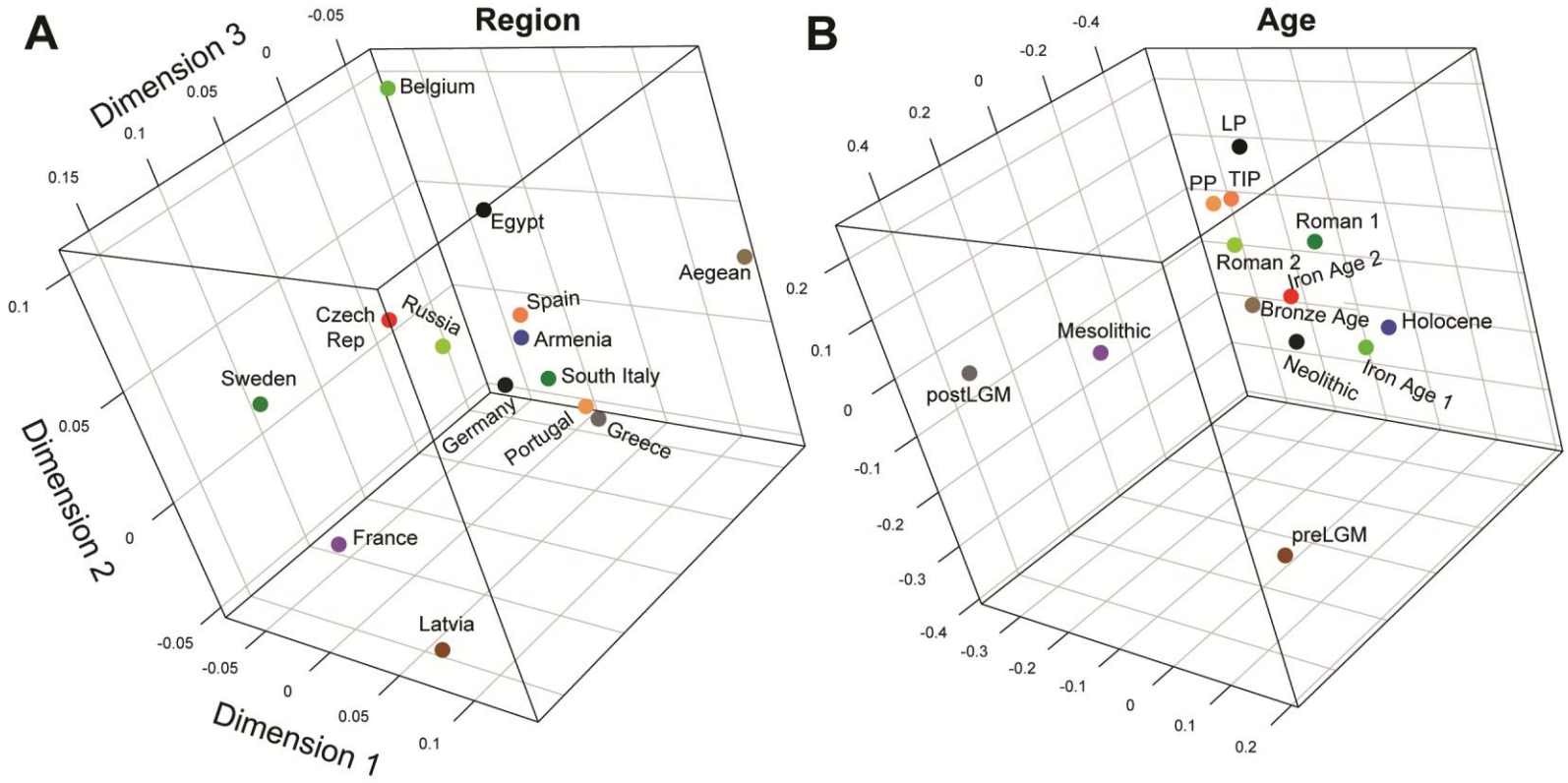

Table S5: Published mtDNA Sequences Used for Multi-Dimensional Scaling and BEAST Analysis (n=357).

Library ID	Location	Time Period	Date (cal BP)/Ranges cal. BCE	Haplogroup	Publication
Kostenki14	Russia	preLGM	37985	U2	(Krause et al., 2010)
GoyetQ116-1	Belgium	preLGM	34795	M	(Posth et al., 2016)
GoyetQ376-3	Belgium	preLGM	33540	M	(Posth et al., 2016)
Cioclovina1	Romania	preLGM	33212	U	(Posth et al., 2016)
Paglicci133	Italy	preLGM	33000	U8c	(Posth et al., 2016)
DolniVestonice13	Czech Republic	preLGM	31155	U8	(Fu et al., 2013)
DolniVestonice14	Czech Republic	preLGM	31155	U5	(Fu et al., 2013)
DolniVestonice15	Czech Republic	preLGM	31155	U5	(Fu et al., 2013)
DolniVestonice16	Czech Republic	preLGM	29977	U5	(Posth et al., 2016)
DolniVestonice43	Czech Republic	preLGM	29977	U5	(Posth et al., 2016)
Paglicci108	Italy	preLGM	28396	U2'3'4'7'8'9	(Posth et al., 2016)
GoyetQ53-1	Belgium	preLGM	27975	U2	(Posth et al., 2016)
LaRochette	France	preLGM	27592	M	(Posth et al., 2016)
GoyetQ55-2	Belgium	preLGM	27520	U2	(Posth et al., 2016)
GoyetQ376-19	Belgium	preLGM	27515	U2	(Posth et al., 2016)
Goyet2878-21	Belgium	preLGM	26662	U5	(Posth et al., 2016)
GoyetQ56-16	Belgium	preLGM	26320	U2	(Posth et al., 2016)
Paglicci71	Italy	postLGM	18585	U5b2b	(Posth et al., 2016)
HohleFels79	Germany	postLGM	15909	U8a	(Posth et al., 2016)
HohleFels10	Germany	postLGM	15470	U8a	(Posth et al., 2016)
HohleFels49	Germany	postLGM	15470	U8a	(Posth et al., 2016)
Rigney1	France	postLGM	15465	U2'3'4'7'8'9	(Posth et al., 2016)
GoyetQ-2	Belgium	postLGM	15005	U8a	(Posth et al., 2016)
Brillenhohle	Germany	postLGM	14780	U8a	(Posth et al., 2016)
Burkhardtshohle	Germany	postLGM	14615	U8a	(Posth et al., 2016)
Oberkassel1998	Germany	Late Glacial	14020	U5b1	(Fu et al., 2013)
Iboussieres39	France	postLGM/LateGlacial	11820	U5b2b	(Posth et al., 2016)
Iboussieres25-1	France	postLGM/LateGlacial	11820	U5b2b	(Posth et al., 2016)
Iboussieres31-2	France	postLGM/LateGlacial	11820	U5b1	(Posth et al., 2016)
Rochedane	France	postLGM/LateGlacial	12960	U5b2b	(Posth et al., 2016)
BLA20	Germany	Holocene	10652	U5a2c3	(Bollongino et al., 2013)
Ranchot88	France	Holocene	10084	U5b1	(Posth et al., 2016)

LesCloseaux3	France	Holocene	9905	U5a2	(Posth et al., 2016)
MareuilLesMeaux1	France	Holocene	9290	U5a2	(Posth et al., 2016)
Falkenstein	Germany	Holocene	9201	U5b2a	(Posth et al., 2016)
Felsdach	Germany	Holocene	8680	U5a2c	(Posth et al., 2016)
HohlensteinStadel	Germany	Holocene	8628	U5b2c1	(Posth et al., 2016)
Ofnet	Germany	Holocene	8292	U5b1d1	(Posth et al., 2016)
CuiryLesChaudardes1	France	Holocene	8205	U5b1b	(Posth et al., 2016)
Bockstein	Germany	Holocene	8173	U5b1d1	(Posth et al., 2016)
BerryAuBac1	France	Holocene	7244	U5b1a	(Posth et al., 2016)
Loschbour	Luxembourg	Holocene	8054	U5b1a	(Fu et al., 2013)
Motala1	Sweden	Neolithic	7953	U5a1	(Lazaridis et al., 2014)
Motala12	Sweden	Neolithic	7953	U2e1	(Lazaridis et al., 2014)
Motala2	Sweden	Neolithic	7953	U2e1	(Lazaridis et al., 2014)
Motala3	Sweden	Neolithic	7953	U5a1	(Lazaridis et al., 2014)
Motala4	Sweden	Neolithic	7953	U5a2d	(Lazaridis et al., 2014)
Motala6	Sweden	Neolithic/Holocene	7953	U5a2d	(Lazaridis et al., 2014)
Motala9	Sweden	Neolithic/Holocene	7953	U5a2	(Lazaridis et al., 2014)
arm1	Armenia	Early Bronze Age	4942	K3	(Margaryan et al., 2017)
arm10	Armenia	Classical	2580*	H13a1a2	(Margaryan et al., 2017)
arm11	Armenia	Late Bronze Age	3200	U3b	(Margaryan et al., 2017)
arm12	Armenia	Medieval	1179*	J1d6	(Margaryan et al., 2017)
arm13	Armenia	Early Iron Age	3000	U2e2a1	(Margaryan et al., 2017)
arm14	Artsakh	Medieval	300	U1a1a	(Margaryan et al., 2017)
arm15	Armenia	Late Bronze Age	3314	H15a1a1	(Margaryan et al., 2017)
arm16	Armenia	Late Bronze Age	3314	K1a12a	(Margaryan et al., 2017)
arm18	Armenia	Late Bronze Age	3314	H15a1a1	(Margaryan et al., 2017)
arm19	Armenia	Late Bronze Age	3314	K1a1b1e	(Margaryan et al., 2017)
arm2	Armenia	Early Bronze Age	4942	R1a1	(Margaryan et al., 2017)
arm20	Armenia	Late Bronze Age	3314*	H8a1	(Margaryan et al., 2017)
arm21	Armenia	Early Iron Age	3161	HV12b1	(Margaryan et al., 2017)
arm22	Armenia	Early Iron Age	3161	H2a	(Margaryan et al., 2017)
arm23	Armenia	Late Bronze Age	3400	R1a1a	(Margaryan et al., 2017)

arm24	Armenia	Early Iron Age	3161	U5a1b	(Margaryan et al., 2017)
arm26	Armenia	Early Iron Age	3161	J1d1b1	(Margaryan et al., 2017)
arm27	Armenia	Early Iron Age	3161*	HV	(Margaryan et al., 2017)
arm28	Armenia	Late Bronze Age	3300	K1a4c1	(Margaryan et al., 2017)
arm29	Armenia	Late Bronze Age	3300	R1b1	(Margaryan et al., 2017)
arm3	Armenia	Early Bronze Age	4942*	K3	(Margaryan et al., 2017)
arm30	Armenia	Late Bronze Age	3400	U8b1a2b	(Margaryan et al., 2017)
arm31	Armenia	Late Bronze Age	3300	T1a9	(Margaryan et al., 2017)
arm32	Armenia	Late Bronze Age	3300	HV1a2	(Margaryan et al., 2017)
arm33	Armenia	Late Bronze Age	3300	W3b	(Margaryan et al., 2017)
arm34	Armenia	Late Bronze Age	3264*	U3b	(Margaryan et al., 2017)
arm35	Armenia	Middle Bronze Age	3900	U3b	(Margaryan et al., 2017)
arm36	Armenia	Late Bronze Age	3400	U2e1e	(Margaryan et al., 2017)
arm37	Armenia	Early Iron Age	3000	H	(Margaryan et al., 2017)
arm39	Armenia	Neolithic	7811*	I1	(Margaryan et al., 2017)
arm4	Armenia	Classical	2000	J1d1b1	(Margaryan et al., 2017)
arm40	Armenia	Early Bronze Age	5353*	H14b2	(Margaryan et al., 2017)
arm42	Armenia	Early Bronze Age	5353	T1	(Margaryan et al., 2017)
arm43	Armenia	Middle Bronze Age	3700	U4a	(Margaryan et al., 2017)
arm44	Armenia	Late Iron Age	2609*	U3b3	(Margaryan et al., 2017)
arm45	Armenia	Middle Bronze Age	3700	T	(Margaryan et al., 2017)
arm46	Armenia	Middle Bronze Age	3700	HV1a1	(Margaryan et al., 2017)
arm48	Armenia	Late Iron Age	2609	I4	(Margaryan et al., 2017)
arm49	Armenia	Late Iron Age	2609	I4	(Margaryan et al., 2017)
arm5	Armenia	Early Bronze Age	4942	J1b1b1	(Margaryan et al., 2017)
arm51	Armenia	Late Iron Age	2609	U3b3	(Margaryan et al., 2017)
arm52	Artsakh	Chalcolithic	6411*	U8b1a1	(Margaryan et al., 2017)
arm7	Armenia	Neolithic	7811	H2+152	(Margaryan et al., 2017)
arm9	Armenia	Neolithic	7811	H15a1	(Margaryan et al., 2017)
rise396	Armenia	Early Iron Age	3007*	H6b	(Margaryan et al., 2017)
rise397	Armenia	Early Iron Age	2909*	T1a2	(Margaryan et al., 2017)

rise407	Armenia	Early Iron Age	2935*	H8a1	(Margaryan et al., 2017)
rise408	Armenia	Early Iron Age	3049*	I5c	(Margaryan et al., 2017)
rise412	Armenia	Early Iron Age	3016*	U4c1	(Margaryan et al., 2017)
rise413	Armenia	Middle Bronze Age	3766*	T2c1f	(Margaryan et al., 2017)
rise423	Armenia	Late Bronze Age	3249*	T2a3	(Margaryan et al., 2017)
HAL16	Germany	Unetice_EBA	2022-1937 calBCE	V	(Haak et al., 2015)
HAL25	Germany	LBK_EN	5206-5052 calBCE	K1a	(Haak et al., 2015)
ESP5	Germany	Corded_Ware_LN	2800-2050 BCE	U5a2d	(Haak et al., 2015)
ESP22	Germany	Corded_Ware_LN	2454-2291 calBCE	X2b4	(Haak et al., 2015)
HAL5	Germany	LBK_EN	5206-5004 calBCE	T2c1d'e'f	(Haak et al., 2015)
ALB2	Germany	Alberstedt_LN	2494-2344 calBCE	H3b	(Haak et al., 2015)
HAL36C	Germany	Halberstadt_LBA	1113-1021 calBCE	H23	Haak et al., 2015/Brotherton et al., 2013
QUEXII6	Germany	Bell_Beaker_LN	2340-2190 calBCE	H13a1a2	(Haak et al., 2015)
ALB3	Germany	Alberstedt_LN	2459-2345 calBCE	HV6'17	(Haak et al., 2015)
ESP26	Germany	Corded_Ware_LN	2454-2291 calBCE	T2a1b1	(Haak et al., 2015)
ESP2	Germany	Unetice_EBA_relative_of_I0117	2131-1979 calBCE	I3a	(Haak et al., 2015)
ESP11	Germany	Corded_Ware_LN	2473-2348 calBCE	U4b1a1a1	(Haak et al., 2015)
ROT3	Germany	Bell_Beaker_LN	2500-2050 BCE	K1a2c	(Haak et al., 2015)
HAL15	Germany	LBK_EN	5030-4948 calBCE	N1a1a1a3	(Haak et al., 2015)
HAL4	Germany	LBK_EN	5032-4946 calBCE	N1a1a1a	(Haak et al., 2015)
ROT4	Germany	Bell_Beaker_LN	2414-2333 calBCE	H3	(Haak et al., 2015)
ESP16	Germany	Corded_Ware_LN	2566-2477 calBCE	W6a	(Haak et al., 2015)
QUEXII4	Germany	Bell_Beaker_LN	2290-2130 calBCE	J1c5	(Haak et al., 2015)
ROT6	Germany	Bell_Beaker_LN	2497-2436 calBCE	H5a3	Haak et al., 2015/Brotherton et al., 2013
ESP3	Germany	Unetice_EBA	1931-1780 calBCE	U5a1	(Haak et al., 2015)
ESP29	Germany	Unetice_EBA	2199-2064 calBCE	I3a	(Haak et al., 2015)
ESP4	Germany	Unetice_EBA	2118-1961 calBCE	W3a1	(Haak et al., 2015)
QUEVIII6	Germany	Unetice_EBA	2012-1919 calBCE	U5b2a1	(Haak et al., 2015)
HAL13	Germany	Rössen_EN	5500-4775 BCE	V1a	(Haak et al., 2015)
BAL16a	Hungary	Lengyel_Neolithic	4900-4500 BCE	N1a1a1	(Haak et al., 2015)
BZH12	Germany	BenzigerodeHeimburg_LN	2204-2136 calBCE	U5a1a2a	(Haak et al., 2015)
BAM25a	Hungary	Starcevo_EN	5710-5530 calBCE	N1a1a1	(Haak et al., 2015)
OSH7	Germany	Rössen_EN	4582-4407 calBCE	H5b	Haak et al., 2015/Brotherton et al., 2013
OAW1	Germany	Gatersleben_EN	4475-3950 BCE	HV6'17	(Haak et al., 2015)

OSH1	Germany	Rössen_EN	4625-4250 BCE	H16a'c'd	Haak et al., 2015/Brotherton et al., 2013
SZEH4b	Hungary	LBKT_EN	5210-4940 calBCE	N1a1a1a3	(Haak et al., 2015)
OSH9	Germany	Rössen_EN	4625-4250 BCE	U5b1b	(Haak et al., 2015)
UzOO74	Russia	Karelia_HG	5500-5000 BCE	C1g	(Haak et al., 2015)
UWS4	Germany	LBK_EN	5209-5070 calBCE	J1c17	(Haak et al., 2015)
BZH4	Germany	BenzigerodeHeimburg_LN	2283-2146 calBCE	H1e	Haak et al., 2015/Brotherton et al., 2013
BZH6	Germany	BenzigerodeHeimburg_LN	2286-2153 calBCE	H1/H1b'ad	Haak et al., 2015/Brotherton et al., 2013
HAL14	Germany	LBK_EN	5206-5052 calBCE	T2b(8)	(Haak et al., 2015)
HAL34	Germany	LBK_EN	5207-5067 calBCE	N1a1a1	(Haak et al., 2015)
HQU5	Germany	Baalberge_MN	3944-3852 calBCE, 3427-3381 calBCE, 3631-3561 calBCE	T2c1d1	(Haak et al., 2015)
Troc7	Spain	Spain_EN	5177-5068 calBCE	V	(Haak et al., 2015)
Troc4	Spain	Spain_EN_relative_of_I0410	5303-5204 calBCE	K1a2a	(Haak et al., 2015)
Mina18a	Spain	Spain_MN	3900-3600 BCE	pre-U5b1i	(Haak et al., 2015)
Mina2	Spain	Spain_MN	3900-3600 BCE	J2a1a1	(Haak et al., 2015)
Troc3	Spain	Spain_EN	5178-5066 calBCE	pre-T2c1d2	(Haak et al., 2015)
Mina6b	Spain	Spain_MN	3900-3600 BCE	K1b1a1	(Haak et al., 2015)
Troc5	Spain	Spain_EN	5310-5206 calBCE	N1a1a1	(Haak et al., 2015)
Mina3	Spain	Spain_MN	3900-3600 BCE	K1a1b1	(Haak et al., 2015)
Troc1	Spain	Spain_EN	5311-5218 calBCE	J1c3	(Haak et al., 2015)
DEB36	Germany	LBK_EN	5500-4775 BCE	U5a1a'g	(Haak et al., 2015)
QLB18A	Germany	Baalberge_MN	3640-3510 calBCE	T2e1	(Haak et al., 2015)
KAR22A	Germany	Karsdorf_LN	2564-2475 cal BCE	T1a1	(Haak et al., 2015)
QLB15D	Germany	Baalberge_MN	3645-3537 calBCE	HV6'17	(Haak et al., 2015)
QLB6B	Germany	Baalberge_MN	3950-3400 BCE	U5b2a2	(Haak et al., 2015)
BENZ18/BENZ15?	Germany	Bernburg_MN	3101-2919 calBCE	W1c'i	(Haak et al., 2015)
SALZ7A	Germany	Salzmünde_MN	3400-3025 BCE	H5	(Haak et al., 2015)
SALZ3B	Germany	Salzmünde_MN	3400-3025 BCE	U3a1	(Haak et al., 2015)
BENZ14	Germany	Bernburg_MN	3104-2919 cal BCE	U5a2b4	(Haak et al., 2015)
QLB2A	Germany	Baalberge_MN	3950-3400 BCE	U8a1	(Haak et al., 2015)
SALZ88A	Germany	Salzmünde_MN	3237-3171 calBCE	J1c	(Haak et al., 2015)
HAL2	Germany	LBK_EN	5079-4997 calBCE , 5066-4979 calBCE	N1a1a1a2	(Haak et al., 2015)
ESP24	Germany	Esperstedt_MN	3360-3086 calBCE	T2b	(Haak et al., 2015)
SALZ21B	Germany	Schöningen_MN	4100-3950 BCE	H1e	Haak et al., 2015/Brotherton et al., 2013
SALZ18A	Germany	Schöningen_MN	4172-4089 calBCE	H10e'f'g	Haak et al., 2015/Brotherton et al., 2013

QLB28b	Germany	Bell_Beaker_LN	2296-2206 calBCE	H1	Haak et al., 2015/Brotherton et al., 2013
EUL41a	Germany	Unetice_EBA	2115-1996 calBCE	H4a1a1	Haak et al., 2015/Brotherton et al., 2013
QLB26a	Germany	Bell_Beaker_LN	2360-2190 calBCE	H1	Haak et al., 2015/Brotherton et al., 2013
SALZ57A	Germany	Salzmünde_MN	3334-3262 calBCE	H3	Haak et al., 2015/Brotherton et al., 2013
HAL24	Germany	LBK_EN	5034-4942 calBCE	pre-X2d1	Haak et al., 2015
EUL57b	Germany	Unetice_EBA	2131-1982 calBCE	H3	Haak et al., 2015/Brotherton et al., 2013
KAR16A	Germany	LBK_EN	5500-4775 BCE	H46b	Haak et al., 2015/Brotherton et
KAR11B	Germany	LBK_EN	5500-4775 BCE	H	Haak et al., 2015/Brotherton et al., 2013
HQU3	Germany	Baalberge_MN	3630-3581 calBCE	K1e	Haak et al., 2015
SALZ77A	Germany	Salzmünde_MN	3400-3025 BCE	H3	Haak et al., 2015/Brotherton et al., 2013
HAL37	Germany	LBK_EN	5298-5247 calBCE	W1c'i	Haak et al., 2015
ESP30	Germany	Baalberge_MN	3887-3797 calBCE	H1e1a	Haak et al., 2015/Brotherton et al., 2013
HQU4	Germany	Baalberge_MN	3950-3400 BCE	H7d	Haak et al., 2015/Brotherton et al., 2013
LBK1992	Germany	LBK_EN	5500-4800 BCE	T2b	(Haak et al., 2015)
LBK2172	Germany	LBK_EN	5500-4800 BCE	H40	(Haak et al., 2015)
LBK2155	Germany	LBK_EN	5500-4800 BCE	T2b	(Haak et al., 2015)
LBK1979	Germany	LBK_EN	5500-4800 BCE	H	(Haak et al., 2015)
LBK1254	Germany	LBK_EN	5500-4800 BCE	HV6'17	(Haak et al., 2015)
LBK1581	Germany	LBK_EN	5500-4800 BCE	T2b	(Haak et al., 2015)
LBK1976	Germany	LBK_EN	5500-4800 BCE	T2e	(Haak et al., 2015)
LBK1988	Germany	LBK_EN	5500-4800 BCE	W1c'i	(Haak et al., 2015)
LBK1577	Germany	LBK_EN	5500-4800 BCE	T2e	(Haak et al., 2015)
SVP3	Russia	Yamnaya	2910-2875 calBCE	U4a1	(Haak et al., 2015)
SVP10	Russia	Yamnaya	3500-2700 BCE	H13a1a1	(Haak et al., 2015)
SVP44	Russia	Samara_HG	5650-5555 calBCE	U5a1d	(Haak et al., 2015)
SVP57	Russia	Yamnaya	3500-2700 BCE	W3a1a	(Haak et al., 2015)
SVP5	Russia	Yamnaya	3090-2910 calBCE	W6c	(Haak et al., 2015)
SVP2	Russia	Yamnaya	3500-2700 BCE	K1b2a	(Haak et al., 2015)
SVP38	Russia	Yamnaya	3339-2917 calBCE	T2c1a2	(Haak et al., 2015)
SVP50	Russia	Yamnaya	3021-2635 calBCE	U5a1a1	(Haak et al., 2015)
SVP52	Russia	Yamnaya	3305-2925 calBCE	U5a1a1	(Haak et al., 2015)

SVP58	Russia	Yamnaya	3335-2881 calBCE	H6a1b	(Haak et al., 2015)
SVP54	Russia	Yamnaya	3010-2622 calBCE	H2b	(Haak et al., 2015)
BLA7	Germany	Neolithic	3666	H5	(Bollongino et al., 2013)
BLA10	Germany	Neolithic	3418	H1c3	(Bollongino et al., 2013)
BLA11	Germany	Neolithic	-	U5b2b(2)	(Bollongino et al., 2013)
BLA13	Germany	Neolithic	3513	H5	(Bollongino et al., 2013)
Theo5	Greece/Anatolia	Mesolithic	7605-7529	K1c	(Hofmanova et al., 2016)
Theo1	Greece/Anatolia	Mesolithic	7288-6771	K1c	(Hofmanova et al., 2016)
Rev5	Greece/Anatolia	Neolithic	6438-6264	X2b	(Hofmanova et al., 2016)
Bar31	Greece/Anatolia	Neolithic	6419-6238	X2m	(Hofmanova et al., 2016)
Bar8	Greece/Anatolia	Neolithic	6212-6030	K1a2	(Hofmanova et al., 2016)
Pal7	Greece/Anatolia	Neolithic	4452-4350	J1c1	(Hofmanova et al., 2016)
Klei10	Greece/Anatolia	Neolithic	4230-3995	K1a2	(Hofmanova et al., 2016)
StPet12	Ukraine	Neolithic	4519-4343	U5b2	(Jones et al., 2017)
StPet2	Ukraine	Mesolithic	9193-8641	U4a1d	(Jones et al., 2017)
ZVEJ28	Latvia	Neolithic	3089-2676	U5a1	(Jones et al., 2017)
ZVEJ31	Latvia	Neolithic	4229-3800	U4	(Jones et al., 2017)
ZVEJ26	Latvia	Neolithic	4251-3976	U4a1	(Jones et al., 2017)
ZVEJ27	Latvia	Neolithic	5302-4852	U5a2d	(Jones et al., 2017)
ZVEJ25	Latvia	Neolithic	5841-5636	U2e1	(Jones et al., 2017)
ZVEJ32	Latvia	Neolithic	6467-6249	U5a1c	(Jones et al., 2017)
LaBrana1	Spain	Mesolithic	6980 +/-50	U5b2c1	(Sánchez-Quinto et al., 2012)
CroMagnon	France	Medieval	690 +/- 39	T2b1	(Fu et al., 2013)
BS11	China	Neolithic	7368 +/- 34	B4c1a	(Fu et al., 2013)
ESP15	Germany	Neolithic	3904 +/- 47	H6a1a	(Brotherton et al., 2013)
ROT2	Germany	Neolithic?	n/a	H5a3	(Brotherton et al., 2013)
OSH2	Germany	Neolithic?	n/a	H89	(Brotherton et al., 2013)
HAL11	Germany	Neolithic?	n/a	H	(Brotherton et al., 2013)
DEB9	Germany	Neolithic?	n/a	H88	(Brotherton et al., 2013)
HAL32	Germany	Neolithic?	n/a	H26	(Brotherton et al., 2013)
KAR6a	Germany	Neolithic?	n/a	H1	(Brotherton et al., 2013; Haak et al., 2015)
Mina4	Germany	Neolithic	3900-3600 BCE	H1	(Haak et al., 2015)
Sardinia	Sardinia	Neolithic	3398 +/-26	H1aw1	(Brotherton et al., 2013)
OSH3	Germany	Neolithic	n/a	H1	(Brotherton et al.,

					2013)
DEB21	Germany	Neolithic	6151 +/-27	H1j	(Brotherton et al., 2013)
HAL39	Germany	Neolithic	6145+/-30	H1e	(Brotherton et al., 2013)
ALB1	Germany	Neolithic	3858 +/-57	H3b	(Brotherton et al., 2013)
KZ1	Poland	Neolithic	5375 ± 35 BP	U5b2a1a	(Juras et al., 2017)
KZ2	Poland	Neolithic	5370 ± 40 BP	K1c	(Juras et al., 2017)
KZ3	Poland	Neolithic	na	H3d	(Juras et al., 2017)
KZ4	Poland	Neolithic	5330 ± 65 BP	K1a4	(Juras et al., 2017)
Tyrolean Iceman	Astro-Italian Border of Alps	Neolithic/Copper Age	5350-5100	K1	(Ermini et al., 2008)
JK2127	Egypt	Ptolemaic Period	cal BC 358-208	W6	(Schuenemann et al., 2017)
JK2128	Egypt	Ptolemaic Period	cal BC 185-107	HV21	(Schuenemann et al., 2017)
JK2130	Egypt	Roman	cal AD 91-212	M1a1	(Schuenemann et al., 2017)
JK2131	Egypt	Third Intermediate Period	cal BC 749-517	U3b	(Schuenemann et al., 2017)
JK2132	Egypt	Roman	cal AD 83-208	T	(Schuenemann et al., 2017)
JK2133	Egypt	Third Intermediate Period	cal BC 750-525	X	(Schuenemann et al., 2017)
JK2134	Egypt	Third Intermediate Period	cal BC 776-569	J1d	(Schuenemann et al., 2017)
JK2135	Egypt	Third Intermediate Period	cal BC 992-923	M1a2a	(Schuenemann et al., 2017)
JK2136	Egypt	Late Period	cal BC 405-394	R0a2	(Schuenemann et al., 2017)
JK2137	Egypt	Ptolemaic Period	cal BC 164-60	J2a2b	(Schuenemann et al., 2017)
JK2139	Egypt	Roman	cal AD 54- 124	K1a	(Schuenemann et al., 2017)
JK2141	Egypt	Ptolemaic Period	cal BC 358- 204	J2a2e	(Schuenemann et al., 2017)
JK2142	Egypt	Ptolemaic Period	cal BC 382- 234	U6a	(Schuenemann et al., 2017)
JK2143	Egypt	Third Intermediate Period	cal BC 801- 777	T1a7	(Schuenemann et al., 2017)
JK2150	Egypt	Third Intermediate Period	cal BC 759-551	K1a4	(Schuenemann et al., 2017)
JK2153	Egypt	Roman	cal BC 43-cal AD 15	R0a1a	(Schuenemann et al., 2017)
JK2155	Egypt	Roman	cal AD 386-426	T	(Schuenemann et al., 2017)
JK2158	Egypt	Roman	cal AD 261-382	X1c	(Schuenemann et al., 2017)
JK2165	Egypt	Ptolemaic Period	cal BC 364-211	W3a1	(Schuenemann et al., 2017)
JK2169	Egypt	Ptolemaic Period	cal BC 355-204	W8	(Schuenemann et al., 2017)

JK2866	Egypt	Ptolemaic Period	cal BC 395-263	R0a2	(Schuenemann et al., 2017)
JK2870	Egypt	Third Intermediate Period	cal BC 899-841	R0a	(Schuenemann et al., 2017)
JK2872	Egypt	Roman	cal AD 81-132	HV1a2a	(Schuenemann et al., 2017)
JK2873	Egypt	Third Intermediate Period	cal BC 804-792	T2	(Schuenemann et al., 2017)
JK2874	Egypt	Ptolemaic Period	cal BC 151-48	U	(Schuenemann et al., 2017)
JK2875	Egypt	Roman	cal AD 340-395	N	(Schuenemann et al., 2017)
JK2876	Egypt	Ptolemaic Period	cal BC 151-46	T1a8a	(Schuenemann et al., 2017)
JK2878	Egypt	Ptolemaic Period	cal BC 344-126	T1a7	(Schuenemann et al., 2017)
JK2880	Egypt	Third Intermediate Period	cal BC 770-567	T1a2	(Schuenemann et al., 2017)
JK2881	Egypt	Ptolemaic Period	cal BC 367-212	T2c1	(Schuenemann et al., 2017)
JK2884	Egypt	Ptolemaic Period	cal BC 158-54	T1a5	(Schuenemann et al., 2017)
JK2885	Egypt	Third Intermediate Period	cal BC 1304-1136	R2'JT	(Schuenemann et al., 2017)
JK2886	Egypt	Late Period	cal BC 398-373	T1a7	(Schuenemann et al., 2017)
JK2887	Egypt	Third Intermediate Period	cal BC 1388-1311	J2a1a1	(Schuenemann et al., 2017)
JK2888	Egypt	Ptolemaic Period	cal BC 97-2	U6a2	(Schuenemann et al., 2017)
JK2889	Egypt	Third Intermediate Period	cal BC 797-674	U7	(Schuenemann et al., 2017)
JK2890	Egypt	Third Intermediate Period	cal BC 794-671	I	(Schuenemann et al., 2017)
JK2893	Egypt	Third Intermediate Period	cal BC 797-771	H5	(Schuenemann et al., 2017)
JK2895	Egypt	Roman	cal AD 25-111	K 16T	(Schuenemann et al., 2017)
JK2899	Egypt	Third Intermediate Period	cal BC 795-674	T1a7	(Schuenemann et al., 2017)
JK2900	Egypt	Third Intermediate Period	cal BC 804-786	HV	(Schuenemann et al., 2017)
JK2902	Egypt	Third Intermediate Period	cal BC 902-842	I	(Schuenemann et al., 2017)
JK2903	Egypt	Ptolemaic Period	cal BC 87-cal AD 2	U5a	(Schuenemann et al., 2017)
JK2904	Egypt	Ptolemaic Period	cal BC 362-210	R0a1a	(Schuenemann et al., 2017)
JK2907	Egypt	Roman	cal AD 26-84	HV1a'b'c	(Schuenemann et al., 2017)

JK2911	Egypt	Third Intermediate Period	cal BC 769-560	M1a1	(Schuenemann et al., 2017)
JK2913	Egypt	Third Intermediate Period	cal BC 895-834	X1	(Schuenemann et al., 2017)
JK2914	Egypt	Late Period	cal BC 510-408	T2	(Schuenemann et al., 2017)
JK2916	Egypt	Third Intermediate Period	cal BC 1111-998	R0	(Schuenemann et al., 2017)
JK2918	Egypt	Roman	cal AD 84-129	J2a2e	(Schuenemann et al., 2017)
JK2919	Egypt	Third Intermediate Period	cal BC 790-671	J2a2c	(Schuenemann et al., 2017)
JK2920	Egypt	Third Intermediate Period	cal BC 758-552	U8b1a1	(Schuenemann et al., 2017)
JK2921	Egypt	Roman	cal AD 35-120	R0a1	(Schuenemann et al., 2017)
JK2922	Egypt	Ptolemaic Period	cal BC 352-200	R	(Schuenemann et al., 2017)
JK2923	Egypt	Third Intermediate Period	cal BC 753-544	U8b1a1	(Schuenemann et al., 2017)
JK2925	Egypt	Roman	cal AD 5-54	U7	(Schuenemann et al., 2017)
JK2950	Egypt	Ptolemaic Period	cal BC 357-206	H6b	(Schuenemann et al., 2017)
JK2951	Egypt	Ptolemaic Period	cal BC 344-169	U8b1b1	(Schuenemann et al., 2017)
JK2952	Egypt	Third Intermediate Period	cal BC 790-603	J2a2c	(Schuenemann et al., 2017)
JK2953	Egypt	Ptolemaic Period	cal BC 37-cal AD 48	M1a1	(Schuenemann et al., 2017)
JK2955	Egypt	Ptolemaic Period	cal BC 391-260	L3	(Schuenemann et al., 2017)
JK2956	Egypt	Third Intermediate Period	cal BC 823-785	U1a1a3	(Schuenemann et al., 2017)
JK2957	Egypt	Third Intermediate Period	cal BC 788-595	J2a2c	(Schuenemann et al., 2017)
JK2958	Egypt	Roman	cal AD 27-83	I	(Schuenemann et al., 2017)
JK2960	Egypt	Roman	cal BC 44-cal AD 16	N1'5	(Schuenemann et al., 2017)
JK2961	Egypt	Ptolemaic Period	cal BC 87-cal AD 1	T1a7	(Schuenemann et al., 2017)
JK2963	Egypt	Third Intermediate Period	cal BC 1211-1126	M1a1i	(Schuenemann et al., 2017)
JK2965	Egypt	Third Intermediate Period	cal BC 979-914	T2c1c	(Schuenemann et al., 2017)
JK2966	Egypt	Ptolemaic Period	cal BC 384-235	T1a7	(Schuenemann et al., 2017)
JK2970	Egypt	Ptolemaic Period	cal BC 357-206	U1a1	(Schuenemann et al., 2017)

JK2972	Egypt	Ptolemaic Period	cal BC 156-53	T1a5	(Schuenemann et al., 2017)
JK2973	Egypt	Ptolemaic Period	cal BC 347-168	U6a3	(Schuenemann et al., 2017)
JK2974	Egypt	Third Intermediate Period	cal BC 889-803	H	(Schuenemann et al., 2017)
JK2975	Egypt	Roman	cal BC 43-cal AD 45	R	(Schuenemann et al., 2017)
JK2977	Egypt	Ptolemaic Period	cal BC 389-235	T2e	(Schuenemann et al., 2017)
JK2978	Egypt	Third Intermediate Period	cal BC 975-905	N1a1a2	(Schuenemann et al., 2017)
JK2979	Egypt	Ptolemaic Period	cal BC 369-211	HV1a2a	(Schuenemann et al., 2017)
JK2980	Egypt	Ptolemaic Period	cal BC 357-204	I	(Schuenemann et al., 2017)
JK2981	Egypt	Ptolemaic Period	cal BC 399-376	M1a1e	(Schuenemann et al., 2017)
JK2985	Egypt	Ptolemaic Period	cal BC 352-195	HV1a'b'c	(Schuenemann et al., 2017)
JK2986	Egypt	Late Period	cal BC 508-406	HV	(Schuenemann et al., 2017)
JK2987	Egypt	Ptolemaic Period	cal BC 342-117	HV1a'b'c	(Schuenemann et al., 2017)
JK2879	Egypt	Roman	cal BC 45-cal AD 4	U3b	(Schuenemann et al., 2017)
JK2883	Egypt	Third Intermediate Period	cal BC 799-781	T1a	(Schuenemann et al., 2017)
JK2896	Egypt	Ptolemaic Period	cal BC 394-239	HV1b2	(Schuenemann et al., 2017)
JK2959	Egypt	Roman	cal BC 44-cal AD 16	T1a	(Schuenemann et al., 2017)
JK2962	Egypt	Late Period	cal BC 756-545	H13c1	(Schuenemann et al., 2017)
JK2982	Egypt	Ptolemaic Period	cal BC 92-1	T1a5	(Schuenemann et al., 2017)
JK2984	Egypt	Roman	cal AD 32-122	U7	(Schuenemann et al., 2017)
1622BM	Egypt	Third Intermediate Period	cal BC 806- 784	R0a2f	(Schuenemann et al., 2017)
A2197	Greece	Neolithic	5419 +/- 41 cal BCE	K1a26	(Lazaridis et al., 2017)
Lasithi4	Greece	Bronze Age	2000-1700 BCE	U5a1	(Lazaridis et al., 2017)
Lasithi2	Greece	Bronze Age	2000-1700 BCE	H13a1	(Lazaridis et al., 2017)
Lasithi7	Greece	Bronze Age	2000-1700 BCE	H	(Lazaridis et al., 2017)
Lasithi9	Greece	Bronze Age	2000-1700 BCE	H5	(Lazaridis et al., 2017)
Lasithi17	Greece	Bronze Age	2000-1700 BCE	H	(Lazaridis et al., 2017)
Salamis31	Greece	Bronze Age	1411-1262 cal BCE	X2d	(Lazaridis et al., 2017)
S-EVA 1263 Armenoi 503	Greece	Bronze Age	1370-1340 BCE	U5a1	(Lazaridis et al., 2017)
12V t2 Odigitria	Greece	Bronze Age	2900-1900 BCE	J2b1a1	(Lazaridis et al., 2017)

13V t2 Odigitria	Greece	Bronze Age	2900-1900 BCE	I5	(Lazaridis et al., 2017)
14V t2 Odigitria	Greece	Bronze Age	2900-1900 BCE	H+163	(Lazaridis et al., 2017)
16V Odigitria	Greece	Bronze Age	2900-1900 BCE	U3b3	(Lazaridis et al., 2017)
19V t2 Odigitria	Greece	Bronze Age	2900-1900 BCE	K1a2	(Lazaridis et al., 2017)
Galatas19	Greece	Bronze Age	1700-1200 BCE	X2	(Lazaridis et al., 2017)
Peristeria4	Greece	Bronze Age	1416-1280 cal BCE	H	(Lazaridis et al., 2017)
Galatas4	Greece	Bronze Age	1700-1200 bCE	X2	(Lazaridis et al., 2017)
A4-1	Turkey	Bronze Age	2558-2295 cal BCE	H	(Lazaridis et al., 2017)
UC1	Turkey	Bronze Age	2836-2472 cal BCE	K1a2	(Lazaridis et al., 2017)
G3-95	Turkey	Bronze Age	2500-1800 BCE	T2b	(Lazaridis et al., 2017)
CabecoArruda117B	Portugal	Neolithic/Chalcolithic	~3500 BC	J1c1b	(Martiniano et al., 2017)
CabecoArruda122A	Portugal	Neolithic/Chalcolithic	~3500 BC	H1e1a	(Martiniano et al., 2017)
CovaMoura364	Portugal	Neolithic Chalcolithic	~3500 BC	H	(Martiniano et al., 2017)
CovaMoura9B	Portugal	Neolithic/Chalcolithic	~3500 BC	J1c1	(Martiniano et al., 2017)
DolmenAnsiao96B	Portugal	Neolithic/Chalcolithic	~3500 BC	K1b1a	(Martiniano et al., 2017)
LugarCanto41	Portugal	Neolithic	4200–3500 BC	U5b1+16189+@16192	(Martiniano et al., 2017)
LugarCanto42	Portugal	Neolithic	4200–3500 BC	H3	(Martiniano et al., 2017)
LugarCanto44	Portugal	Neolithic	4200–3500 BC	H1e1a2	(Martiniano et al., 2017)
MonteGato104	Portugal	Bronze Age	1740–1430 BCE	U5b3	(Martiniano et al., 2017)
TV32032extra	Portugal	Bronze Age	1740–1430 BCE	X2b+226	(Martiniano et al., 2017)
TV3831	Portugal	Bronze Age	1740–1430 BCE	H1+152	(Martiniano et al., 2017)
ValeDoOuro10207	Portugal	Bronze Age	1740–1430 BCE	U5b1+16189+@16192	(Martiniano et al., 2017)

4.10 References

Attema P, van Leusen A. 2004. The Early Roman Colonization of South Lazio: A Survey of Three Landscapes. In: Attema P, editor. Centralization, Early Urbanization, and Colonization in First Millenium BC Italy and Greece. Leuven: Peeters:157–195.

Barberena R, Durán VA, Novellino P, Winocur D, Benítez A, Tessone A, Quiroga MN, Marsh EJ, Gasco A, Cortegoso V, Lucero G, Llano C, Knudson KJ. 2017. Scale of human mobility in the southern Andes (Argentina and Chile): a new framework based on strontium isotopes. Am J Phys Anthropol:305–320.

Bentley RA. 2006. Strontium isotopes from the earth to the archaeological skeleton: a review. J Archaeol Method Theory 13:135–187.

Boattini A, Martinez-Cruz B, Sarno S, Harmant C, Useli A, Sanz P, Yang-Yao D, Manry J, Ciani G, Luiselli D, Quintana-Murci L, Comas D, Pettener D, Adhikarla S, Adler CJ, Balanovska E, Balanovsky O, Bertranpetit J, Clarke AC, Cooper A, Der Sarkissian CSI, Dulik MC, Gaieski JB, GaneshPrasad AK, Haak W, Haber M, Jin L, Kaplan ME, Li H, Li S, Matisoo-Smith EA, Merchant NC, Mitchell RJ, Owings AC, Parida L, Pitchappan R, Platt DE, Renfrew C, Lacerda DR, Royyuru AK, Santos FR, Schurr TG, Soodyall H, Hernanz DFS, Swamikrishnan P, Tyler-Smith C, Santhakumari AV, Vieira PP, Vilar MG, Wells RS, Zalloua PA, Ziegle JS. 2013. Uniparental markers in Italy reveal a sex-biased genetic structure and different historical strata. PLoS One 8:e65441.

Bollongino R, Nehlich O, Richards MP, Orschiedt J, Thomas MG, Sell C, Fajkošová Z, Powell A, Burger J. 2013. 2000 years of parallel societies in stone age central Europe. Science 342:479-481.

Bos KI, Herbig A, Sahl J, Waglechner N, Fourment M, Forrest SA, Klunk J, Schuenemann VJ, Poinar D, Kuch M, Golding GB, Dutour O, Keim P, Wagner DM, Holmes EC, Krause J, Poinar HN. 2016. Eighteenth century Yersinia pestis genomes reveal the long-term persistence of an historical plague focus. Elife 5:1–11.

Bouwman AS, Brown KA, Prag AJNW, Brown TA. 2008. Kinship between burials from grave circle B at Mycenae revealed by ancient DNA typing. J Archaeol Sci 35:2580–2584.

Bowen GJ. 2010. Isoscapes: spatial pattern in isotopic biogeochemistry. Annu Rev Earth Planet Sci 38:161–187.

Bradley KR. 1994. Slavery and Society at Rome. Cambridge: Cambridge University Press.

Brandt G, Szécsényi-Nagy A, Roth C, Alt KW, Haak W. 2015. Human paleogenetics of Europe - the known knowns and the known unknowns. J Hum Evol 79:73–92.

Brent L, Prowse T. 2014. Grave Goods, Burial Practices and Patterns of Distribution in the Vagnari Cemetery. In: Small A, editor. Beyond Vagnari: New Themes in the Study of Roman South Italy. Bari: Edipuglia:99–110.

Brooks R, Small A, Ward-Perkins J. 1966. Trial Excavations on the Site of Botromagno, Gravina di Puglia, 1966. Pap Br Sch Rome1 34:131–150.

Brotherton P, Haak W, Templeton J, Brandt G, Soubrier J, Jane Adler C, Richards SM, Sarkissian C Der, Ganslmeier R, Friederich S, Dresely V, van Oven M, Kenyon R, Van der Hoek MB, Korlach J, Luong K, Ho SYW, Quintana-Murci L, Behar DM, Meller H, Alt KW, Cooper A, Adhikarla S, Ganesh Prasad AK, Pitchappan R, Varatharajan Santhakumari A, Balanovska E, Balanovsky O, Bertranpetit J, Comas D, Martínez-Cruz B, Melé M,

Clarke AC, Matisoo-Smith EA, Dulik MC, Gaieski JB, Owings AC, Schurr TG, Vilar MG, Hobbs A, Soodyall H, Javed A, Parida L, Platt DE, Royyuru AK, Jin L, Li S, Kaplan ME, Merchant NC, John Mitchell R, Renfrew C, Lacerda DR, Santos FR, Soria Hernanz DF, Spencer Wells R, Swamikrishnan P, Tyler-Smith C, Paulo Vieira P, Ziegle JS. 2013. Neolithic mitochondrial haplogroup H genomes and the genetic origins of Europeans. Nat Commun 4:1764.

Buikstra J, Ubelaker D. 1994. Standards for Data Collection from Human Skeletal Remains. Arkansas Archeological Survey, Fayetteville.

Capelli C, Brisighelli F, Scarnicci F, Arredi B, Caglia' A, Vetrugno G, Tofanelli S, Onofri V, Tagliabracci A, Paoli G, Pascali VL. 2007. Y chromosome genetic variation in the Italian peninsula is clinal and supports an admixture model for the Mesolithic-Neolithic encounter. Mol Phylogenet Evol 44:228–239.

Capocasa M, Anagnostou P, Bachis V, Battaggia C, Bertoncini S, Biondi G, Boattini A, Boschi I, Brisighelli F, Calò CM, Carta M, Coia V, Corrias L, Crivellaro F, De Fanti S, Dominici V, Ferri G, Francalacci P, Franceschi ZA, Luiselli D, Morelli L, Paoli G, Rickards O, Robledo R, Sanna D, Sanna E, Sarno S, Sineo L, Taglioli L, Tagarelli G, Tofanelli S, Vona G, Pettener D, Bisol GD. 2014. Linguistic, geographic and genetic isolation: a collaborative study of Italian populations. J Anthropol Sci 92:201–231.

Chenery CA, Pashley V, Lamb AL, Sloane HJ, Evans JA. 2012. The oxygen isotope relationship between the phosphate and structural carbonate fractions of human bioapatite. Rapid Commun Mass Spectrom 26:309–319.

Chilvers ER, Bouwman AS, Brown KA, Arnott RG, Prag AJNW, Brown TA. 2008. Ancient DNA in human bones from Neolithic and Bronze Age sites in Greece and Crete. J Archaeol Sci 35:2707–2714.

Cornell T. 1995. The Beginnings of Rome: Italy and Rome From the Bronze Age to the Punic Wars (c. 1000 - 264 BC). London: Routledge.

Crawford M. 2001. Early Rome and Italy. In: Boardman J, Griffin J, Murray O, editors. The Oxford Illustrated History of the Roman World. Oxford: Oxford University Press:387-417.

Dabney J, Knapp M, Glocke I, Gansauge M-T, Weihmann A, Nickel B, Valdiosera C, García N, Pääbo S, Arsuaga J-L, Meyer M. 2013. Complete mitochondrial genome sequence of a middle Pleistocene cave bear reconstructed from ultrashort DNA fragments. Proc Natl Acad Sci 110:15758–63.

Darriba D, Taboada GL, Doallo R, Posada D. 2012. jModelTest 2: more models, new heuristics and parallel computing. Nat Methods 9:772–772.

De Ligt L, Northwood S. 2008. People, Land, and Politics: Demographic Developments and the Transformation of Roman Italy, 300 BC - AD 14. Leiden: Brill.

Derenko M, Malyarchuk B, Grzybowski T, Denisova G, Rogalla U, Perkova M, Dambueva I, Zakharov I. 2010. Origin and post-glacial dispersal of mitochondrial DNA haplogroups C and D in Northern Asia. PLoS One 5:1–9.

Duggan AT, Perdomo MF, Piombino-Mascali D, Marciniak S, Poinar D, Emery M V, Buchmann JP, Duchêne S, Jankauskas R, Humphreys M, Golding GB, Southon J, Devault A, Rouillard JM, Sahl JW, Dutour O, Hedman K, Sajantila A, Smith GL, Holmes EC, Poinar HN. 2016. 17th century Variola virus reveals the recent history of smallpox. Curr Biol 26:3407–3412.

Edgar RC, Drive RM, Valley M. 2017. MUSCLE : multiple sequence alignment with high accuracy and high throughput. Nucleic Acids Res 32:1792–1797.

Emery MV, Stark R, Murchie TJ, Elford S, Schwarcz H., Prowse TL. Mapping the origins of imperial Roman workers (1st – 4th century CE) at Vagnari, southern Italy, using 87Sr/86Sr and δ18O variability. Am J Phys Anthropol In Review.

Ermini L, Olivieri C, Rizzi E, Corti G, Bonnal R, Soares P, Luciani S, Marota I, De Bellis G, Richards MB, Rollo F. 2008. Complete mitochondrial genome sequence of the Tyrolean iceman. Curr Biol 18:1687–1693.

Excoffier L, Smouse PE, Quattro JM. 1992. Analysis of molecular variance inferred from metric distances among DNA haplotypes: Application to human mitochondrial DNA restriction data. Genetics 131:479–491.

De Fanti S, Barbieri C, Sarno S, Sevini F, Vianello D, Tamm E, Metspalu E, Van Oven M, Hübner A, Sazzini M, Franceschi C, Pettener D, Luiselli D. 2015. Fine dissection of human mitochondrial DNA haplogroup HV lineages reveals paleolithic signatures from European Glacial refugia. PLoS One 10:1–19.

Fu Q, Mittnik A, Johnson PLF, Bos K, Lari M, Bollongino R, Sun C, Giemsch L, Schmitz R, Burger J, Ronchitelli AM, Martini F, Cremonesi RG, Svoboda J, Bauer P, Caramelli D, Castellano S, Reich D, Pääbo S, Krause J. 2013. A revised timescale for human evolution based on ancient mitochondrial genomes. Curr Biol 23:553–559.

Di Gaetano C, Voglino F, Guarrera S, Fiorito G, Rosa F, Di Blasio AM, Manzini P, Dianzani I, Betti M, Cusi D, Frau F, Barlassina C, Mirabelli D, Magnani C, Glorioso N, Bonassi S, Piazza A, Matullo G. 2012. An overview of the genetic structure within the Italian population from genome-wide data. PLoS One 7:e43759.

Ghirotto S, Tassi F, Fumagalli E, Colonna V, Sandionigi A, Lari M, Vai S, Petiti E, Corti G, Rizzi E, de Bellis G, Caramelli D, Barbujani G. 2013. Origins and evolution of the Etruscans' mtDNA. PLoS One 8:e55519.

Gill MS, Lemey P, Faria NR, Rambaut A, Shapiro B, Suchard MA. 2013. Improving bayesian population dynamics inference: A coalescent-based model for multiple loci. Mol Biol Evol 30:713–724.

Giustini F, Brilli M, Patera A. 2016. Mapping oxygen stable isotopes of precipitation in Italy. J Hydrol Reg Stud 8:162–181.

Gomez-Carballa A, Pardo-Seco J, Amigo J, Martinon-Torres F, Salas A. 2015. Mitogenomes from The 1000 Genome Project reveal new Near Eastern features in present-day Tuscans. PLoS One 10:1–12.

Gregoricka LA, Sheridan SG. 2017. Continuity or conquest? A multi-isotope approach to investigating identity in the Early Iron Age of the Southern Levant. Am J Phys Anthropol 162:73–89.

Haak W, Lazaridis I, Patterson N, Rohland N, Mallick S, Llamas B, Brandt G, Nordenfelt S, Harney E, Stewardson K, Fu Q, Mittnik A, Bánffy E, Economou C, Francken M, Friederich S, Pena RG, Hallgren F, Khartanovich V, Khokhlov A, Kunst M, Kuznetsov P, Meller H, Mochalov O, Moiseyev V, Nicklisch N, Pichler SL, Risch R, Rojo Guerra M a., Roth C, Szécsényi-Nagy A, Wahl J, Meyer M, Krause J, Brown D, Anthony D, Cooper A, Alt KW, Reich D. 2015. Massive migration from the steppe was a source for Indo-European languages in Europe. Nature 522:207–211.

Hartl D, Clark A. 1997. Principles of Population Genetics. 3rd Editio. Sunderland, Massachusetts: Sinauer Associates.

Hofmanova Z, Kreutzer S, Hallenthal G, Sell C, Diekmann Y. 2016. Early farmers from across Europe directly descended from Neolithic Aegeans. Proc Natl Acad Sci 113:6886–6891.

Jones ER, Zarina G, Moiseyev V, Manica A, Pinhasi R, Bradley DG, Lightfoot E, Nigst PR. 2017. The Neolithic transition in the Baltic was not driven by admixture with early European farmers. Curr Biol 27:576–582.

Jónsson H, Ginolhac A, Schubert M, Johnson PLF, Orlando L. 2013. MapDamage2.0: Fast approximate Bayesian estimates of ancient DNA damage parameters. Bioinformatics 29:1682–1684.

Juras A, Chyleński M, Krenz-Niedbała M, Malmström H, Ehler E, Pospieszny Ł, Łukasik S, Bednarczyk J, Piontek J, Jakobsson M, Dabert M. 2017. Investigating kinship of Neolithic post-LBK human remains from Krusza Zamkowa, Poland using ancient DNA. Forensic Sci Int Genet 26:30–39.

Kearse M, Moir R, Wilson A, Stones-Havas S, Cheung M, Sturrock S, Buxton S, Cooper A, Markowitz S, Duran C, Thierer T, Ashton B, Meintjes P, Drummond A. 2012. Geneious Basic: An integrated and extendable desktop software platform for the organization and analysis of sequence data. Bioinformatics 28:1647–1649.

Killgrove K, Montgomery J. 2016. All roads lead to Rome: Exploring human migration to the eternal city through biochemistry of skeletons from two imperial-era cemeteries (1st-3rd c AD). PLoS One 11:1–30.

Kircher M, Sawyer S, Meyer M. 2012. Double indexing overcomes inaccuracies in multiplex sequencing on the Illumina platform. Nucleic Acids Res 40:1–8.

Krause J, Fu Q, Good JM, Viola B, Shunkov M V, Derevianko AP, Pääbo S. 2010. The complete mitochondrial DNA genome of an unknown hominin from southern Siberia. Nature 464:894–897.

Lacan M, Keyser C, Ricaut F-X, Brucato N, Durathon F, Guilaine J, Crubezy E, Ludes B. 2011. Ancient DNA reveals male diffusion through the Neolithic Mediterranean route. PNAS 108:9788–9791.

Lazaridis I, Mittnik A, Patterson N, Mallick S, Rohland N, Pfrengle S, Furtwängler A, Peltzer A, Posth C, Vasilakis A, McGeorge PJP, Konsolaki-Yannopoulou E, Korres G, Martlew H, Michalodimitrakis M, Özsait M, Özsait N, Papathanasiou A, Richards M, Roodenberg SA, Tzedakis Y, Arnott R, Fernandes DM, Hughey JR, Lotakis DM, Navas PA, Maniatis Y, Stamatoyannopoulos JA, Stewardson K, Stockhammer P, Pinhasi R, Reich D, Krause J, Stamatoyannopoulos G. 2017. Genetic origins of the Minoans and Mycenaeans. Nature 548:214-218.

Lazaridis I, Patterson N, Mittnik A, Renaud G, Mallick S, Kirsanow K, Sudmant PH, Schraiber JG, Castellano S, Lipson M, Berger B, Economou C, Bollongino R, Fu Q, Bos KI, Nordenfelt S, Li H, de Filippo C, Prüfer K, Sawyer S, Posth C, Haak W, Hallgren F, Fornander E, Rohland N, Delsate D, Francken M, Guinet J-M, Wahl J, Ayodo G, Babiker H a., Bailliet G, Balanovska E, Balanovsky O, Barrantes R, Bedoya G, Ben-Ami H, Bene J, Berrada F, Bravi CM, Brisighelli F, Busby GBJ, Cali F, Churnosov M, Cole DEC, Corach D, Damba L, van Driem G, Dryomov S, Dugoujon J-M, Fedorova S a., Gallego Romero I, Gubina M, Hammer M, Henn BM, Hervig T, Hodoglugil U, Jha AR, Karachanak-Yankova S, Khusainova R, Khusnutdinova E, Kittles R, Kivisild T, Klitz W, Kučinskas V, Kushniarevich A, Laredj L, Litvinov S, Loukidis T, Mahley RW, Melegh B, Metspalu E, Molina J, Mountain J, Näkkäläjärvi K, Nesheva D, Nyambo T, Osipova L, Parik J, Platonov F, Posukh O, Romano V, Rothhammer F, Rudan I, Ruizbakiev R, Sahakyan H, Sajantila A, Salas A, Starikovskaya EB, Tarekegn A, Toncheva D, Turdikulova S, Uktveryte I, Utevska O, Vasquez R, Villena M, Voevoda M, Winkler CA, et al. 2014. Ancient human genomes suggest three ancestral populations for present-day Europeans. Nature 513:409–13.

Li H, Durbin R. 2009. Fast and accurate short read alignment with Burrows-Wheeler transform. Bioinformatics 25:1754–1760.

Longinelli A, Selmo E. 2003. Isotopic composition of precipitation in Italy: A first overall map. J Hydrol 270:75–88.

Marciniak S, Prowse TL, Herring DA, Klunk J, Kuch M, Duggan AT, Bondioli L, Holmes EC, Poinar HN. 2016. Plasmodium falciparum malaria in 1st–2nd century CE southern Italy. Curr Biol 26:1220–1222.

Margaryan A, Derenko M, Hovhannisyan H, Malyarchuk B, Heller R, Khachatryan Z, Avetisyan P, Badalyan R, Bobokhyan A, Melikyan V, Sargsyan G, Piliposyan A, Simonyan H, Mkrtchyan R, Denisova G, Yepiskoposyan L, Willerslev E, Allentoft ME. 2017. Eight Millennia of Matrilineal Genetic Continuity in the South Caucasus. Curr Biol 27:e80673.

Marsteller SJ, Knudson KJ, Gordon G, Anbar A. 2017. Biogeochemical reconstructions of life histories as a method to assess regional interactions: Stable oxygen and radiogenic strontium isotopes and Late Intermediate Period mobility on the Central Peruvian Coast. J Archaeol Sci Reports 13:535–546.

Martiniano R, Cassidy LM, O'Maolduin R, McLaughlin R, Silva NM, Manco L, Fidalgo D, Pereira T, Coelho MJ, Serra M, Burger J, Parreira R, Moran E, Valera A, Porfirio E, Boaventura R, Silva AM, Bradley DG. 2017. The population genomics of archaeological transition in west Iberia. bioRxiv:1–41.

Meyer M, Kircher M. 2010. Illumina sequencing library preparation for highly multiplexed target capture and sequencing. Cold Spring Harb Protoc 5:10.1101/pdb.prot5448.

Olalde I, Schroeder H, Sandoval-Velasco M, Vinner L, Lobón I, Ramirez O, Civit S, Borja PG, Salazar-García DC, Talamo S, Fullola JM, Oms FX, Pedro M, Martínez P, Sanz M, Daura J, Zilhão J, Marquès-Bonet T, Gilbert MTP, Lalueza-Fox C. 2015. A common genetic origin for early farmers from mediterranean cardial and central european LBK cultures. Mol Biol Evol 32:3132–3142.

Omrak A, Günther T, Valdiosera C, Svensson EM, Malmström H, Kiesewetter H, Aylward W, Storå J, Jakobsson M, Götherström A. 2016. Genomic evidence establishes Anatolia as the source of the European Neolithic gene pool. Curr Biol 26:270–275.

van Oven M. 2015. PhyloTree Build 17: Growing the human mitochondrial DNA tree. Forensic Sci Int Genet Suppl Ser 5:e392–e394.

Pala M, Achilli A, Olivieri A, Kashani BH, Perego UA, Sanna D, Metspalu E, Tambets K, Tamm E, Accetturo M, Carossa V, Lancioni H, Panara F, Zimmermann B, Huber G, Al-Zahery N, Brisighelli F, Woodward SR, Francalacci P, Parson W, Salas A, Behar DM, Villems R, Semino O, Bandelt HJ, Torroni A. 2009. Mitochondrial haplogroup U5b3: a distant echo of the epipaleolithic in Italy and the legacy of the early Sardinians. Am J Hum Genet 84:814–821.

Paoli U. 1973. Rome: Its People, Life, and Customs. Norforlk: Lowe and Brydone Ltd.

Pellegrini M, Pouncett J, Jay M, Pearson MP, Richards MP. 2016. Tooth enamel oxygen "isoscapes" show a high degree of human mobility in prehistoric Britain. Sci Rep 6:34986.

Perry MA, Jennings C, Coleman DS. 2017. Strontium isotope evidence for long-distance immigration into the Byzantine port city of Aila, modern Aqaba, Jordan. Archaeol Anthropol Sci 9:943–964.

Peruzzi B. 2016. Populating Peucetia: Central Apulian Grave Good Assemblages From the Classical Period (late 6th-3rd centuries B.C.). Unpublished PhD Dissertation, University of Cincinnati, Arts and Sciences:Classics.

Peschel EM, Carlsson D, Bethard J, Beaudry MC. 2017. Who resided in Ridanäs?: A study of mobility on a Viking Age trading port in Gotland, Sweden. J Archaeol Sci Reports 13:175–184.

Posth C, Renaud G, Mittnik A, Drucker DG, Rougier H, Cupillard C, Valentin F, Thevenet C, Furtwängler A, Wißing C, Francken M, Malina M, Bolus M, Lari M, Gigli E, Capecchi G, Crevecoeur I, Beauval C, Flas D, Germonpré M, Van Der Plicht J, Cottiaux R, Gély B, Ronchitelli A, Wehrberger K, Grigorescu D, Svoboda J, Semal P, Caramelli D, Bocherens H, Harvati K, Conard NJ, Haak W, Powell A, Krause J. 2016. Pleistocene mitochondrial genomes suggest a single major dispersal of non-africans and a late glacial population turnover in Europe. Curr Biol 26:827–833.

Prowse TL. 2016. Isotopes and Mobility in the Ancient Roman World. In: De Ligt L, Tacoma L, editors. Migration and Mobility in the Early Roman Empire. Leiden: Brill:205–233.

Prowse TL, Barta J, Hunnius T, Small A. 2010. Stable isotope and mtDNA evidence for geographic origins at the site of Vagnari, South Italy. In: Eckardt H, editor. Roman Diasporas: Archaeological Approaches to Mobility and Diversity in the Roman Empire. Portsmouth: Journal of Roman Archaeology Supplementary Series 78:175–198.

Quintana-Murci L, Veitia R, Fellous M, Semino O, Poloni ES. 2003. Genetic structure of mediterranean populations revealed by Y-chromosome haplotype analysis. Am J Phys Anthropol 121:157–171.

Renaud G, Slon V, Duggan AT, Kelso J. 2015. Schmutzi: estimation of contamination and endogenous mitochondrial consensus calling for ancient DNA. Genome Biol 16:1–18.

Renaud G, Stenzel U, Kelso J. 2014. LeeHom: Adaptor trimming and merging for Illumina sequencing reads. Nucleic Acids Res 42:e141.

Salmon E. 1955. Roman expansion and Roman colonization in Italy. Phoenix 9:36–75.

Sánchez-Quinto F, Schroeder H, Ramirez O, Ávila-Arcos MC, Pybus M, Olalde I, Velazquez AM V, Marcos MEP, Encinas JMV, Bertranpetit J, Orlando L, Gilbert MTP, Lalueza-Fox C. 2012. Genomic affinities of two 7,000-year-old Iberian hunter-gatherers. Curr Biol 22:1494–1499.

Sarno S, Tofanelli S, De Fanti S, Quagliariello A, Bortolini E, Ferri G, Anagnostou P, Brisighelli F, Capelli C, Tagarelli G, Sineo L, Luiselli D, Boattini A, Pettener D. 2016. Shared language, diverging genetic histories: high-resolution analysis of Y-chromosome variability in Calabrian and Sicilian Arbereshe. Eur J Hum Genet 24:600–606.

Schuenemann VJ, Peltzer A, Welte B, Pelt WP van, Molak M, Wang C-C, Furtwängler A, Urban C, Reiter E, Nieselt K, Teßmann B, Francken M, Harvati K, Haak W, Schiffels S, Krause J. 2017. Ancient Egyptian mummy genomes suggest an increase of Sub-Saharan African ancestry in post-Roman periods. Nat Commun 8:e15694.

Schweissing MM, Grupe G. 2003. Stable strontium isotopes in human teeth and bone: A key to migration events of the late Roman period in Bavaria. J Archaeol Sci 30:1373–1383.

Skoglund P, Malmstrom H, Raghavan M, Stora J, Hall P, Willerslev E, Gilbert MTP, Gotherstrom A, Jakobsson M. 2012. Origins and genetic legacy of Neolithic farmers and hunter-gatherers in Europe. Science 336:466–469.

Small A. 1992. Botromagno: An Introduction. In: Small A, editor. Gravina: An Iron Age and Republican Settlement in Apulia. Volume 1: London: British School at Rome:3–15.

Small A. 2002. Apulia before and after the Roman conquest: Recent evidence from Botromagno. J Rom Archaeol 15:375–379.

Small A, Small C. 2007. Excavation in the Roman cemetery at Vagnari in the territory of Gravina in Puglia. Pap Br Sch Rome LXXV:162–213.

Small AM, Volterra V, Hancock RG V. 2000. New evidence from tile-stamps for imperial properties near Gravina , and the topography of imperial estates in SE Italy. J Rom Archaeol 122:179–199.

Soares P, Achilli A, Semino O, Davies W, Macaulay V, Bandelt HJ, Torroni A, Richards MB. 2010. The archaeogenetics of Europe. Curr Biol 20:174–183.

Stek T, Pelgrom J. 2014. Roman Republican Colonization: New Perspectives From Archaeology and Ancient History. Volume 62. Rome: Palombi Editori.

Tassi F, Ghirotto S, Caramelli D, Barbujani G. 2013. Genetic evidence does not support an etruscan origin in Anatolia. Am J Phys Anthropol 152:11–18.

Taylor J, Dorrell P, Small A. 1976. Gravina-Di-Puglia III Houses and a Cemetery of the Iron Age and Classical Period. Pap Br Sch Rome1 44:48–132.

La Torre G. 2011. Reflections on the Lucanians and Bruttians in Calabria Between Hannibal and the Principate: Coloniae, Foederatae, Municipia. In: Colivicchi F, editor. Local Cultures of South Italy and Sicily in the Late Republican Period2. Journal of Roman Archaeology Supplementary Series 83:139–159.

Wagner DM, Klunk J, Harbeck M, Devault A, Waglechner N, Sahl JW, Enk J, Birdsell DN, Kuch M, Lumibao C, Poinar D, Pearson T, Fourment M, Golding B, Riehm JM, Earn DJD, DeWitte S, Rouillard JM, Grupe G, Wiechmann I, Bliska JB, Keim PS, Scholz HC, Holmes EC, Poinar H. 2014. Yersinia pestis and the Plague of Justinian 541-543 AD: A genomic analysis. Lancet Infect Dis 14:319–326.

Ward-Perkins J, Cotton M, Vander Poel H, Macnamara E, Taylor J, Carter A. 1969. Excavations at Botromagno, Gravina di Puglia: Second Interim Report, 1967-68. Pap Br Sch Rome 37:100–157.

Weissensteiner H, Pacher D, Kloss-Brandstätter A, Forer L, Specht G, Bandelt H-J, Kronenberg F, Salas A, Schönherr S. 2016. HaploGrep 2: mitochondrial haplogroup classification in the era of high-throughput sequencing. Nucleic Acids Res 44:W58-63.

Whittaker C. 1994. Frontiers of the Roman Empire: A Social and Economic History. Baltimore: The John Hopkins University Press.

Wilhelmson H, Price TD. 2017. Migration and integration on the Baltic island of Öland in the Iron Age. J Archaeol Sci Reports 12:183–196.

Williams D. 1997. The Reach of Rome: A History of the Imperial Roman Frontier 1st - 5th Centuries AD. New York: St. Martin's Press.

Wong EHM, Khrunin A, Nichols L, Pushkarev D, Khokhrin D, Verbenko D, Evgrafov O, Knowles J, Novembre J, Limborska S, Valouev A. 2017. Reconstructing genetic history of Siberian and Northeastern European populations. Genome Res 27:1–14.

Wright LE, Schwarcz HP. 1998. Stable carbon and oxygen isotopes in human tooth enamel: Identifying breastfeeding and weaning in prehistory. Am J Phys Anthropol 106:1–18.

Chapter 5.0 - Conclusions

Taken together, the genetic and isotopic data presented in this dissertation are analyzed within the expansive theoretical orientation of Braudel's *Longue Durée* (Braudel, 1949, 1958). Such historical framing is focused on deciphering long-term patterns in the historic and archaeological records over hundreds to thousands of years (Ames, 1991). In the case of Iron Age and Roman period southern Italy, the mtDNA and isotopic evidence, situated in an archaeological, historic, and archaeogenetic context, provide a foundation to interpret long-term demographic change in a complex region of the Mediterranean. The following expands on the themes explored here into a continuous narrative that captures key changes in South Italy across time.

5.1 Reimagining the Longue Durée in pre-Roman and Roman Southern Italy

The peopling of Europe by Anatomically Modern Humans (AMH) occurred approximately 55 ka, during the Upper Paleolithic (Posth et al., 2016). These early European populations experienced major climatic changes with the onset of the last Ice Age. By 22 ka, continent-wide ice sheets were present across northern Eurasia, known as the Last Glacial Maximum (LGM) (Soares et al., 2010). The advancing ice sheets and dramatic drop in temperatures across the northern hemisphere pushed temperate adapted species (flora and fauna) further South, sequestering them in refugia across parts of southern and eastern Europe (including Italy), and the Near East (Pala et al., 2009, 2012; De Fanti et al., 2015). Following the retreat of the glaciers, and a second cooling phase (the Younger Dryas event), humans re-expanded back into parts of central and northern Europe (~14 ka) (Pereira et al., 2005). Successive population contractions, paired with the influx of migrants stemming from eastern

Europe and the Near East (Anatolia), resulted in several founding events that can be directly measured in DNA obtained from archaeological remains (Lazaridis et al., 2017).

5.2 The Origins of Iron Age Populations in Southern Italy

The maximum clade credibility tree composed of 246 mtDNA sequences analyzed in Chapter 2 (Table S1) suggest that apart from haplogroup H (Iron Age libraries, or LIAV, 32, 33, and 40), which originated in Eurasia before the LGM, 12 out of 15 Iron Age mtDNA haplogroups postdate the LGM, indicating mtDNA turnover in Italy following the retreat of the ice sheets. Haplogroup U2 is comprised of samples from Iron Age Italy LIAV 43 (hg U2e3), pre-LGM samples from Russia (Kostenki 14) and Belgium (Goyet), and Bronze and Iron Age samples from Armenia. Previous mtDNA analysis showed that haplogroup U2 originated in eastern Europe and spread into central Europe prior to the LGM (Krause et al., 2010). It is likely that subsequent founding events by U2 subclusters occurred post-LGM, also concentrated in eastern Europe, leading to the diversification of haplogroup U2 sub-lineages in this area after the Ice Age (Malyarchuk et al., 2017). The presence of mtDNA subcluster U2e3 indicates that the ancestors likely originated from eastern Europe, and moved into central Europe and eventually Italy sometime after the retreat of the glaciers.

Haplogroup U3b (LIAV 37, U3b1b) likely originated in either the Caucases or Anatolia during the LGM (Derenko et al., 2013; Fernández et al., 2014). However, its absence from western European Neolithic assemblages suggests a more recent entry into southwestern Europe. One possibility for the diffusion of sublineage U3b1b into southern Europe was through expansion of Ionian Greek colonies in southern Italy, a hypothesis that is substantiated by the presence of U3b1b among the *Iapygians* from Botromagno, however it is unknown whether this

haplogroup entered western Europe prior to Greek colonization. Subclades U4a and U4b contain LIAV 4 (U4b1a1a1) and LIAV 38 (U4a1), together with samples obtained from Mesolithic Ukraine, Neolithic Russia, Latvia, and Germany, Bronze and Iron Age Armenia. Node ages suggest that U4a and U4b split approximately 26.3 ka, likely in eastern Europe, indicating that mtDNA sublineages U4a and U4b arose in eastern European refugia and dispersed into western Europe sometime after the LGM (Pala et al., 2012).

LIAV 20 (U5b2c) falls basal to samples obtained from Mesolithic Spain (LaBranã1) and Germany (Hohlenstein Stadel). It is possible that U5b2c evolved in Italy during the LGM and represents maternal continuity from that time up to the end of the Iron Age. If this is true, then both U5b3 and U5b2c represent two deeply rooted mitochondrial lineages in southern Italy (Pala et al., 2009). Subclade U5a1 (LIAV 31) is comprised of samples obtained from Neolithic Germany, Sweden, and Latvia. A coalescent age estimates for U5a1 was measured at 16.2 ka (95% CI 11.8 – 20.7 ka), which support an expansion from an eastern refugia between the Pyrenees, Balkans, and Ukraine, and across western Europe sometime after ~16 ka (Malyarchuk et al., 2010).

Subclade V contains LIAV 7 (V18) and samples from Neolithic Spain and Germany, and Bronze Age Germany. Haplogroup V likely evolved and expanded out of the Franco-Cantabrian refuge following the LGM, along with H1 (LIAV 8) and H3 (Torroni et al., 2001; Achilli et al., 2004; García et al., 2011). An alternative hypothesis suggests that haplogroup V, although common across western Europe, diversified in the East following the split of HV0a from HV (Soares et al., 2009). LIAV 32, 33, and 40 belong to superhaplogroup H, a Eurasian clade that accounts for approximately 40% of modern day European mtDNA diversity (Torroni et al., 1998, 2006). Haplogroup H arose in southwest Asia sometime between 20 and 25 ka, and arrived in

Europe before the LGM (Brotherton et al., 2013). Recent analysis has shown that this transformative period and increase in H mtDNAs occurred during the Neolithic (~6 ka) (Brotherton et al., 2013). LIAV 33 (H) shares a common ancestor with a sample obtained from Neolithic Sardinia (H1), pointing to either a post-LGM or Neolithic origins for this undefined sublineage. LIAV 32 and 40 (H) share a common ancestor with LIAV 45 (H2). Current analysis suggests that H2 originated in the Caucasus, likely during the LGM, and expanded West into central Europe during the Late Glacial period. It is unknown whether the ancestors of LIAV 32 and 40 migrated to Italy following the Late Glacial period, or represent recent influx from the Near East or central Europe after the onset of the Neolithic. Haplogroup H5'36 (LIAV 29) and H6a1a (LIAV11) is found most frequently in western Asia, eastern Europe, and the Caucasus. The H5 subclade is comprised of samples that date from the early to late German Neolithic, while H6a1a forms a subclade with samples from Neolithic Russia (Yamnaya) and Germany, and early Iron Age Armenia. Subsequent founding events of H5 and H6 are likely linked to migrations originating from the eastern European plains during the Neolithic. Subclade J2 is represented by two samples, LIAV 12 (J2b1a2) and Mina 2 (J2a1a), from Neolithic Spain. Haplogroup J2b1 is believed to be entirely European in origin, expanding into Europe after the Late Glacial period from the Balkans (Pala et al., 2012). Together, *Iapygian* mtDNA variation suggests that their ancestors originated as early as the Mesolithic, from parts of central and eastern Europe, or as late as the Neolithic and Bronze Ages, from eastern Europe and the Near East.

5.3 Roman Conquest of South Italy and the Local Population at Vagnari

Archaeological evidence indicates that the *Iapygians* traded and incorporated Hellenistic

elements into their material and cultural traditions (Small, 1992; Peruzzi, 2016). These changes are most apparent in burial custom and ceramic production, and become increasingly prominent by 2400 BP (Peruzzi, 2016). Further evidence shows that Iron Age communities across South Italy retracted in size amidst ongoing conflict between colonies in *Magna Graecia*, and Rome and Carthage (Small, 1992). This apparent change was interpreted as a decline in local populations throughout the region. However, Bayesian Skygrid analysis using the mtDNA profiles of 15 *Iapygians* and 30 Roman period individuals suggest that female effective population size was comparable between the two populations. In Chapter 4, population distance (measured as population pairwise Φ_{ST} values) across a range of mtDNAs obtained from the pan-Mediterranean, European, and western Asian regions suggest closer maternal affinities to Neolithic and Bronze Age populations from the eastern Mediterranean as a cohort, than with Iron Age Italians. This finding points to moderate mtDNA turnover, and is likely the consequence of Roman gene flow stemming from central and northern Italy via the migration and subsequent occupation by Roman colonies after 2250 BP.

Roman Imperial pursuits peaked by ~2050 BP. This extension of power, coupled with an increase in food and materials procurement, was driven by a substantial labour force comprised of both low status Romans and slaves (Harris, 1980; Bradley, 1987, 1994, 2000). Although several attempts have been made to quantify the number of slaves required to maintain the Roman economy, it is unknown what fraction of the Roman population was slave-owned (~approximately 1 to 3 million by 2050 BP) (Scheidel, 2005). Rome's slave acquisition during the early centuries of the Republic was likely maintained through military campaigns and conquest, a trend that is well documented in Italy (Scheidel, 1997, 1999, 2005; Harris, 1999; Small, 2002). However, once territory was secured, local slave populations were likely

maintained through one or a combination of the following: i) the importation of slaves from non-local regions, ii) were born to slave-owned parents, or iii) were voluntarily self-enslaved to acquire subsistence (Harris, 1999). The importation of foreign slaves was likely more costly than maintaining a self-reproducing slave population, especially in rural areas. As such, rural Roman necropoleis, such Vagnari, provide an opportune case to determine the local versus non-local demographic. Archaeological evidence suggests that Vagnari was involved in agriculture and industrial procurement, and was likely staffed by low-class individuals possibly including slaves (Small et al., 2000). However, without direct archaeological or epigraphic evidence, it is impossible to identify the proportion of slaves at rural sites.

Instead, integrating multiple lines of historic and isotopic evidence has begun to clarify these elusive questions about the Roman past. Stable isotope evidence for Roman mobility has show that immigration was more common in large-city centres, such as Rome, than in rural areas like Vagnari, and that these migrants included women and children (Emery et al. in review; Prowse et al., 2007, 2010; Killgrove and Montgomery, 2016; Prowse, 2016). Stable $\delta^{18}O$ analysis of Roman remains has expanded to include $^{87}Sr^{86}Sr$ analysis. This multi-isotopic approach has improved our ability to identify local and non-local inhabitants buried in Roman cemeteries. However, the ability to spatially locate (or match) the $^{87}Sr^{86}Sr$ values from teeth, and thus the ability to infer childhood geographic origins, has so far eluded Roman bioarchaeologists. To advance this lack of spatial $^{87}Sr^{86}Sr$ resolution for Italy, I generated the first $^{87}Sr^{86}Sr$ variation map using a variety of disparate $^{87}Sr^{86}Sr$ data sources spanning the Italian peninsula (Chapter 3). $^{87}Sr^{86}Sr$ variation across Italy reflects its long and complex geological history. The $^{87}Sr^{86}Sr$ spatial analysis confirms that Italian $^{87}Sr^{86}Sr$ varies along a N-S axis, with lower $^{87}Sr^{86}Sr$ values characterizing southern Italy, generally progressing to higher $^{87}Sr^{86}Sr$ values in the Italian Alps.

Spatial $^{87}Sr^{86}Sr$ analysis of Italy provided the necessary baseline from which to directly assess the $^{87}Sr^{86}Sr$ values, and therefore geographic origins, for a subset of the Vagnari dental assemblage. The isotope values presented in Chapter 3 obtained from 56 Roman individuals buried at Vagnari suggest that over half (58%) were born directly at Vagnari, with a further 34% originating from South Italy. Only 7% (3/43 with both $\delta^{18}O$ and $^{87}Sr/^{86}Sr$ values) of the individuals sampled resulted in isotope values non-local to the southern peninsula. Two of these individuals originated from either northern Italy or, more broadly, from central Europe, while one individual likely originated from North Africa. Overall, the isotope data suggest a low number of immigrants at Vagnari, which conforms with the population pairwise (Φ_{ST}) data for the Iron Age and Roman mtDNAs, and suggests that as the Romans occupied the region, they populated their Imperial properties with people from central Italy (possible the region of Latium, and the surrounding environs of Rome). These results also integrate with the historical evidence concerning the Roman slave economy during the Imperial period. Future research using a larger comparative dataset comprised of pre-Roman and Roman period mtDNAs, $\delta^{18}O$ and, $^{87}Sr/^{86}Sr$ results will refine the interpretations outlined here.

The results presented in this thesis directly advance our understanding about the population history of classical southern Italy through the theoretical lens of the *longue durée*. The biochemical (mtDNA) and chemical ($^{87}Sr^{86}Sr$ and $\delta^{18}O$) results obtained for the Botromagno and Vagnari assemblages reflect a variety of evolutionary and geomorphological processes that helped shaped the biology and chemistry of the individuals analyzed here. The complicated and yet unresolved nature of the peopling of Europe is reflected in the mtDNAs from both Iron Age and Roman skeletal assemblages, and their $^{87}Sr^{86}Sr$ compositions similarly reflect the intricate geological history of the lanscape they once inhabited. Future analysis using the methodologies

outlined in this document will, whether conscious or not, be utilizing a theoretical lens oriented towards millenia of change, a narrative across Braudel's *longue durée* (Braudel, 1958).

5.4 Future Directions

The skeletal material processed for mtDNA and isotopic information represent a portion of the total material available for study. Expansion on the results presented in this dissertation require further isotopic and aDNA investigation. Additional $^{18}O/^{16}O$, $^{87}Sr/^{86}Sr$, $^{13}C/^{12}C$, and $^{15}N/^{14}N$ results, including sulphur ($^{34}S/^{32}S$) and lead ($^{206}Pb/^{204}Pb$, $^{207}Pb/^{204}Pb$, and $^{208}Pb/^{204}Pb$) isotope analysis of the Botromagno and Vagnari remains will lead to more accurate interpretations about migration and diet at these sites (e.g., Montgomery et al., 2010; Linderholm et al., 2014; Nehlich, 2015; Moghaddam et al., 2016; Sharpe et al., 2016). The interpretation of specific provenancing isotopes, such as $^{87}Sr/^{86}Sr$, depend on a robust understanding of $^{87}Sr/^{86}Sr$ variation of the local biosphere (Bowen, 2010). The preliminary $^{87}Sr/^{86}Sr$ variation map presented in Chapter 3 is a step towards obtaining new $^{87}Sr/^{86}Sr$ values from bioavailable sources. This step will circumvent the inherent problems with using geological, spring water, and other non-bioavailable sources of $^{87}Sr/^{86}Sr$, which may misrepresent bioavailable $^{87}Sr/^{86}Sr$ variation through environmental transportation processes. Obtaining additional bioavailable $^{87}Sr/^{86}Sr$ results will further resolve $^{87}Sr/^{86}Sr$ variation across the Italian peninsula.

Ancient DNA analysis is limited by the amount of endogenous DNA recovered from ancient specimens, and is characterized by highly fragmented and damaged molecules. The processes leading to DNA degradation are determined by environmental conditions, confounded by modern human and bacterial contamination, and time. Under exceptional environmental conditions, such as permafrost or low-pore water anoxic environments, the decay rate of DNA

may slow over time. These conditions are exceptions to the rule, and more recent attempts to amplify and sequence fragmented DNA now use target enrichment-based techniques followed by high-throughput sequencing, a move that has drastically increased our chances of recovering a large amount of genetic information over the short term. Although DNA degredations continues to be a limiting factor in the field, technological advancements in laboratory experimentation, sequencing, and read processing, has improve whole-genome depth and resolution for a number of ancient specimens. 'Next-next-generation', or third generation platforms, are currently being employed (i.e., Single Molecule Real Time, Illumina Tru-Seq, and Nanopore sequencing platforms) (Hoenen et al., 2016; Lee et al., 2016). Future mtDNA analysis, paired with NRY-chromosome, whole-genome SNP, and pathogen analysis, will similarly improve interpretation regarding ancestry, migration, and the spread and prevalence of disease in South Italy over greater periods of time. At the local scale, however, these targets will further substantiate the possible kin-based relationships across the cemetery, leading to more nuanced interpretations about the biosocial structure of rural Roman period cemeteries in this region of Italy.

Traditional attempts to determine whether or not individuals recovered from archaeological contexts were born domestic- or foreign-born, or were ancestrally linked to the geographic spaces they occupied relied primarily on artifacts and textual records. Modern bioarchaeological analyses use a suite of cutting-edge scientific technologies that allow us to investigate the biogeographic diversity of archaeological specimens down to the molecular and atomic scales. Advances in the archaeological sciences will continue to add to the rich repertoire of information about the past previously thought unattainable, and as an extension, our ability to reconstruct the lifestyles and habits of our ancestors.

6.0 References (Chapters 1 and 5)

Achilli A, Rengo C, Magri C, Battaglia V, Olivieri A, Scozzari R, Cruciani F, Zeviani M, Briem E, Carelli V, Moral P, Dugoujon J-M, Roostalu U, Loogväli E-L, Kivisild T, Bandelt H-J, Richards M, Villems R, Silvana Santachiara-Benerecetti A, Semino O, Torroni A. 2004. The molecular dissection of mtDNA haplogroup H confirms that the Franco-Cantabrian glacial refuge was a major source for the European gene pool. Am J Hum Genet 75:910–918.

Ames KM. 1991. The archaeology of the longue durée: Temporal and spatial scale in the evolution of social complexity on the southern Northwest Coast. Antiquity 65:935–945.

Armitage D. 2012. What's the big idea? Intellectual history and the *longue durée*. Hist Eur Ideas 38:493–507.

Attema P, van Leusen A. 2004. The Early Roman Colonization of South Lazio: A Survey of Three Landscapes. In: Attema P, editor. Centralization, Early Urbanization, and Colonization in First Millenium BC Italy and Greece. Leuven: Peeters:157–195.

Batiuk SD. 2013. The fruits of migration: understanding the "*longue dureé*" and the socio-economic relations of the early transcaucasian culture. J Anthropol Archaeol 32:449–477.

Ben-Shlomo D, Uziel J, Maeir AM. 2009. Pottery production at Tell es-Safi/Gath: a Longue Durée perspective. J Archaeol Sci 36:2258–2273.

Benelli E. 2001. The Romanization of Italy Through the Epigraphic Record. In: Keays S, Terrenato N, editors. Italy and the West: Comparative Issues in Romanization. Oxford: Oxford Books:7–17.

Bernard S. 2016. Food Distribution and Immigration in Imperial Rome. In: De Ligt L, Tacoma L, editors. Migration and Mobility in the Early Roman Empire. Leiden: Brill:50–71.

Biers W. 1992. Art, Artefacts, and Chronology in Classical Archaeology. London and New York: Routledge.

Bowen GJ. 2010. Isoscapes: spatial pattern in isotopic biogeochemistry. Annu Rev Earth Planet Sci 38:161–187.

Bradford E. 1971. Mediterranean: Portrait of a Sea. London: Hodder and Stoughton.

Bradley KR. 1987. On the Roman slave supply and slavebreeding. Slavery Abolit 8:42–64.

Bradley KR. 1994. Slavery and Society at Rome. Cambridge: Cambridge University Press.

Bradley KR. 2000. Animalizing the slave: the truth of fiction. J Rom Stud 90:110–125.

Braudel F. 1949. La Méditerranée et le Monde Méditerranéen à L'époque de Philippe II. Paris: Armand Colin.

Braudel F. 1958. Histoire et sciences sociales : la longue durée. Ann Économies, Sociétés, Civilisations 13:725–753.

Breeze D. 2011. The Frontiers of Imperial Rome. South Yorkshire: Pen and Sword Military.

Brotherton P, Haak W, Templeton J, Brandt G, Soubrier J, Jane Adler C, Richards SM, Sarkissian C Der, Ganslmeier R, Friederich S, Dresely V, van Oven M, Kenyon R, Van der Hoek MB, Korlach J, Luong K, Ho SYW, Quintana-Murci L, Behar DM, Meller H, Alt KW, Cooper A, Adhikarla S, Ganesh Prasad AK, Pitchappan R, Varatharajan Santhakumari A, Balanovska E, Balanovsky O, Bertranpetit J, Comas D, Martínez-Cruz B, Melé M, Clarke AC, Matisoo-Smith EA, Dulik MC, Gaieski JB, Owings AC, Schurr TG, Vilar MG, Hobbs A, Soodyall H, Javed A, Parida L, Platt DE, Royyuru AK, Jin L, Li S, Kaplan ME, Merchant NC, John Mitchell R, Renfrew C, Lacerda DR, Santos FR, Soria Hernanz DF, Spencer Wells R, Swamikrishnan P, Tyler-Smith C, Paulo Vieira P, Ziegle JS. 2013. Neolithic mitochondrial haplogroup H genomes and the genetic origins of Europeans. Nat Commun 4:17-64.

Burgers G. 2004. Urbanization in Magna Graecia: Settlement, Landscape, and Social Dynamics in a Regional Life. In: Attema P, editor. Centralization, Early Urbanization, and Colonization in First Millenium BC Italy and Greece. Leuven: Peeters. p 121–136.

Campagna L. 2011. Exploring Social and Cultural Change in Provincia Sicilia: Relfections of the Study of Urban Landscapes. In: Colivicchi F, editor. Local Cultures of South Italy and Sicily in the Late Republican Period. Dexter: Thomson Shore:161–185.

Cary M. 1981. The Geographic Background of Greek and Roman History. Westport, Connecticut: Greenwood Press Publishers.

Christ K. 1984. The Romans: An Introduction to Their History and Civilization. London: The Hogarth Press.

Colivicchi F. 2011. The Long Good-Bye: The Local Elites of Daunia Between Continuity and Change. In: Colivicchi F, editor. Local Cultures of South Italy and Sicily in the Late Republican Period. Journal of Roman Archaeology Supplementary Series 83:112–139.

Colombo A, Hill C, Kast D, Petito F, Raineri E, Carr EH. 2006. Elisabetta Brighi " One man alone "? A longue durée approach to Italy's foreign policy. Mod Italy 41:278–297.

Cool H. 2010. Finding the Foreigners. In: Eckardt H, editor. Roman Diasporas: Archaeological Approaches to Mobility and Diversity in the Roman Empire. Portsmouth: Journal of Roman Archaeology, Supplementary Series Number 78:27–44.

Cornell T. 1995. The Beginnings of Rome: Italy and Rome From the Bronze Age to the Punic Wars (c. 1000 - 264 BC). London: Routledge.

Crawford M. 2001. Early Rome and Italy. In: Boardman J, Griffin J, Murray O, editors. The Oxford Illustrated History of the Roman World. Oxford: Oxford University Press:387-417.

Curti E, Dench E, Patterson J. 1996. The archaeology of central and southern Roman Italy: recent trends and approaches. J Rom Archaeol 86:170–189.

De Ligt L. 2012. Peasants, Citizens and Soldiers: Studies in the Demographic History of Roman Italy 225 BC-AD100 AD. Cambridge: Cambridge University Press.

De Ligt L, Tacoma L. 2016. Approaching Migration in the Early Roman Empire. In: De Ligt L, Tacoma L, editors. Migration and Mobility in the Early Roman Empire. Leiden: Brill:1–22.

Derenko M, Malyarchuk B, Bahmanimehr A, Denisova G, Perkova M, Farjadian S, Yepiskoposyan L. 2013. Complete mitochondrial DNA diversity in Iranians. PLoS One 8:e80673.

Dietler M. 2007. The Iron Age in the Western Mediterranean. In: Scheidel W, Morris I, Saller R, editors. The Cambridge Economic History of the Greco-Roman World. Cambridge: Cambridge University Press:242–276.

Dudley D. 1970. The Romans: 850 BC - AD 337. New York: Alfred A. Knopf.

Dunbabin TJ. 1979. The Western Greeks: The History of Sicily and South Italy From the Foundation of the Greek Colonies to 480 BC. Chicago: ARES Publisher Inc.

Dyson S. 1985. The Creation of the Roman Frontier. New Jersey: Princeton University Press.

Elton H. 1996. Frontiers of the Roman Empire. Indianapolis: Indiana University Press.

Emery MV, Stark R, Murchie TJ, Elford S, Schwarcz H., Prowse TL. Mapping the origins of imperial Roman workers (1st – 4th century CE) at Vagnari, southern Italy, using $^{87}Sr/^{86}Sr$ and $\delta^{18}O$ variability. Am J Phys Anthropol In Review.

Erdkamp P. 2016. Seasonal Labour and Rural-Urban Migration in Roman Italy. In: De Ligt L, Tacoma L, editors. Migration and Mobility in the Early Roman Empire. Leiden: Brill. p 33–49.

De Fanti S, Barbieri C, Sarno S, Sevini F, Vianello D, Tamm E, Metspalu E, Van Oven M, Hübner A, Sazzini M, Franceschi C, Pettener D, Luiselli D. 2015. Fine dissection of human mitochondrial DNA haplogroup HV lineages reveals paleolithic signatures from European Glacial refugia. PLoS One 10:1–19.

Fernández E, Pérez-Pérez A, Gamba C, Prats E, Cuesta P, Anfruns J, Molist M, Arroyo-Pardo E, Turbón D. 2014. Ancient DNA analysis of 8000 B.C. Near Eastern farmers supports an early Neolithic pioneer maritime colonization of mainland Europe through Cyprus and the Aegean Islands. PLoS Genet 10:e1004401.

Finley M. 1979. Ancient Sicily. London: Chatto and Windus.

Fischer-Hansen T. 1993. Apulia and Etruria in the Early Hellenistic Period. In: Guldager P, Nielsen I, Nielsen M, editors. Aspects of Hellenism in Italy. Copenhagen: Museum Tusculanum Press:53–91.

Fletcher RN. 2007. Patterns of Imports in Iron Age Italy. Oxford: Archeopress.

Foubert L. 2016. Mobile Women in P. Oxy and the Port Cities of Roman Egypt: Tracing Women's Travel Behaviour in Papyrological Sources. In: De ligt L, Tacoma L, editors. Migration and Mobility in the Early Roman Empire. Leiden: Brill:285–304.

Fulford M. 2010. Roman Britain: Immigration and Material Culture. In: Eckardt H, editor. Roman Diasporas: Archaeological Approaches to Mobility and Diversity in the Roman Empire2. Portsmouth: Journal of Roman Archaeology Supplementary Series 78:67–78.

Galinsky K. 1992. Classical and Modern Interactions: Postmodern Architecture, Multiculturalism, Decline, and Other Issues. Austin: University of Texas Press.

García O, Fregel R, Larruga JM, Álvarez V, Yurrebaso I, Cabrera VM, González AM. 2011. Using mitochondrial DNA to test the hypothesis of a European post-glacial human recolonization from the Franco-Cantabrian refuge. Heredity 106:37–45.

Garnsey P, Saller R. 2014. Roman Empire: Economy, Society, and Culture. Oakland: California Press.

Gejvall N, Henschen F. 1968. Two late Roman skeletons with malformations and close family relationships from ancient Corinth. Opusc Athenia 8:179–193.

Gibbon E. 1869. The History of the Decline and Fall of the Roman Empire. London: Methuen and Co. Ltd.

Graeme B. 1995. A Mediterranean Valley: Landscape Archaeology and Annales History in the Biferno Valley. London: Leicester University Press.

Guido M. 1973. Southern Italy: An Archaeological Guide: The Main Prehistoric, Greek, and Roman Sites. New Jersey: Noyes Press.

Guldi J, Armitage D. 2014. The History Manifesto. Cambridge: Cambridge University Press.

Gwynn D. 2012. The Roman Republic: A Very Short Introduction. Oxford: Oxford University Press.

Haeussler R. 2013. Becoming Roman? Diverging Identities and Experiences in Ancient Northwest Italy. Walnut Creek: Left Coast Press.

Handberg S, Jacobsen JK. 2011. Greek or Indigenous? From Potsherd to Identity in Early Colonial Encounters. In: Gleba M, Horsnaes HW, editors. Communicating Identity in Italic Iron Age Communities. Oxford: Oxbow Books:177–197.

Harding J. 2005. Rethinking the great divide: long- term structural history and the temporality of event. Nor Archaeol Rev 38:88–101.

Harris W. 1980. Towards a Study of the Roman Slave Trade. In: D'Arms JH, Kopff EC, editors. The Seaborne Commerce of Ancient Rome: Studies in History and Archaeology. Memoirs of the American Academy in Rome 36:117–140.

Harris W. 1999. Demography, geography, and the sources of Roman slaves. J Rom Stud 89:62–75.

Hassall M. 1999. Homes for the Heroes: Married Quarters for Soldiers and Veterans. In: Haynes A, editor. The Roman Army as a Community: Journal of Roman Archaeology Supplement 34. Portsmouth:35–40.

Haywood J. 2008. The Great Migrations: From the Earliest Humans to the Age of Globolization. London: Quercus.

Hedeager L. 1992. Iron-Age Societies: From Tribe to State in Northern Europe, 500 BC to AD 700. Oxford: Blackwell.

Hedeager L. 2000. Migration Period Europe: The Formation of a Political Mentality. In: Theuws F, Nelson J, editors. Rituals of Power: From Late Antiquity to the Early Middle Ages. Leiden: Brill:15–57.

Hodos T. 2006. Local Responses to Colonization in the Iron Age Mediterranean. London: Routledge.

Hodos T. 2009. Colonial engagements in the global Mediterranean Iron Age. Cambridge Archaeol J 19:221–241.

Hoenen T, Groseth A, Rosenke K, Fischer RJ, Hoenen A, Judson SD, Martellaro C, Falzarano D, Marzi A, Squires RB, Wollenberg KR, De Wit E, Prescott J, Safronetz D, Van Doremalen N, Bushmaker T, Feldmann F, McNally K, Bolay FK, Fields B, Sealy T, Rayfield M, Nichol ST, Zoon KC, Massaquoi M, Munster VJ, Feldmann H. 2016. Nanopore sequencing as a rapidly deployable Ebola outbreak tool. Emerg Infect Dis 22:331–334.

Hopkins K. 1980. Taxes and trade in the Roman empire (200 BC - AD 400). J Rom Stud 70:101–125.

Jeskins P. 1998. The Environment and the Classical World. London: Bristol Classical Press.

Karlsson L. 1993. Did the Romans Allow the Sicilian Greeks to Fortify Their Cities in the Third Century BC? In: Guldager P, Nielsen I, Nielsen M, editors. Aspects of Hellenism in Italy. Copenhagen: Museum Tusculanum Press:31-51.

Killgrove K. 2010. Identifying Immigrants to Imperial Rome Using Strontium Isotope Analysis. In: Eckardt H, editor. Roman Diasporas: Archaeological Approaches to Mobility and Diversity in the Roman Empire. Portsmouth: Journal of Roman Archaeology Supplementary Series 78:157–174.

Killgrove K, Montgomery J. 2016. All roads lead to Rome: Exploring human migration to the eternal city through biochemistry of skeletons from two imperial-era cemeteries (1st-3rd c AD). PLoS One 11:1–30.

Krause J, Fu Q, Good JM, Viola B, Shunkov M V, Derevianko AP, Pääbo S. 2010. The complete mitochondrial DNA genome of an unknown hominin from southern Siberia. Nature 464:894–897.

Lazaridis I, Mittnik A, Patterson N, Mallick S, Rohland N, Pfrengle S, Furtwängler A, Peltzer A, Posth C, Vasilakis A, McGeorge PJP, Konsolaki-Yannopoulou E, Korres G, Martlew H, Michalodimitrakis M, Özsait M, Özsait N, Papathanasiou A, Richards M, Roodenberg SA, Tzedakis Y, Arnott R, Fernandes DM, Hughey JR, Lotakis DM, Navas PA, Maniatis Y, Stamatoyannopoulos JA, Stewardson K, Stockhammer P, Pinhasi R, Reich D, Krause J, Stamatoyannopoulos G. 2017. Genetic origins of the Minoans and Mycenaeans. Nature 548:214-218.

Lee H, Gurtowski J, Yoo S, Nattestad M, Marcus S, Goodwin S, McCombie WR, Schatz M. 2016. Third-generation sequencing and the future of genomics. bioRxiv:48603.

Di Lieto M. 2011. The Northern Lucanian Area in the Roman Republic Period. In: Colivicchi F, editor. Local Cultures of South Italy and Sicily in the Late Republican Period: Between Hellenism and Rome. Dexter, Michigan: Thomson Shore:44–57.

Linderholm A, Fornander E, Eriksson G, Mörth C-M, Lidén K. 2014. Increasing mobility at the Neolithic/Bronze Age transition – sulphur isotope evidence from Öland, Sweden. Internet Archaeol 37:10.11141/ia.37.10.

Lomas K. 1993. Rome and the Western Greeks. London and New York: Routledge.

Lomas K. 2000. The Polis in Italy: Ethnicity, Colonization, and Citizenship in the Western Mediterranean. In: Brock R, Hodkinson S, editors. Alternatives to Athens. Oxford: Oxford University Press:167–189.

Lomas K. 2016. Magna Graecia 270 BC-AD 200. In: Cooley A, editor. A Companion to Roman Italy. Malden: Wiley Blackwell:253–268.

Malfitana D. 2011. The View From the Material Culture Assemblage of Late Republican Sicily. In: Colivicchi F, editor. Local Cultures of South Italy and Sicily in the Late Republican Period. Dexter, Michigan: Thomson Shore:185–203.

Malyarchuk BA, Derenko M V., Litvinov AN. 2017. The macrohaplogroup U structure in Russians. Russ J Genet 53:498–503.

Malyarchuk B, Derenko M, Grzybowski T, Perkova M, Rogalla U, Vanecek T, Tsybovsky I. 2010. The Peopling of Europe From the Mitochondrial Haplogroup U5 Perspective. PLoS One 5:16–20.

Marciniak S, Prowse TL, Herring DA, Klunk J, Kuch M, Duggan AT, Bondioli L, Holmes EC, Poinar HN. 2016. Plasmodium falciparum malaria in 1st–2nd century CE southern Italy. Curr Biol 26:1220–1222.

Mattingly D, Hitchner R. 1995. Roman Africa: an archaeological review. J Rom Stud 85:135–213.

McEvoy B, Richards M, Forster P, Bradley DG. 2004. The Longue Durée of genetic ancestry: multiple genetic marker systems and Celtic origins on the Atlantic facade of Europe. Am J Hum Genet 75:693–702.

Moghaddam N, Müller F, Hafner A, Lösch S. 2016. Social stratigraphy in Late Iron Age Switzerland: stable carbon, nitrogen and sulphur isotope analysis of human remains from Münsingen. Archaeol Anthropol Sci 8:149–160.

Montgomery J, Evans J, Chenery C, Pashley V, Killgrove K. 2010. Gleaming, White and Deadly: Using Lead to Track Human Exposure and Geographic Origins in the Roman Period in Britain. In: Eckardt H, editor. Roman Diasporas: Archaeological Approaches to Mobility and Diversity in the Roman Empire. Portsmouth: Journal of Roman Archaeology Supplementary Series 78:199–226.

Morel J. 2007. Early Rome and Italy. In: Scheidel W, Morris I, Saller R, editors. The Cambridge Economic History of the Greco-Roman World. Cambridge: Cambridge University Press:487-511.

Morley N. 2001. The transformation of Italy, 225-28 BC. J Rom Stud 91:50–62.

Negbi I. 1992. Early Phoenician presence in the mediterranean islands: a reappraisal. Am J Archaeol 96:599–615.

Nehlich O. 2015. The application of sulphur isotope analyses in archaeological research: A review. Earth-Science Rev 142:1–17.

North J. 1981. The development of Roman imperialism. J Rom Stud 71:1–9.

Pala M, Achilli A, Olivieri A, Kashani BH, Perego UA, Sanna D, Metspalu E, Tambets K, Tamm E, Accetturo M, Carossa V, Lancioni H, Panara F, Zimmermann B, Huber G, Al-Zahery N, Brisighelli F, Woodward SR, Francalacci P, Parson W, Salas A, Behar DM, Villems R, Semino O, Bandelt HJ, Torroni A. 2009. Mitochondrial haplogroup U5b3: a distant echo of the epipaleolithic in Italy and the legacy of the early Sardinians. Am J Hum Genet 84:814–821.

Pala M, Olivieri A, Achilli A, Accetturo M, Metspalu E, Reidla M, Tamm E, Karmin M, Reisberg T, Kashani BH, Perego UA, Carossa V, Gandini F, Pereira JB, Soares P, Angerhofer N, Rychkov S, Al-Zahery N, Carelli V, Sanati MH, Houshmand M, Hatina J, MacAulay V, Pereira L, Woodward SR, Davies W, Gamble C, Baird D, Semino O, Villems R, Torroni A, Richards MB. 2012. Mitochondrial DNA signals of late glacial recolonization of europe from near eastern refugia. Am J Hum Genet 90:915–924.

Paoli U. 1973. Rome: Its People, Life, and Customs. Norforlk: Lowe and Brydone Ltd.

Parker H. 1935. History of the Roman World - From AD 138 to 337. London: Methuen and Co. Ltd.

Pedley J. 1990. Paestum: Greeks and Romans in Southern Italy. London: Thames and Hudson Ltd.

Pereira L, Richards M, Goios A, Alonso A, Albarrán C, Garcia O, Behar DM, Gölge M, Hatina J, Al-Gazali L, Bradley DG, Macaulay V, Amorim A. 2005. High-resolution mtDNA evidence for the late-glacial resettlement of Europe from an Iberian refugium. Genome Res 15:19–24.

Peruzzi B. 2016. Populating Peucetia: Central Apulian Grave Good Assemblages From the Classical Period (late 6th-3rd centuries B.C.). Unpublished PhD Dissertation, University of Cincinnati, Arts and Sciences:Classics.

Petersen J. 2011. Constructing Identities in the Multicultural Milieux: The Formation of Orphism in the Black Sea Region and Southern Italy in the Late 6th and Early 5th Centuries BC. In: Gleba M, Horsnaes H, editors. Communicating Identity in Italic Iron Age Communities. Oxford: Oxford Books:167–177.

Posth C, Renaud G, Mittnik A, Drucker DG, Rougier H, Cupillard C, Valentin F, Thevenet C, Furtwängler A, Wißing C, Francken M, Malina M, Bolus M, Lari M, Gigli E, Capecchi G, Crevecoeur I, Beauval C, Flas D, Germonpré M, Van Der Plicht J, Cottiaux R, Gély B, Ronchitelli A, Wehrberger K, Grigorescu D, Svoboda J, Semal P, Caramelli D, Bocherens H, Harvati K, Conard NJ, Haak W, Powell A, Krause J. 2016. Pleistocene mitochondrial

genomes suggest a single major dispersal of non-africans and a late glacial population turnover in Europe. Curr Biol 26:827–833.

Prowse TL. 2016. Isotopes and Mobility in the Ancient Roman World. In: De Ligt L, Tacoma L, editors. Migration and Mobility in the Early Roman Empire. Leiden: Brill:205–233.

Prowse TL, Barta J, Hunnius T, Small A. 2010. Stable isotope and mtDNA evidence for geographic origins at the site of Vagnari, South Italy. In: Eckardt H, editor. Roman Diasporas: Archaeological Approaches to Mobility and Diversity in the Roman Empire. Portsmouth: Journal of Roman Archaeology Supplementary Series 78:175–198.

Prowse TL, Schwarcz HP, Garnsey P, Knyf M, Macchiarelli R, Bondioli L. 2007. Isotopic evidence for age-related immigration to imperial Rome. Am J Phys Anthropol 128:2–13.

Rawson E. 2001. The Expansion of Rome. In: Boardman J, Griffin J, Murray O, editors. The Oxford Illustrated History of the Roman World. Oxford: Oxford University Press:39–60.

Redman CL, Kinzig AP. 2003. Resilience of past landscapes: Resilience theory, society, and the Longue Durée. Ecol Soc 7:1-4.

Reich J. 1979. Italy Before Rome. Oxford University Press: Oxford. London.

Revell L. 2009. Roman Imperialism and Local Identities. Cambridge: Cambridge University Press.

Rosen AM, Rivera-Collazo I. 2012. Climate change, adaptive cycles, and the persistence of foraging economies during the late Pleistocene/Holocene transition in the Levant. Proc Natl Acad Sci 109:3640–3645.

Rostovtzeff M. 1971. The Social and Economic Hisotry of the Roman Empire. Oxford: Oxford University Press.

Salmon E. 1955. Roman expansion and Roman colonization in Italy. Phoenix 9:36–75.

Salmon E. 1968. A History of the Roman World From 30 BC to AD 138. London: Methuen and Co. Ltd.

Sampson G. 2008. The Defeat of Rome: Crassus, Carrhae, and the Invasion of the East. South Yorkshire: Pen and Sword Books Ltd.

Samuel A. 1988. The Promise of the West: The Greek World, Rome, and Judaism. London: Routledge.

Scheidel W. 1997. Quantifying the sources of slaves in the Roman empire. J Rom Archaeol 87:159–169.

Scheidel W. 1999. The slave population of Roman Italy: speculations and constraints. Topoi 9:129–144.

Scheidel W. 2005. Human mobility in Roman Italy II: the slave population. J Rom Stud 95:64–79.

Sharpe AE, Kamenov GD, Gilli A, Hodell DA, Emery KF, Brenner M, Krigbaum J. 2016. Lead (Pb) isotope baselines for studies of ancient human migration and trade in the Maya region. PLoS One 11:1–28.

Small A. 1992. Botromagno: An Introduction. In: Small A, editor. Gravina: An Iron Age and Republican Settlement in Apulia. Volume 1: London: British School at Rome:3–15.

Small A. 2002. Apulia before and after the Roman conquest: Recent evidence from Botromagno. J Rom Archaeol 15:375–379.

Small A, Small C. 2007. Excavation in the Roman cemetery at Vagnari in the territory of Gravina in Puglia. Pap Br Sch Rome LXXV:162–213.

Small AM, Volterra V, Hancock RG V. 2000. New evidence from tile-stamps for imperial properties near Gravina , and the topography of imperial estates in SE Italy. J Rom Archaeol 122:179–199.

Smith CJ. 1999. Medea in Italy: Barter and Exchange in the Archaic Mediterranean. In: Tsetskhladze GR, editor. Ancient Greeks West and East. Brill, Leiden:179-207.

Soares P, Achilli A, Semino O, Davies W, Macaulay V, Bandelt HJ, Torroni A, Richards MB. 2010. The archaeogenetics of Europe. Curr Biol 20:174–183.

Soares P, Ermini L, Thomson N, Mormina M, Rito T, Röhl A, Salas A, Oppenheimer S, Macaulay V, Richards MB. 2009. Correcting for purifying selection: an improved human mitochondrial molecular clock. Am J Hum Genet 84:740–759.

Stark R. 2016. Ancient Lives in Motion.Unpublished PhD Dissertation, McMaster University, Hamilton, Canada.

La Torre GF. 2011. Reflections on the Lucanians and Bruttians in Calabria Between Hannibal and the Principate: Coloniae, Foederatae, Municipia. In: Colivicchi F, editor. Local Cultures of South Italy and Sicily in the Late Republican Period: Between Hellenism and Rome. Journal of Roman Archaeology, Supplementary Series Number 83:139–159.

Torroni A, Achilli A, Macaulay V, Richards M, Bandelt HJ. 2006. Harvesting the fruit of the human mtDNA tree. Trends Genet 22:339–345.

Torroni A, Bandelt H-J, Lahermo P, Moral P, Sellitto D, Rengo C, Forster P, Savontaus M-L, Bonné-Tamir B, Scozzari R. 1998. mtDNA analysis reveals a major Late Paleolithic population expansion from southwestern to northeastern Europe. Am J Hum Genet 62:1137–1152.

Torroni A, Bandelt H-J, Macaulay V, Richards M, Cruciani F, Rengo C, Martinez-Cabrera V, Villems R, Kivisild T, Metspalu E, Parik J, Tolk H-V, Tambets K, Forster P, Karger B, Francalacci P, Rudan P, Janicijevic B, Rickards O, Savontaus M-L, Huoponen K, Laitinen V, Koivumäki S, Sykes B, Hickey E, Novelletto A, Moral P, Sellitto D, Coppa A, Al-Zaheri N, Santachiara-Benerecetti AS, Semino O, Scozzari R. 2001. A signal, from human mtDNA, of postglacial recolonization in Europe. Am J Hum Genet 69:844–852.

Van Dommelen P. 1998. Colonial constructs: colonialism and archaeology in the Mediterranean. World Archaeol 28:305–323.

Wells C. 1984. The Roman Empire. Standford: Stanford University Press.

Whittaker C. 1994. Frontiers of the Roman Empire: A Social and Economic History. Baltimore: The John Hopkins University Press.

Williams D. 1997. The Reach of Rome: A History of the Imperial Roman Frontier 1st - 5th Centuries AD. New York: St. Martin's Press.

Wilson A. 1966. Emigration From Italy in Republican Age Rome. Manchester: Manchester University Press.

Winks R, Mattern-Parkes S. 2004. The Ancient Mediterranean World: From the Stone Age to AD 600. Oxford: Oxford University Press.